Epigenetic control of ribosome biogenesis homeostasis

Jérôme Deraze

Université Pierre et Marie Curie

Ecole doctorale : Complexité du Vivant

IBPS – UMR7622 Laboratoire de Biologie du Développement UPMC CNRS

Epigenetic control of developmental homeostasis and plasticity

Epigenetic Control of Ribosome Biogenesis Homeostasis

Par Jérôme Deraze

Thèse de doctorat de Biologie Moléculaire et Cellulaire

Dirigée par Frédérique Peronnet et Sébastien Bloyer

Présentée et soutenue publiquement le 19 Septembre 2017

Devant un jury composé de :

Pr Anne-Marie MARTINEZ	Professeur	Rapporteur
Dr Jacques MONTAGNE	Directeur de Recherche	Rapporteur
Dr Olivier JEAN-JEAN	Directeur de Recherche	Examinateur
Dr Michel COHEN-TANNOUDJI	Directeur de Recherche	Examinateur
Dr Françoise JAMEN	Maître de Conférences	Examinateur
Dr Nicolas NEGRE	Maître de Conférences	Examinateur
Dr Frédérique PERONNET	Directrice de Recherche	Directrice de thèse
Pr Sébastien BLOYER	Professeur	Co-directeur de thèse

Table of contents

Table of figures

Table of abreviations

aaRS	aminoacyl-tRNA Synthetase
ADP	Adenosine Disphosphate
AMP	Adenosine Monophosphate
AMPK	AMP-activated protein Kinase
ASL	Anticodon Stem Loop
ATP	Adenosine Triphosphate
BAC	Bacterial artificial chromosome
BMP	Bone morphogenetic protein
CDK	Cycin-dependent Kinase
cDNA	complementary DNA
CDS	Coding sequence
ChIP	Chromatin immunoprecipitation
CortoCD	Chromodomain of Corto
CRISPR	Clustered regularly interspaced short palindromic repeats
CTD	Carboxy-terminal domain
DFC	Dense Fibrillar Component
DNA	Deoxyribonuceic Acid
dsDNA	double strand DNA
ER	Endoplasmic reticulum
ES	Expansion Segment
ES cells	Embryonic stem cells
ETP	Enhancers of Trithorax and Polycomb
ETS	Externally Transcribed Sequence
FA	Fluctuating asymmetry
FC	Fibrillar Centre
FRET	Fluorescence resonnance energy transfer
GAC	GTPase Activating Centre
GC	Granular Component
GDP	Guanosine Diphosphate
GO	Gene Ontology
GSC	Germinal stem cells
GTP	Guanosine Triphosphate
HDR	Homologous directed repair
HIF	Hypoxia-inducible factor
HRMA	High Resolution Melting Analysis
IDR	Irreproducible Discovery Rate
IF	Initiation Factor
IPC	Insulin-producing cell
IRES	Internal Ribosome Entry Site
ITS	Internaly Transcribed Sequence
LB	Luria broth
LNA	Locked Nucleic Acid
lncRNA	long non coding RNA
LSU	Large Sub-Unit
MAPK	Mitogen-actvated protein kinase
miRNA	micro RNA
MMR	methyl-directed mismatch repair
MPF	Mitosis promoting factor

mRNA	messenger RNA
NAC	Nascent chain-associated complex
NHEJ	Non-homologous end joining
NLS	Nuclear localisation signal
NMD	Nonsense Mediated Decay
NoDS	Nucleolar detention signal
NoLS	Nucleolar localisation signal
NTD	amino-terminal domain
ORF	Open Reading Frame
OTE	Off-target effect
PABP	Poly(A)-Binding Protein
PAM	Protospacer Adjacent Motif
PcG	Polycomb group
PCR	Polymerase chain reaction
PIC	Pre-Initiation Complex
PNB	Pre-nucleolar bodies
PRC1	Polycomb repressive complex 1
PRC2	Polycomb repressive complex 2
PR-DUB	Polycomb repressive deubiquitinase complex
PTC	Peptidyl Transferase Centre
PTM	Post-translational modification
PTTH	prothoracicotropic hormone
qPCR	quantitative PCR
RAP	Ribosome Associated Proteins
RBP	RNA binding proteins
rDNA	ribosomal DNA
RER	Rough endoplasmic reticulum
RISC	RNA-induced Silencing Complex
RNA	Ribonucleic Acid
RNAi	RNA interference
RNAPolI	RNA Polymerase I
RNAPolII	RNA Polymerase II
RNAPolIII	RNA Polymerase III
RNP	Ribonucleoparticle
RPG	Ribosomal protein gene
r-protein	ribosomal protein
rRNA	ribosomal RNA
RT-qPCR	Reverse transcription quantitative PCR
SDS	sodium dodecyl sulfate
SDS-PAGE	sodium dodecyl sulfate polyacrylamide gel electrophoresis
sgRNA	single guide RNA
snoRNA	small nucleolar RNA
snoRNP	Small nucleolar ribonucleoparticle
SOP	Sensory organ precursor
SRP	Signal recognition particle
ssDNA	single strand DNA
ssODN	single strand oligodeoxynucleotide
SSU	Small Sub-Unit
TAF	TBP-Associated Factor
TBP	TATA-Binding Protein
TC	Ternary Complex

TES	Transcription End Site
TMAC	tetramethylammonium chloride
TOP	5' terminal oligopyrimidine
tracrRNA	trans-activating CRISPR RNA
tRNA	transfer RNA
trxG	trithorax group
TSS	Transcription Start Site
UBF	Upstream Binding Factor
uORF	upstream Open Reading Frame
UPR	Unfolded protein response
UTR	Untranslated region
VR	Variable Region

Introduction

The notion of homeostasis can be traced back to the work of Claude Bernard in sugar metabolism and thermoregulation. Indeed, he proposed that “all the vital mechanisms, varied as they are, have only one object, that of preserving constant the conditions of life in the internal environment”. Specifically, he enunciated that “far from […] being indifferent to their surroundings, they are on the contrary in close and intimate relation to them, so that their equilibrium is the result of compensation established as continually and as exactly as if by a very sensitive balance.” The term homeostasis was first used by Walter B. Cannon: “The coordinated physiological reactions which maintain most of the steady states in the body are so complex, and are so peculiar to the living organism, that [I have] suggested … that a specific designation for these states be employed — *homeostasis*” (For review: Cooper, 2008 and references therein).

Homeostasis was thus defined as a dynamic equilibrium at the level of an organism. However, it can also be envisioned at smaller scales. For instance, a cell also maintains an equilibrium state within its boundaries, which is commonly referred to as “cell homeostasis”. By extension, the notion of homeostasis is often applied to the scale of a metabolic process like ribosome biogenesis. The latter however derogates from the notion of a homeostatic system because it does not maintain a constant equilibrium. Indeed, its intensity is modulated in response to a number of cues, which allows cells to adapt to stressful environments or lack of energetic resources. In this aspect, ribosome biogenesis is an important component of cell homeostasis, at extensive interplay with other cellular processes.

Yet, the idea that ribosome biogenesis would be homeostatic remains a very useful working hypothesis. Indeed, while its intensity is highly modulable, the relative abundance of its components is retained at all times, through the action of a myriad of feedback mechanisms. Thus, it can be approximated to a homeostatic system with externally modulable equilibrium. Under this hypothesis, a perturbation of any component of ribosome biogenesis would echo onto the whole system, and experimental data are generally consistent with that idea. To further the analogy with a homeostatic system, ribosome biogenesis also displays the ability to modify the external environment, *i.e.* the cell. Indeed, a surge of observations described ribosome biogenesis components regulating cell metabolism.

The extra-ribosomal functions of ribosomal proteins may couple ribosome biogenesis and cell homeostasis. Indeed, they have been shown to carry feedback mechanisms towards ribosome biogenesis components, but also to regulate other cell processes. The loss of such coupling may lead to dramatic consequences, as underlined by the paradoxical statement that both an increase or decrease of ribosome biogenesis intensity may drive tumorigenesis (Barna et al., 2008; Cai et al., 2015). In this context, it is likely that the study of extra-ribosomal functions will yield important discoveries regarding the ability of cells to monitor and regulate their ribosome synthesis activity. These could have implications in growth metabolism, development and cancer biology.

The interaction between ribosomal protein uL11 and epigenetic factor Corto, which I have been working on, can be seen as a bridge between two worlds: ribosome biology and epigenetics. My team has been thoroughly investigating the functions of Corto, and its partners in transcription and epigenetics. However, the ribosomal side of this project was yet mostly unexplored. Thus, I felt that introducing this work through its context in ribosome biology would bring reflection material to understand the extra-ribosomal function of uL11. In this manuscript, I tried to first give an overview of ribosomal function and biogenesis, then to summarize their interplay with cell metabolism from the most general to the most specific features.

I. The ribosome

The ribosome was observed as early as the mid-50s as an electron-dense particle abundantly present in the cytoplasm. It was soon established that it possessed a polymerase activity, assembling proteins of any sequence. However, precise insight about its inner working remained elusive due to the lack of atomic-resolution structural data. The first crystal structures published in 2000 (Ban et al., 2000; Wimberly et al., 2000), which won the 2009 chemistry Nobel prize, started a new era in ribosome research.

The recent surge of data on ribosome structure has brought valuable insight in the mechanism of translation and the precise role of the different ribosome components. In the following chapter, I will first describe ribosome composition and the mechanism of translation. I will then describe the process by which ribosomes are assembled, termed « Ribosome biogenesis ».

A. Ribosome and translation

The translating ribosome is a complex particle made of two distinct subunits. Both contain ribosomal proteins (r-proteins) assembled onto ribosomal RNA (rRNA). The large and small sub-units (LSU and SSU) display a similar organization between all three domains of life. Nevertheless, archaeal and eukaryotic ribosomes are bigger and contain specific additions as compared to the bacterial ribosome, suggesting additional complexity in the mechanism of translation. For clarity purpose, this thesis will focus on the eukaryotic ribosome, unless explicitly specified. Additionally, r-proteins will be named following the recently proposed nomenclature (Ban et al., 2014). A conversion table for r-protein names can be found in appendix (Tables S1 and S2). It should also be noted that the previous yeast nomenclature was proposed in 1998 (Planta and Mager, 1998). Thus, another table is provided to convert to earlier r-protein names (Table S3).

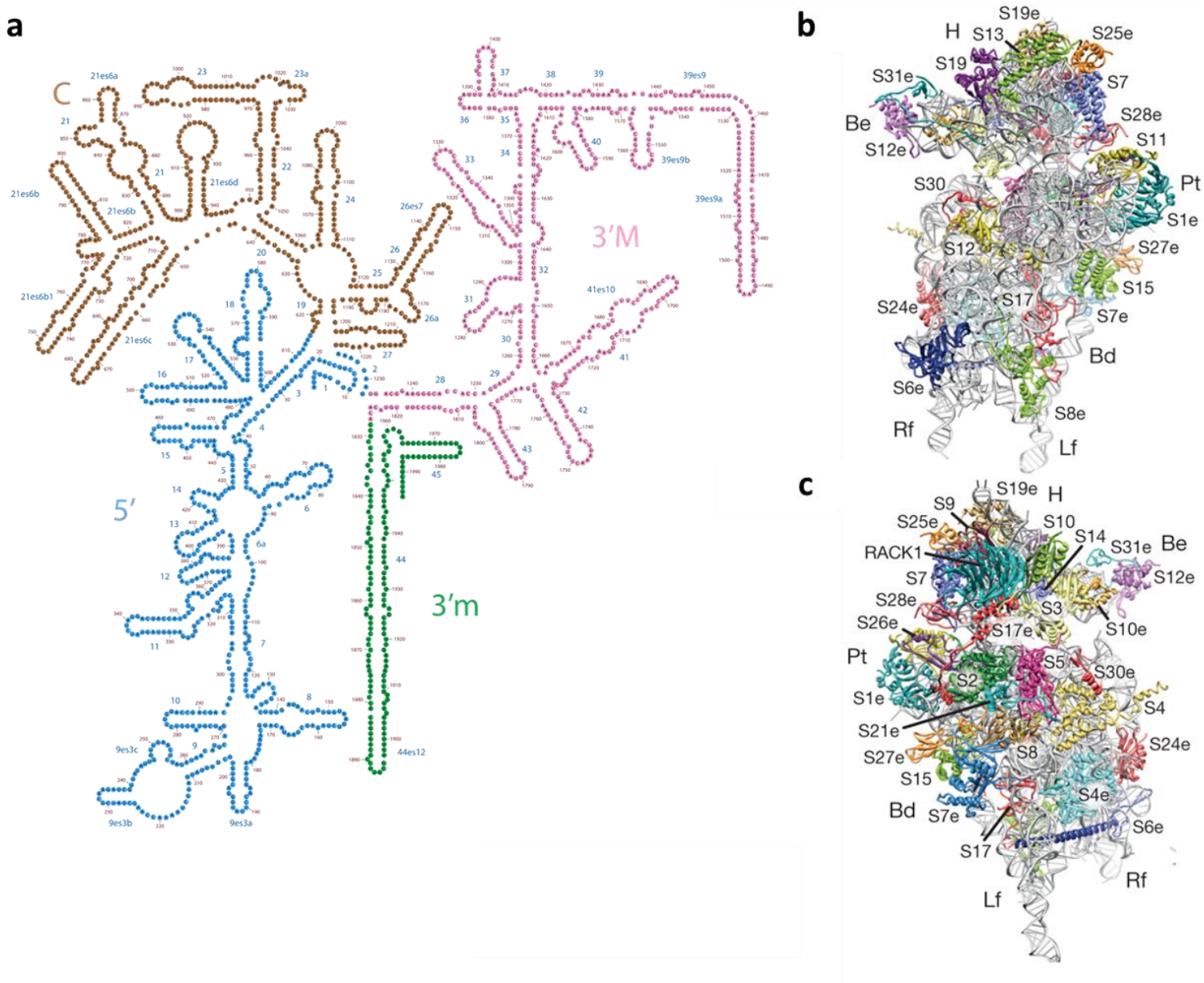

Figure 1. Structure of the 40S subunit of the ribosome.
a, *Secondary structure of the Drosophila melanogaster 18S rRNA (Petrov et al., 2014). Taken from http://apollo.chemistry.gatech.edu/RiboVision.* ***b, c,*** *Interface (b) and solvent (c) view of the human 40S ribosome subunit with rRNA shown in grey and r-proteins coloured. H, head; Bd, body; Pt, platform. Taken from (Anger et al., 2013).*

The core of the 40S subunit of the ribosome is the 18S rRNA. Its secondary structure allows to distinguish four domains, which correspond to the landmarks of the 40S-SSU (**Fig 1**). The 5' and 3' minor (3'm) domains make up the body, while the 3' major (3'M) domain forms the head of the SSU. Meanwhile, the central domain (C) makes up the platform. The organisation of the 18S rRNA is very similar to that of its bacterial counterpart (16S rRNA), with the exception of 5 regions containing additional nucleotides, termed expansion segments (ES), and 5 variable regions (VR). Thirty-three r-proteins can be found assembled on the 18S rRNA, six of which are specific to eukaryotes (For review: Wilson and Cate, 2012).

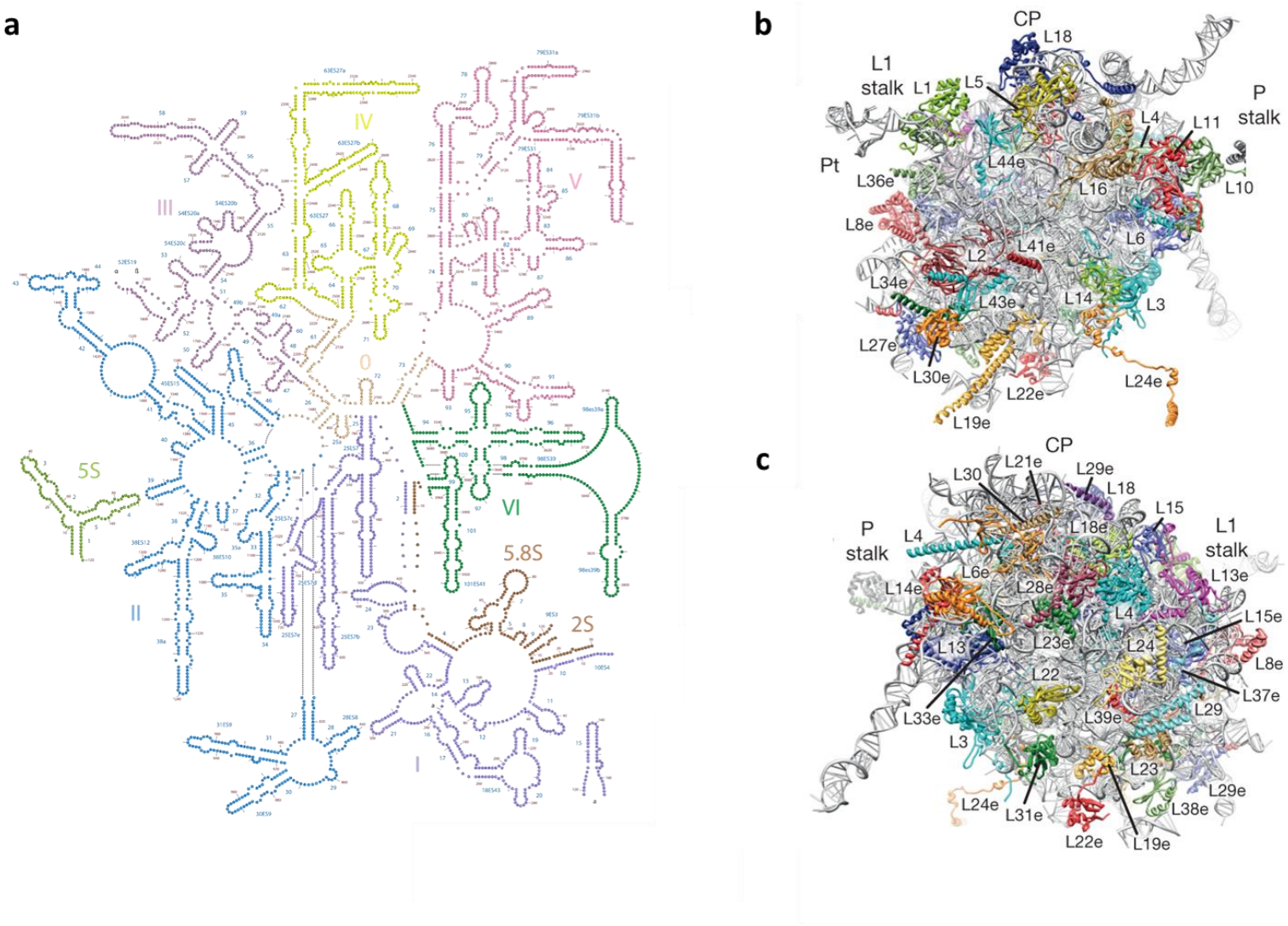

Figure 2. Structure of the 60S subunit of the ribosome

a, *Secondary structure of the Drosophila melanogaster 28S, 5,8S, 5S and 2S rRNA (Petrov et al., 2014). Taken from* http://apollo.chemistry.gatech.edu/RiboVision*.* ***b, c,*** *Interface (b) and solvent (c) view of the human 60S ribosome subunit with rRNA shown in grey and r-proteins coloured. CP, central protuberance. Taken from (Anger et al., 2013).*

The 60S subunit contains three rRNA species in most eukaryotes: 28S, 5.8S and 5S. Together, they organize into domains I to VII, with the 5S rRNA as domain VII (**Fig 2**). Eukaryotic rRNA of the LSU display 16 expansion segments as compared to bacterial counterparts, as well as two variable regions. The 60S subunit harbours 47 r-proteins (46 in yeast), among which 7 are specific to eukaryotes. The LSU displays three structural landmarks in the form of stalks: The P stalk, the L1 stalk and the central protuberance (CP) (**Fig 2**) (For review: Wilson and Cate, 2012). As an exception to eukaryotic LSU organisation, insects display an additional 2S rRNA which is homologous to the 3' end of the 5.8S rRNA in other species (Pavlakis et al., 1979). Insects also display a cleavage of the 28S rRNA in expansion segment 19, separating the 28S rRNA into the 28α and 28β rRNA (Ware et al., 1985).

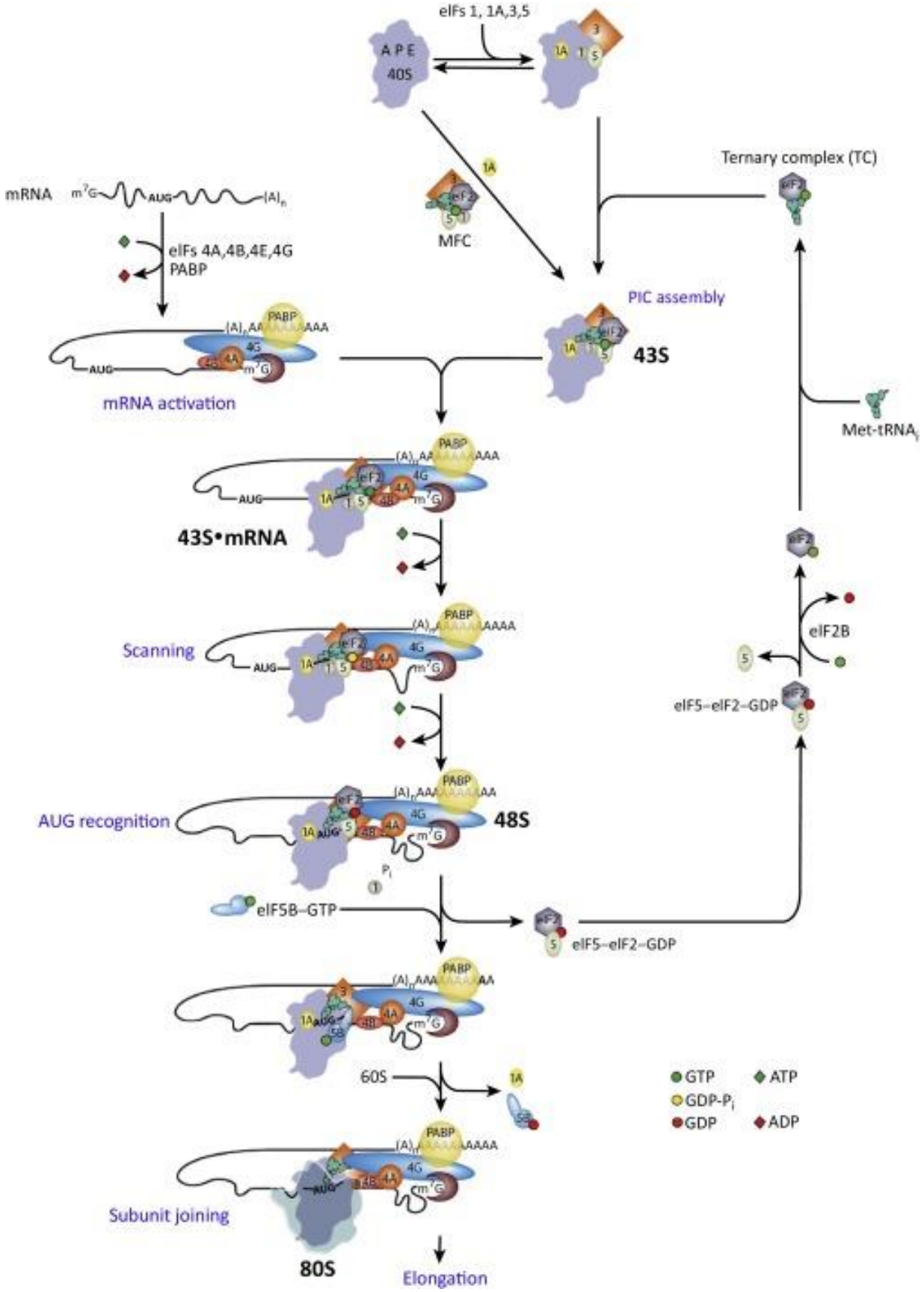

Figure 3. Assembly of the 80S initiation complex and recognition of the initiation codon

Protein synthesis requires that the ribosome assembles onto an mRNA over an AUG codon, a step called translation initiation. The small subunit is first loaded with several initiation factors (IF): eIF1, eIF1A, eIF5 and the eIF3 complex. These factors further promote the binding of the ternary complex (TC) containing the methionyl-tRNA and eIF2 bound to a GTP molecule. This 43S pre-initiation complex (PIC) is then recruited onto mRNAs through the interaction between eIF3 and the eIF4F complex that assembles on the 5'-m^7G cap (For review: Kim, 2017). The eIF4A helicases from the eIF4F complex then unwind RNA secondary structures in an ATP-dependent manner to allow the PIC to scan for a proper AUG initiation codon. Inside the PIC, the methionyl-tRNA is bound with its anticodon close to the peptydil decoding center (P site). Steric clashes with eIF1 prevent it from fully entering the P site. Upon reaching a proper AUG codon, perfect base complementarity relocates it completely into the P site, dislodging eIF1 and causing a shift in the conformation of other eIFs. This results in the 40S subunit taking a closed conformation that stops it from moving further along the mRNA (Hinnebusch, 2017). The conformation shift allows the release of eIF2 and eIF5. The 60S subunit joining is then catalysed by eIF5B in a GTP-dependent manner (Pestova et al., 2000), resulting in the formation of a translation competent 80S initiation complex.

3. Translation elongation

At the end of the initiation stage of translation, the 80S ribosome is assembled on a mRNA with the methionyl-tRNA bound at the P site over the initiation codon, while the acceptor site (A site) is free. Translational elongation is a cycle consisting in delivery of the proper aminoacyl-tRNA to the A site, formation of the peptide bond, translocation of the ribosome and release of the deacylated tRNA (**Fig 4**).

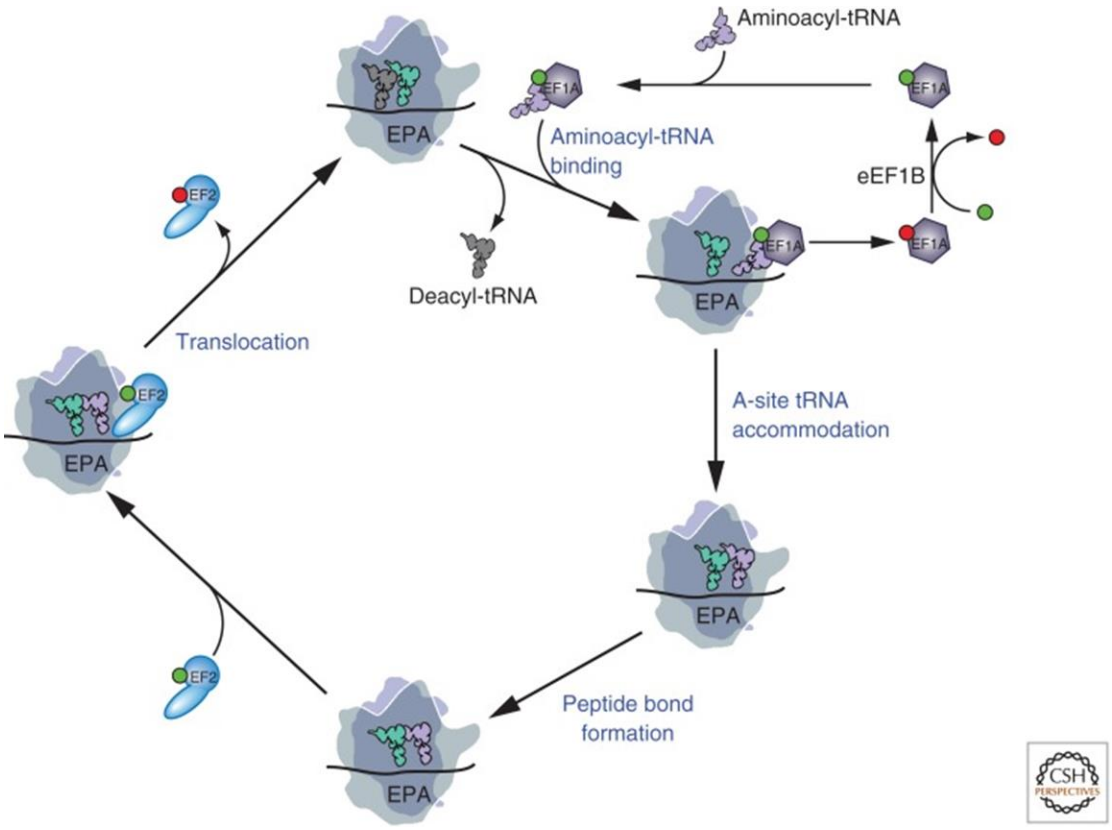

Figure 4. Model of the eukaryotic translation elongation pathway.
In this model, the large ribosomal subunit is drawn transparent to visualize tRNAs, factors, and mRNA binding to the decoding center at the interface between the large and small subunits and tRNAs interacting with the peptidyl transferase center in the large subunit. Throughout, GTP is depicted as a green ball and GDP as a red ball; also, the positions of the mRNA, tRNAs, and factors are drawn for clarity and are not meant to specify their exact places on the ribosome. Taken from (Dever and Green, 2012).

The aminoacyl-tRNA is delivered to the A site as part of a ternary complex with GTP-bound eukaryotic Elongation Factor 1A (eEF1A). The ternary complex is able to sample the codon in the A site, but cannot fit completely inside of it. A perfect match between the A site codon and the tRNA anticodon triggers hydrolysis of the GTP molecule by eEF1A, and their release from the ribosome. The free aminoacyl-tRNA can subsequently fully enter the A site, stabilized by its interaction with the A site codon and the 18S rRNA (Dever and Green, 2012).

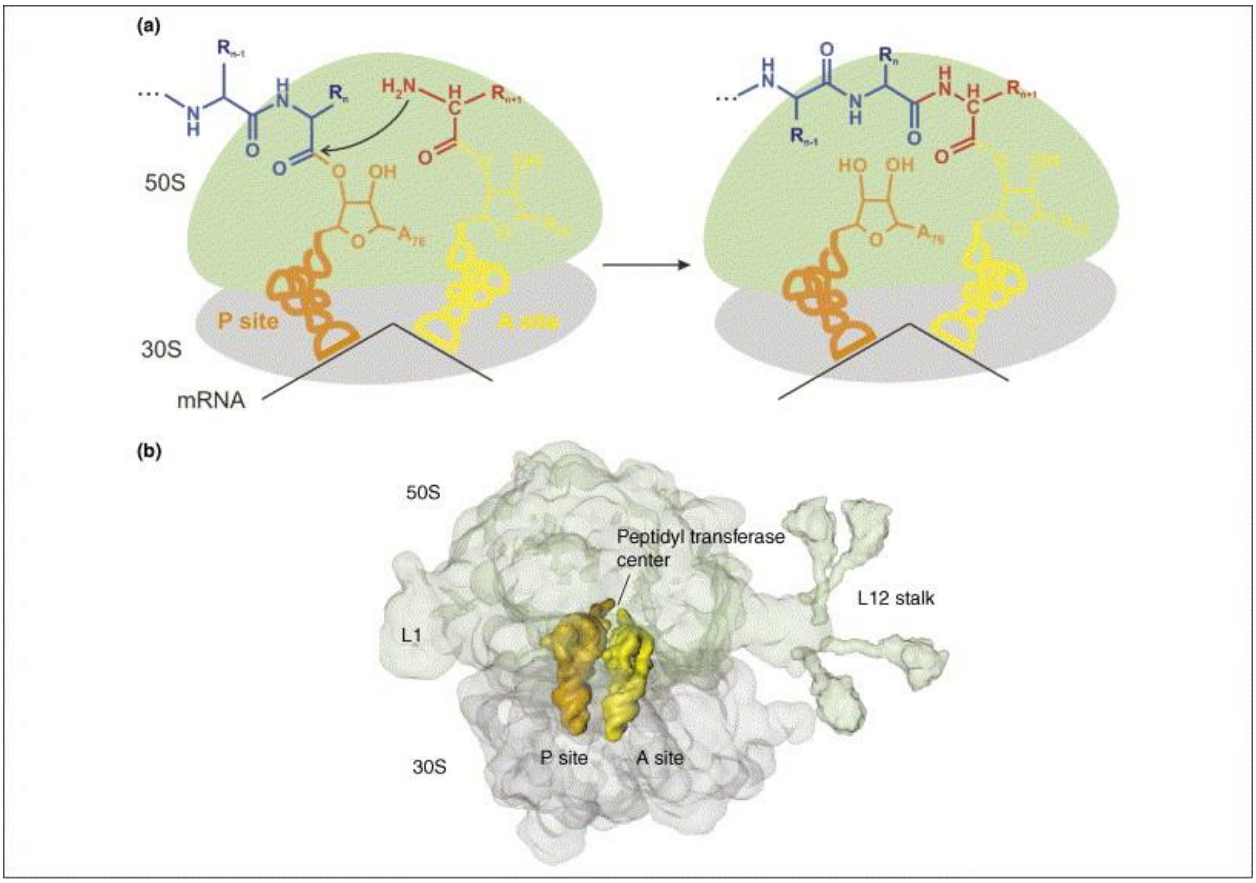

Figure 5. Peptide bond formation on the ribosome.
(a) Reaction scheme. The α-amino group of aminoacyl-tRNA in the A site (yellow) attacks the carbonyl carbon of the peptidyl-tRNA in the P site (orange). (b) Structure of the prokaryotic ribosome with bound tRNAS. Taken from (Rodnina et al., 2007).

While bound to the A and P sites, tRNAs point their 3' end towards a cleft in interface side of the large subunit, the so-called Peptidyl transferase centre (PTC). Interactions between the 28S rRNA and the universal 3' end of the tRNAs positions the aminoacyl close to the peptidyl chain. This allows the peptide bond formation through a nucleophilic attack of the amine function of the aminoacyl on the ester carbonyl group of the peptidyl-tRNA (**Fig 5**, Rodnina et al., 2007). The structure of the PTC is considered superimposable between eukaryotic and prokaryotic ribosomes, suggesting that the mechanism of peptide-bond formation is conserved in both kingdoms of life (Klinge et al., 2011).

Following the peptide bond formation, the tRNA takes a hybrid conformation where their 3' end shift to the E and P sites while their anticodon stem loop (ASL) are still in the A and P sites. Binding of GTP-bound eukaryotic Elongation Factor 2 (eEF2) stabilizes this conformation, and causes a 6° rotation of the SSU in regard to the LSU. This rotation causes a displacement of the ASL of both tRNAs towards the E and P sites. Subsequent GTP hydrolysis causes a conformational change in eEF2, allowing it to enter the A site and sever the connection between the A site tRNA and the decoding center. This triggers a conformational change in the SSU that completes the translocation of the ASL of both tRNA to the E and P sites. eEF2 is then released from the ribosome, allowing the SSU to rotate back to its initial conformation (Taylor et al., 2007). The E site tRNA then dissociates from the ribosome either spontaneously or under an allosteric effect of the binding of the next tRNA at the A site (Chen et al., 2011).

Interestingly, fungi have a unique requirement among eukaryotes for a third elongation factor: eEF3. This stabilizes the L1 stalk in an open conformation that facilitates the release of the deacylated tRNA from the E site (Andersen et al., 2006). Interestingly, eEF3 carries a chromodomain suspected to interact with uL5, uS13, eS25 and the 5S rRNA. Although this domain is not required for eEF3 to bind the ribosome, it is necessary for its ATPase activity. It is thought that the binding of the chromodomain to the ribosome triggers an allosteric effect that enhances ATP hydrolysis rates (Sasikumar and Kinzy, 2014).

4. Translation termination

Translation termination occurs when the ribosome stumbles upon a UGA, UAG or UAA codon in the A site. STOP codons are decoded in a similar way as others, albeit with a tRNA-shaped protein instead. Indeed, eukaryotic Release Factor 1 (eRF1) exists as a ternary complex with eRF3 and a GTP molecule off the ribosome. Its N-terminal domain is able to sample the codon in the A site, and the presence of any STOP codon allows it to bind the ribosome. Subsequent interaction between eRF3 and the PABP bound at the poly(A) site of the mRNA stimulates GTP hydrolysis (Uchida et al., 2002), resulting in the release of eRF3 and GDP from the ribosome. This reaction also leads to the positioning of the middle domain of eRF1 into the PTC, where it triggers hydrolysis of the peptidyl-tRNA bond (Salas-Marco and Bedwell, 2004).

B. Ribosome biogenesis

Ribosome biogenesis is the process that leads to the assembly of translationally competent ribosomes. It is considered the most energy demanding mechanism in cell metabolism, accounting for more than half of a cell's whole energy (Moss and Stefanovsky, 2002). Ribosome biogenesis starts in a dedicated organelle: the nucleolus, where ribosomal components accumulate. From the transcription of ribosomal RNA to the assembly of the last ribosomal proteins on the 80S ribosome, a plethora of maturation and assembly steps is required. These occur sequentially during the entire journey from the nucleolus fibrillar centre to the cytoplasm. In this part, I will provide an overview of the mechanical steps that are required to produce ribosomes and translation factors. As there are differences in nomenclature for ribosomal components and assembly factors, I will use mammalian nomenclature for clarity purpose, unless explicitly specified.

1. Ribosomal RNA transcription

rRNA account for more than 80 % of the RNA content in proliferating cells. Accordingly, rRNA gene organization and transcription display many unique features that allow for such intense activity.

Expression of the 47S rRNA

The 28S, 18S and 5.8S rRNA are transcribed from hundreds of clustered gene copies, mostly organized in tandem arrays. Within the cluster, each repetition contains one copy of each gene. The number of units as well as the number of rDNA loci varies within species and individuals. For instance, human cells carry approximately 400 repeats, while yeast only contain around 150 (Birch and Zomerdijk, 2008;

Nomura et al., 2013). Their transcription is responsible for the formation of a specialized organelle: the nucleolus (Mélèse and Xue, 1995). Consequently, these rDNA cluster regions are termed Nucleolar Organizer Regions (NOR).

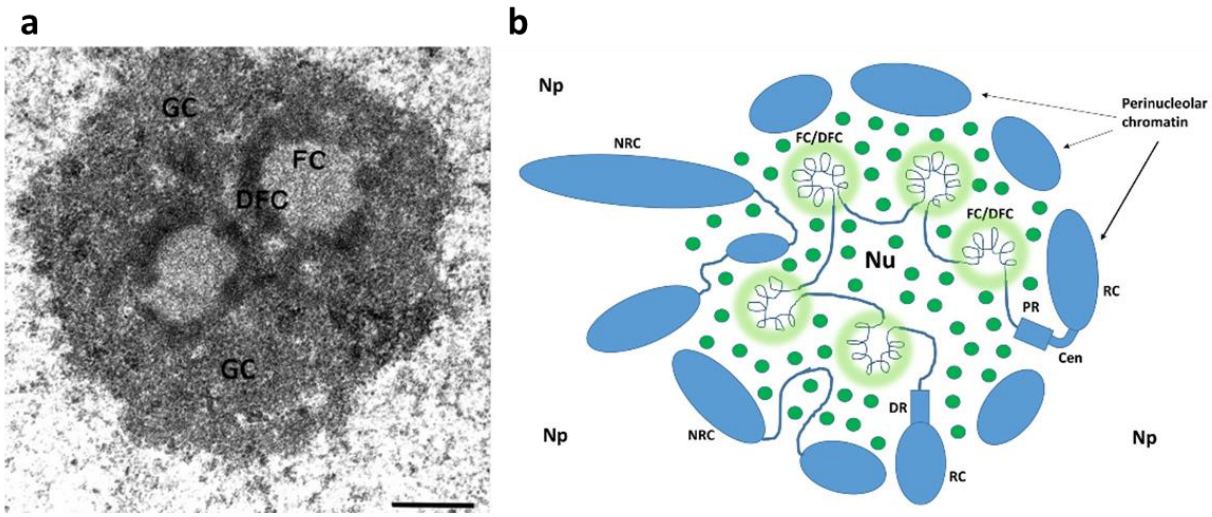

Figure 6. Organization of the nucleolus.
(a) Electron micrograph of a nucleolus in HeLa Cells. (b) Schematic representation of nucleolus-associated DNA. FC, Fibrillar Center; DFC, Dense Fibrillar Component; GC, Granular component; Nu, nucleolus; RC, ribosomal chromosome; NRC, non-ribosomal chromosome. Adapted from (Sirri et al., 2002; Smirnov et al., 2016)

Among the rRNA genes, only a subset is actively transcribed. The proportion of active *versus* inactive repeats may vary between species (Madalena et al., 2012) and cell types (Sanij et al., 2008). Inactive repeats display heterochromatin characteristics with methylated DNA, high histone compaction and repressive histone marks (methylation of Histone 3 lysines 9 and 27, and histone 4 lysine 20) (Németh and Längst, 2011). On the contrary, active rDNA repeats are characterized by acetylated histones, hypo-methylated DNA, and an open chromatin state. The latter correlates with an enrichment in the Upstream Binding Factor protein (UBF), which participates in the maintenance of eukaryotic rDNA by displacing repressive histone H1 (Németh and Längst, 2011). Active rDNA repeats form a sub-compartment of the nucleolus: the Fibrillar Center (FC), a region characterized by low density in electron microscopy (**Fig. 6a**). Interestingly, electron microscopy studies showed that the transcription of active rDNA repeats occurs in the neighbouring compartment: the Dense Fibrillar Component (DFC), or at the border between the FC and the DFC (Koberna et al., 2002). Meanwhile, chromatin capture analysis showed that the promoter and terminator region of active rDNA contact each other, and several other loci in the rDNA repeat. Thus a “core-helix” model has been proposed where the rDNA unit forms loops at the FC/DFC interface, anchored in the FC by its joined promoter and terminator (**Fig 6b**, Denissov et al., 2011).

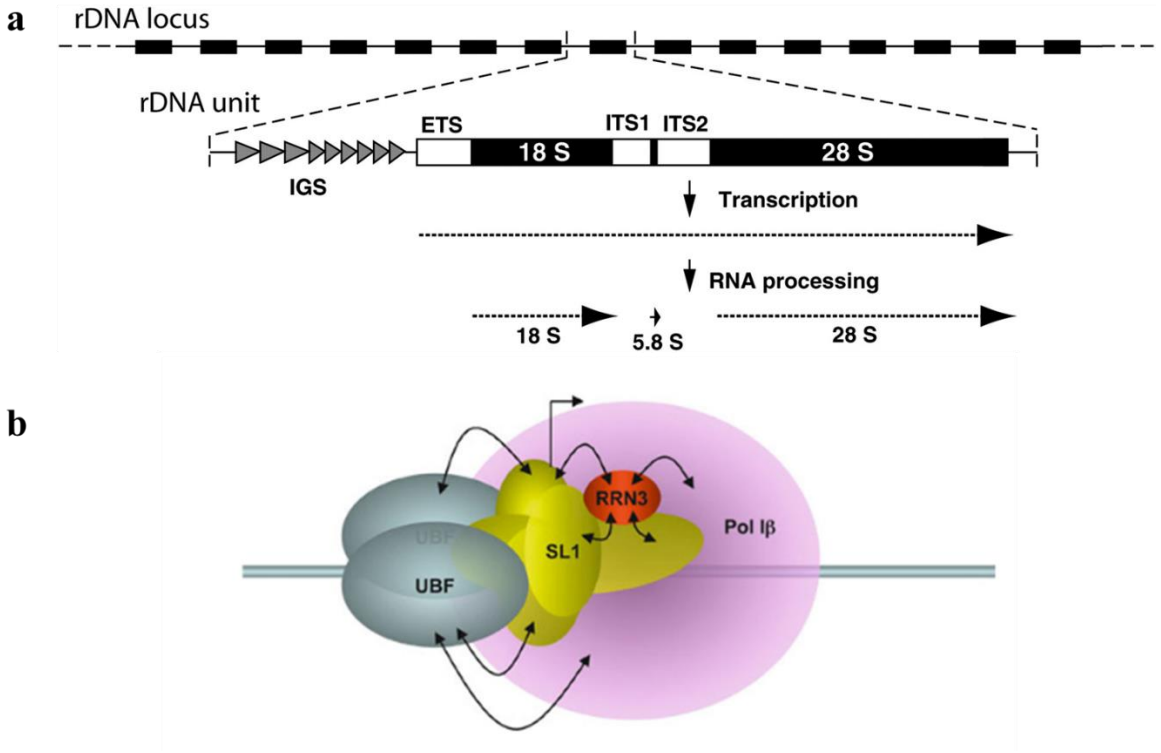

Figure 7. Transcription of the rRNA genes.
(a) Organization of the rRNA genes in eukaryotes. IGS, InterGenic Spacer; ETS, Externally Transcribed Sequence; ITS, Internally Transcribed Sequence. Taken from (Eickbush and Eickbush, 2007). (b) Schematic of the mammalian PolI pre-initiation complex. Taken from (Goodfellow and Zomerdijk, 2012).

The organization of rDNA repeats is conserved among eukaryotes. A single transcription unit contains the genes for the 28S, 18S and 5.8S rRNA; and gives rise a pre-rRNA whose size varies greatly within species (13kb in mammals *vs* 6.9 in yeast). The rRNA genes are separated by an Intergenic Spacer (IGS) that contains many regulatory elements including a core promoter, repetitive enhancers and a terminator (**Fig. 7a**). RNA polymerase I (RNAPolI) is dedicated to the transcription of this locus, and it relies on the assembly of a specific pre-initiation complex for its recruitment. In mammalians, it is the SL1 complex, made of the TATA-binding Protein (TBP), and several PolI-specific TBP-associated factors (TAF). Among them, TAF_I110, TAF_I63 and TAF_I48 bind DNA directly and are thought to be responsible for the promoter selectivity of SL1 (Beckmann et al., 1995). RNAPolI binds the SL1 complex by interacting with TAFs. Furthermore, SL1 binds UBF and stabilizes its interaction with rDNA at the core promoter, which is required for transcription (Friedrich et al., 2005). After PIC assembly, productive transcription requires that RNAPolI dissociates from the SL1 complex, a process called promoter escape. This step is rate-limiting for *in vitro* transcription suggesting that it is a major target in the regulation of PolI activity (Panov et al., 2001). In mammals, promoter escape requires the release of PolI subunit RRN3, which is triggered by its phosphorylation by Casein Kinase 2 (Bierhoff et al., 2008). The association of UBF within the PIC is also important to facilitate promoter escape though the underlying mechanism is unclear (Panov et al., 2006). The dissociation of RNAPolI leaves SL1 and UBF still assembled on the core promoter, and competent for recruitment of another RNAPolI complex. Additionally, the promoter and terminator regions of active rDNA repeats are juxtaposed, allowing for rapid re-initiation after RNAPolI reaches the terminator. Thus, the looping organization of active rDNA repeats participate in the high efficiency of RNAPolI transcription (Panov et al., 2001).

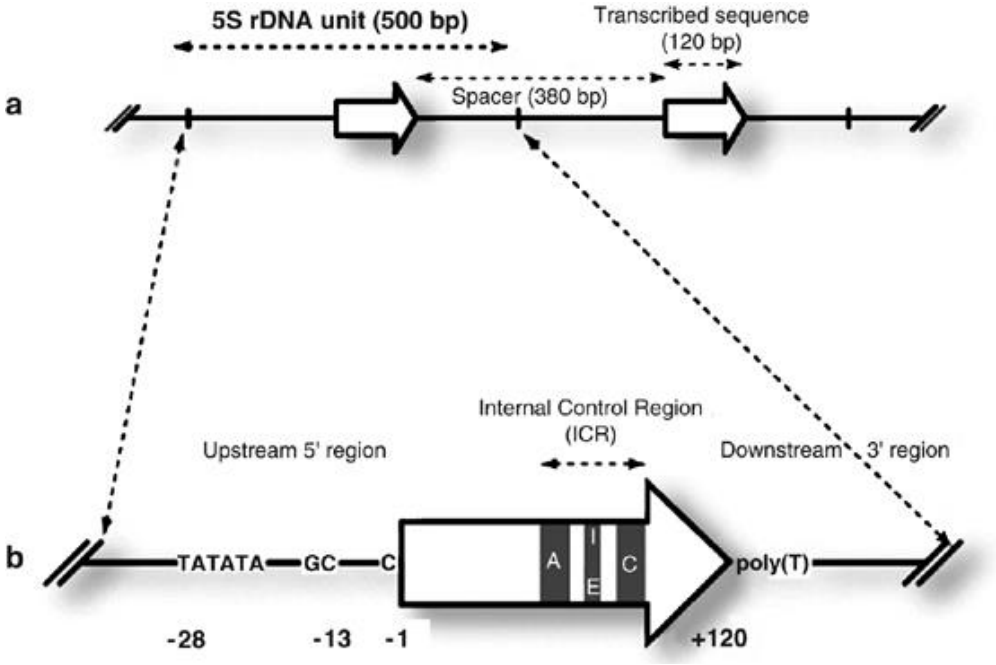

Figure 8. Structure of A. thaliana 5S rDNA units.
*(**a**) Two tandemly organized 5S rDNA units. (**b**) One 5S rDNA unit with the 120 bp-transcribed sequence containing the internal promoter composed of box A (A), intermediate element (IE) and box C (C). The upstream region contains three motifs necessary for transcription at -28, -13 and -1. The downstream region contains the poly-T cluster used as transcription terminator. Taken from (Douet and Tourmente, 2007).*

Similarly to the other rRNA species, the 5S rRNA is encoded by hundreds of clustered gene copies. However the 5S rRNA clusters are separated from NOR loci in most eukaryotes (with *S.cerevisiae* as an exception) and can be found on euchromatic regions. Their length and number vary among species. Their organization is quite similar to the NOR: a short transcribed sequence is separated from other repeats by an intergenic spacer (**Fig. 8a**). As the 47S rRNA cluster, only a subset of 5S rRNA genes are active, with their chromatin state showing high level of histone acetylation (Douet and Tourmente, 2007).

Transcription of the 5S rRNA gene is performed by RNA polymerase III (RNAPolIII), which specializes in short non-coding RNAs. Unlike PolI, its transcription activity does not occur inside the nucleolus. FISH experiments showed that RNAPolIII transcribes the 5S rRNA in a nucleoplasmic foci that tends to localize near the nucleolus in yeast (Haeusler and Engelke, 2006).

As with other polymerases, the recruitment of RNApolIII on target genes is dependent on the assembly of a specific pre-initiation complex. In the case of the 5S rRNA, sequences responsible for recruitment of the PIC are intragenic (**Fig. 8b**). The intragenic promoter contains three conserved elements: box A, box C and an Intermediate element, which are all recognized by the zinc-finger protein TFIIIA (Clemens et al., 1992). The PIC then forms with the sequential binding of TFIIIC and TFIIIB. The latter is a multimeric complex that contains TBP and binds the TATA box upstream of the 5S rRNA gene. Once bound, TFIIIB is able to recruit RNAPolIII and position it over the initiation region (Kassavetis et al., 1990). RNAPolIII is then able to initiate transcription without displaying significant pausing at the promoter (Bhargava and Kassavetis, 1999). It then transcribes the 5S rRNA gene through the binding sites for TFIIIA without dissociating the PIC from chromatin (Bogenhagen et al., 1982). Finally, RNAPolIII is able to recognize the poly(T) sequence autonomously and accurately terminates transcription (Cozzarelli et al., 1983).

2. Ribosomal RNA processing

Transcription of the nucleolar rDNA locus by RNAPolI generates a 47S precursor RNA that will subsequently be cleaved into the mature 28S, 18S and 5.8S rRNA. The processing of ribosomal RNA is a complex cascade of events that requires the activity of many endo- and exonucleases. The different cleavage events follow a precise order, extensively reviewed in Henras et al., 2015 (**Fig. 9**). Importantly, these maturation steps are coupled to rRNA folding and assembly of r-proteins, and occur at all steps of the journey from the nucleolus to the cytoplasm.

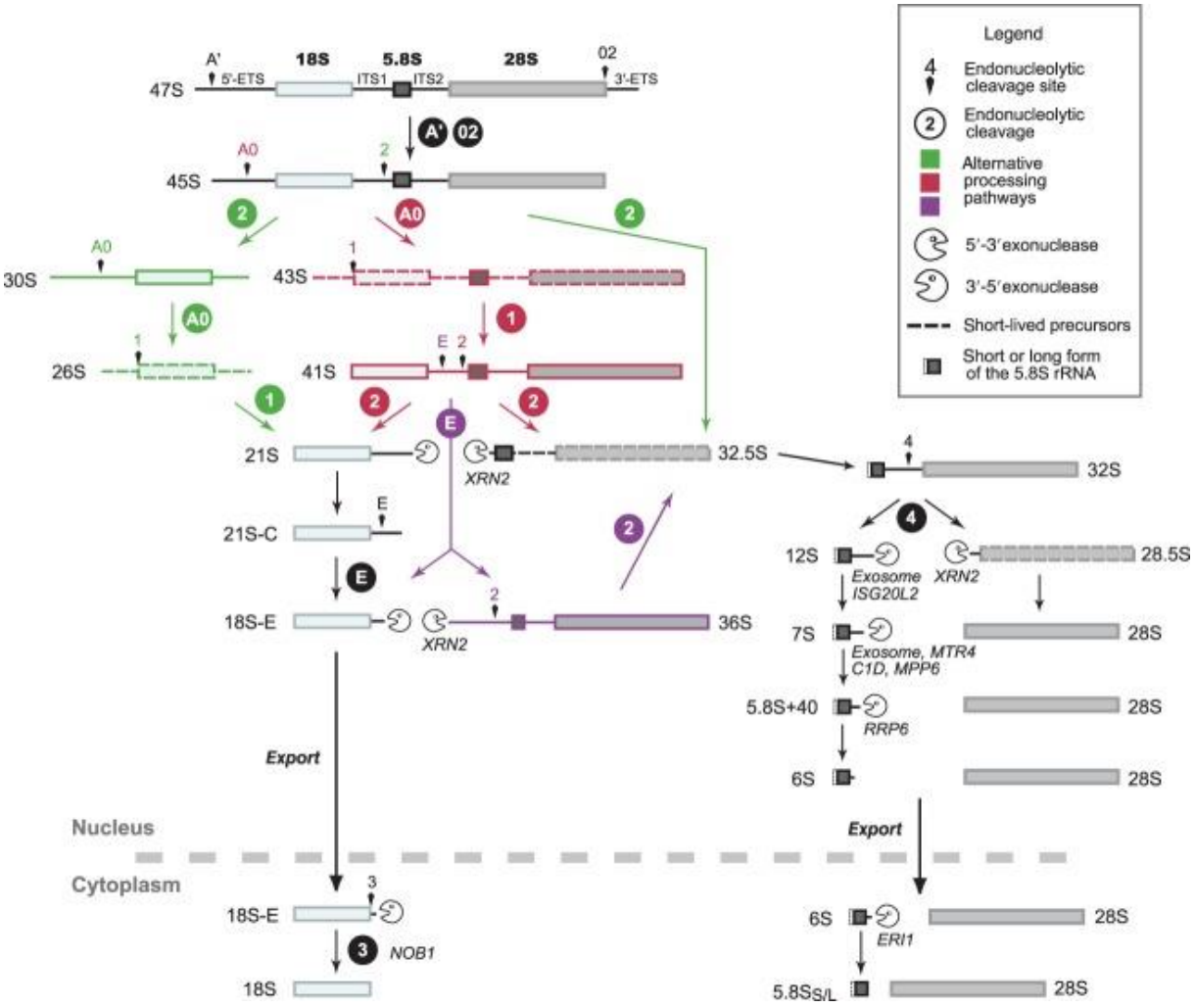

Figure 9. Pre-ribosomal RNA processing in mammalian cells.
Taken from (Henras et al., 2015)

One of the early steps of maturation of the precursor rRNA is an endo-nucleolytic cleavage at site 2 in the ITS1, resulting in the separation of the small subunit pre-rRNA from the large subunit pre-rRNAs. This event occurs quickly after transcription, and even co-transcriptionally in yeast (Kos and Tollervey, 2010). Following this event, the pre-subunits undergo independent processing pathways. The pre-40S is quickly exported to the nucleus where its maturation continues, and then to the cytoplasm where it is achieved. Meanwhile, the pre-60S lingers in the granular component of the nucleolus (**Fig. 6a** and

Hernandez-Verdun et al., 2010). While the 28S rRNA maturation is completed prior to export, the 5.8S undergoes the last steps of its maturation in the cytoplasm.

In contrast to the complex processing of the 47S pre-rRNA, the maturation of the 5S rRNA is very straightforward. It is transcribed with a 7-13nt 3' expansion that is removed by exonucleases Rex1p, Rex2p, and Rex3p in yeast (Hoof et al., 2000).

Importantly, the processing of ribosomal RNA is monitored by the so-called "nucleolar surveillance pathway". Improperly processed rRNA are quickly targeted for degradation, through the addition of a short poly-adenosine tail in 3' by the TRAMP4 and TRAMP5 in yeast, and PAPD5 in mammals (Houseley and Tollervey, 2006; LaCava et al., 2005; Shcherbik et al., 2010). The recognition mechanism for defective rRNA is currently unclear. Interestingly, it has been reported that a delay in processing the 18S pre-rRNA also triggers degradation (Wery et al., 2009), leading to the theory that pre-rRNA routinely carry the ability to be recruited for degradation, which they only escape through timely maturation (Dez et al., 2006). In mammals, rRNA degradation relies on the activity of 5'→3' exonuclease XRN2, which trims the 5' ends of rRNA after each endo-nucleolytic cleavage during normal processing (**Fig. 9**). Therefore, these exonucleolytic steps of rRNA processing could also serve as quality checks targeting pre-rRNA to either continued maturation or degradation (Wang and Pestov, 2011).

Mature ribosomal RNAs are known to be heavily modified: approximately 200 sites have been identified in humans (http://people.biochem.umass.edu/fournierlab/3dmodmap/ and Piekna-Przybylska et al., 2008). Among them, 2'O-methylation of the ribose cycle and isomerisation of uridine to pseudouridine (Ψ) are the most common, being ten times more frequent than base modifications. Importantly, these modifications are distributed in several clusters that correspond to functional sites in the mature ribosome, among which the peptidyltransferase center, and the decoding center (**Fig. 10** and Decatur and Fournier, 2002).

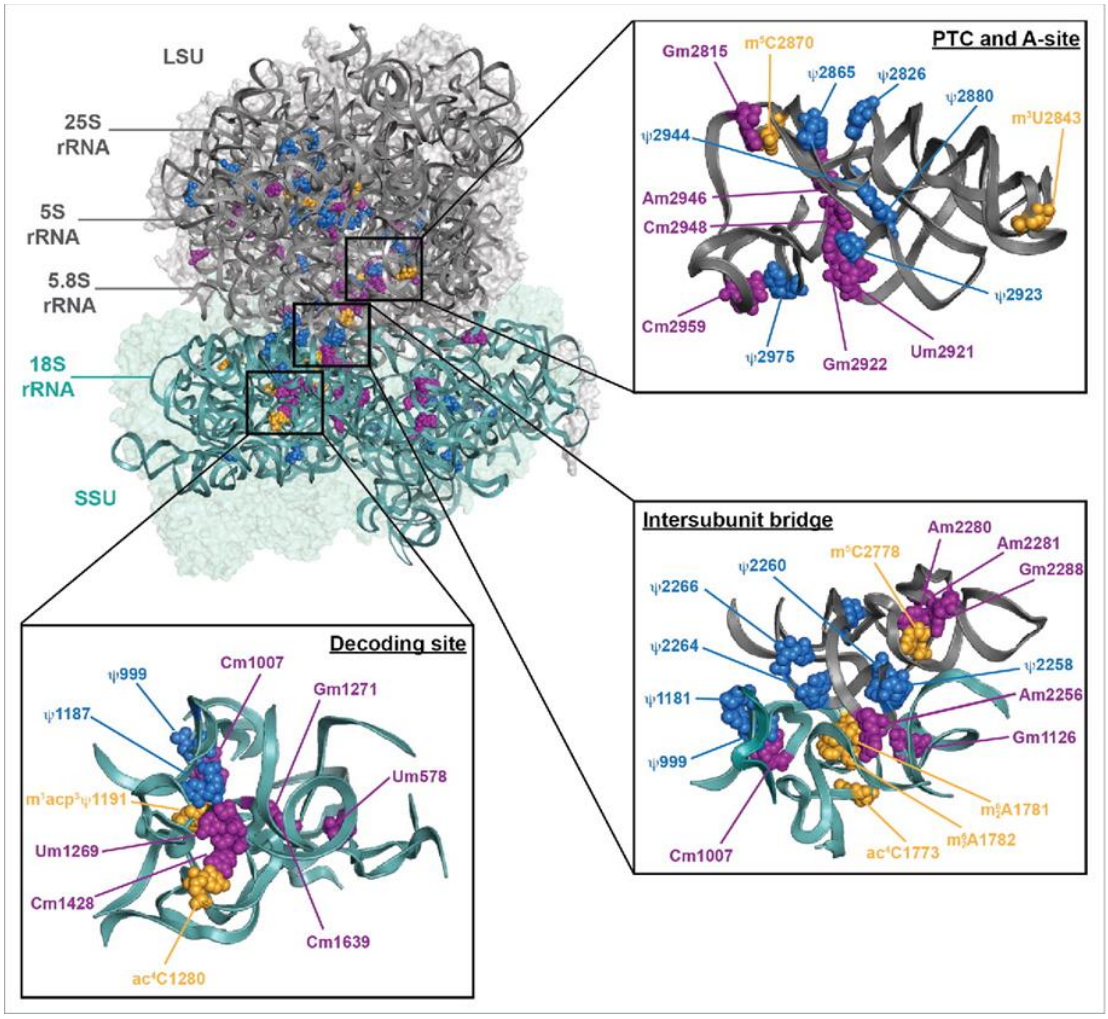

Figure 10. Distribution of rRNA modifications on the yeast ribosome.
The S. cerevisiae 80S ribosome (PBD 4V88)6 is shown – 40S in teal and 60S in gray. The positions of 2'-O-methylations (purple), pseudouridines (blue) and base modification installed by stand-alone enzymes (orange) are indicated. Three functionally important regions of the ribosome, the peptidyltransferase center (PTC), the decoding site and the intersubunit bridge eB14, are also shown in a magnified view. Taken from (Sloan et al., 2016).

While 2'O-methylation and pseudouridylation are crucial for ribosome function (Esguerra et al., 2008; Tollervey et al., 1993), the loss of individual modifications display mostly subtle phenotypes (Esguerra et al., 2008). On the contrary, loss of several modifications in the same functional region of the ribosome often displays severe phenotypes, showing that they do carry functional importance in

ribosome activity (King et al., 2003; Liang et al., 2009). Indeed, these modifications stabilize RNA secondary structures: 2'O-methylations increase base stacking, while pseudouridines establish more hydrogen bonds than their unmodified counterpart (Helm, 2006).

The bulk of these modifications is catalysed by two classes of small nucleolar RNPs. The boxH/ACA snoRNPs complexes contains an eponymous snoRNA, along with the pseudouridine synthetase Dyskerin (Cfb5 in yeast, Lafontaine et al., 1998). In a similar manner, the boxC/D snoRNAs enter a second snoRNP complex that contains the methyltransferase fibrillarin (Nop1 in yeast, Tollervey et al., 1993). In both cases, the snoRNA recognizes a specific site on ribosomal rRNA through base pairing, allowing the enzymatic subunit to catalyse rRNA modification.

There are approximately 700 snoRNA expressed in humans, and most of them belong to the box HA/ACA and box C/D families. A significant proportion possesses more than one target (Jorjani et al., 2016). In yeast, snoRNAs are mostly expressed from independent or polycystronic transcripts by RNAPolII. In contrast, vertebrate snoRNA are mainly processed from the introns of protein-coding genes, most of which participate in ribosome biogenesis (Dieci et al., 2009; Filipowicz et al., 1999). This coupling between snoRNA and coding genes raised the idea that this peculiar organization underlies a coordination between several steps in ribosome biogenesis. Additionally, some snoRNA display strong tissue specificity (Cavaillé et al., 2000). Accordingly, some snoRNA-catalyzed modifications appear to be sub-stoichiometric, suggesting that rRNA modifications could also underlie ribosome heterogeneity (Krogh et al., 2016; Taoka et al., 2016).

4. Ribosomal proteins biogenesis

While rRNA make up the core of the ribosome, both structurally and functionally, r-proteins form its surface layer. In eukaryotes, 80 r-proteins are found in the mature ribosome (79 in yeast). The severe phenotypes associated to their loss of function underscore their importance in the synthesis of functional ribosomes (Marygold et al., 2007; Terzian and Box, 2013). However, their role in translation has mostly been associated to folding and stabilizing the rRNA.

r-protein genes characteristics

	Human	Fly	Worm	Yeast
Gene length (bp)	4316	922	742	764
CDS length (bp)	541	524	520	498
Number of exons	5.3	2.5	3.0	1.6
Exon length (bp)	103	206	172	303
Intron length (bp)	888	258	110	413

Table 1. Ribosomal protein gene features among model organisms
Taken from (Yoshihama et al., 2002)

Ribosomal protein coding genes (*RPG*) are scattered throughout the genome, but they share some characteristic features. *RPG* are small genes with a highly-conserved coding sequence (CDS): their human CDS display 59 % homology with their yeast counterpart, and 69% with *Drosophila's*. They possess short 5' and 3'UTR sequences, and in humans, their initiation codon is always located near the splice site for the first intron, either on the first or second exon. Interestingly, the position of the introns in the CDS is conserved between species: for instance, 80% of *Drosophila RPG* introns are also found in humans. This may be linked with the presence of snoRNA within *RPG* introns (cf. I.A.3.). In humans, their transcription start site (TSS) is always a cytosine located inside an oligopyrimidine tract (5'TOP), and while their promoter is rich in GC, most *RPG* exhibit a TATA box or a TATA-like sequence in 5' (Yoshihama et al., 2002). Another feature of *RPG* in several species is the existence of duplicates, either functional or pseudogenes. The most notorious example is the baker's yeast, *S. cerevisiae*, where an ancient whole genome duplication event gave rise to duplicates. While only 12 % gene pairs conserved a paralog, almost 75 % of *RPG* did (59 out of 79) (Kellis et al., 2004; Planta and Mager, 1998). In contrast, mammalians carry thousands of *RPG* duplications, 99.8% of which stem from retro-transposition events. Interestingly, analysis of their evolutionary trajectory shows that they are under strong purifying selection, particularly when they display transcriptional activity. It is thought that the opposed selection trajectory between yeast and mammalian duplicates is a consequence of the duplication pattern. Indeed, whole genome duplications does not modify the relative stoichiometry within a gene family, while retro-transposition may severely compromise it (Dharia et al., 2014).

r-protein shuttling

Given that r-proteins are translated in the cytoplasm and associate with the pre-ribosome in the nucleolus, they must be imported into the nucleus. Most r-proteins do so through redundant β-karyopherins (Kap123, Kap108, Kap121) from yeast to humans (Jäkel et al., 2002; Rout et al., 1997). Some r-

protein also use specific import pathways: uL5 and uL18 are imported together by the combination of a β-karyopherin and the symportin Syo1 (Kressler et al., 2012). Similarly, uL11 enters the nucleus through importin11, and not by the general mechanism of r-protein import (Plafker and Macara, 2002).

The use of active shuttling pathways may seem intriguing, given that r-proteins are mostly small enough to diffuse passively through the nuclear pore. However, several studies showed that free ribosomal proteins are rapidly ubiquitylated and degraded in the nucleus (Lam et al., 2007; Sung et al., 2016a). Further evidence pointed out that r-proteins can escape this degradation pathway by forming complexes with other proteins, protecting their ubiquitylation sites (Bursać et al., 2012; Kim et al., 2006). The interaction between r-proteins and importins may serve the same purpose. Indeed, several recent studies report that r-protein chaperones bind their substrate co-translationally, and escort them all the way to their assembly site in the ribosome (Pausch et al., 2015; Pillet et al., 2015; Schütz et al., 2014). This precautious importation system is thought to prevent the nuclear accumulation of r-protein, which displays deleterious properties. Indeed, free r-proteins often display large unstructured domains (Gunasekaran et al., 2004; Lupas and Alva, 2017), and their basic expansions can bind nucleic acids unspecifically. The combination of these properties with their massive number allow r-proteins to form aggregates in the presence of polyanions. Their binding by importins have been shown to cover their basic domains and prevent the formation of such aggregates (Jäkel et al., 2002). Thus, the combination of active importation by chaperones and degradation of free supernumerary r-proteins may serve as a safeguard for cell metabolism.

In the absence of r-proteins, the rRNA rapidly folds into secondary and tertiary structures that resemble normal ribosomes. However, they can follow different folding pathways, and more than half fold into kinetically trapped structures *in vitro* (Adilakshmi et al., 2005; Woodson, 2011). r-proteins bind specific rRNA secondary structure, and stabilize them. By assembling at all steps of rRNA folding, they constrain it into following the proper folding pathway. An interesting property of r-protein assembly is their cooperative behaviour: primary binding r-proteins first engage rRNA in a weak association. The conformational changes induced by this interaction allow the binding of secondary r-proteins, which stabilizes the rRNA further, and strengthens the binding of primary r-proteins. Tertiary r-protein can then bind, with the same effect (Ferreira-Cerca et al., 2007; Ohmayer et al., 2013).

Because r-protein induced folding of the rRNA is a necessary prelude to pre-rRNA cleavage, loss of functions of r-proteins often causes the accumulation of pre-ribosomal particles stalled at a certain point of rRNA maturation. It is therefore possible to pinpoint the step at which r-proteins assemble by analysing these kinetically trapped pre-ribosomes.

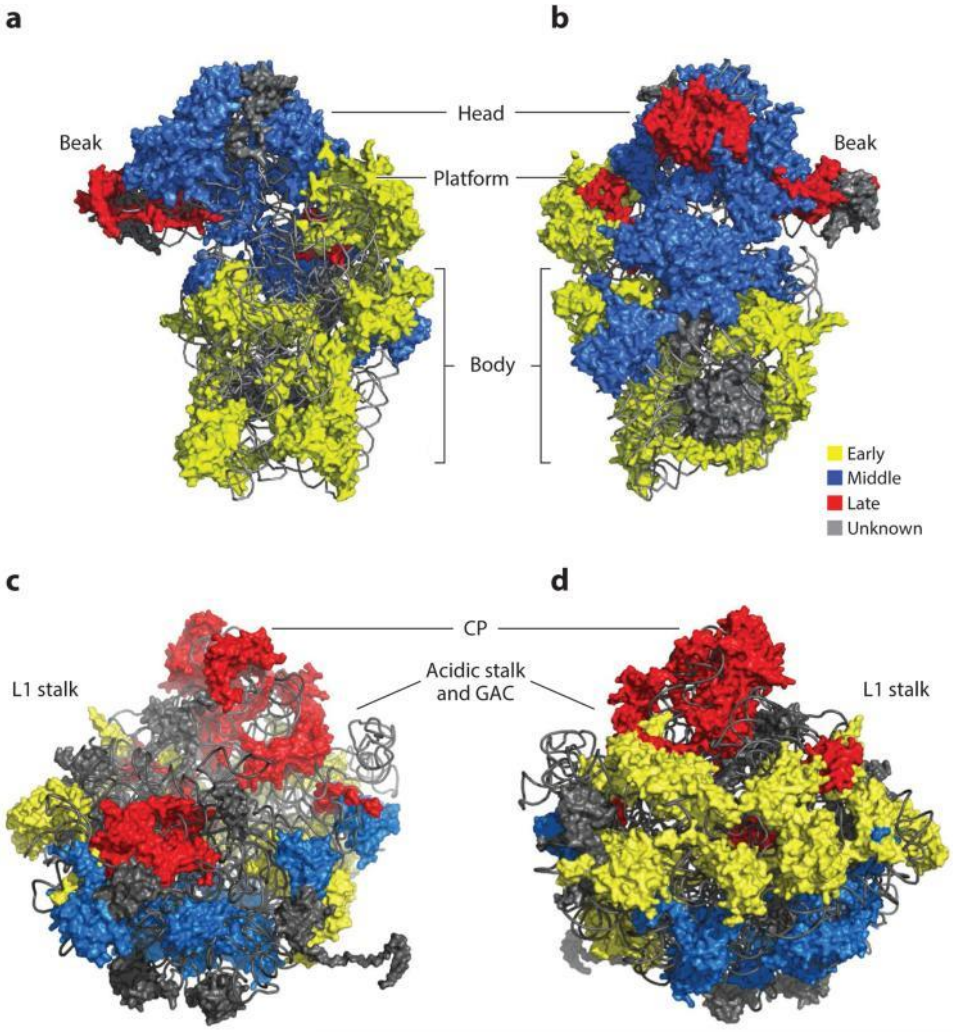

Figure 11. Correlation of function and location of the small subunit and large subunit r-proteins of Saccharomyces cerevisiae

*Early-acting (*yellow*), middle-acting (*blue*), and late-acting (*red*) r-proteins are mapped onto the crystal structure. (*a,c*) The subunit interface of the SSU and LSU, respectively. (*b,d*) The solvent-exposed surface of the SSU and LSU, respectively. Ribosomal RNA (rRNA) and r-proteins are shown in cartoon and surface representation, respectively.*

Abbreviations: CP, central protuberance; GAC, GTPase-activation center. The crystal structure is adapted from Protein Data bank codes 3U5D and 3U5E. Taken from (de la Cruz et al., 2015).

The first r-proteins assemble onto the 5' domain of the pre-18S, and form the body of the small subunit (**Fig. 11a, b**, yellow). Their deficiency blocks the earliest steps of rRNA processing in the 5'ETS (**Fig. 6**). The next group of r-protein bind the head domain of the SSU (**Fig. 11a, b**, blue), and are necessary for the cleavage of the ITS1, which happens very early after transcription in mammals, and co-transcriptionally in yeast (Ferreira-Cerca et al., 2007; Osheim et al., 2004). Those proteins, which make up 70% of the SSU r-proteins, must therefore bind co-transcriptionally in yeast, and at least very early in mammals. The last r-proteins to assemble are not necessary for pre-SSU export, and are therefore thought to participate only to cytoplasmic maturation (**Fig. 11a, b**, red). With the exception of RACK1 (Asc1 in yeast), they localize near the mRNA-binding channel (For review: de la Cruz et al., 2015).

While the 60S subunit seems somewhat monolythic due to its rRNA domains forming intertwined structures, large subunit r-proteins also bind in a hierarchical fashion. The first 12 r-proteins are required before the very first processing steps of the pre-60S rRNA (removal of the ITS1 3' region). They bind mostly to the domains I and II of the 28S rRNA, and are located on the solvent-exposed surface (**Fig 11c, d**, yellow). The next 11 r-proteins are necessary for the cleavage of the ITS2 that separates the pre-5.8S and pre-28S rRNA. They bind the 28S rRNA domains I and III, and the 5.8S rRNA, and clusterize around the polypeptide exit tunnel (PET). An additional set of r-proteins is required for further processing of the pre-5.8S rRNA, and localizes on the interface side of the LSU (**Fig11c, d**, blue). The last group of r-protein to bind the pre-60S subunit assembles either right before export or in the cytoplasm, and clusterize around the central protuberance. Among them, uL5 and uL18 bind the pre-ribosome as a complex with the 5S rRNA, between 28S rRNA domains II and IV (**Fig. 11c, d**, red, for review: de la Cruz et al., 2015).

Ribosomal particles that are exported to the cytoplasm are not competent for translation. Indeed, several pre-ribosomal factors are still bound to pre-subunits, and thus several maturation steps remain. In most cases, these factors are bound at functional sites of the ribosome, and prevent the premature subunits from engaging in translation activity (Strunk et al., 2011). Interestingly, these cytoplasmic events also serve as quality controls, allowing maturation to complete only if the pre-subunit is properly folded.

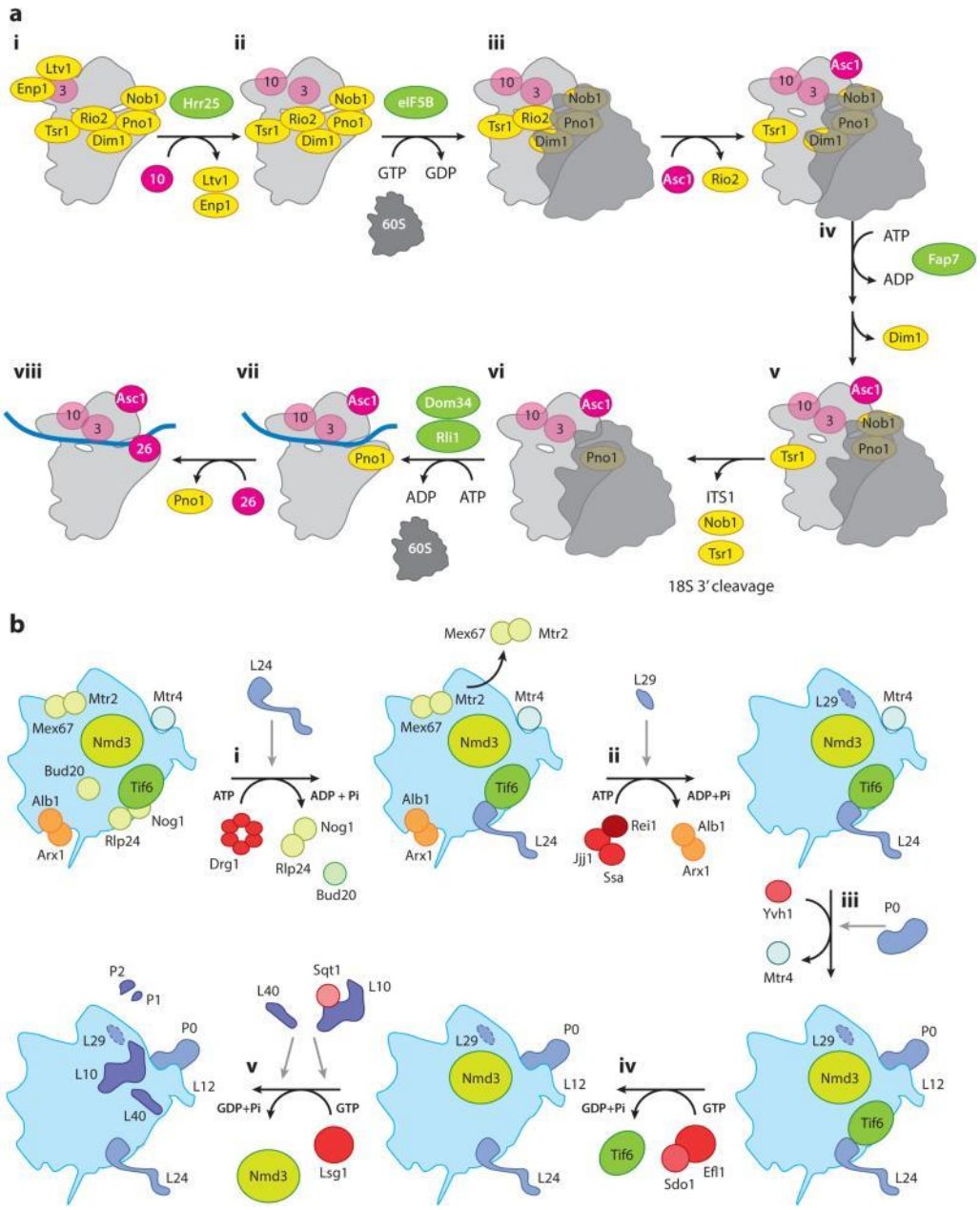

Figure 12. Overview of the ribosome cytoplasmic maturation steps
(a) Cytoplasmic steps of 40S incorporation. (b) Cytoplasmic steps of pre-60S subunit maturation. Taken from (de la Cruz et al., 2015)

On the pre-40S, seven assembly factors are bound on the beak, intersubunit surface, and platform. Notably, Ltv1 and Enp1, bound at the beak, prevent uS3 from taking its final conformation, thus preventing the binding of eS10 (Strunk et al., 2011). Their release is triggered by the phosphorylation of Ltv1 by Hrr25 (Ghalei et al., 2015), and allows the final maturation of the mRNA entry channel. The pre-40S is subsequently bound by eIF5B, promoting the recruitment of a mature 60S subunit. This 80S-like complex is not able to perform translation since assembly factors Rio2 and Tsr1 are blocking the mRNA channel and tRNA binding site (Strunk et al., 2012). It is in that 80S-like particle that the last step of 18S rRNA processing (removal of the ITS1) occurs (García-Gómez et al., 2014), as well as the removal of most remaining assembly factors. Notably, the release of the 60S subunit requires the binding of Rli1 which shares its binding site with Tsr1, and its cofactor Dom34, which binds in the decoding center (Strunk et al., 2012). To sum it up, completion of this translation-like cycle requires that the pre-40S subunit displays the ability to bind and release 60S subunits, and that its decoding center and mRNA channel be properly structured. Hence, this maturation step is considered to work as a final quality control.

Similarly, the pre-60S subunit carries a number of assembly factors in the cytoplasm. Those are located at functional sites: the GTPase activating center (GAC) and the PTC. Cytoplasmic maturation is required to dissociate Tif6 from the pre-60S, which prevents its association with 40S subunits (Si and Maitra, 1999). Assembly factor Rlp24 is first removed and replaced by eL24, which triggers further removal of several AFs (Saveanu et al., 2003). Meanwhile, uL11 recruits Yvh1, which displaces Mrt4, allowing irreversible binding of acidic ribosomal protein P0 at the GAC. P0 then serves as a platform for the binding of P1 and P2 heterodimers that form the acidic stalk (Lo et al., 2009). The assembly of the stalk is required to recruit the GTPase Elf1 (Lo et al., 2010). The integrity of the peptidyl-transferase site is then probed by a flexible extension of uL16, which triggers a conformational change in Elf1, triggering the GTP-dependent release of Tif6 (Bussiere et al., 2012). The 60S subunit can then engage in translation. Interestingly, P0 and the acidic stalk have been shown to be able to assemble in the nucleus in absence of Mrt4 (Francisco-Velilla et al., 2013). Thus, Mrt4 and possibly other factors could function as placeholders, delaying the formation of active structures of the ribosome. For instance, preventing nuclear formation of the stalk bans inappropriate interactions with translation factors before completion of ribosome maturation (Panse and Johnson, 2010).

7. tRNA biogenesis

The activity of the ribosome relies on the unique properties of transfer RNA (tRNA) to polymerize polypeptides. These small RNAs amount for 15 % of all cell RNA, making it the second prominent class, after rRNA. Their biogenesis is very conserved among eukaryotes, and shares some similarities with rRNA biogenesis.

Eukaryotes typically harbour hundreds of tRNA genes (274 in yeast). They are scattered throughout the genome, although they are sometimes found in clusters of variable size. Whereas their sequence is highly conserved, their organization shows considerable variation even between close species (Bermudez-Santana et al., 2010). Actively transcribed tRNA have been shown to cluster together at the nucleolus in yeast (Thompson et al., 2003), but whether this organization is conserved in other eukaryotes is not obvious. For instance RNAPolIII transcription has been described to occur in numerous foci throughout the nucleus in HeLa cells, suggesting some sort of spatial clustering, but not with the nucleolus (Pombo et al., 1999).

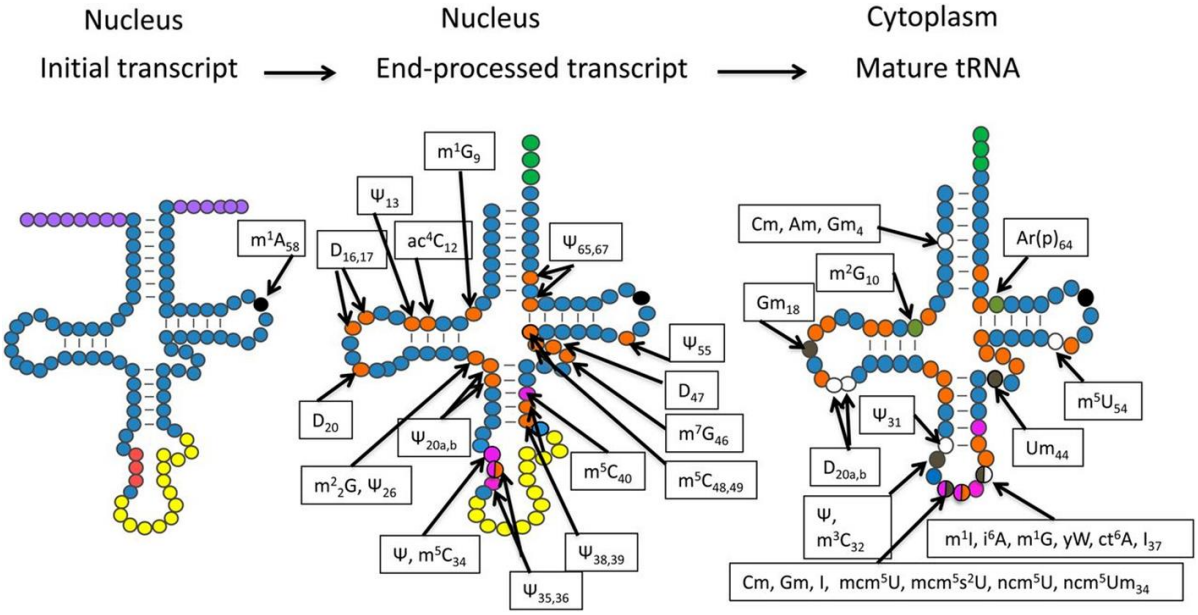

Figure 13. Overview of tRNA processing and modification.
Purple circles indicate the 5' leader and 3' trailer sequences, red ones indicate the anticodon while yellow circles are intronic bases. Solid black circle indicates a modification known to occur on initial pre-tRNAs. Several modifications occur in the nucleus; magenta circles indicate those modifications that require the substrate to contain an intron, whereas orange circles indicate modifications that do not appear to require intron-containing tRNAs as substrate. Numerous other modifications occur in the cytoplasm; those that require that the intron first be spliced are brown, whereas those with no known substrate specificity or are restricted to tRNAs encoded by intronless genes are colored khaki. Open circles are catalyzed by enzymes whose subcellular locations are unknown. Particular nucleosides that can possess numerous different modifications are indicated; half-colored circles indicate that the modifying enzymes have varying substrate specificity and/or subcellular location. Note that modification of G_{37} by Trm5 that requires tRNAs to be spliced occurs in the nucleoplasm after retrograde nuclear import. Taken from (Hopper, 2013).

tRNA genes are transcribed by RNAPolIII. Like 5S RNA genes, they harbour an intragenic promoter responsible for the recruitment of the PIC (Geiduschek and Tocchini-Valentini, 1988). They are transcribed as a long precursor RNA, which contains a 5' leader and 3' trailer sequence. Those are removed by a series of conserved RNAses (for review: Maraia and Lamichhane, 2011). The terminal ends are then processed by RNA polymerases with very peculiar properties. All eukaryotic tRNA require

the post-transcriptional addition of a universal CCA 3' terminus. This is achieved by the tRNA nucleotidyl-transferase, which displays a template-independent polymerase activity (Xiong and Steitz, 2004). Processing of the $tRNA^{His}$ requires the addition of a G in 5' by Thg1, which does so through a 3'→5' polymerisation reaction (Jackman et al., 2012).

A number of tRNA contain an intron that is always positioned one base 3' of the anticodon in eukaryotes (Phizicky and Hopper, 2010). The splicing occurs in the nucleus through a process that bears little resemblance to mRNA splicing. The intron is first spliced out by endonucleolytic cleavages, generating two half tRNAs that are joined by a ligase. A phosphotransferase then removes the extra phosphate produced by the previous reaction (For review : Hopper, 2013).

During their maturation, tRNAs acquire a plethora of modifications, with more than 15 % of their bases being uncanonical (**Fig.13**). Those modifications are located all over the tRNA sequence, with the most variable region being the anticodon, who also carries the most elaborate modifications (a list of modifications and associated enzymes can be found on the Modomics database at http://modomics.genesilico.pl). Their functions range between promoting folding, increasing stability, allowing discrimination by translation factors, or altering the specificity of the anticodon (Anderson et al., 1998; Aström and Byström, 1994). Notably, the deamination of adenosine into inosine (I) at the wobble position (34) allows it to base pair with any A, U or C base on the mRNA (Gerber and Keller, 1999).

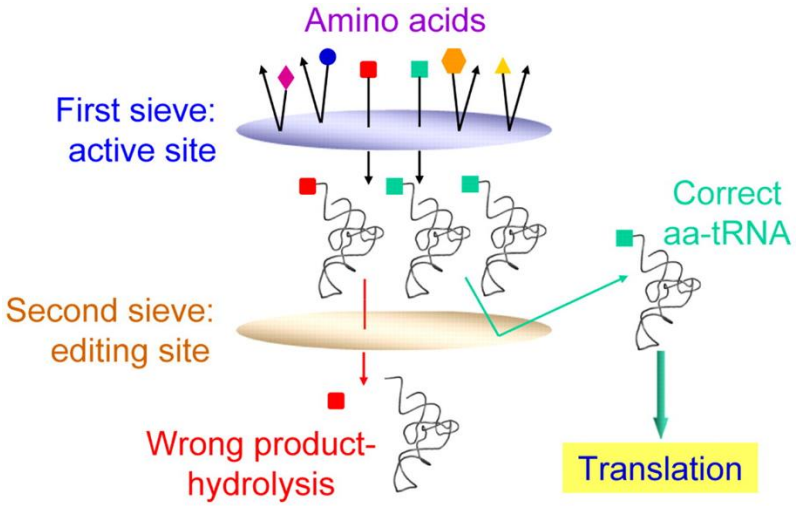

Figure 14. Double-sieve model of editing by aaRSs.
The aaRS aminoacylation active site as the first sieve accepts the cognate (shown in green) and structurally similar near-cognate (i.e., Ser for ThrRS, shown in red) amino acids but rejects the majority of noncognate amino acids. The editing site serves as the second sieve to hydrolyze only the misactivated products (aminoacyl adenylate or aa-tRNA). The correct aa-tRNA is excluded from the editing site and participates in protein synthesis. Taken from (Ling and Söll, 2010).

Mature tRNA must next be charged with the appropriate amino acid before engaging in translation. A set of dedicated enzymes, the aminoacyl-tRNA synthetases (aaRSs) are responsible for this step. Their substrate specificity relies on their ability to probe the tRNA for identity elements, mostly in the 3' acceptor stem - the discriminator base for instance – and the anticodon loop (Breitschopf and Gross, 1994). Because several amino acids are very similar (isoleucine and valine, or glycine and alanine), aaRS are at risk of mischarging tRNA. The frequency of these errors is greatly reduced by the ability of aaRSs to hydrolyse mischarged tRNAs in their editing site (**Fig 14** and Pang et al., 2014).

II. Ribosome biogenesis as a conductor of cell metabolism

Homeostasis has been described as the ensemble of reactions dedicated to keeping biological parameters within a range permissive for survival. As the most energy expensive process in the cell, ribosome biogenesis is at a very strategic place to coordinate cell homeostasis. Indeed, it was found to orchestrate the response to many a cue, being able to adjust cell proliferation tempo, conduct the cell through mitosis, and catch any wrong note in cell metabolism. Accordingly, many processes turn to ribosome biogenesis for directions, thus defining cell fate and organization. The importance of ribosome biogenesis in homeostasis is underscored by the developmental cacophony that follow its impairment in any species.

A. Metabolic cues dictate the activity of ribosome synthesis

Despite its complexity, ribosome biogenesis displays the ability to modulate its activity in a coordinated manner. Even more impressive is the fact that it is reactive to virtually any kind of stress or metabolic event. Indeed, ribosome biogenesis components have been found to be the target of many signalling pathways. Those are intimately intricated, thus providing a regulatory network integrating metabolic cues, and regulating ribosome biogenesis in turn.

In order to maintain their ability to synthetize proteins, cells need to double their number of ribosomes before every division. Indeed, proliferating cells spend most of their energy for ribosome synthesis (Schmidt, 1999). Consistently, increased ribosome production is a feature of fast growing cells, to the point it has become a hallmark of cancer (Drygin et al., 2010). Signalling pathways that induce cell growth and proliferation regulate ribosome biogenesis at many levels, allowing for tight coupling of proliferation and ribosome production. Notably, the Ras-ERK and PI3K-mTor pathways are most remarkable for their ability to induce ribosome synthesis at multiple levels.

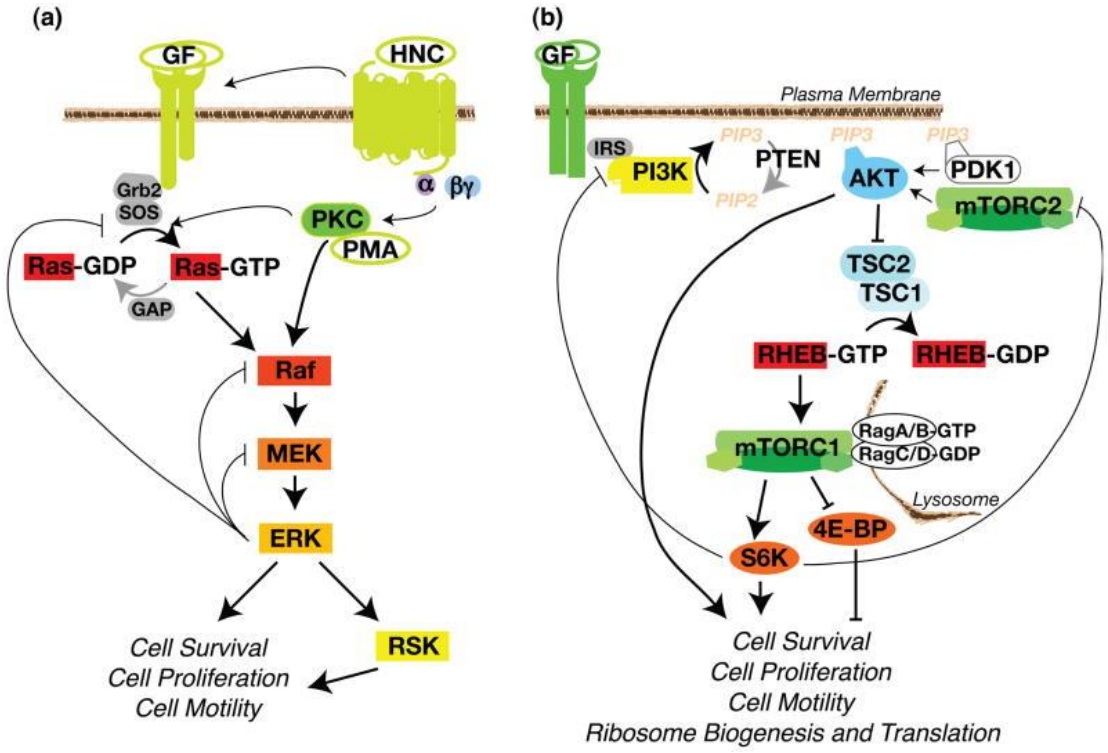

Figure 15. Core components of the Ras-ERK and PI3K-mTor pathways
(a) The Ras-ERK-MAPK Pathway. In quiescent cells, inactive Ras-GDP associates with the plasma membrane and inactive Raf, MEK, and ERK are largely cytoplasmic. GF (growth factor) binding activates RTK auto-phosphorylation, generating binding sites for the SHC and GRB2 adaptor molecules that recruit SOS, the RasGEF (GTPase exchange factor), to the membrane. SOS catalyzes Ras GTP exchange and Ras-GTP then recruits Raf to the membrane, where it gets activated. HNC (polypeptide hormone, neurotransmitter, and chemokine) activation of GPCRs feed into the MAPK cascade by trans-activating upstream RTKs, thereby inducing SOS translocation, and/or Raf activation. Cell-permeable phorbol esters such as PMA directly bind and activate PKC by mimicking the natural PKC ligand diacylglycerol. The mechanism by which PKC activates ERK is not resolved and could be through activation of SOS or Raf. Raf activates MEK and MEK activates ERK via activation loop phosphorylation. ERK also feeds back to negatively regulate the pathway. (b) The PI3K-mTOR Pathway. In quiescent cells, the lipid phosphatase PTEN maintains low levels of PIP3, resulting in AKT inactivation. TSC2, in complex with TSC1, maintains RHEB in the GDP-bound state. Insulin and IGF1 bind their cognate RTKs, and subsequent receptor autophosphorylation creates binding sites that then recruit IRS, an adaptor protein for PI3K. Different RTKs activate PI3K through distinct docking proteins, such as FRS (FGF Receptor Substrate) or GAB (c-Met or EGFR), or via direct binding of PI3K (Platelet-derived Growth Factor Receptor). Activated PI3K phosphorylates PIP2 to generate membrane-bound PIP3. Pleckstrin homology (PH) domains in AKT and PDK1 recognize PIP3 and translocate to the membrane. PDK1 phosphorylates the activation loop and mTORC2 phosphorylates the hydrophobic motif of AKT, thus promoting AKT activation and phosphorylation of TSC2. This TSC2 phosphorylation inhibits TSC2 GAP activity. RHEB-GTP localizes to the lysosome and activates mTORC1 following its recruitment by the Rag GTPases. Taken from (Mendoza et al., 2011).

Cell proliferation signalling pathways can be triggered by a number of external cues including growth factors, hormones and neurotransmitters. Both the Ras-ERK and PI3K-mTor pathways are triggered by the binding of such molecules to a cognate receptor. Subsequent activation of the receptor kinase activity triggers a cascade of events that results in the activation of effector proteins, which has been extensively reviewed in Mendoza et al., 2011 (**Fig. 15**). Importantly, both pathways are largely intricated, with the Ras-ERK pathway able to cross-activate the PI3K-mTor effector complexes. Additionally, their substrates are largely overlapping with the effector kinases S6K, AKT, RSK and PKC displaying very close target specificity.

More unintuitively, both pathways also display the ability to cross-inhibit each other, and this may be necessary to prevent intense pathway activation leading to deleterious consequences and subsequent cell cycle arrest and senescence (Cheung et al., 2008).

Activation of either pathway induces numerous regulatory events, promoting cell survival, proliferation and motility. Strikingly, many of their targets are involved in ribosome synthesis and translation. A most impressive feature of these pathways is their ability to regulate transcription by the three RNA Polymerases, enhancing the synthesis of all ribosome components in a coordinated manner.

Transcription of the rRNA precursor is one of the limiting factors for ribosome synthesis. The activity of RNAPolI requires the assembly of a specific pre-initiation complex containing TIF-1A (RRN3) and UBF (cf. I.B.1). The ability of TIF-1A to associate with SL1 (TIF-1B) and RNAPolI to promote transcription is regulated by multiple phosphorylations. After Ras-ERK pathway activation, the RSK kinases phosphorylates TIF-1A on serine 649, which is required for its transcriptional activity. Serine 633 can be subsequently phosphorylated by ERK, resulting in further increased efficiency (Zhao et al., 2003). Activation of the PI3K-mTor pathway also regulates the phosphorylation pattern of TIF-1A. Its activity requires the phosphorylation of serine 44 which is catalysed by CDK2 and removed by PP2A. PI3K-mTor mediated repression of PP2A is thus necessary to prevent TIF-1A inactivation (Mayer et al., 2004). In addition, UBF activity is also regulated by the PI3K-mTor pathway. Indeed, mTor activation triggers an increase in CycD1 translation, improving the activity of CDK4 which phosphorylates Rb. In turn, phospho-Rb releases UBF, allowing for increased RNAPolI inititation (Nader et al., 2005). Furthermore, activation of S6K induces UBF phosphorylation indirectly, and this is required for it to bind SL1 (Hannan et al., 2003).

Ribosome synthesis and translation require the transcription of both the 5S and transfer RNAs by RNAPolIII which is also regulated by the PI3K-mTor pathway. Indeed, mTor binds chromatin over the 5S and tRNA genes, and associates with PIC component TFIIIC (Kantidakis et al., 2010; Tsang et al., 2010). It has also been shown to phosphorylate the RNAPolIII repressor Maf1 on several residues, notably serine 75. While the exact consequences remain unclear, a phospho-deficient variant of Maf1 has been shown to repress RNAPolIII transcription more efficiently than wild type Maf1, suggesting that these phosphorylations adversely regulate Maf1 activity as a repressor (Shor et al., 2010). Consistently, dephosphorylation of Maf1 by mTor antagonist PP2A in yeast promotes its accumulation in the nucleus and subsequent association to RNAPolIII (Roberts et al., 2006). In a similar way, inhibition of Ras-ERK signalling in *Drosophila* has been shown to increase the nuclear localization of Maf1 and reduce tRNA synthesis in a Maf1-dependent manner (Sriskanthadevan-Pirahas et al., 2016). Thus, Maf1 is could function as a master regulator of RNAPolIII transcription by integrating positive and negative feedback from both Ras-ERK and PI3K-mTor signalling.

In addition to stimulating transcription by RNA Polymerases I and III, the PI3K-mTor pathway also modulates the activity of several transcription factors involved in r-protein genes regulation. The yeast transcription factor FHL1 is a striking example: it is constitutively bound to *RPG* promoters and exerts

its regulatory activity through the recruitment of co-factors. The trans-activator IHF1 and trans-repressor CRF1 compete for binding to FHL1. Upon inactivation of the Tor pathway, CRF1 can accumulate in the nucleolus, compete with IHF1, and switch FHL1-mediated regulation from activation to repression of *RPG* (Martin et al., 2004). In a somewhat similar fashion, the yeast transcription factor Sfp1 binds *RPG* promoters under permissive growth conditions, but is relocated to the cytoplasm upon Tor pathway inactivation (Marion et al., 2004). While these two examples illustrate the mechanisms through which the Tor pathway regulates *RPG* expression, it should be noted that several other transcription factors (Abf1, Hmo1, Rap1) link this pathway to ribosomal protein gene expression regulation (Berger et al., 2007; Fermi et al., 2016; Klein and Struhl, 1994).

Chief among PI3K-mTor and Ras-ERK effectors, the transcription factor Myc regulates the activity of all three polymerases. Myc exists as a family of proteins (c-Myc, N-Myc, L-Myc) with overlapping biological function in mammals (Eilers and Eisenman, 2008). It activates transcription of RNAPolII genes by associating with its co-factor Max, and competes with its antagonist Mad to do so. Myc activity is enhanced by the PI3K-mTor and Ras-ERK pathways in two ways. First, Myc is phosphorylated by ERK, which increases its stability (Sears et al., 2000). Secondly, Mad is phosphorylated by RSK and S6K, which triggers its degradation, thus alleviating the competition for Max binding (Zhu et al., 2008). Myc has been described to bind up to 15 % gene loci in several species, and has profound effect on gene expression patterns (Fernandez et al., 2003; Orian et al., 2003).

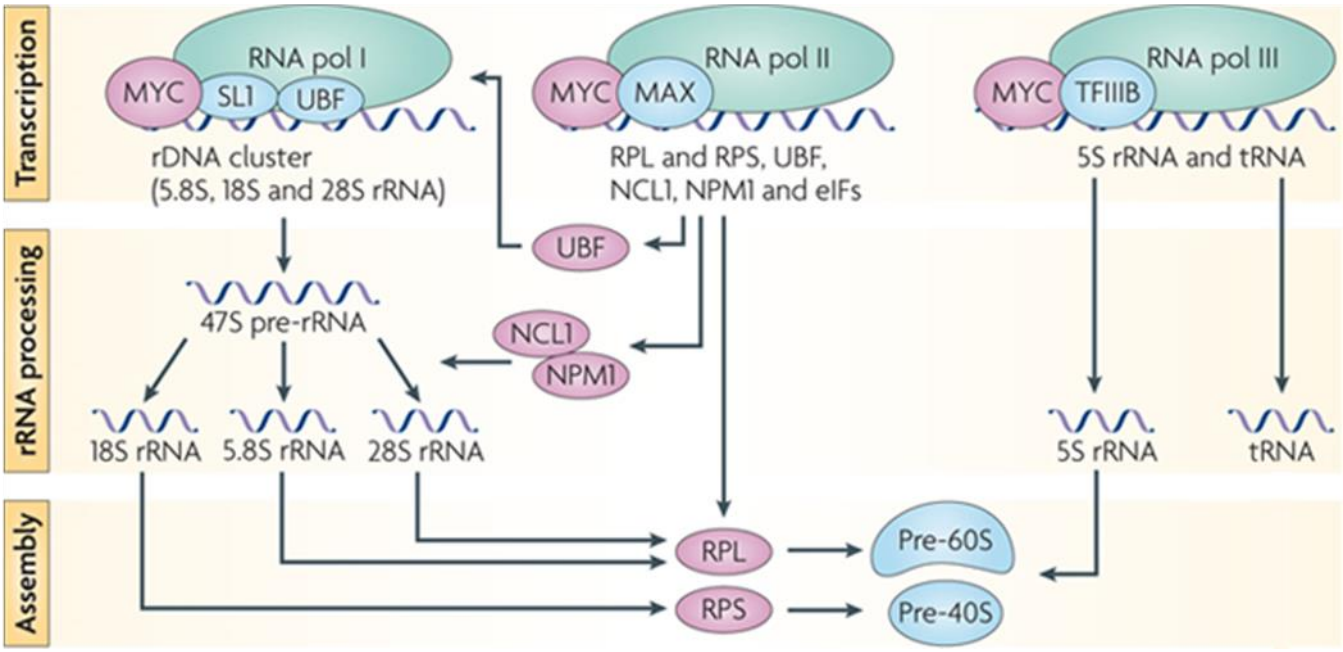

Figure 16. Coordinated regulation of ribosome biogenesis by the transcription factor Myc
Adapted from (van Riggelen et al., 2010).

Indeed, Myc binds the human rDNA promoter and terminator regions, and facilitates the recruitment of RNAPolI by interacting with the Pre-initiation complex component SL1 (Grandori et al., 2005). It also recruits TRRAP and the histone acetyltransferases (HATs) GCN5 and Tip60, promoting acetylation of histones H3 and H4, further increases rDNA transcription through chromatin remodelling (Arabi et al., 2005).

Similarly, Myc also activates RNAPolIII transcription of the 5S rRNA and tRNA genes though direct association with the pre-initiation complex component TFIIIB (Gomez-Roman et al., 2003). Upon

binding, Myc recruits its co-factor TRRAP and in turn, GCN5 which facilitates transcription by acetylating histone H3 (Kenneth et al., 2007).

Myc also localizes to RNAPolII promoters as an heterodimer with Max, where it binds E-box elements (CACA/GTG), but also non-consensus motives, or adaptor proteins such as Miz1 (Blackwell et al., 1993; Staller et al., 2001). It serves as a platform for the recruitment of chromatin remodelling factors, such as HATs (GCN5, Tip60, CBP and p300), nucleosome exchange factors (p400), chromatin remodelling complexes ATPase subunits (TIP48 and TIP49) and DNA methyltransferases (DNMT3a) (Brenner et al., 2005; Fuchs et al., 2001; McMahon et al., 2000; Vervoorts et al., 2003; Wood et al., 2000). Additionally, Myc recruits transcription factors such as the Mediator and pTef-b complexes (Bouchard et al., 2004). Depending on the recruited factors, Myc can function either as an activator or repressor of transcription. Its mode of action varies considerably and seems to depend on cellular context. However, as a general feature, Myc has no effect on RNAPolII recruitment, and rather regulates promoter clearance and elongation (Brenner et al., 2005; Eberhardy and Farnham, 2001). Among target genes, Myc activates the transcription of r-protein genes, translation factors, rRNA processing factors, and transcription factors such as UBF, which further increases rDNA transcription (For review : Adhikary and Eilers, 2005).

In addition to increasing transcription of ribosome biogenesis components, the activation of cell proliferation signalling pathways regulate the translation of their messenger RNA. Indeed, most r-protein and translation factors mRNAs display a 5'TOP motif (cf I.B.4). These mRNA display very specific translation kinetics, with poor translation initiation efficiency under even optimal conditions. Strikingly, their translation is drastically reduced upon inhibition of either Ras-ERK or PI3K-mTor pathways (Patursky-Polischuk et al., 2009; Romeo et al., 2013). However, the molecular mechanisms of this regulation are largely unknown. Many RNA binding factors have been shown to associate with TOP mRNAs and proposed to mediate their regulation. However, in each case contradictory evidence challenged the requirement of the proposed factor for TOP mRNA regulation. These data suggest that the regulation of TOP mRNA by signalling pathways may involve a complex network and differ with cell types or stimuli (For review: Meyuhas and Kahan, 2015)

2. The cell cycle

Tightly linked to cell proliferation, progression into the cell cycle triggers many changes in transcription, protein localization or nuclear organization. Ribosome synthesis activity is no exception to this rule, as evidenced by the disruption of the nucleolus during mitosis in mammalian cells. Indeed, several mechanisms regulate both the transcription and assembly of ribosome components in a phase specific manner, leading to the observation that rRNA synthesis is inhibited during mitosis, gradually recovers during G1 phase, and peaks during S and G2 phases (Klein and Grummt, 1999).

The entry into prophase is accompanied by the release of ribosomal processing factors from the nucleolus, and followed by the inhibition of rDNA transcription (Gébrane-Younès et al., 1997). Interestingly, the RNAPolI transcription machinery stays associated to rDNA through the whole mitotic phase, which may allow rapid resumption of transcription in G1 phase (Jordan et al., 1996). Their activity is however inhibited by a series of phosphorylations orchestrated by the Mitosis Promoting Factor (MPF). The phosphorylation of the pre-initiation complex SL1 prevents its interaction with UBF, which is necessary for promoter escape (Heix et al., 1998). This inhibition is further mediated by the inactivation of UBF in mitosis (Klein and Grummt, 1999). Additionally, the termination factor TTF-1 is also phosphorylated by the MPF complex, lowering its affinity for rDNA and thus possibly interfering with its role in active rDNA chromatin remodelling (Sirri et al., 1999). Similarly, the pre-initiation

complex for RNAPolIII is inactivated during mitosis by the phosphorylation of TFIIIB subunits Bdp1 and Brf1 by the MPF complex, preventing the transcription of the 5S and transfer RNAs (Fairley et al., 2003).

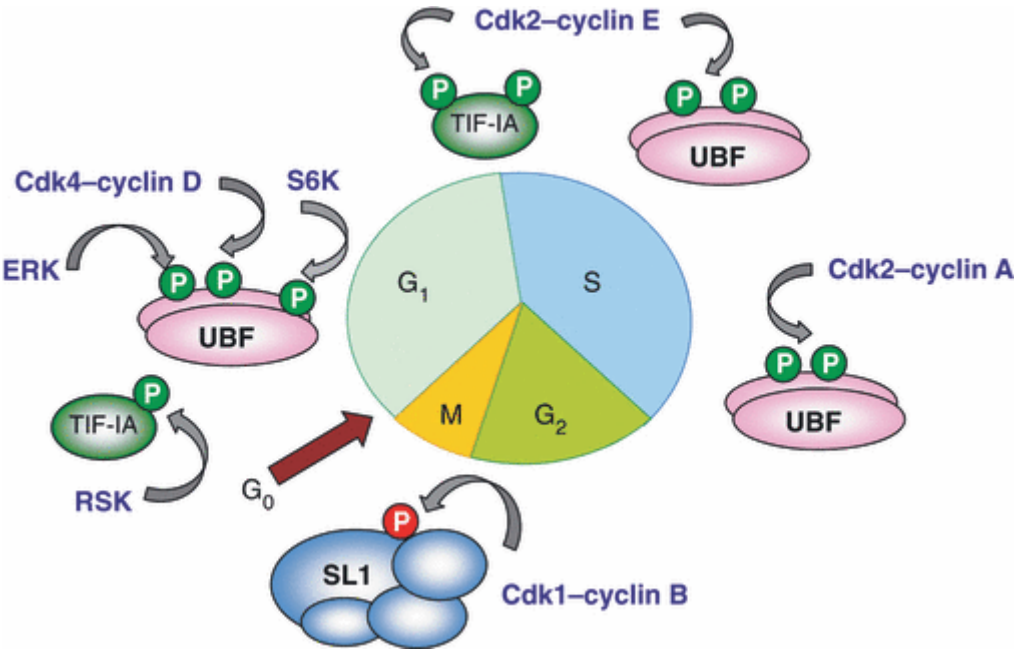

Figure 17. Regulation of RNAPolI during the cell cycle
Regulation of Pol I transcription during the cell cycle. During progression through the G_1-phase and S-phase, UBF is activated by phosphorylation of Ser484 by Cdk4–cyclin D and Ser388 and Cdk2–cyclin E/A, respectively. In addition, mTOR-dependent and ERK-dependent pathways activate TIF-IA by phosphorylation of Ser44, Ser633 and Ser649. At entry into mitosis, Cdk1–cyclin B phosphorylates TAF_I110, a subunit of the TAF_I–TBP complex SL1, at Thr852. Phosphorylation at Thr852 inactivates SL1, leading to repression of Pol I transcription during mitosis. At the exit from mitosis, Cdc14B dephosphorylates Thr852, leading to recovery of SL1–TIF-IB activity. Activating phosphorylations are marked in green, and inhibiting ones in red. Transcription is low in resting cells (G_0), and resumption of full transcriptional activity on re-entry into the cell cycle requires phosphorylation of TIF-IA by ERK/RSK and phosphorylation of UBF by ERK, Cdk4–cyclin D and S6K. Taken from (Grummt, 2010).

The onset of anaphase triggers the degradation of the MPF, and subsequently alleviates the inhibition of rRNA transcription. Interestingly, RNAPolI transcription only resumes gradually during the G1 phase, and requires both removal of inhibitory phosphorylations and renewal of activating ones. Interestingly, the different factors that participate to rDNA transcription are reactivated at different rates. Indeed, SL1 is fully functional as early as the exit of mitosis, but UBF is still inactive during early G1 phase. The inhibitory phosphorylation deposited by the MPF complex needs to be removed by the PP2A phosphatase for UBF to recover its trans-activator properties (Klein and Grummt, 1999). Its ability to promote transcription is then progressively restored throughout interphase by the phosphorylation of serines 484 and 388 by the Cdk4/CyclinD, Cdk2/CyclinE and Cdk2/CyclinA complexes (Grummt, 2003).

Ribosome assembly is also halted during mitosis as the nucleolar components are released in early prophase. Strikingly, they have been shown to tether around condensing chromosomes and form the peri-chromosomal compartment (Gautier et al., 1992). This layer surrounds the chromosome arms and has been shown to contain r-proteins, rRNA processing factors, partially processed rRNAs and snoRNAs (Gautier et al., 1994; Piñol-Roma, 1999). Interestingly, FRET analysis of the interaction between rRNA processing factors showed that Fibrillarin, Nop52, Bop1 and NPM co-localize but do not interact in this compartment, suggesting that their assembly into processing complexes may also be regulated in a cycle-dependent manner (Angelier et al., 2005). The assembly of nucleolar proteins into a peri-

chromosomal compartment is believed to allow equal distribution of ribosomal components between daughter cells upon division, and is a conserved mechanism among many species (Van Hooser et al., 2005). During telophase, nucleolar components are released and assemble into pre-nucleolar bodies (PNB). Interestingly, rRNA processing factors traffic between reforming nucleoli and PNB, which gradually disappear as their pre-rRNA contents are released. Thus, PNB may function as extra-nucleolar sites that ensure the maturation of the partially processed rRNAs that were distributed to the peri-chromosomal layer during mitosis (Carron et al., 2012).

3. Energy levels

Ribosome synthesis and translation require the activity of hundreds of energy releasing enzymes such as GTP and ATP hydrolases (For review: Strunk and Karbstein, 2009). Indeed, a large portion of cell energy is dedicated to these processes under permissive conditions. However, energy can become scarce under poor environmental conditions, and several mechanisms are dedicated to reorganizing cell metabolism under these circumstances. As a common feature, most of these mechanisms monitor energy levels to maintain the activation of the PI3K-mTor pathway specifically under permissive conditions, and are thus necessary to sustain ribosome biogenesis.

Amino-acids availability

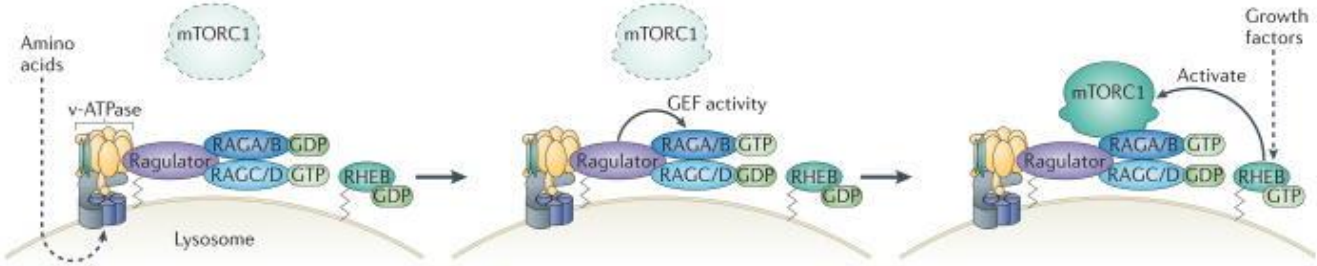

Figure 18. Amino-acid dependent activation of mTor at the lysosome
Amino acids are thought to accumulate within the lysosomal lumen and to signal to vacuolar H^+-ATPase (v-ATPase) through an 'inside–out' mechanism. v-ATPase controls RAG GTPase–Ragulator binding, and therefore Ragulator guanine exchange factor (GEF) activity and RAGA and RAGB guanine nucleotide loading (RAGA/B·GTP). The active RAG complex (RAGA/B·GTP–RAGC/D·GDP) binds to mammalian target of rapamycin complex 1 (mTORC1) and recruits it to the lysosome, through an unknown mechanism, possibly in close proximity to RHEB (RAS homologue enriched in brain). Downstream of growth factor signalling, GTP-bound RHEB potently activates mTORC1. Taken from (Jewell et al., 2013).

A comfortable supply of amino-acids is necessary for sustained protein synthesis. Their availability is monitored by several mechanisms that feed into the PI3K-mTor pathway. Indeed, nutrient intake results in the accumulation of amino-acids in the lysosome lumen. This is required for Rag GTPases-mediated activation of the mTORC1 complex at the lysosome membrane (**Fig. 18** and Jewell et al., 2013). Importantly, amino-acids are also sensed from the cytoplasm and Golgi apparatus to activate mTORC1 (Goberdhan et al., 2016). Additionally, amino-acids starvation induces an increase in uncharged tRNA, which can bind and activate GCN2. This kinase is able to phosphorylate the translation initation factor eIF2α, which represses general translation (Wang and Proud, 2008). The activation of GCN2 together with the repression of the PI3K-mTor pathway further triggers autophagic responses to the lack of amino-acids. Importantly, ribosomes are specifically degraded in autophagosomes, in a process called "ribophagy". Interestingly, free inactive ribosomes are selectivally degraded, suggesting that this mechanism could serve both in restoring amino-acid levels and eliminate defective ribosomes (Cebollero et al., 2012).

Oxygen levels

In a similar manner, appropriate oxygen levels are required for energy production by the mitochondria. The hypoxia-inducible factor (HIF) family of transcriptions factors are hydroxylated in a O2-dependent manner under normoxia (Semenza, 2014). When oxygen levels decrease, their stabilization allows them to activate the transcription of a set of genes involved in energetic metabolism. Among them,

REDD1 encodes a protein that competes with TSC2 for binding 14-3-3. The hypoxia-induced release of TSC2 allows it to inactivate mTORC1 and thus inhibit the PI3K-mTor pathway (DeYoung et al., 2008). Hypoxia also induces a shift from respiration to fermentation, allowing the production of energy in the absence of oxygen. The fermentation process is less efficient in producing energy, and is accompanied by the release of lactic acid in the environment. The latter triggers an acidification of the extracellular compartment, termed acidosis. This condition correlates with a reduction in nucleolus size and rDNA synthesis which requires the acidosis-induced relocalization of the tumor suppressor VLH into the nucleolus. While the underlying mechanism is unclear, it is interesting to note that contrary to RNAPolI inhibitors, prolonged hypoxia response does not jeopardize the architecture of the nucleolus. It has thus been postulated that a reduction in ribosome synthesis allows to adapt energy expenditure to the reduced energy production efficiency of fermentation (Mekhail et al., 2006).

NAD+ availability

Production of energy through the mitochondrial respiration pathway requires constant regeneration of the NADH supply. Accordingly, NAD+ availability results from the balance between metabolic activity and energy production. This metabolite is a required co-factor for a family of deacetylases with a broad range of substrates: the sirtuins. They are activated in conditions of energy deficiency and trigger many adaptive changes (Covington and Bajpeyi, 2016). Interestingly, ribosomal components are among their substrates, possibly linking NAD+ metabolism to ribosome biogenesis homeostasis. Indeed, SIRT1 has been shown to reduce rRNA synthesis by deacetylating the TAF_I68 subunit of SL1, thus reducing Pol I initiation (Blander and Guarente, 2004). In addition, it has been shown to promote epigenetic silencing of rDNA by deacetylating H3K9 (Murayama et al., 2008). More confusingly, SIRT7 has been shown to increase RNAPolI and RNAPolIII transcription, but repress transcription of r-protein genes (Blank and Grummt, 2017). As a general feature, the amount of sirtuin family proteins correlates with proliferation, and their activity is regulated by stress cues. Indeed, their activity is subject to additional layers of regulation besides NAD+ levels(Chung et al., 2010; Yang and Chen, 2014). Thus, the apparently contradictory behaviour of sirtuins in regard to ribosome biogenesis may reflect the complexity of their regulation by different stress signalling pathways.

ATP levels

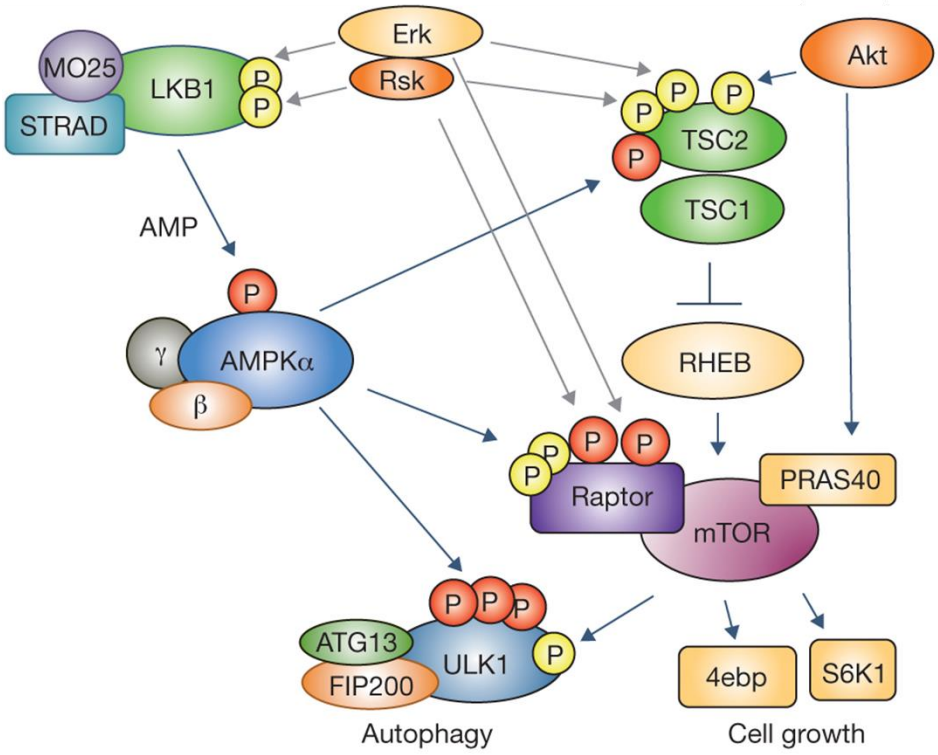

Figure 19. The AMPK pathway interacts with the PI3K-mTor and Ras-ERK pathway
Inhibiting phosphorylations are depicted in yellow while activating phosphorylations are displayed in red. Adapted from (Mihaylova and Shaw, 2011).

Cells store chemical energy in the form of ATP, which is necessary to catalyse a myriad of enzymatic reactions. Sustenance of the cell metabolism require a balance between production and consumption of ATP. The ratio between ATP and its hydrolysed counterparts, ADP and AMP, are therefore a good measure of the cell's energy reserves. ATP levels are monitored by the AMP-activated protein kinase (AMPK). Its activation requires two steps: phosphorylation by the upstream kinase LKB1, followed by a conformational change that prevents subsequent dephosphorylation. While ADP binding to the γ subunit of AMPK promotes only the latter, AMP binding enhances both steps of AMPK activation (Oakhill et al., 2011; Xiao et al., 2011). The activation of the AMPK pathways triggers the renewal of mitochondria by promoting both mitophagy and mitochondrial biogenesis. Importantly, it also triggers a reduction in ribosome metabolism by activating the mTORC1 repressor TSC2 (For review: Mihaylova and Shaw, 2011). In addition, activated AMPK has been shown to directly phosphorylate TIF-IA which prevents its interaction with SL1, thus impairing RNAPolI recruitment and rRNA synthesis (Hoppe et al., 2009).

4. Metabolic stress

Cells display the ability to thrive in environments that fluctuate to a certain extent. However, their survival can be endangered under adverse conditions. Such stress can be induced by a number of ways, and generally disrupts the metabolism at many levels. The activation of stress response mechanisms allows cells to quickly reorganize their energy expenditure to survive.

Endoplasmic reticulum stress

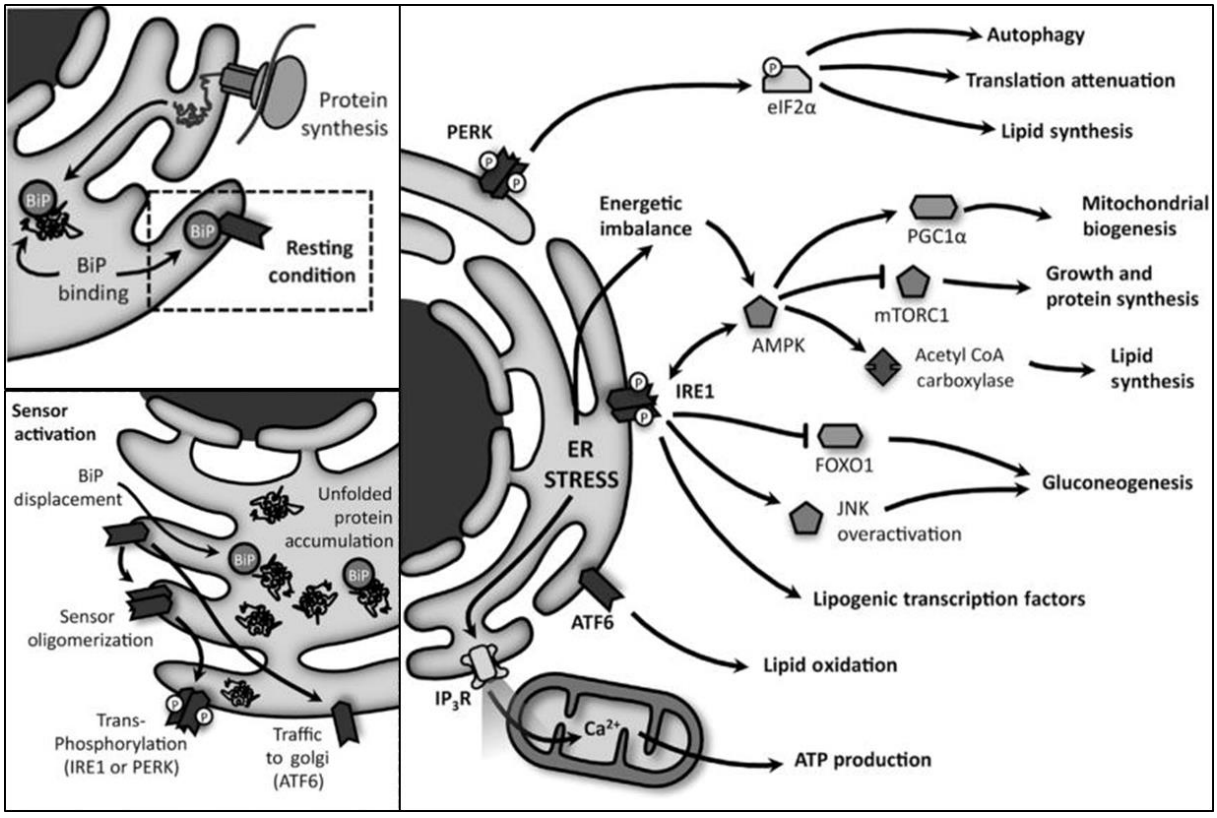

Figure 20. The unfolded protein response pathway
Upper left panel: In resting conditions, the stress sensors IRE1, PERK and ATF6 interact with Bip/GRP78. Lower left panel: Accumulation of misfolded proteins in the ER lumen separates the chaperone from each sensor. IRE1α and PERK activation involves oligomerization and transphosphorylation of their cytosolic effector region. ATF6 activation, on the other hand, requires its transport to the Golgi, where it is sequentially cleaved by S1P and S2P. Right panel: PERK induces global attenuation in protein anabolism, and favours lipid synthesis, both effects via eIF2α phosphorylation. IRE1 cooperates with these responses and stimulates mitochondrial biogenesis through the regulation of master metabolic switches, such as PGC1α, mTOR, AMPK and FOXO1. ATF6, on the other hand, stimulates lipid utilization. Calcium released by IP3R increases mitochondrial activity during ER stress, in order to revert energy imbalance. Adapted from (Bravo et al., 2013).

The endoplasmic reticulum (ER) is a critical hub of cell metabolism, which regulates calcium concentrations, lipid metabolism and synthesis, and vesicle trafficking. Ribosomes bind its membrane, forming the rough endoplasmic reticulum (RER) compartment. Indeed, the presence of a hydrophobic signal in the N-terminal part of a nascent polypeptide can be recognized by the signal recognition particle (SRP), which induces a pause in translation, and the translocation of the ribosome-SRP complex to the RER membrane (Corsi and Schekman, 1996). The nascent polypeptide traverses the membrane through a pore, allowing it to enter the RER, which contains a variety of chaperone proteins. Thus, it

also plays a crucial role in protein folding. Several stress cues can disturb ER metabolism such as calcium depletion and oxidative stress, lipid perturbation, or increased protein load (Görlach et al., 2015; Ozcan et al., 2008; Volmer and Ron, 2015). Those lead to an increase in misfolded proteins inside the ER lumen, which trigger the activation of the Unfolded Protein Response (UPR) pathway (**Fig. 20**).

The most immediate response to an increase in misfolded proteins is the transient inhibition of translation. Indeed, activated PKR-like endoplasmic reticulum kinase (PERK) phosphorylates eIF2α, thus inhibiting general translation (cf. II.A.3 and Harding et al., 2000). In addition, eIF2α phosphorylation promotes the dissociation of RRN3 and RNAPolI from rDNA, further reducing protein synthesis capacity (DuRose et al., 2009). Another consequence of ER stress is the release of calcium to the cytoplasm, activating CaMKKβ which in turn phosphorylates AMPK, thus leading to activation of the AMPK pathway (Høyer-Hansen and Jäättelä, 2007). This activation can also be mediated by the UPR effector IRE1 under nitric oxide stress conditions (Meares et al., 2011). In both cases, AMPK activation leads to the inactivation of mTORC1 and reduction of ribosome biogenesis (cf. II.A.1).

Heat shock

Temperature variation is another common source of metabolic distress. Indeed, an acute increase in temperature, or heat shock, may induce protein misfolding and denaturation thus damaging cells. Heat stressed cells display an acute reorganization upon heat shock, among which the inhibition of translation and ribosome synthesis is of paramount importance. Indeed, newly synthetized peptides are particularly sensitive to misfolding and aggregation upon heat shock (Zhou et al., 2014) In addition, heat stressed cells display formation of stress granules (Anderson and Kedersha, 2009). These aggregates of proteins and mRNA have been shown to protect their components from degradation and permit their return to activity during recovery (Wallace et al., 2015).

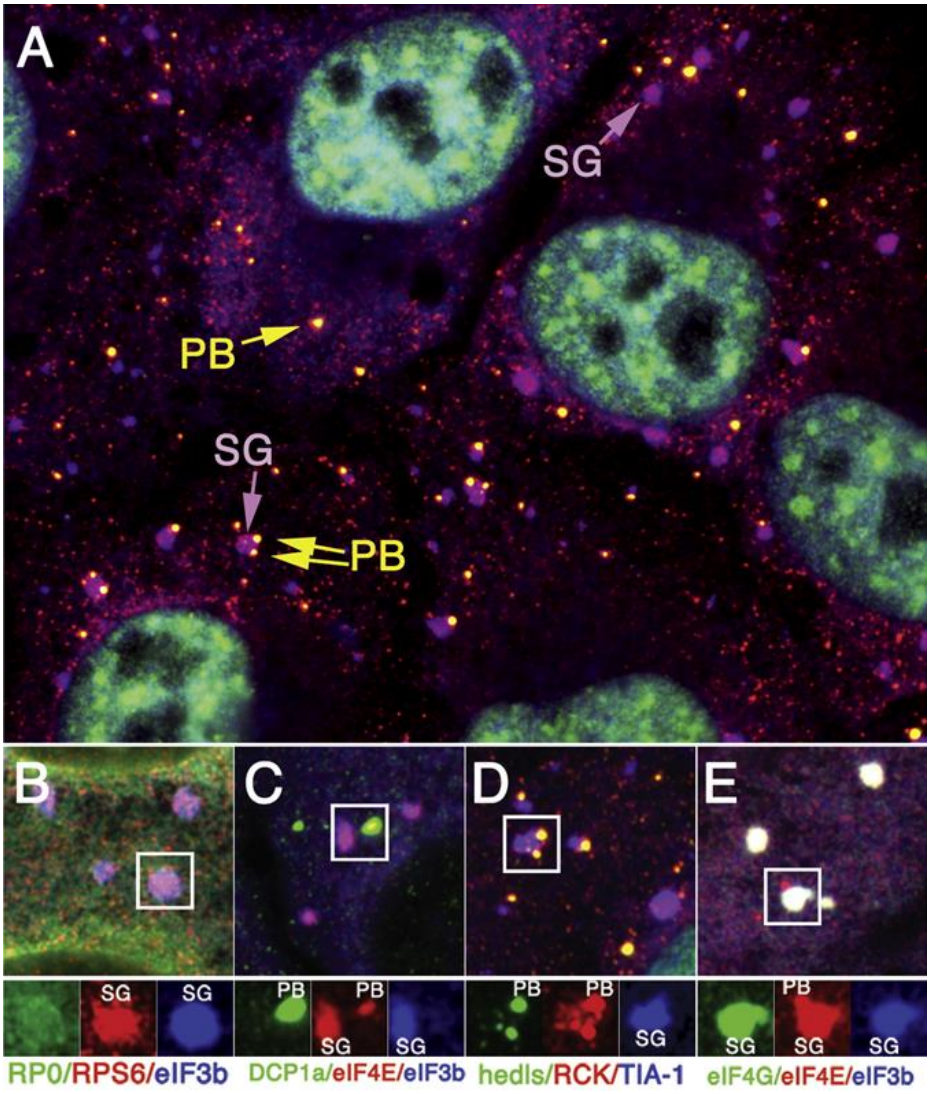

Figure 21. Stress granules and P-bodies in arsenite-treated human U2OS cells
(A) Stress granules (SG, purple arrows) are visualized by staining for TIA-1 (blue), a translational silencer. As stress granules also contain the RNA helicase RCK1 (stained in red), the merged colors appear purple. Similarly, P-bodies (PB, yellow arrows) are visualized by hedls/GE-1 staining (green) but appear yellow due to RCK1 colocalization. A single cell can contain isolated P-bodies and stress granules, as well as interacting pairs of stress granules and P-bodies. (B) Large ribosomal subunits (RP0, green) are excluded from stress granules or localized to the edges, defined by small ribosomal subunits (RPS6, red) and eIF3b (blue). (C) P-bodies (DCP1a, green) and stress granules (eIF3b, blue) both contain eIF4E (red). (D) A region of (A), showing separated colors in the inset. (E) Stress granules exclusively contain eIF3b (blue) and eIF4G (green), whereas eIF4E (red) is found both in stress granules and in a

bound P-body. Insets show the separate colors within the boxed regions. Taken from (Anderson and Kedersha, 2009).

Importantly, the majority of proteins sequestered in stress granules are linked to translation, notably initiation and elongation factors, and aminoacyl-tRNA synthetases. Ribosome biogenesis factors also accumulate in insoluble nuclear deposits, although separately from stress granules (Cherkasov et al., 2015). Stress granules are also specifically enriched in r-protein mRNAs in *Arabidopsis*, further preventing *de novo* ribosome synthesis during stress (Merret et al., 2017). In addition, heat shock induces a reduction in RNAPolI activity. First, the heat-dependent sequestration of CK2 in the nuclear matrix prevents it from activating TIF-1A through Serines 170/172 phosphorylation. Secondly, heat induced transcription of the long non coding RNA (lncRNA) PAPAS in antisense of the rDNA repeat recruits the chromatin remodelling complex NuRD to deacetylate histones on the rDNA promoter, further silencing transcription (Zhao et al., 2016).

During recovery from heat shock, aggregates dissociate under the control of the heat shock proteins chaperones, allowing resumption of translation. Interestingly, the amount of free 40S and 60S subunits does not decrease following translation resumption, suggesting that it is newly synthetized ribosomes that engage in translation. Consistently, it was observed that ribosome subunits can be ubiquitinated under stress conditions or translation inhibition, leading to altered translation or degradation (Higgins et al., 2015; Kraft et al., 2008). It was thus hypothesized that pre-existing ribosome subunits may be altered during heat shock, possibly because they are not shielded from modification through aggregation (Merret et al., 2017).

Cold shock

While an elevation of temperature triggers stress responses, so does its reduction. Cold shock has been shown to trigger an elevation of the AMP/ATP ratio, thus triggering the AMPK pathway. In addition, it causes a release of Ca_{2+} to the cytoplasm, thus activating CaMKKβ. Both events lead to the phosphorylation of eIF2α, resulting in the inhibition of translation (Knight et al., 2015). Interestingly, cold stress has also been shown to induce the SUMOylation of EXOSC10, which impedes its activity in rRNA and snoRNA processing, and degradation of non-functional RNA. This event impedes rRNA biogenesis at specific steps of 18S rRNA processing, leading to the accumulation of partially processed 40S subunits. It has thus been postulated that besides reducing global translation activity, this could permit completion of 40S processing upon recovery, thus allowing rapid resumption of translation (Knight et al., 2016).

B. Ribosome biogenesis regulates homeostasis

1. Ribosome biogenesis is monitored at several stages of cell life

As previously demonstrated, ribosome biogenesis activity is tightly regulated and can be inhibited a number of ways in times of metabolic distress. Thus, ribosome synthesis can be considered a proxy for cell health. Indeed, several mechanisms monitor the state of ribosome biogenesis and regulate cell fate in accordance.

Cell cycle commitment

One such example is the progression into the cell cycle. Indeed, the transition from G1 phase to S phase, implies a commitment to cell division, and is subject to extensive regulation. Passing the G1/S checkpoint requires to reach a critical size, and the same condition applies for the G2/M checkpoint (for review: Barnum and O'Connell, 2014). As ribosomes constitute the largest part of the cell material, their abundance may serve to evaluate cell size. In turn, ribosome number may be measured through translation capacity. Indeed, it has been shown that in yeast, the depletion of many translation factors and tRNA biosynthesis genes induce an arrest of the cell cycle in G1 phase, suggesting that G1 to S phase transition is translation-dependent (Yu et al., 2006). Indeed, translation of the yeast Cln3p was shown to be required to pass this checkpoint (Barbet et al., 1996). Cln3p is an extremely unstable protein, so its accumulation requires intense translation (Tyers et al., 1992). In addition, the presence of an upstream open reading frame (uORF) in the 5' UTR of the Cln3p mRNA represses its translation when the amount of ribosomes is limited (Polymenis and Schmidt, 1997). Thus, accumulation of Cln3p is only possible after ribosome number reaches a certain point.

Interestingly, a study pointed out that depletion of an rRNA processing factor triggered defects in cell cycle progression before the number of ribosomes or translation capacity started to dwindle, in a Cln3p-independent manner. These data suggest that ribosome biogenesis activity may also be monitored at the level of newly synthetized subunits to trigger cell cycle progression (Bernstein et al., 2007). In addition, the depletion of r-proteins in yeast caused stage specific cell-cycle arrest. Many of them caused G1 phase arrest, consistent with monitoring of either ribosome biogenesis or steady-state levels. Interestingly, nine r-proteins of the large subunit triggered an arrest in G2 phase, suggesting that they are required at the G2/M checkpoint. This specific defect could result from another mechanism than G1 arrest. Strikingly, all nine r-proteins cluster on the solvent side of the 60S subunit, where they could interact with non-ribosomal factors. Thus, they may be needed either as part of "specialized" ribosomes, or they could participate in cytoplasmic export of G2 phase-specific factors, through "ribosome riding" (cf. II.B.2) (Thapa et al., 2013).

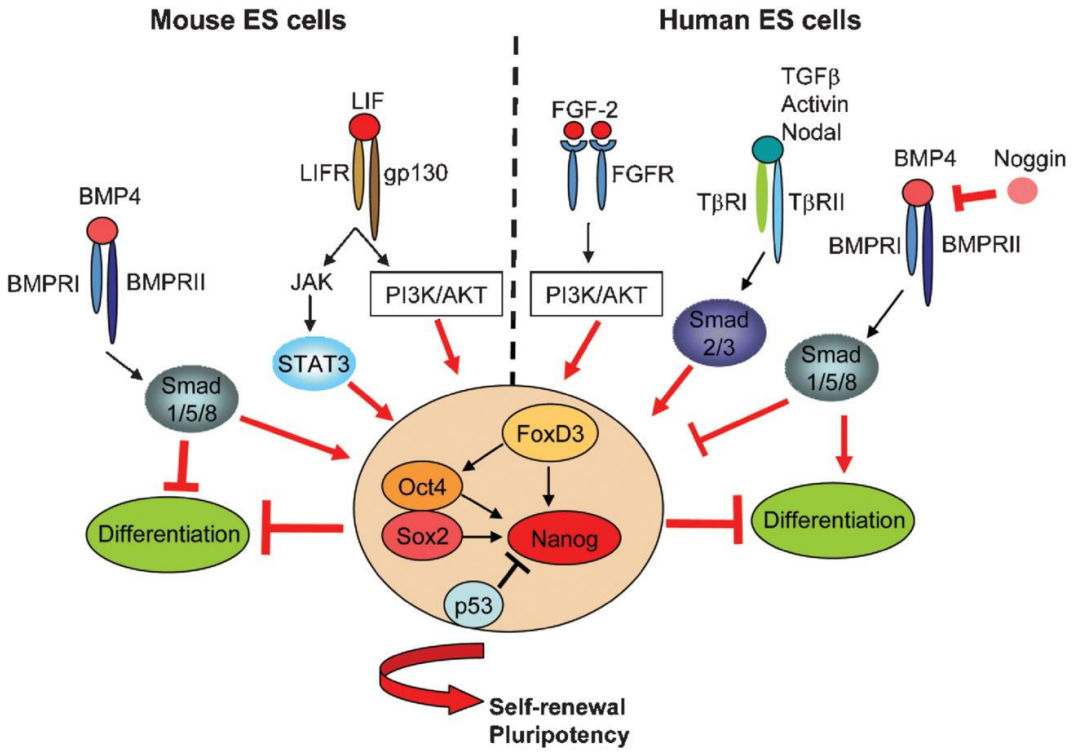

Figure 22. Extrinsic and intrinsic regulation of ES cell self-renewal and differentiation
Oct4*, Sox2, and* Nanog *are master genes causing formation of the core transcription regulatory network and control embryonic stem cell pluripotency. The activity of the core regulatory network is modulated by multiple extrinsic factors, which are different for human ES cells and mouse ES cells. Taken from (Zhang and Wang, 2008).*

The integrity of ribosome biogenesis is of utmost importance for stem cells, which carry the responsibility of self-renewal. Maintenance of the stem cell state depends on a network of transcription factors and external signals, whose disturbance leads to aberrant differentiation (for review Zhang and Wang, 2008). In embryonic stem cell models, disruption of fibrillarin and six genes of the small subunit processome induced early differentiation. Strikingly, the overexpression of fibrillarin prolonged ES cells pluripotency in the absence of external stemness maintenance cues (Watanabe-Susaki et al., 2014; You et al., 2015). It was postulated that sufficient ribosome capacity is required to keep the expression of key pluripotence-promoting transcription factors above a threshold level (**Fig. 22**). Another explanation for the aberrant differentiation phenotype would be the prolongation of G1 phase upon ribosome biogenesis impairment. Indeed, pluripotence loss upon depletion of the nucleolar GTPase nucleostemin was rescued upon depletion of cell cycle inhibitors, concomitantly with G1 phase shortening (Qu and Bishop, 2012). Indeed, embryonic stem cells are particularly sensitive to differentiation cues during G1 phase, whose prolongation increases the likelihood of committing to differentiation (For review: Orford and Scadden, 2008).

Developmentally regulated differentiation events are also affected by ribosome biogenesis impairments. Loss of several ribosome components in zebrafish triggered early differentiation of neural stem cells, correlating with a down-regulation of Notch pathway targets (Essers, 2013). Similarly, *Drosophila* egg chambers mutant for subunits of the SL1 complex displayed early differentiation of GSC into cyst cells, correlated with a down-regulation of the BMP pathway factor Mothers against decapentaplegic (Zhang et al., 2014). In both cases, wild type stem cells were shown to display higher ribosome biogenesis intensity than their differentiated sister cell, suggesting that high

translation capacity is required pluripotence. Consistently, the rRNA processing U3 snoRNP component Wicked segregates asymmetrically to stem cells during mitosis, and has been shown to be required for maintenance of germ stem cells and neural stem cells during development (Fichelson et al., 2009). Similarly, the SL1 component Under-developped was shown to segregate preferentially to germ stem cells during asymmetric mitosis (Zhang et al., 2014). The requirement for high ribosome capacity and preferential repartition of ribosome components in stem cells suggest that pluripotence indeed relies on functional ribosome biogenesis.

Cell competition

Many heterozygous mutants for ribosomal protein genes or ribosomal assembly factors are viable, at the expense of a range of developmental defects (cf. II.B.4). Indeed, cells can live with reduced ribosome synthesis activity, despite the importance of ribosomal functions. However, these otherwise viable cells undergo apoptosis in a genetic mosaic context, in the presence of wild type cells. This observation led to the discovery that disadvantaged cells are eliminated by a process called “cell competition” (Morata and Ripoll, 1975).

Extensive research on the underlying mechanisms yielded the idea that adjacent cells compare their fitness, and that the outcompeted cells trigger apoptosis. However, the precise nature of the criteria that are evaluated remain elusive. Indeed, besides ribosomal components, mutations for genes involved in many signalling pathways have been shown to provide such disadvantage (For review: Baker, 2017). Among them, the transcription factor Myc was shown to be a master regulator of cell competition, with its overexpression turning cells into “supercompetitors” able to induce apoptosis in wild type cells (Moreno and Basler, 2004). The ability of Myc and many competition-inducing genes to regulate ribosome biogenesis led to the idea that there is a direct relationship between cell fitness and ribosome number. However, loss of Wnt/Wg or JAK/STAT signalling was shown to induce cell competition independently of Myc and ribosome biogenesis regulation (Rodrigues et al., 2012; Vincent et al., 2011). These data suggest that while ribosome biogenesis is critical for cell fitness, other parameters may also weight into the competition between cells.

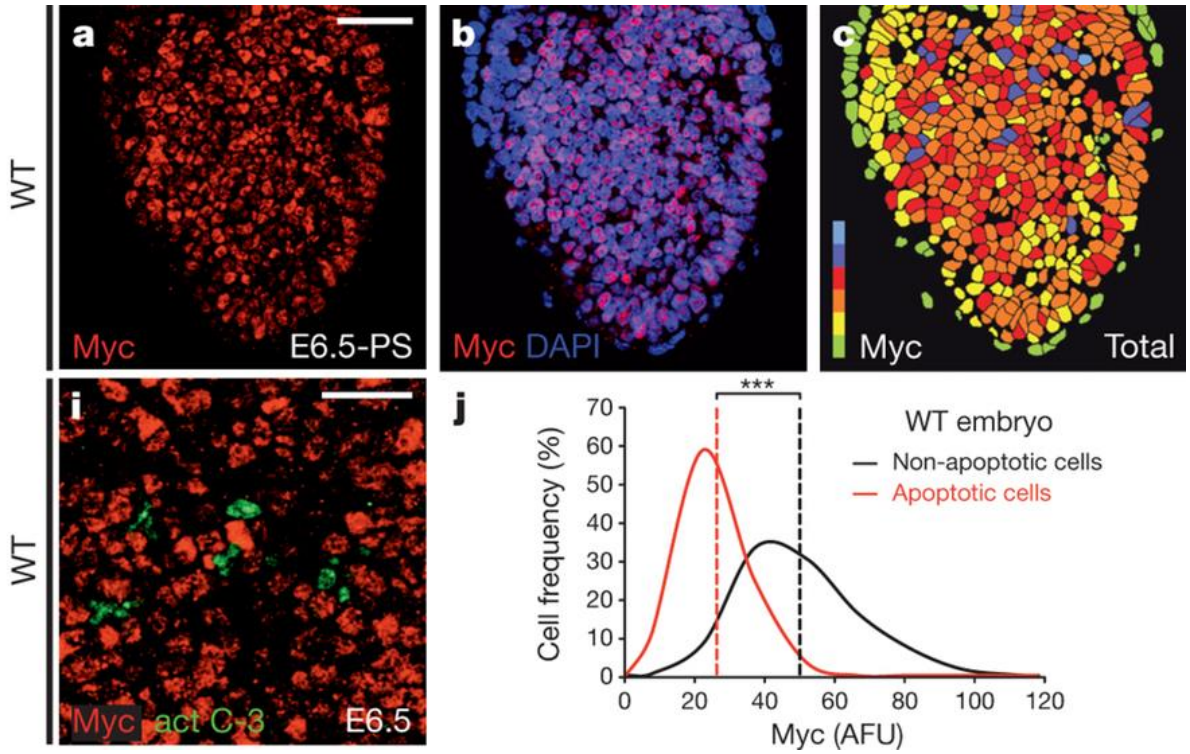

Figure 23. Myc heterogeneity may drive cell competition in wild type mammalian embryos
a, b *Confocal sections showing Myc expression. Scale bars, 50 µm.* ***c*** *Colour coding of Myc levels; green indicates the lower and blue the higher Myc levels in arbitrary fluorescence units* ***i****, Detail of Myc and active caspase-3 expression in the wild-type epiblast. Scale bar, 50 µm.* ***j****, Distribution of Myc levels in non-apoptotic and apoptotic wild-type epiblast cells (n = 8 embryos, 2,376 cells). Embryos in* ***j*** *were collected from various genetically equivalent litters and represent biological replicates. Dashed lines in* ***j*** *indicate averages. ***P < 0.001 by a mixed linear model with different variances per level. Taken from (Clavería et al., 2013)*

The physiological relevance of this mechanism has long been questioned since it had been observed only in genetically manipulated context. However, recent studies provided data suggesting that cell competition plays a role in physiological conditions. Indeed, it was shown that differences in Myc levels drive cell competition in mice embryos. Concomitantly, cells contain variable amounts of endogenous Myc in these embryos, and apoptosis occurs during early development in the cells that contain the least Myc (**Fig. 23** and Clavería et al., 2013). As Myc levels are the consequence of many signalling pathways regulated by metabolic health (cf. II.A), this could participate to remove unfit cells from the embryo. In addition, another study showed that BMP defective and tetraploid embryonic stem cells are eliminated from mice embryos before the onset of gastrulation. It was postulated that cell competition allows to identify and remove defective stem cells before the next developmental stages, where they undergo intense proliferation. Strikingly, Myc level differences were again shown to be necessary to establish cell competition in this case, suggesting that ribosome biogenesis intensity may be a vital parameter to select fit cells (Sancho et al., 2013).

2. Ribosome biogenesis drives cellular organization

The nucleolus is a membrane-less organelle, thought to form upon coalescence of ribosome biogenesis factors around the site of rDNA transcription. It has thus been described as an organelle made by the act of building ribosomes (Mélèse and Xue, 1995). One of its functions is to concentrate ribosome biogenesis factors at the site of ribosome production, but the nucleolus also plays an important role in nuclear organization. Not only does it separate many proteins from the nucleoplasm, it also recruits specific chromatin domains shaping genomic spatial organization and therefore gene expression. Importantly, the nucleolus is a highly dynamic structure, which disappears and reassembles during each cell cycle (cf. II.A.2). Being the site of ribosome synthesis, it is also very responsive to stress. Indeed, many cues that inhibit ribosome biogenesis trigger morphological changes, up to sheer disruption of the nucleolus, and these phenotypes are termed “nucleolar stress” (Boulon et al., 2010). Through this mechanism, ribosome biogenesis impairments impact the whole nuclear organization, causing massive changes in both gene expression and cell metabolism.

The nucleolar associated domains

The nucleolus forms around active rRNA genes, which can be found in the fibrillar centre in a de-condensed state (cf I.B.I). Meanwhile, inactive rDNA genes can be found in a layer of heterochromatin that surrounds the nucleolus, and that localization is required for rDNA stability (Guetg et al., 2010). But rDNA repeats are not the only residents of this peri-nucleolar heterochromatin layer. Indeed, many chromosomal loci are recruited in there, following a reproducible pattern. For instance, the Y and inactive X chromosomes associate preferentially to the peri-nucleolar layer in humans (Bobrow et al., 1971; Zhang et al., 2007). These Nucleolus Associated Domains (NADs) contain a high amount of satellite DNA, notably centromeric, and pericentromeric sequences (Németh and Längst, 2011). In *Drosophila* , their recruitment is mediated by the nucleolar protein Modulo, and is necessary to maintain the silencing of repetitive regions and maintain proper chromosome segregation during mitosis (Padeken et al., 2013). Telomeric sequences have also been shown to associate with nucleolar heterochromatin. In *Arabidopsis*, this association requires uc1, and its disruption results in drastic telomere shortening. Nucleolar heterochromatin also contains RNAPolII genes and transposable elements, which are maintained in a transcriptionally repressed state (Pontvianne et al., 2016).

NADs also contain a high amount of RNAPolIII genes, among which 5S rRNA, tRNA and U6 snoRNA genes (Németh and Längst, 2011; Thompson et al., 2003). Those have been shown to induce silencing of nearby RNAPolII promoters. This repression is dependent on active transcription by RNAPolIII and indeed, it is alleviated upon inhibition of ribosome biogenesis. As the loss of nucleolar localization correlated with the de-repression of proximal RNAPolII genes, it was postulated that tRNA silence nearby genes by changing their sub-nuclear localization (Wang et al., 2005). Interestingly, tRNA genes have also been shown to display insulator properties, and prevent the spread of heterochromatin. Unlike their function in proximal gene silencing, this property is independent of transcription by RNAPolIII (Raab et al., 2012). Indeed, the minimal requirement for this heterochromatin barrier activity is the binding of the pre-assembly complex component TFIIIC, which binds the B box on the tRNA genes internal promoter (Simms et al., 2008). As many tRNA genes cluster near the pericentromeric heterochromatin, their insulator property is thought to be necessary to delimit its boundaries (Noma et al., 2006). Another property of tRNA genes is their ability to establish cohesion points with the sister chromatin, further participating to genome stability. Importantly, this cohesion requires not only the binding of TFIIIC, but also active transcription by RNAPolIII (Dubey and Gartenberg, 2007).

Nucleolar sequestration

One could expect that all residents of the nucleolus take part in ribosome biogenesis but such is not the case. Among 4500 nucleolar proteins and molecules, only a third have been involved with ribosome biogenesis (Boulon et al., 2010). Indeed, the nucleolus is now thought to participate into several processes, including the biogenesis of many ribonucleoparticles (Boisvert et al., 2007; Pederson, 1998). However, one of its major functions is to alternatively sequester or release a number of proteins, thus allowing a rapid change in nuclear composition in response to stress cues (Nalabothula et al., 2010).

The nucleolus is a highly dynamic structure which continually exchanges proteins with other nuclear sub-compartments and with the nucleoplasm (Hernandez-Verdun, 2006). Several peptides sequences have been identified as nucleolar localization signals (NoLS), but no consensus could be described (For review: Emmott and Hiscox, 2009). Importantly, different NoLS target proteins to different components of the nucleolus, and the addition of a GC NoLS to the DFC protein fibrillarin was sufficient to mislocalize it, suggesting that nucleolar localization works in a hierarchical manner. Interestingly, in this experiment, Nop56 which interacts with fibrillarin, was also re-localized to the granular component, suggesting that its nucleolar localization is in fact driven by protein-protein interactions Lechertier et al., 2007). Indeed, nucleolar proteins form an intricate network of protein-protein interactions, and several key residents may work as hub proteins, *i.e.* proteins with more than ten specific interacting partners (Krasowski et al., 2008). For instance, nucleolin and nucleophosmin contain long disordered domains, which increases their surface, facilitating the binding of multiple ligands at the same time (Lam and Trinkle-Mulcahy, 2015). Thus, nucleolar localization may not be a consequence of an import machinery but rather that of specific interactions with either nucleolar proteins or nucleic acids.

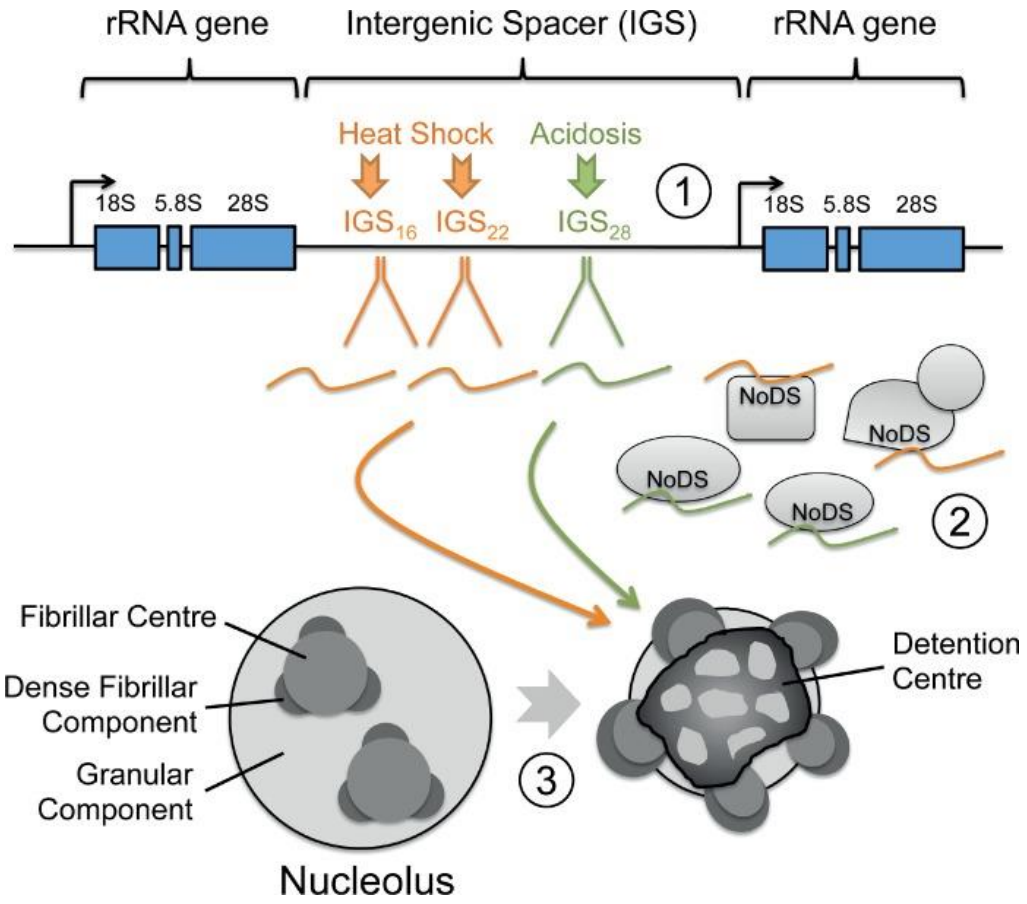

Figure 24. Structural/functional reorganization of the nucleolus in response to stress
(1) Stress stimulus-specific induction of long non-coding RNA transcripts from distinct regions of the intergenic spacer (IGS). (2) IGS transcripts bind and sequester/immobilize a diverse range of cellular proteins within the nucleolus. Interaction is mediated via a discrete nucleolar detention sequence (NoDS). (3) Formation of the nucleolar detention centre leads to restructuring of nucleolar architecture and silencing of ribosome biogenesis. Taken from (Lam and Trinkle-Mulcahy, 2015).

In response to many stress cues, the nucleolus changes its morphology. The severity of the changes varies depending on the nature and intensity of the stimulus, but a typical stress response is the topological separation of the nucleolus compartments, or "nucleolar segregation". As part of this mechanism, several long non-coding RNAs are transcribed by RNAPolI from the rDNA intergenic spacer (**Fig. 24**). These lncRNA display the ability to bind proteins containing a nucleolar detention signal (NoDS) and immobilize them inside a newly formed component of the segregated nucleolus: the detention centre (Audas et al., 2012; Jacob et al., 2013). On the contrary, many nucleolar proteins are released to the nucleoplasm upon ribosomal stress (Nalabothula et al., 2010). As a general feature, the nucleolar localization of these proteins isolates them from their co-factors or targets. The most extensively studied example is the nucleolar regulation of p53. Indeed, activating the "gatekeeper" first requires protecting it from its antagonist MDM2. This can be done a number of ways, notably by the $p14^{ARF}$ ($p19^{ARF}$ in mice) protein. It is however sequestered in the nucleolus through its interaction with the nucleolar hub protein nucleophosmin (NPM1). In response to genotoxic stress, both NPM1 and $p14^{ARF}$ are released to the nucleoplasm. The latter is then able to interact with MDM2, disrupting its association with p53 (Kruse and Gu, 2009).

3. Phenotypic consequences of ribosome biogenesis defects

Considering the absolute necessity for protein synthesis at the cellular level, it comes as no surprise that mutations affecting ribosome biogenesis are associated with dire phenotypes. Most of them adversely impact viability and fertility, but they also generate a very broad range of phenotypes, some of which can be hard to link with translation. While there is a considerable amount of data about the specific effects of ribosome impairments, some general features do emerge.

r-protein mutations in *S. cerevisiae*

The study of *S. cerevisiae* phenotypes upon ribosome biogenesis impairments provides insight about its importance at the cellular level. It comes as no surprise that the complete loss of most ribosomal proteins prevents proliferation. Indeed, 64 out of 79 r-protein genes are essential, and their conditional inhibition triggers the arrest of the cell cycle at specific checkpoint. They can however be studied by using heterozygous deletion strains. In most cases, they display a slow growth phenotype (Steffen et al., 2012; Thapa et al., 2013). Molecular study of the effect of their depletion on ribosome synthesis showed that the lack of any essential r-protein impairs the production of mature ribosomes. Indeed, mutant cells accumulate pre-subunits stalled at different maturation stages depending on the lacking r-protein (Ferreira-Cerca et al., 2005; Pöll et al., 2009). In contrast, non-essential r-proteins are not required for the production of mature ribosomes. They do however take part in its translational function, and their mutations most often result in very slow growth phenotypes (Baronas-Lowell and Warner, 1990; Briones et al., 1998; DeLabre et al., 2002; Peisker et al., 2008; Remacha et al., 1995). Thus, the reduction in growth rate is thought to result from a limitation of translation capacity.

Ribosomal protein gene loss of function alleles have been studied for almost a hundred years in *Drosophila*, where they are known as "*Minute*" mutations. They have puzzled researchers for decades. Indeed, mutations at more than 50 loci in the genome gave rise to similar phenotypes sharing the same genetic properties (Schultz, 1929). The latter were extensively studied, providing exceptional insight about the requirements for ribosomal protein genes in a developing organism.

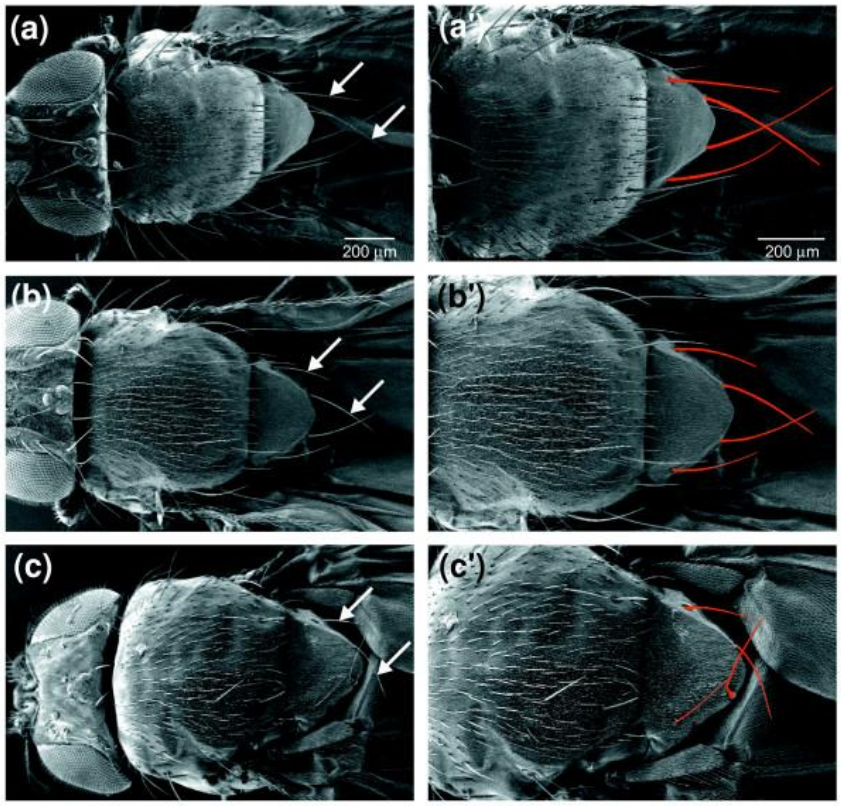

Figure 25. The Minute bristle phenotype
Minute flies have shorter and thinner bristles than wild type flies. This is most clearly seen by comparing the scutellar bristles, indicated here by the arrows and pseudocoloring. ***(a, a')*** *Wild type.* ***(b, b')*** *uS15^{1} heterozygotes.* ***(c, c')*** ***e****L14^{1} heterozygotes. Taken from (Marygold et al., 2007).*

All *Minute* mutations are dominant and lethal when homozygous. *Minute* mutants were first described for displaying thin and short (minute) bristles, together with prolonged development (Brehme, 1939). The vast majority of *Minute* mutations strongly impact viability and fertility, to the point that several *Minute* loci could only be identified through transient aneuploidy experiments and were proposed to be "extreme *Minute*" (Lindsley et al., 1972). Interestingly, the combination of different *Minute* mutations shows no cumulative effect on bristle length or development length. Additionally, *Minute* mutations display the same interactions with genetic modifiers. These data led to the hypothesis that *Minute* mutations affected different components of a single "*Minute* reaction", which requires all *Minute* genes to function. Furthermore, in triploid flies, these mutations were found to be recessive to two copies of a wild type allele. On the opposite, two copies of a *Minute* allele were lethal in presence of a single wild type allele. These experiments showed that the dominance of *Minute* mutations is the consequence of haplo-insufficiency. Thus, the core *Minute* phenotypes were attributed to the limitation of the "*Minute* reaction", consequence of the reduction in expression of one of its components (Schultz, 1929). *Minute* loci have been characterized over time and the *Minute* genes have now been identified to encode r-proteins with very few exceptions (Cook et al., 2012; Marygold et al.,

2007). Indeed, all the characteristics of *Minute* mutations are consistent with the "*Minute* reaction" corresponding to the synthesis of mature ribosomes.

In addition to bristle and development length phenotypes, *Minute* mutants display a broad range of developmental defects, which have been remarkably summarized by Jack Schultz: "*The eyes are larger and rougher than normal; the wings are blunt in shape, sometimes beaded. Their venation is slightly plexus-like, and the fifth vein may stop short of the wing margin.* Minute *flies have weak legs, and a somewhat pale body colour; the aristae may be reduced, the abdominal sclerites irregular. The post-vertical bristles of the head are frequently missing, and other bristles (notably the alars) are occasionally duplicated. The total body size may be smaller than normal. Females are likely to be sterile, and are generally weaker than males. Most striking of all the characters of the* Minutes*, however, are the retardation of development and the elimination of chromosomes in somatic cells*" (Schultz, 1929). Indeed, it was proposed that certain tissues are more dependent on rapid translation ability during development, thus explaining why *Minute* phenotypes appear organ-specific. However, different *Minute* mutations trigger specific sets of organ failures. If all *Minute* phenotypes were the consequence of suboptimal synthesis of ribosomes, one could expect that every *Minute* mutation should give rise to the same phenotypes, albeit with varying severity. Several hypotheses can reconcile these observations. First, ribosome composition may differ between tissues, which would thus display specific sensitivity to the loss of only a subset of r-proteins. Indeed, r-proteins have been shown to possess tissue-specific expression patterns in *Drosophila* and mammals (Kearse et al., 2011; Kondrashov et al., 2011). A second explanation would be that r-proteins impact development through their numerous ribosome-independent functions (Warner and McIntosh, 2009). The relative contribution of the ribosomal and extra-ribosomal functions of r-proteins to the *Minute* phenotypes still remain to be investigated.

Mutations in ribosome biogenesis components are responsible for a series of rare human diseases termed “ribosomopathies”. Like *Minute* mutations, they are associated to a number of organ-specific failures and congenital malformations. The different ribosomopathies and their pathology have been extensively reviewed in Danilova and Gazda, 2015; Nakhoul et al., 2014.

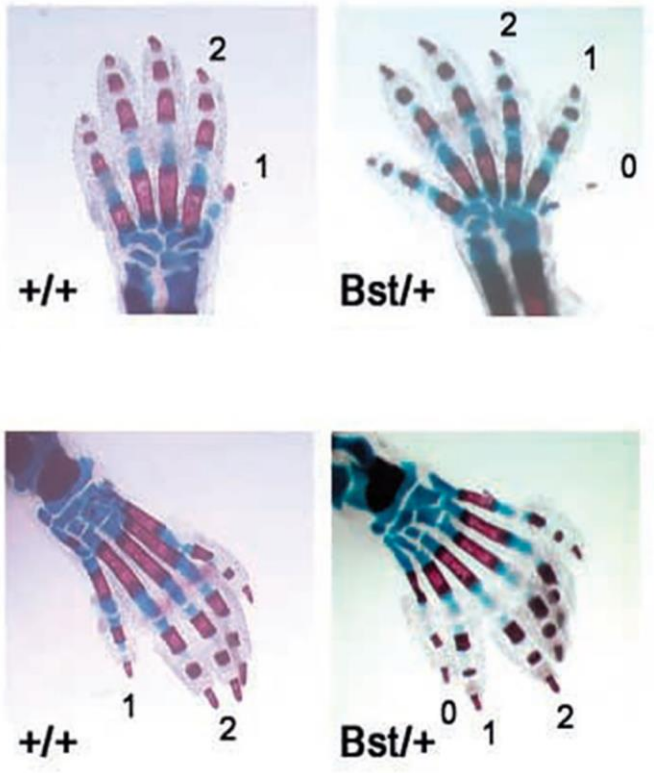

Figure 26. Duplicated digits and phalanges in mice heterozygous for eL24.
Skeletal stain of newborn fore limbs (upper) and hind limbs (lower). Mice heterozygous for a mutation in eL24 *(*Bst*/+ phenotype) show preaxial polydactyly (0) and triphalangy of the first digit (1). Taken from (Oliver et al., 2004)*

Mutation in several ribosomal protein genes (*eS7, 10, 17, 19, 24, 26, 27, 28; uS14; eL15, 27, 31, 33; uL5, 18, 24*) have been associated to Diamond-Blackfan Anemia (DBA) in humans. This syndrome is characterized by pure red cell aplasia, growth retardation and congenital malformations of the head, upper limb, kidney or heart. They also display increased cancer predisposition. These phenotypes are conserved to some extent in different species, which are used as models to study ribosomopathies (For review: Yelick and Trainor, 2015). For instance, the belly spot tail mutation (loss of function of *eL24*) in mice leads to the formation of a supernumerary finger, and malformation of the first digit, which is similar to abnormalities observed in Diamond-Blackfan Anemia patients (**Fig 26**, Oliver et al., 2004).

Similarly to *Minute* mutants, the rationale behind global translation defect giving rise to such specific phenotypes is poorly understood. One explanation for the consistent phenotypes between different ribosomopathies is the observed upregulation of p53 activity. This was proposed to cause apoptosis in erythropoietic progenitors and neural crest cells, thus leading to bone marrow failure and craniofacial malformations. Indeed, inhibition of p53 rescued the differentiation defect phenotypes in *uL18* and *eS19* mutant mice (Singh et al., 2014). But despite there being a set of core common phenotypes, different mutations do cause unique phenotypes. For instance, mutations in *uL5* gives rise to thumb malformation, while disruption of *uL18* leads to cleft palate formation (Bursać et al., 2012). Similarly,

mutations in *eL33* cause genito-urinary malformations (Boria et al., 2010). Several observations offer a basis to reconcile the ubiquity of ribosome biogenesis with the specificity of ribosomopathies' phenotypes: i) ribosomes participate in tissue-specific functions, notably gene regulation. ii) ribosome components carry important functions out of the ribosome.

III. Ribosomes regulate gene expression: the second lives of the housekeepers

The idea that some genes are dedicated to the cell's basic metabolism has been longstanding. These housekeeping genes would be constitutively expressed in all cells, at all times (Eisenberg and Levanon, 2013). Logically, they would be essential for cell survival and require no regulation mechanism whatsoever. Ribosomal biogenesis components perfectly fitted that idea, and were thus considered housekeepers. Unfortunately, "nature was not designed to make life easy for biologists" (Tudge, 2006), which came to realize that even the housekeepers have days off. Indeed, beside doing the cell's laundry, housekeeping genes have a life of their own, and engage in many activities. Thus began the quest for biologists to discover what the housekeepers do when they are not polishing the silverware (after re-counting the silver spoons, though).

A. Ribosome-mediated regulation of translation

In the absence of powerful techniques to study proteins, mRNA levels have long been used as proxies to estimate protein abundance. The advent of quantitative mass spectrometry and its tremendous improvements in the recent years opened new perspectives in gene expression research (Ong and Mann, 2005). Notably, the correlation between mRNA and corresponding protein levels were soon found to be surprisingly low. Indeed, depending on organisms and environmental context, mRNA abundance only explain around 40% of the variation in protein levels, suggesting that translation and degradation are major components of gene expression regulation (Abreu et al., 2009; Vogel and Marcotte, 2012). Apprehending the importance of translation regulation has raised concerns, as it seems to render transcription regulation somewhat superfluous. However, a study showed that upon drug treatment, differentially expressed mRNA correlated with protein levels more than steady mRNA (Koussounadis et al., 2015). These data imply that, as expected, transcriptional regulations are reflected at the protein level. Indeed, it has been proposed recently that under steady-state conditions, protein levels could be estimated from mRNA levels by applying to each gene an RNA-To-Protein (RTP) ratio. Strikingly, this ratio was found to vary by orders of magnitude between genes, but to be independent of cell type (Edfors et al., 2016; Silva and Vogel, 2016). Paradoxically, these theories question in turn the necessity for translational regulation. It should however be considered that they spawn from high-throughput analyses and reflect general trends. As such, they do not account for individual genes or gene groups. Furthermore, it is questionable whether they still hold true under stress induction, when ribosome biogenesis is heavily altered. Indeed, an exciting hypothesis would be that regulation of transcription and translation serve different purposes. For instance, it is believed that translational regulation has a much quicker impact on metabolism that transcriptional regulation, and is thus more fit to accommodate stress response mechanisms.

1. Ribosomes interact with mRNA cis-regulatory elements

While many mechanisms tune general translation through the number of ribosomes (cf. II.A), it is important to note that translational activity can be regulated in a mRNA-specific manner. The affinity of the ribosome for specific mRNA, and the efficiency of translation are critical parameters in gene expression. Indeed, cells contain a finite pool of ribosomes and translation factors, for which mRNAs must compete (Chu et al., 2011; Raveh et al., 2016). Accordingly, their untranslated sequences abound with cis-regulatory elements which influence ribosome recruitment or initiation rate, and allow spatiotemporal control of protein synthesis (For review: Araujo et al., 2012).

The Kozak sequences

Translation initiation typically requires that the initiation complex scans a mRNA until finding an appropriate codon (cf I.A.2.). However, some mRNA displays leaky scanning, where the first AUG codon is not always selected for initiation (Kozak, 2002). Indeed, the sequence context has been shown to be critical for initiation efficiency, directly influencing translation rate and start codon choice. The optimal sequence, also known as the Kozak sequence (GCC**A/G**CCaug**G**), has been shown to yield 20 times more protein than weak sequences. Interestingly, the presence of a purine at the [-3] position and a guanine at [+4] contributes the most to initiation efficiency (Kozak, 1986). It was postulated that AUG codon selection was enhanced by ribosome stalling mediated by base specific interactions. Indeed, uS19 interacts with both a U or G at the [+4] position, though other bases were not tested. More interestingly, uS7 interacts with a U at the [-3] position but not with a G, possibly underlying base discrimination mechanisms for AUG selection. Similarly, eS26 was shown to bind a U between positions [-8] and [-11] (Pisarev et al., 2006). Strikingly, ribosomes lacking eS26 were shown to translate mRNA with weak Kozak sequences more than complete ribosomes. Those mRNA are enriched for specific stress response pathways. Cells lacking eS26 expression constitutively activate those response pathways suggesting that incorporation of eS26 in the ribosome may be a mechanism that modulates the translational landscape (Ferretti, 2015, 10th EMBO conference on ribosome synthesis, unpublished data).

Upstream open reading frames

Initiation codon selection is a determinant factor in translation. Indeed, many mRNA possess several potential initiation sites, with different outcomes for gene expression. Strikingly, a huge proportion of mRNAs contain AUG codons 5' of the canonical initiation site (44% in mice, 49% in humans) (Calvo et al., 2009). While those may promote the translation of long isoforms of the canonical protein, most of them are not in frame with the main coding sequence, or are separated from it by a termination codon. In the latter two occurrences, ribosomes can be recruited to translate the upstream open reading frame (uORF), which may either inhibit or facilitate translation of the canonical CDS, depending on mRNA topology.

The presence of an uORF typically results in a 30-80% reduction of the translation of the main ORF. Several mechanisms participate to this repression: i) the majority of ribosomes may dissociate after translation of the uORF, thus never reaching the main ORF. Ii) the uORF may overlap with the main ORF, thus preventing the scanning of the AUG proper. iii) preventing ribosomes from translating the main ORF may facilitate degradation of the mRNA by the NMD pathway (For review: Somers et al., 2013). However, some uORFs positively affect gene expression by reducing the translational inhibition induced by *cis*-regulatory elements. For instance, translation of an uORF was shown to allow ribosomes to skip a repressive stem loop structure in the 5'UTR of a mRNA and reach the main ORF, a process called ribosome shunting (Hemmings-Mieszczak et al., 2000).

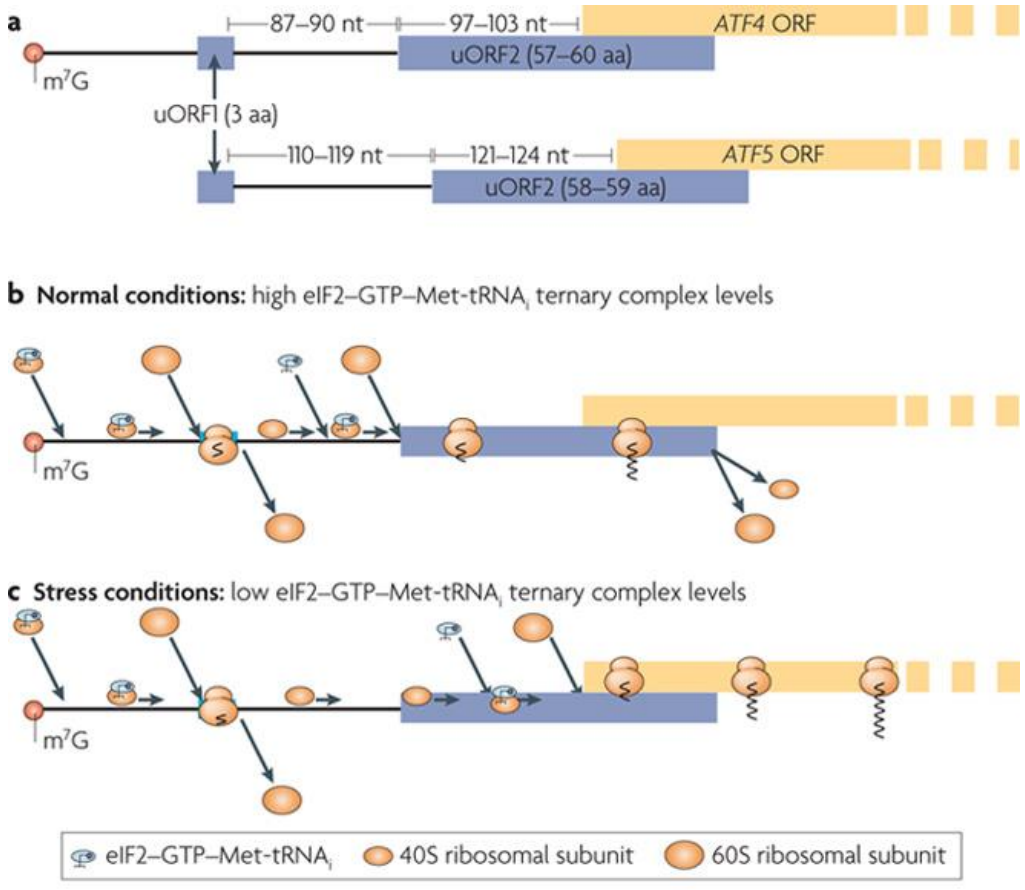

Figure 27. The mechanism of regulation of ATF4 and ATF5 mRNA translation.
(a) Diagram of the two upstream open reading frames (uORFs) in human, mouse, rat, cow and chicken activating transcription factor 4 (ATF4) mRNAs and the four mammalian ATF5 mRNAs. (b) The pattern of translation in control (unstressed) conditions, when eukaryotic initiation factor 2 (eIF2)–GTP–Met-tRNA$_i$ ternary complexes (eIF2-TCs) are abundant. In this case, most of the 40S subunits that resume scanning after uORF1 translation will acquire a new eIF2-TC in time to initiate translation of uORF2, and ribosomes that translate this second uORF will

be unable to initiate at the ATF4 or ATF5 AUG. (c) Pattern of translation in stressed conditions, when eIF2-TC availability is low, for instance owing to eIF2 phosphorylation. Most of the 40S subunits that resume scanning after translating uORF1 acquire a new eIF2-TC only after they have migrated past the uORF2 initiation codon, but in time to initiate at the next AUG, which is at the start of the ATF ORF in both cases. Taken from (Jackson et al., 2010)

The disposition of uORFs and their combination with other regulatory elements are the basis of very elaborate regulation schemes. For instance, the *Drosophila* female-specific factor Sex lethal (Sxl) was shown to bind the 5'UTR of the *male specific lethal 2* (*msl-2*) mRNA, resulting in the activation of an uORF, and the repression of the main ORF (Moschall et al., 2017). In another instance, uORF translation also permits stress-dependent activation of a specific ORFs, owing to a delay in a translation re-initiation (**Fig. 27** and Jackson et al., 2010). Thus, gene expression can be regulated during development or stress induction through the affinity of ribosomes for different AUG codons.

Messenger RNAs can display secondary structures, and those who are located in the 5'UTR region generally antagonize translation (Davuluri et al., 2000). Indeed, stable stem-loop structures were shown to block the scanning 43S PIC and prevent initiation of translation (Gray and Hentze, 1994). Some structures, however, have the paradoxical ability to recruit ribosomes to mRNAs independently of the scanning mechanism. They are thus called internal ribosome entry sites (IRES).

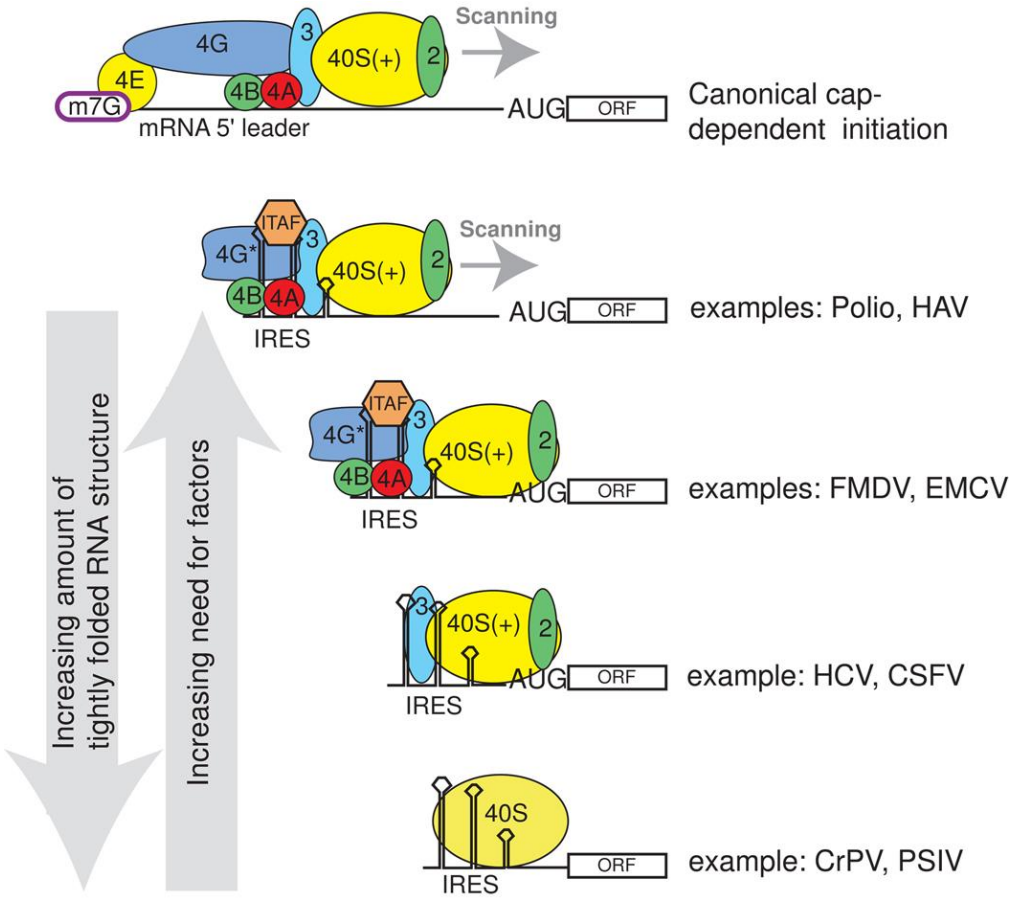

Figure 28. Examples of the diversity of viral IRES factor requirements
Canonical initiation requires the full complement of translation eIFs (top), while IRES initiation can use subsets of these factors as well as IRES trans-acting factors (ITAFs). Shown are examples of some viral IRES with the factors each requires. For simplicity, all the factors associated with the 40S subunit are not shown. As a trend, IRES RNAs with the most inherent stably folded structures (left arrow) are those that require the fewest factors, and as the IRES becomes less inherently structured, more ITAFs and eIFs are needed (right arrow). Taken from (Filbin and Kieft, 2009)

IRES elements were first discovered in viral mRNAs, and found to allow the translation of these cap-less messengers. They are not restricted to viruses, and it has been estimated that more than 10% of cellular mRNAs may possess IRES features. These elements share remarkably few structural features, which complicates their systematic discovery. However, they do share the property to recruit the pre-initiation complex in a cap-independent manner, with reduced requirements for translation initiation factors (**Fig. 28**). Thus, IRES-mediated translation escapes general repression of translation by 4E-BP or limiting initiation factor concentrations. Indeed, IRES-containing messengers are still translated under stress conditions (Spriggs et al., 2008).

Interestingly, different IRES groups show specific requirements for ribosome components and modifications. Thus was it found that a defect in rRNA pseudouridylation caused by the impairment of

DKC1 caused a specific loss of IRES-mediated translation of a subset of mRNAs, including *p53* (Montanaro et al., 2010; Yoon et al., 2006). Similarly, the recruitment of ribosomes to some groups of IRES has been shown to require specific r-proteins (Horos et al., 2012; Landry et al., 2009). Furthermore, it was found that viral IRES-bound ribosomes display a different pattern of ribosomal protein methylation than host mRNA-bound ribosomes (Ong and Mann, 2005). Altogether, these data suggest that mRNA translation specificity may be regulated not only by ribosomal protein contents, but also by rRNA and r-protein modifications.

Ribosomal proteins are abundant, bind nucleic acids unspecifically, are susceptible to aggregation, and populate all cellular components. Those properties hinder the analysis of their interactions with other molecules. Indeed, they have historically been discarded as contaminants from classical molecular biology experiments, up to even recent mass-spectrometry analysis workflows (Dahlberg et al., 2003; Mellacheruvu et al., 2013). Indeed, while many translation regulators are known, their regulatory mechanism is only poorly understood.

RNA binding factors

Experimental studies have identified more than 800 mRNA binding proteins in mammals, many of which potentially regulate translation (Baltz et al., 2012; Castello et al., 2012). Several such regulators have already been characterized which display context dependant activity. The *Drosophila* sex lethal protein represses translation in females (cf III.A.1), and the Iron Response Element binding protein (IRE-BP) does the same in the absence of iron (Hentze and Kühn, 1996; Moschall et al., 2017). Similarly, the expression of 15-lipoxygenase is repressed by hnRNPK and hnRNPE1 at the translational level in erythroid precursors (Ostareck et al., 2001).

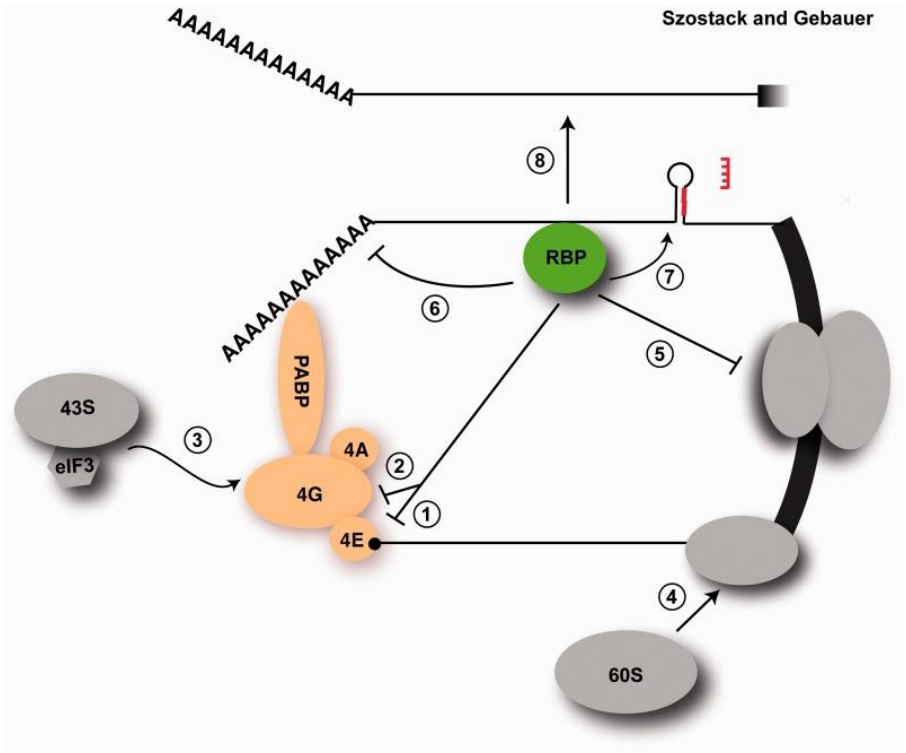

Figure 29. Mechanisms of translational regulation by 3'-UTR-binding proteins.
Large ovals depict the small (43S) and large (60S) ribosomal complexes. The initiation factors that participate in closed-loop formation are indicated. A miRNA, as well as its binding site on the target mRNA, is also highlighted. (1) Recruitment of eIF-4E isoform eIF4EHP which displays low affinity for eIF-4G. (2) Inhibition of eIF-4G binding to eIF-4E. (3) Inhibition of ribosome recruitment. (4) Inhibition of 60S subunit joining. (5) Attenuation of translational elongation. (6) Deadenylation of the poly(A) tail. (7) Modulation of miRNA activity. (8) Promotion of inter-molecular interactions. Taken from (Szostak and Gebauer, 2013).

RBP are mostly repressors that may interfere with a number of translation steps. As a general feature, they primarily target the initiation step, by hindering ribosome recruitment (**Fig. 29, 1-4**). The mechanistic bases for this repression are rather poorly known, and do not necessarily involve interaction with ribosomes. On the other hand, a few examples of alternative mechanisms have been shown, which specifically target translating ribosomes. For instance, human PUM2 and hnRNP E1 were shown to induce ribosome stalling during translation elongation (Friend et al., 2012; Hussey et al., 2011).

Among regulators of translation, micro RNAs (miRNAs) are particularly important for their ability to coordinate the expression of hundreds of transcripts. miRNA display the ability to both inhibit translation and promote mRNA degradation. However, to know which mechanism is responsible for the bulk of miRNA-mediated regulation of mRNA expression is a decade-long debate (Jonas and Izaurralde, 2015; Wilczynska and Bushell, 2015). Furthermore, the mechanisms by which miRNA affect translation are also unclear. All steps of translation have been proposed to be regulated by miRNAs, including ribosome recruitment, initiation, elongation, and termination (Gu et al., 2009; Mathonnet et al., 2007; Nottrott et al., 2006; Petersen et al., 2006; Pillai et al., 2005). Most of these data are however subject to controversy. However, it is interesting to note that the small subunit r-protein RACK1 has been shown to interact with components of the RISC complex in worms and humans, and is necessary for the association of miRNAs with polyribosomes (Jannot et al., 2011). These data suggest that direct interaction with the ribosome may underlie a part of miRNA functions in translational repression.

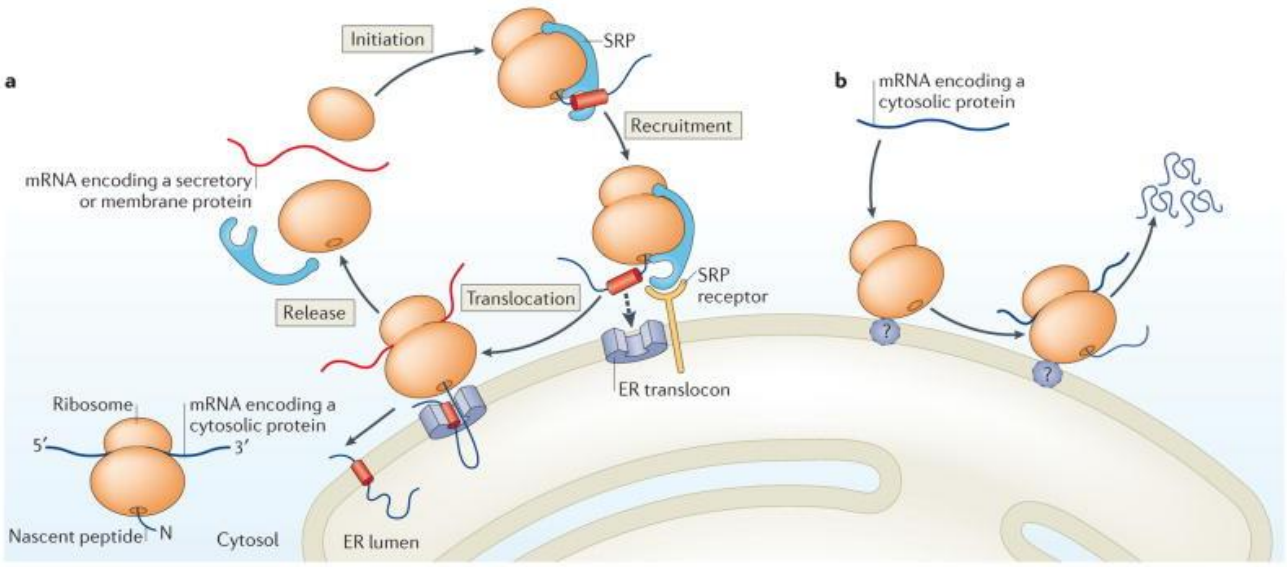

Figure 30. Model for translational compartmentalization.
***a** | Translation initiation begins in the cytosol. Ribosomes translating mRNAs encoding cytosolic proteins that lack a topogenic endoplasmic reticulum (ER)-targeting signal remain in the cytosol. By contrast, ribosomes translating mRNAs that encode a protein containing a signal peptide or a transmembrane domain (such as secretory and integral membrane proteins) are targeted to the ER co-translationally by the SRP. **b** | Translation initiation can occur directly on the ER. Moreover, mRNAs that encode cytosolic proteins can also be translated by ER-bound ribosomes. Thus, a large fraction of the proteome can be translated by ER-associated ribosomes. Taken from (Reid and Nicchitta, 2015).*

Many proteins are addressed to a specific subcellular compartment. In most cases, this is achieved by the recognition of a proteic signal and subsequent import by a variety of shuttling pathways. However, as an alternative, proteins can be translated at the location that requires their function. Indeed, several such instances have been reported, with the most famous one being the translation of proteins at the ER membrane (**Fig. 30**). Indeed, upon recognizing signal sequences on nascent polypeptides, the signal recognition particle (SRP) binds the ribosome by contacting rRNA and r-proteins uL23 and uL29. Interestingly, while the SRP can bind signal sequences post-translationally, these interactions with the ribosome greatly improve its binding affinity. SRP binding induces a halt in translational elongation, and the translocation of the ribosome to the ER membrane, where it binds the SRP receptor and resumes translation (For review: Akopian et al., 2013). In a very similar manner, the Nascent chain-associated complex (NAC) is able to bind peptides co-translationally, and promotes the association of ribosomes with the mitochondria outer membrane (George et al., 2002; Wang et al., 1995).

One of the most puzzling cases of local translation comes from neurones. These highly polarized cells display extreme specialized morphology. Neuronal translation not only occurs at the periphery of the nucleus, but also in dendrites with functions in synaptic plasticity, and developing axons to promote growth, guidance and regeneration (for review: Rangaraju et al., 2017). Local translation requires the presence of the translation machinery in the dedicated subcomponents, and indeed, ribosomes have been identified in both axons and dendrites. Interestingly, axonal ribosomes are found in discrete cortical plaque-like structures termed periaxoplasmic ribosomal plaques, where they are bound to a matrix (Koenig and Martin, 1996). In addition, ribosomes have been found tethered to the membrane in axons and dendrites by association with the receptor DCC. Indeed, DCC was shown to interact with a number of small and large subunit r-proteins through its cytoplasmic domain, therefore inhibiting

translation. Upon the binding of its ligand Netrin-1, it dissociates from ribosomes, thus allowing translation to initiate in a signal-dependent and local manner (Tcherkezian et al., 2010).

3. Ribosome heterogeneity

For a coding gene to be transcribed does not guarantee that it will be translated. Many regulatory mechanisms participate in translation regulation, from *cis*-regulatory elements to *trans*-acting factors. The importance of those mechanisms was epitomized by the discovery of *Hox* mRNA translational regulation in mammals (Xue et al., 2015). Indeed, some of those genes, which display exquisite transcriptional regulation patterns studied for decades, were shown to simply not be translated in the absence of r-protein eL38. This example is only part of a rising amount of data on translation regulation mechanisms, which have led to the general idea that studying transcription alone is not sufficient to explain gene expression. This domain of genetics is still largely unexplored, and many questions remain open. While it is now admitted that different mRNAs have unique affinity for ribosomes, it should be considered whether the reverse is true. Are all ribosomes the same? Or can translation be regulated by tampering with the translator?

The Ribo-interactome

The ribosome possesses a large solvent exposed surface, where protein-protein and RNA-protein interactions are likely to occur. Indeed, many proteins bind the ribosome, and participate in translational regulation (cf. III.A.1 and III.A.2). However, many known examples involve ribosome binding in a nascent peptide or mRNA specific manner. An inventory of proteins that associate to the ribosome itself has recently been described in mouse embryonic stem cells, and termed the ribo-interactome (**Fig. 31** and Simsek et al., 2017).

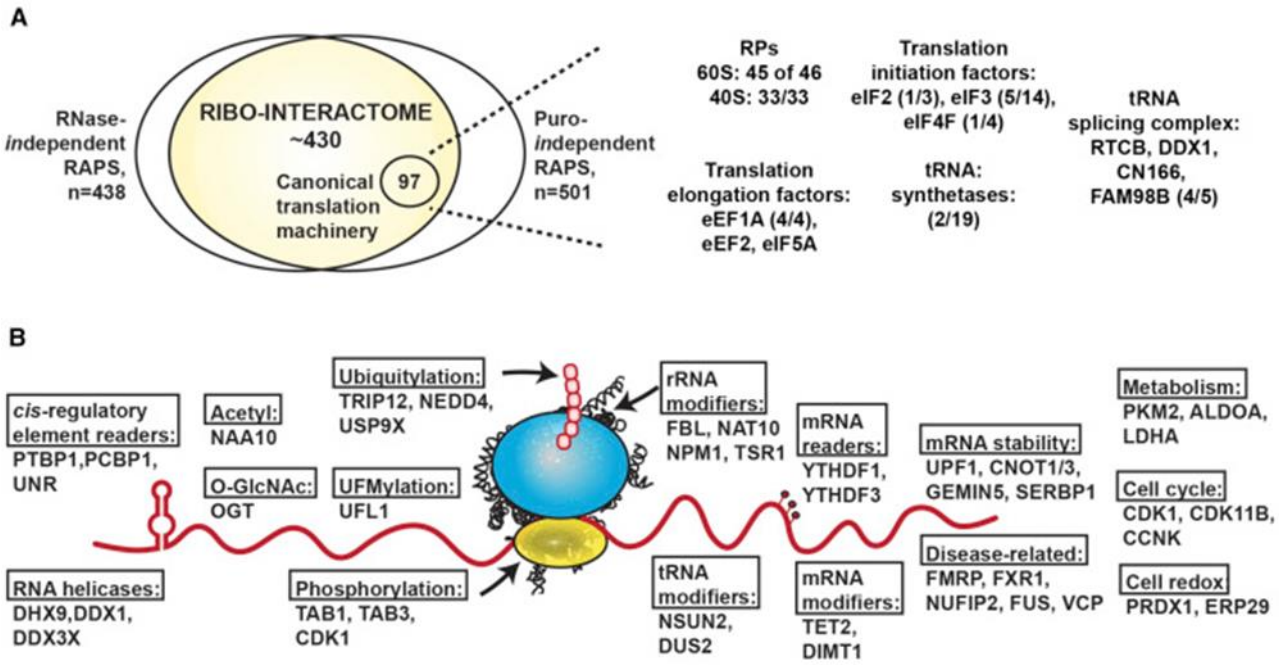

Figure 31. The ribo-interactome consists of diverse functional groups of proteins.
(A) The ribo-interactome is defined as the intersection of RNase-independent and puromycin-independent interactions. The number of identified proteins related to canonical translation machinery in the MS experiments is presented along with the known number of factors in each class. (B) The ribosome as a hub for interactions

with a multitude of proteins with diverse functions. Representative examples of direct ribosome interactors found in each functional group are presented. In the schematic, the pink circles represent the nascent peptides; red circles on the mRNA represent mRNA modifications. Taken from (Simsek et al., 2017).

Strikingly, more than 400 proteins were found to bind the ribosome, and belong to a variety of functional groups. Further study of the association of PMK with the ribosome showed that it only bound a sub-pool of ER-bound ribosomes. These data prove that Ribosome associated proteins (RAP) can generate ribosome diversity. Indeed, it is expected that all ribosomes are not bound by all four hundred RAPs at the same time. It is also likely that the repertoire of RAPs may differ between cell types or upon cue induction. Thus, the combination of ribosome interactants can generate nearly unlimited ribosome diversity with so far unknown effects on their translational activity

Along with the idea that ribosomal components were housekeeping genes, existed the assumption that they would be monotonously expressed in all cell types. The ribosome has thus long been envisioned as a molecular complex with fixed stoichiometry. However, it has been known for a long time that r-protein genes are expressed at different levels across tissues (Bortoluzzi et al., 2001). In addition, r-protein mutations have been known to cause tissue-specific phenotypes, and to affect the translation of a subset of mRNAs (Kondrashov et al., 2011). These data led to the idea that ribosome composition could be variable, with consequences on gene expression.

The study of the duplicated r-protein genes in *S. cerevisiae* provided invaluable information. Indeed, it was observed that deletion of any duplicated r-protein gene conferred different phenotypes than its paralog, contradicting the hypothesis of redundancy. It was thus hypothesized that ribosome composition could be modulated by r-protein composition or post-translational modifications. The limitless amount of possible combinations may thus be considered a "ribosome code", giving rise to a variety of functionally different ribosomes, and controlling the translational program (Komili et al., 2007). While the difference in phenotypes for paralogs deletion has now been proposed to rise from gene expression specificity rather than translational function differences, the ribosome code hypothesis has now been reinforced by a large amount of data (Parenteau et al., 2015).

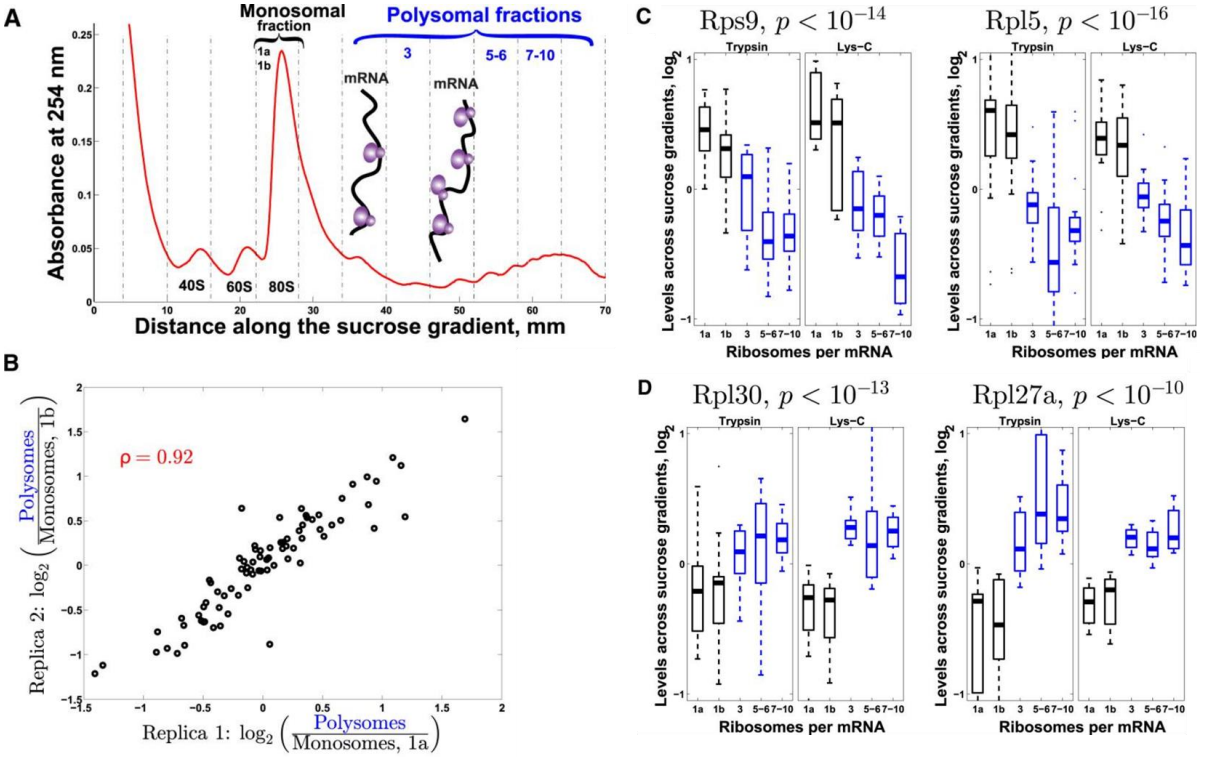

Figure 32. The Stoichiometry among r-proteins in Mouse Ribosomes Depends on the Number of Ribosomes per mRNA.

(A) Velocity sedimentation in sucrose gradients allow separating ribosomes that are free or bound to a single mRNA (monosomes, depicted in black) from multiple ribosomes bound to a single mRNA (polysomes, depicted in blue). The vertical dashed lines indicate the boundaries of the collected fractions. Fractions are labeled at the top with numbers reflecting the number of ribosomes per mRNA. (B) Replicate MS measurements of the monosomes (A and B) indicate reproducible estimates for r-protein enrichment in polysomes. (C and D) Some r-proteins are enriched in monosomes (C) and others in polysomes (D). The relative levels of each r-protein are quantified as the

median levels of its unique peptides, and the probability that the r-protein levels do not change across the quantified fractions is computed from ANOVA (indicated at the top). The distribution levels of all unique peptides from trypsin (left panels) and from lys-C (right panels) digestions are juxtaposed as boxplots to depict the consistency of the estimates across proteases, different peptides, and experiments. Adapted from (Slavov et al., 2015).

Importantly, it was found that the stoichiometry of r-proteins within ribosomes is variable. Indeed, most of them are enriched in either heavy polyribosomes or monosomes in yeast and mammals (**Fig. 32** and Slavov et al., 2015). Moreover, substitution of the energy source from ethanol to glucose triggered a change in r-protein stoichiometry in yeast, correlating with an increase in polyribosome to monosome ratio. The fact that r-proteins display different stoichiometry implies that they are not contained in every ribosome, and by consequence, that ribosomes are heterogenous. Importantly, the pattern of r-protein enrichment in regard to translational activity was found to be conserved between yeast and mouse, suggesting that it may underlie a conserved mechanism.

Another important concern rises from the biogenesis of such diverse ribosomes. Indeed, it is puzzling that ribosomes lacking r-proteins would be routinely generated while so many r-proteins are required for their maturation. An important clue may come from the observation that the r-proteins that vary the most are located at the surface of the ribosome, while the ones that are steadier are usually buried within. Interestingly, r-proteins located at the periphery of the ribosome are known to dissociate more easily than the innermost ones (Piir et al., 2014). Furthermore, it was shown that uL13 is both phosphorylated and released from the ribosome in response to interferon-γ signalling (Mazumder et al., 2003). It is thus tempting to hypothesized that ribosomes would be matured as complete complexes, and that the surface-most r-proteins would be able to dissociate under specific conditions.

Both the ribosomal RNA and proteins are heavily modified in mature ribosomes (cf. I.B.3 and Lee et al., 2002; Yu et al., 2005). Many such modifications are believed to be required for canonical maturation of the ribosome, and to be therefore constitutive. For instance, mutation of histidine 243 residue site of uL3 to an alanine was found to trigger the accumulation of pre-rRNA intermediates and defects in translational elongation (Al-Hadid et al., 2016a). However, snoRNAs expression is known to fluctuate with the circadian rhythm and change between cell types, suggesting that some rRNA modifications may also be the target of regulations (Castle et al., 2010; Hughes et al., 2012). Similarly, the pattern of r-protein modifications was found to be highly variable between tissues (Williamson et al., 1997), life stages (Mangiarotti, 2002; Ramagopal, 1991), or cell cycle phases (Chang et al., 1978). It is thus likely that ribosome modifications participate in generating ribosome diversity.

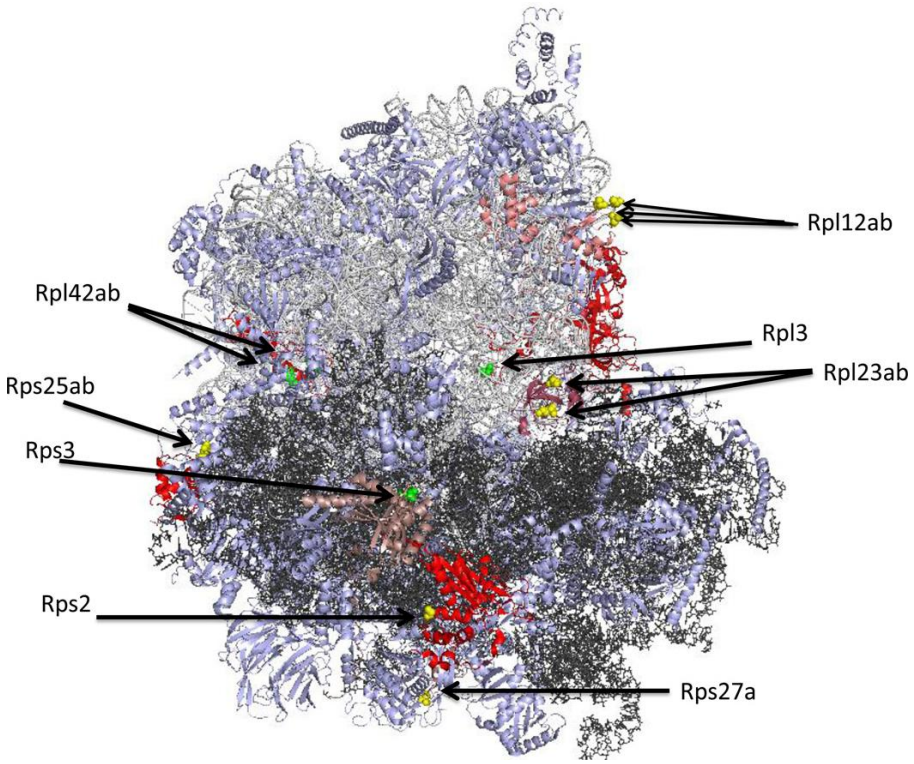

Figure 33. Surface and buried sites of methylation on cytoplasmic ribosomal proteins in the yeast Saccharomyces cerevisiae.
The 25S ribosomal RNA of the large subunit is shown in light gray; the 18S ribosomal RNA of the small subunit is shown in dark gray. Non-methylated proteins are shown in light blue; methylated proteins are shown in pink (Rpl12ab, Rpl23ab, Rps27a, Rps3) and red (Rpl3, Rps2, Rps25ab, Rpl42ab). The approximate positions of surface-exposed methyl groups are shown as yellow spheres; buried methyl groups are represented as green spheres. The illustration was made using PyMOL from the PDB structures 3U5F, 3U5G, 3U5H, and 3U5I. Taken from (Clarke, 2013).

Many r-protein post-translational modifications (PTMs) have been identified, including lysine, di- and tri-methylation, phosphorylation, acetylation, SUMOylation and ufmylation. Their functional significance is however poorly characterized. Interestingly, several such modifications have been shown to be exposed at the surface of the ribosome, where they would be accessible for interactions with translation factors, or other RAPs (**Fig. 33** and Clarke, 2013). Interestingly, the deletion of several

ribosomal protein methyltransferases in yeast caused in most cases no defect in ribosome biogenesis or translation initiation. The deletion mutants however displayed decreased translation fidelity during elongation and termination (Al-Hadid et al., 2016b). These data suggest that r-protein PTMs indeed modulate the translational properties of the ribosome.

B. Extra-ribosomal functions of r-proteins

Once considered full-time constituents of the ribosome, r-proteins are now studied for their participation in many cellular processes. While a substantial part of their contribution to cell metabolism has been attributed to their ability to alter ribosome behaviour with consequences on protein synthesis, it has been known for a long time that some ribosome-free r-proteins also carry regulatory activities, consequently termed “extra-ribosomal functions”. The increasing number of such examples over the last decades led to the idea that those would be a general feature of r-proteins. However, the existence of a genuine extra-ribosomal function is hard to prove and harder to study. Three criteria must be met (Warner and McIntosh, 2009). 1) The r-protein interacts with a non-ribosomal component. 2) This interaction must have a physiological effect. 3) It occurs away from the ribosome. Since tampering with an r-protein is expected to cause translation defects, with extensive effects on physiology, careful attention must be paid to specifically attribute observations to the extra-ribosomal function alone. This can be difficult as most of these functions are involved in the regulation of ribosome biogenesis, or response to nucleolar stress, with expected effects on ribosomal activity. Solving this conundrum is no small feat, explaining why despite numerous observations implicating r-proteins in various processes, readily characterized extra-ribosomal functions are still scarce.

1. When are r-proteins free?

The idea that r-proteins carry regulatory functions out of the ribosome is problematic on several levels. Indeed, extensive studies about their role in ribosome biogenesis yielded the notion that their existence is very tightly controlled, and that they are very unstable on their own. Thus, it seems important to question under which circumstances can r-proteins exert functions out of the ribosome. In the next section, several studies are mentioned which use the r-protein mediated stabilisation of p53 as a readout for the ability for r-proteins to perform their extra-ribosomal functions. For clarity purpose, the underlying mechanism of this stabilisation will be detailed in a further section (cf. III.B.2).

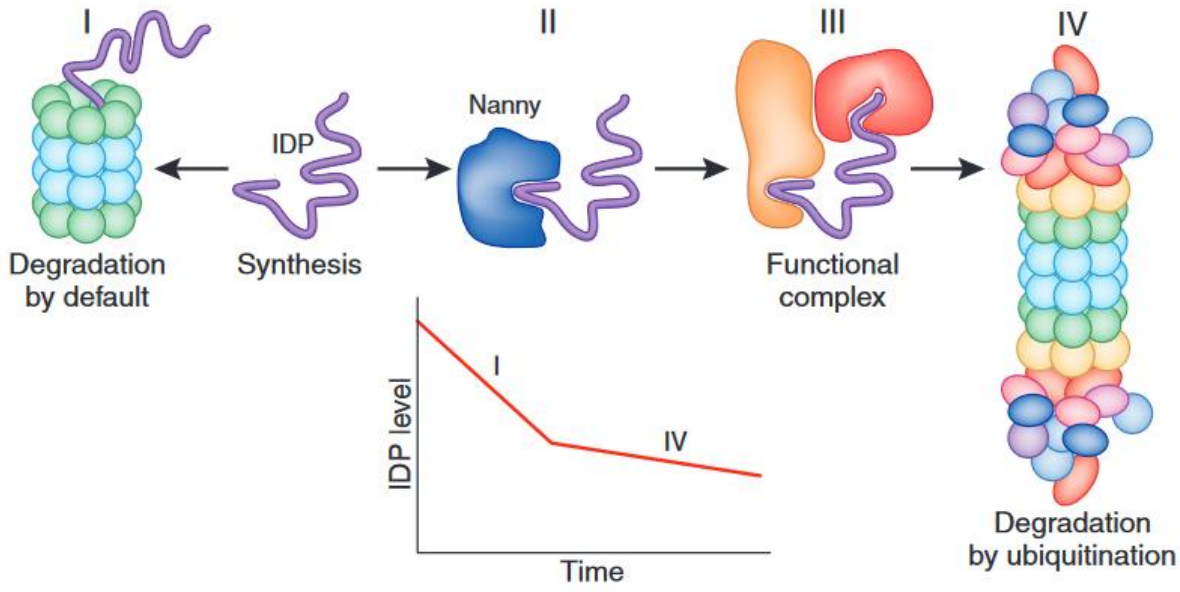

Figure 34. The nanny model.
Once an Intrinsically disordered protein (IDP) is synthesized, it is susceptible for ubiquitin-independent degradation by the 20S proteasome (I) unless the disordered segment is masked by a nanny that binds the newly synthesized IDP (II). The binding of the nanny to the client IDP is a transient process enabling the proper maturation and formation of the functional complex (III). Once in a complex, the IDP is refractory to degradation by default and can only be degraded by the ubiquitin-dependent pathway mediated by the 26S proteasome (IV). The decay kinetics of the two degradation processes (I and IV) are biphasic, as outlined below. Taken from (Tsvetkov et al., 2009)

For r-proteins to carry extra-ribosomal functions means that they must be stable. Ribosomes and their r-protein contents are stable indeed, but free r-proteins are not. Indeed, they are intrinsically disordered proteins, which are known to be targeted for degradation by default by the 20S proteasome (Bloom and Pagano, 2004; Tofaris et al., 2001). Accordingly, it was shown that several r-proteins are degraded by the proteasome upon drug-induced inhibition of rRNA transcription. uL5 and uL18 were exceptions, and accumulated in a mutually dependent manner (Bursać et al., 2012). While the underlying mechanism has not been explained, it is possible that these proteins mutually hide their disorganized regions, in a similar fashion to molecular nannies (**Fig. 34**), thus resulting in protection from ubiquitin-independent degradation. However, it was shown that r-proteins are also degraded in a ubiquitin-dependent manner (Sung et al., 2016a). Importantly, it requires the ubiquitination of specific lysine residues. A number of those were found to be concealed in ribosome-bound r-proteins, explaining the difference in stability (Sung et al., 2016b). Thus, the association of free r-proteins within functional complexes could shield them from degradation, provided they protect critical lysine residues.

Under physiological conditions, r-proteins are quickly imported to the nucleolus after synthesis, where they are delivered on the site of ribosomal assembly. Extreme cases were reported, where some r-proteins are captured co-translationally or released only after binding to the pre-ribosome (Pillet et al., 2015; Schütz et al., 2014). Thus, one could wonder at which point such proteins would be available to perform extra-ribosomal functions.

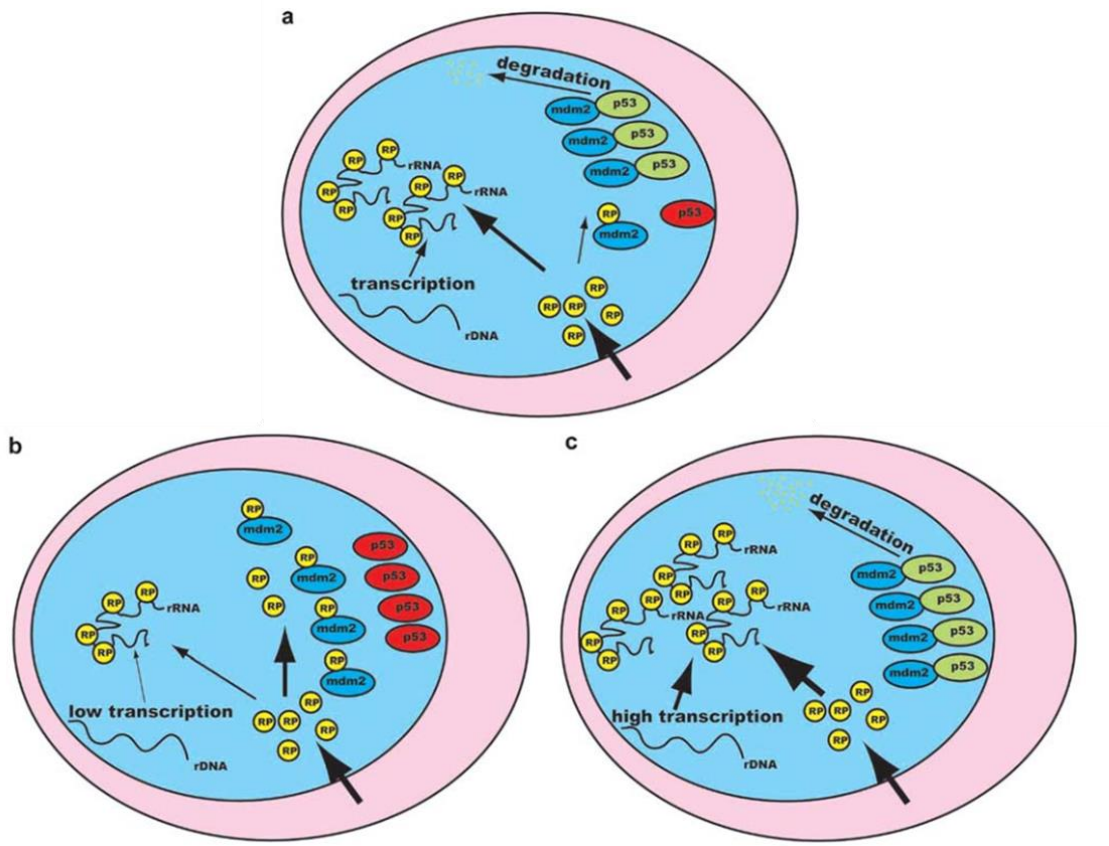

Figure 35. The balance between rRNA and r-protein synthesis regulates p53 levels.
(a) Homeostatic rRNA and ribosomal protein synthesis. r-proteins not used for ribosome building bind to MDM2, thus regulating the MDM2-mediated p53 proteasomal degradation. (b) rRNA synthesis downregulation. Ribosomal proteins no longer engaged in ribosome biogenesis bind in larger amount to MDM2, thus reducing the MDM2-mediated p53 proteasomal degradation with the consequent increase of p53 stabilisation. (c) rRNA synthesis upregulation. A greater amount of ribosomal proteins is used for ribosome building, which are therefore no longer available for MDM2 binding. A greater portion of MDM2 is left free to induce p53 proteasomal degradation. Adapted from (Donati et al., 2011).

An interesting clue came from the study of r-proteins degradation kinetics. Namely, the Tom1 ubiquitin ligase is responsible for the ubiquitin-dependent degradation of a subset of r-proteins. Importantly, Tom1 deletion triggered the aggregation of these r-proteins in insoluble deposits (Sung et al., 2016b). These data suggest that under physiological conditions, there are excess r-proteins to be degraded. Consequently, the limiting factor in steady-state ribosome biogenesis would be either rRNA synthesis or ribosome assembly rate. Indeed, a specific reduction of rRNA synthesis was shown to promote the extra-ribosomal functions of several r-proteins in stabilizing p53 in U2OS cells. Importantly, this regulation was lost when r-proteins were repressed concomitantly to rRNA synthesis, showing that r-protein availability depends on the balance of rRNA and r-protein synthesis. Interestingly, up-

regulation of rRNA synthesis resulted in decreased p53 levels (Donati et al., 2011). These data suggest that p53 stabilization does occur at a basal level under physiological conditions, which would imply that the steady-state amount of free r-proteins is sufficient for them to carry some extra-ribosomal functions (**Fig. 35**).

r-proteins are sequestered in the granular component of the nucleolus and within the ribosomal particles under physiological conditions. However, their extra-ribosomal functions occur in other cell compartments. For instance, many r-proteins are known to bind MDM2, which is mainly located in the nucleoplasm. Despite the abundance of r-proteins, this interaction is only marginal in stress-free conditions, suggesting that there is indeed a compartmental separation between the r-proteins and MDM2. Thus, another pre-requisite for r-proteins to exert regulatory function is that they escape their usual localization.

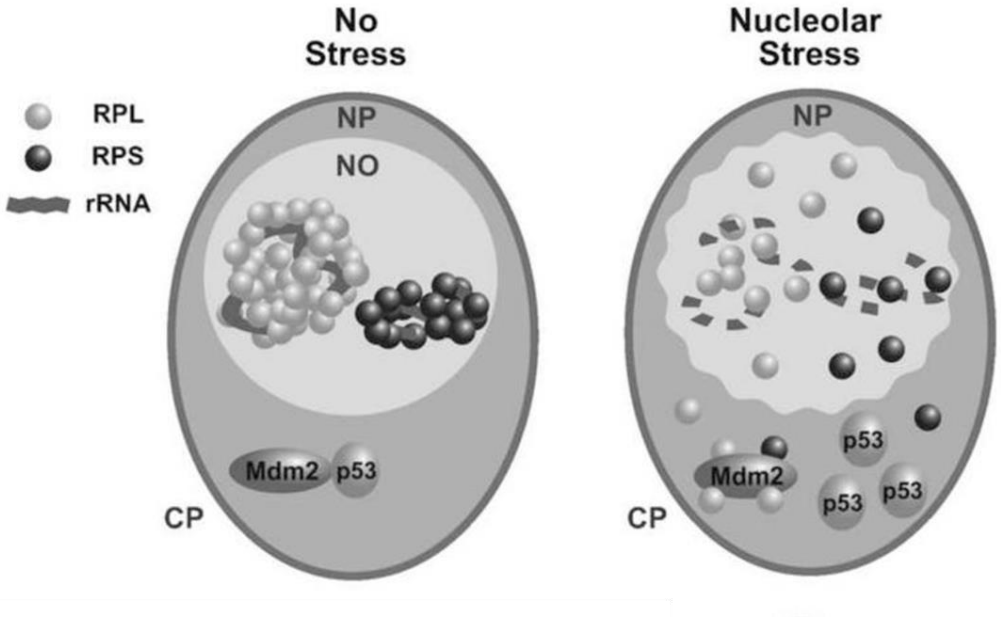

Figure 36. Schematic of RP-MDM2-p53 pathway regulation by nucleolar stress.
Under normal growth conditions (no stress), small (S, 40S) and large (L, 60S) RPs are assembled in the nucleolus (NO) and transported to the cytoplasm (CP) for protein synthesis. Under nucleolar stress, ribosomal biogenesis is inhibited and Ribosome-free forms of RPs (RPL and RPS) enter the nucleoplasm (NP) to interact with MDM2, resulting in p53 stabilization and activation. Similarly, RPs either released from breaking down (indicated by wavy edges) of cytoplasmic Ribosomes or overproduced in the cytoplasm can enter the nucleoplasm to interact with MDM2. Adapted from (Zhang and Lu, 2009).

As the nucleolus is a membrane-less organelle, its contents are very dynamic, shuttling between different nuclear bodies. It was thus proposed that there could be protein exchanges between the nucleolus and the nucleus. Interestingly, ribosomal proteins are indeed able to leave the nucleolus, albeit with slower rates than other nucleolar components. Importantly, their exchange rate was shown to increase upon inhibition of rRNA synthesis (Chen and Huang, 2001). It is thought that r-proteins are retained in the nucleolus because they associate with pre-ribosomes. Thus, an increase of r-proteins relative to ribosome biogenesis activity would give them room to freely shuttle in and out of the nucleolus. More drastically, the inhibition of ribosome biogenesis and a number of cellular stresses cause nucleolar disruption. Depending on the intensity of the cue, the nucleolus can either reduce its size, segregate, or disappear. In each case, r-proteins are massively released in the nucleoplasm (**Fig. 36** and Sirri et al., 2008)). Thus, localization of r-proteins is highly dependent on metabolic cues, making extra-ribosomal functions good candidates for stress response mechanisms.

2. r-proteins participate in cell metabolism

Numerous extra-ribosomal functions have been discovered over the last years, and the number is still on the rise. Several reviews have made attempts to provide a list of these (Bhavsar et al., 2010; Wool, 1996; Zhou et al., 2015). It should however be noted that authentic extra-ribosomal functions are often intermingled with potential functions suggested by circumstantial lines of evidence (for instance uL16 was attributed the extra-ribosomal function "Autism" while eL13 was assigned an extra-ribosomal function for being up-regulated in response to DNA damage). Those should only be considered with caution, as the demonstration of an extra-ribosomal function requires stringent criteria (Warner and McIntosh, 2009). Nevertheless, several of them have been readily characterized, implicating extra-ribosomal functions in a number of metabolic events. Many such functions are the prerogative a single r-protein, and the range of affected processes is broad. For instance an extra-ribosomal function was attributed to eS19 as a monocyte chemotactic factor (Yamamoto, 2000). For these reasons, the next chapter will not contain an exhaustive list of extra-ribosomal functions, but rather describe those that are general features of r-proteins.

The amount of free r-proteins largely depends on their incorporation into pre-ribosomes. They are recruited there in a stoichiometric manner, implying that dysregulation of a single r-protein gene expression would result in either one, or all but one r-proteins accumulating. Free r-proteins were however shown to carry extra-ribosomal functions in the regulation of their own abundance. These mechanisms may coordinate r-protein levels, thus providing robustness to ribosome homeostasis.

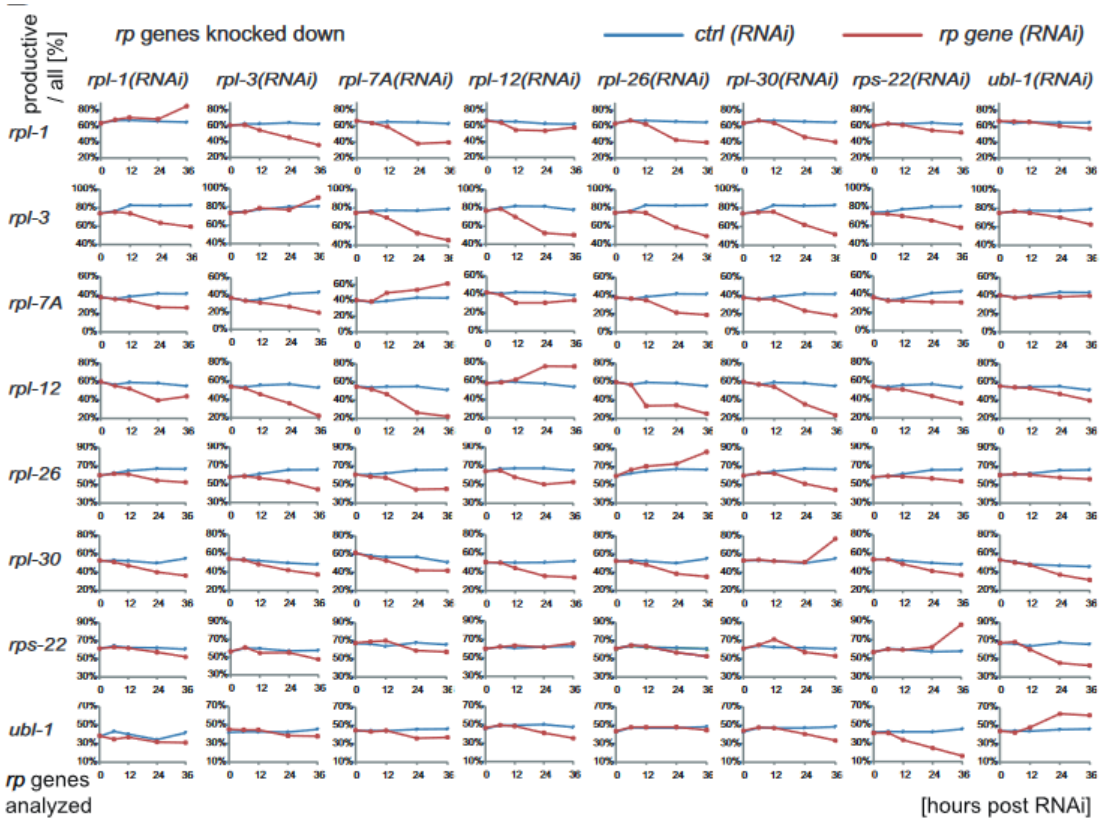

Figure 37. Knockdown r-protein genes expressing unproductive mRNA oppositely affects productive splicing of its own transcript and the other r-protein gene transcripts.
A red line in each graph indicates the change in the molar ratio of the productive mRNA isoform to the sum of the two isoforms of the r-protein gene indicated on the left after feeding with the bacteria for RNAi of the r-protein gene indicated at the top. A blue line indicates the change in worms fed with the control bacteria in a parallel experiment. X-axis indicates the time of feeding for knockdown in hours.
Please note that ubl-1 was C.elegans nomenclature for the newly named eS31.
Taken from (Takei et al., 2016)

On the one hand, free r-proteins can target their expression in a global manner. Indeed, uL5 and uL18 bind the 3'UTR region of the *Myc* mRNA, where they recruit miR24 and the RISC complex, preventing its translation (Challagundla et al., 2011; Liao et al., 2014). In addition, uL5 and uS11 bind the Myc protein and inhibit its activity as a transcriptional activator (Zhou et al., 2013). As Myc is an activator of the transcription of r-protein genes (cf. II.A.1), this is expected to reduce the synthesis of new r-proteins.

On the other hand, many r-proteins were shown to repress their own expression specifically. Strikingly, several r-protein genes were found to generate unproductive mRNA, which are quickly degraded by the nonsense mediated decay (NMD) pathway in worms, flies and humans (Cuccurese et al., 2005; Hansen et al., 2009; Mitrovich and Anderson, 2000). Interestingly, the overexpression of several of

them (uL3, uL11) was shown to increase the proportion of unproductive mRNA for their own gene but not for other r-proteins. While the molecular mechanism has not been solved for most r-proteins, it was shown that uL1 binds its own mRNA over a conserved 39 nt sequence (L10ARE). Binding of uL1 promotes the skipping of a splice site, leading to the integration of a premature stop codon (Takei et al., 2016). As human uS15 and yeast eL30 (thereby named L32 after the pre-1998 nomenclature) were also shown to bind their own mRNA, this feature could be shared by more self-regulating r-proteins (Dabeva and Warner, 1993; Malygin et al., 2007). Strikingly, upon RNAi inactivation of several individual r-protein genes in worms, the proportion of unproductive mRNA decreased for the inactivated gene but increased for all others (**Fig. 37** and Takei et al., 2016) . These data suggest that this mechanism may fulfil a homeostatic function by averaging r-protein levels.

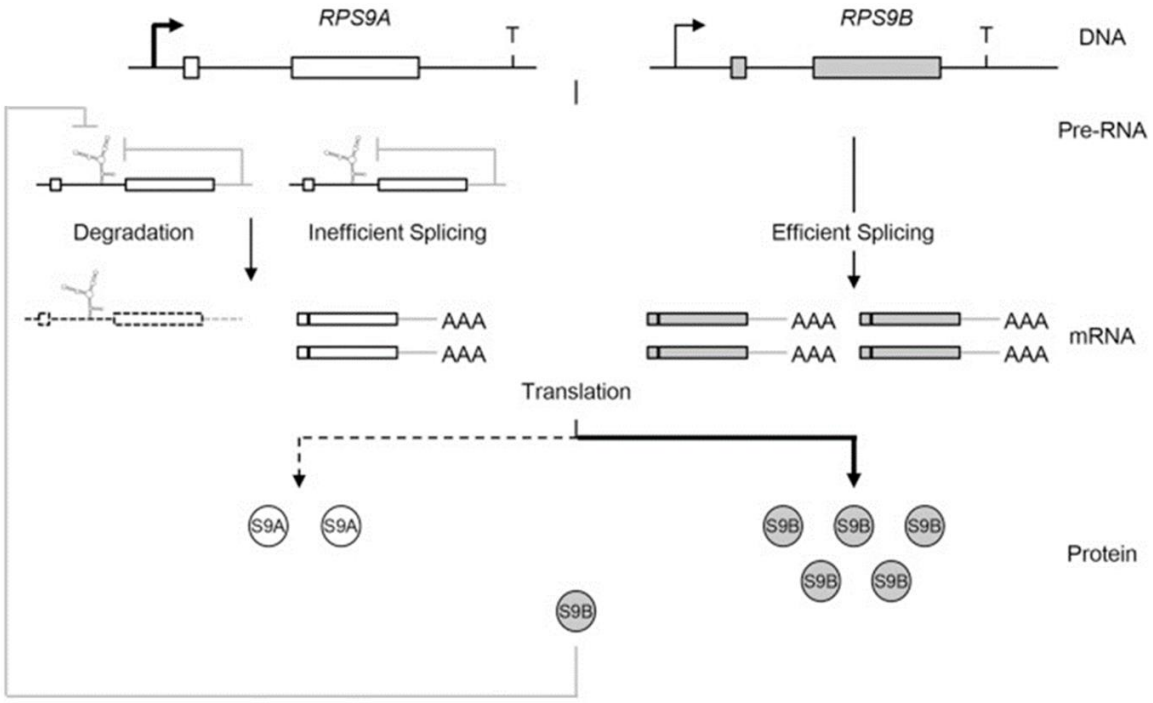

Figure 38. Asymmetric regulation of a pair of r-protein paralog genes
Schematic representation of the multi-level RPS9 (uS4) *regulatory circuit. The differential regulation of* RPS9A *and* RPS9B *is illustrated at different levels of gene expression. The coding regions are shown in the form of boxes and non-coding sequence (introns and UTRs) are shown as lines. The transcription start sites are illustrated by arrows. The secondary structure within the* RPS9A *intron represents the structure required for the inhibition of* RPS9A *splicing. Steady state inhibition and enhancement of splicing are illustrated by grey lines.*

Interestingly, this mechanism was shown to participate in the asymmetric expression of duplicated r-protein genes in *S.cerevisiae*. Indeed, uS4B binds the intron of the *uS4A* mRNA specifically, keeping it from being spliced out. This results in the degradation of the *uS4A* mRNA by the NMD pathway, thus keeping its expression low. In addition, the deletion of the binding locus resulted in decreased splicing efficiency for the *uS4B* mRNA. It was thus concluded that uS4B binds both mRNA with a preference for *uS4A*, establishing a hierarchy in the expression of the paralogs (Petibon et al., 2016). Strikingly, deletion of the intron in the minor paralog r-protein genes was reported to increase their expression in 83% of cases. Furthermore, it caused the hierarchical inversion of the paralog pair in 57% cases. Thus, it is expected that this mechanism would apply to many other r-protein paralogs.

It should however be noted that a previous screen for the regulatory effect of intron in r-protein genes demonstrated that half introns were responsible for gene repression while the other half increased it. Furthermore, in most cases the deletion of an intron triggered a change in the expression of the

paralogous gene. Surprisingly, the effect was opposite to gene compensation in most cases (Parenteau et al., 2015). Thus, paralogous r-protein genes splicing seems to be subject to more than classical negative feedback loops, and it will be interesting to know whether extra-ribosomal functions are involved in these regulatory schemes.

The MDM2-p53-r-protein pathway

Ribosome biogenesis is required for cell growth and proliferation, and is known to be increased in cancer cells (Drygin et al., 2010). Thus, it used to be implicitly admitted that ribosome biogenesis components would behave as oncogenes. Quite oppositely, many ribosome biogenesis components turned out to be tumour suppressors. For instance, 18 out of 28 studied r-protein mutants in zebrafish were paradoxically both growth-impaired and prone to developing malignant tumours (Lai et al., 2009). This apparent contradiction was resolved with the discovery that many r-proteins, while indeed important for translation, also carry extra-ribosomal functions in the regulation of p53 stability.

Under physiological conditions, p53 is bound and ubiquitinated by MDM2, thus targeting it for degradation and keeping it at low levels (Haupt et al., 1997; Kubbutat et al., 1997). The interaction between MDM2 and p53 can be disrupted a number of ways, resulting in an augmentation of p53 levels and activity (Moll and Petrenko, 2003). Under various conditions ranging from genotoxic stress to ribosome biogenesis defects, r-proteins are released from the nucleolus (cf. III.B.1 and **Fig. 36**). Strikingly, 14 of them can bind MDM2 and separate it from p53 (Kim et al., 2014 and **Fig. 35**). Interestingly, while each individual r-protein can suppress MDM2, uL5 and uL18 seem to carry a critical role in this regulation. Indeed, they were found to be required for p53 activation in human cells, while uS14 and eS7 were not (Fumagalli et al., 2012). Thus, a part of these r-proteins seems to be redundant in activating p53. A few theories have been proposed to address their functional significance. On the one hand, the binding of several r-proteins may have a cooperative effect on MDM2, or be a requirement for its inactivation. On the second hand, specific sets of r-proteins could be released from the nucleolus depending on the nature of the stress cues (Kim et al., 2014).

It is expected that other r-proteins will be added to the list of p53 regulators in the years to come. In addition, they may regulate p53 at other levels than its interaction with MDM2. For instance, r-protein uL24 was shown to bind the 5'UTR region of the *p53* mRNA and enhance its translation, under both basal and stress conditions (Takagi et al., 2005).

3. r-proteins are bound to chromatin

A fascinating development in the field of r-protein study was the observation that many of them can be found associated to chromatin (Brogna et al., 2002). While the idea of extra-ribosomal functions in gene expression immediately spring to the mind, only a couple examples where chromatin-bound r-proteins regulate transcription have been properly documented (Dai et al., 2007; Wan et al., 2007). Other functions have been proposed, but lack compelling evidence (Ni et al., 2006; Tchórzewski et al., 1999). In addition, the number of r-proteins detected on chromatin questions whether they are recruited individually, or as part of ribosome-like or pre-ribosomal subunits. Thus, r-protein activity on chromatin typically enters the category of potential extra-ribosomal functions in need of supporting evidence. Indeed, the significance of their binding to chromatin remains subject to considerable speculation and controversy.

The association of r-proteins with chromatin has been shown in several ways. In Drosophila, immunofluorescence assays on polytene chromosomes allowed to identify 20 such r-proteins (**Fig. 39** and Brogna et al., 2002).

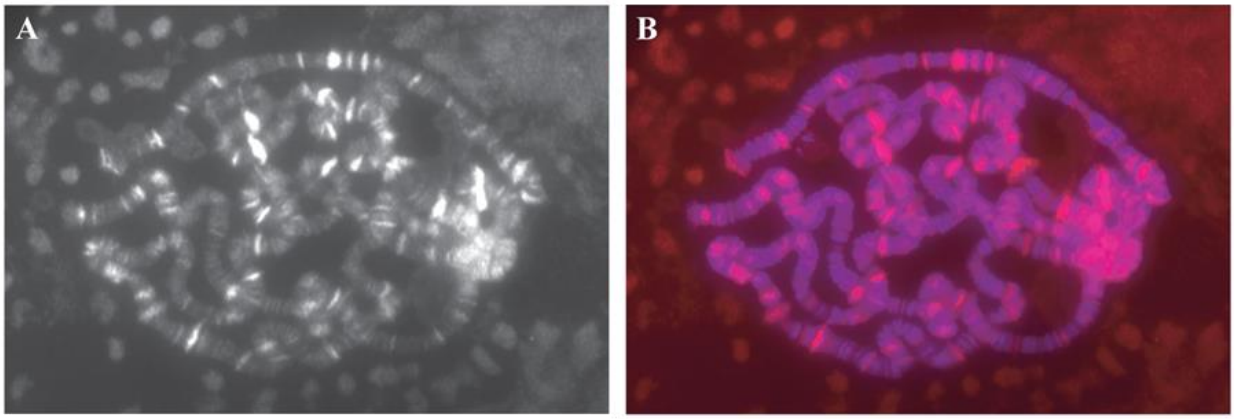

Figure 39. eS30 associates with transcription sites.
*(**A**) Single-channel showing the typical banding pattern produced by anti-RpS30 detected with a Cy3 (indocarbocyanine)-labelled secondary antibody. (**B**) Same chromosome squash, showing the DAPI (4',6-diamidino-2-phenylindole) signal (blue) to visualize DNA; note that the Cy3 signal (red) highlights a decondensed region of the chromosomes (interbands), which corresponds to transcription sites. Taken from (De and Brogna, 2010).*

Concern was subsequently raised towards antibody specificity and possible contamination by cytoplasmic components during the preparation of the samples (Dahlberg et al., 2003). Chromatin binding was thus validated by *in vivo* imaging of r-protein fusions with fluorescent tags. Furthermore, it was shown that endogenously tagged eL41 also bound chromatin, confirming that r-protein binding to chromatin is not an artefact resulting from ectopic expression (Rugjee et al., 2013). In both studies, r-proteins were found to bind DAPI interbands, which correspond to decondensed chromatin, and are considered sites of active transcription (Zhimulev et al., 2004). While all r-proteins displayed similar banding patterns, it is not known to what extent they co-localize. It is thus not known whether they possess unique binding patterns or bind chromatin through a shared mechanism. Interestingly, the binding of several r-proteins was shown to be reduced upon RNAse treatment in the first study, suggesting that they would bind chromatin through the interaction with RNA.

r-proteins were also found to bind chromatin in yeast. In *S.cerevisiae*, ChIP experiments demonstrated that uL24A, uL30B and eL36B bind some coding and non-coding genes. In the case of protein-coding genes, r-protein signal was found to be enriched in the coding sequence. In addition, the signal was increased upon activation of transcription, and reduced upon RNAse treatment. The authors thus suggested that r-proteins may be recruited in a nascent RNA-dependent manner (Schroder and Moore, 2005). In *S.pombe*, uL5, uL23 and uL30 were also found to bind both coding and non-coding genes, with tRNA genes displaying the most enrichment. Interestingly, the association of uL5 and uL30 to the ACT1 gene was lost upon RNAse treatment, but not that of uL23. It is thus possible that multiple mechanisms underlie r-protein binding to chromatin. Indeed ChIP-on-chip assays revealed that these r-proteins not only bind a subset of genes, but are also enriched in pericentromeric heterochromatin. Surprisingly, this enrichment was also found to be sensitive to RNAse treatment. (De et al., 2011). While it is possible that nascent RNAs stemming from heterochromatin may underlie such association, the authors proposed that other kinds of RNAs may be involved in the binding of r-proteins. For

instance, if r-proteins bind as pre-ribosomal complexes, rRNA integrity could be important to tether them together on chromatin.

Another study in *Drosophila* cells provided another candidate mechanism: r-protein eL22 was found to co-localize and interact specifically with linker histone H1. Surprisingly, eL22 display two alternative subcellular distribution profiles: in the vast majority of cells, it is found throughout the cytoplasm, nucleolus and on chromatin. In that case it partially co-localizes with activating histone mark H3K4me3, suggesting that it is present on actively transcribed regions. On the other hand, in 5 to 10% of cells, it would appear predominantly nuclear and be excluded from such active chromatin. In these cells, its co-localization with histone H1 is enhanced. The authors proposed that this association could be transient, and may be regulated during the cell cycle. ChIP experiments showed that the binding of eL22 and uL30 on several coding genes was reduced upon depletion of histone H1, confirming that it participates in their recruitment to chromatin (Ni et al., 2006). A number of other r-proteins were found to interact with histone H1. In the aforementioned study, 19 were identified, whereas a study in human cells found 4 r-proteins to interact with H1.2 (Kim et al., 2008). More recently, mass-spectrometry analysis of histone H1.0 interactants in human cells identified 24 r-proteins. Interestingly, only three of them were found to no longer bind H1.0 upon RNAse treatment (eS1, uS15, eL22) (Kalashnikova et al., 2013).

To summarize, many r-proteins bind chromatin. They can be found both on actively transcribed regions, and pericentromeric chromatin. They may be recruited through different mechanisms, one being dependent of some kind of RNA, the other on histone H1. It is not known whether they bind alone or in a complex. Similarly, it is not known to what extent they share binding sites and function on chromatin.

Proposed functions of r-proteins on chromatin

Finding so many r-proteins bound to chromatin at regions of active transcription is strikingly reminiscent of the organisation of gene expression in prokaryotes and archaea, where transcription and translation occur at the same time and influence each other (French et al., 2007; Yanofsky, 1981). Indeed, these observations sparkled interest for the idea of a form of nuclear ribosome performing regulatory functions on nascent RNAs.

A first theory proposed that they may scan nascent mRNA for premature termination codons. Supporting lines of evidence include the fact that these codons induce perturbations in mRNA splicing, which occurs co-transcriptionally, suggesting a very early surveillance mechanism (Aoufouchi et al., 1996; Gersappe et al., 1999). However, alternate hypotheses may explain these observations in the absence of nuclear mRNA scanning (Dahlberg et al., 2003). Furthermore, in yeast, r-proteins are found associated to non-coding genes such as tRNA and their binding is unaffected by the introduction of a nonsense mutation in a coding gene (Schroder and Moore, 2005). Thus, there seems to be rather weak supporting data in favour of this hypothesis.

Another explanation proposed that chromatin bound r-proteins may engage in nuclear translation. The presence of most translation factors in the nucleus, as well as the detection of nuclear peptidyl-transferase activity support this theory. While several interesting developments arose in this evermore controversial field, reported nuclear translation activity did not display particular association with chromatin (Al-Jubran et al., 2013; Apcher et al., 2013; Dahlberg and Lund, 2012; David et al., 2012). Furthermore, it was reported that unlike r-proteins, translation factors did not bind chromatin efficiently, suggesting that if there is indeed some form of nuclear translation, it would be away from chromatin (Schroder and Moore, 2005). Additionally, r-proteins are bound indifferently to coding and non-coding genes, but also on pericentromeric chromatin (De et al., 2011). It is thus unlikely that nuclear translation would be responsible for the whole pattern of r-proteins binding.

In this context, the precise role for chromatin-bound r-proteins remain elusive. One could wonder whether they all possess unique functions, binding sites and recruitment mechanisms, or whether they are recruited as a whole. Indeed, many r-proteins display similar binding patterns (Brogna et al., 2002; De et al., 2011; Rugjee et al., 2013). However, the few documented studies show little common ground between individual r-proteins. While uL5 is recruited through its interaction with a transcription factor, eS22 interacts with a histone protein and uS3 binds DNA over specific sequences. Similarly, uS3 and uL5 display non-autonomous trans-activating or -repressing properties, while eS22 is described as a repressor, and P1 as an activator (Dai et al., 2007; Ni et al., 2006; Tchórzewski et al., 1999; Wan et al., 2007). To date, there is still too little data to determine whether individual r-protein functions are the exception, or the rule.

IV. Regulation of ribosome homeostasis by uL11 and Corto

The idea that uL11 may carry extra-ribosomal functions in the regulation of transcription is not new (Tu et al., 2011). However, it remained undemonstrated for lack of evidence that it interacted with a non-ribosomal component out of the ribosome. In these conditions, the discovery that transcription factor Corto recognized uL11 specifically provided an unprecedented opportunity to investigate its involvement in transcription regulation. Subsequent work provided the robust demonstration of an extra-ribosomal function with implications in ribosome biogenesis homeostasis (Coléno-Costes et al., 2012).

A. The ribosomal protein uL11

Ribosomal protein uL11 has had a number of aliases over the years. Mostly known as RpL12 in eukaryotes, it used to be named YL23 or L15 in yeast (See Tables S1, S2 and S3 for conversion). The nomenclature of r-proteins has indeed always led to confusions. In particular, bacterial r-protein counterparts followed a different numeration, in such a way that eukaryotic RpL12 was in fact homologous to bacterial RpL11. Even among eukaryotes, the use of different terminologies between species sometimes led to important misinterpretations. For instance, in 2002, RpL12 was reported to bind chromatin on polytene chromosomes as detected by immunofluorescence (Brogna et al., 2002). Unfortunately, the antibody had been described to recognize eL12, which is the *Artemia salina* nomenclature for ribosomal protein P2 (Elkon et al., 1986). While the new nomenclature should solve this problem, it remains important to avoid any further ambiguity between eukaryotic and prokaryotic homologs. For this reason, I will use the uL11 appellation for the eukaryotic r-protein, and refer to the bacterial one as bL11.

1. General features of Drosophila uL11

Drosophila uL11 is encoded by a unique gene (*RpL12*/*CG3195*/*FBgn0034968*) located on the right arm of chromosome 2, at cytogenetic position 60B7. Three annotated transcripts encode the same 165 amino-acids protein. Surprisingly, none of them carries a 5' terminal oligo-pyrimidine tract. However, an 18 nucleotide-long stretch of pyrimidines can be found within the first 50 nucleotides of two annotated transcripts. As transcriptional start sites (TSS) are often curated based on bioinformatical predictions, it remains conceivable that a non-annotated TSS may produce a 5'TOP mRNA. uL11 epression is ubiquitous and described as "very high" to "extremely high" in all tissues, developmental stages, and cell lines.

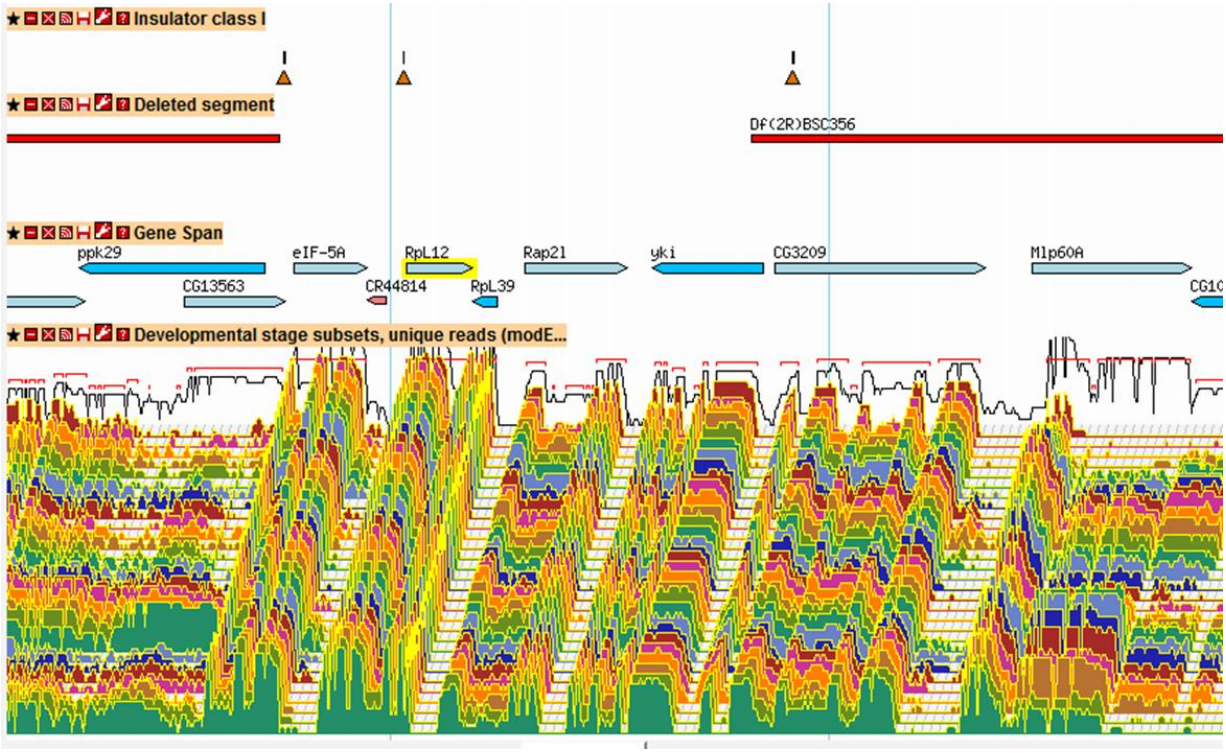

Figure 40. The RpL12/uL11 genomic locus.
Orange triangles mark predicted insulator sites. Red boxes indicate regions of the genome for which a deletion mutant is available. Blue arrows: coding genes. Light red arrow: non-coding gene. The bottom panel displays gene expression data, each line corresponding to a different developmental stage. Taken from FlyBase (http://flybase.org/).

Interestingly, *uL11/RpL12* is located within a cluster of highly and ubiquitously expressed genes (**Fig. 40**). They are encompassed by predicted insulator sites, which demarcate an area of the genome for which no deletion mutant is available. Two such deletions have however been described. The first one - *Df(2R)bw*^{VDe2L}*Px*^{KR} - was defined to cover cytological regions 59E1 to 60D1, thus encompassing the whole *uL11/RpL12* area. However, in a recent personal communication to FlyBase, Kevin R Cook proposed that the cytological borders of this deletion did not cover the *uL11/RpL12* region (http://flybase.org/reports/FBrf0230794.html). The second one - *Df(2R)Exel6081* – was described to delete regions 60B4 to 60C6. It was however not molecularly mapped, and was considered lost when homozygotes were found in the stock (http://flybase.org/reports/FBrf0206661.html). Thus, no evidence remains that flies can accommodate aneuploidy at this locus, which is indeed described as

haplo-lethal (Cook et al., 2012; Lindsley et al., 1972). It is likely that *uL11/RpL12* contributes to this phenotype: no classical allele has been described and its ubiquitous RNAi-mediated inactivation is lethal during the first larval instar. However, another r-protein gene (*eL39/RpL39*), and several essential genes (*eIF5A*, *yki*) are found in the vicinity of *uL11/RpL12* (Huang et al., 2005; Park et al., 2010). For this reason, which genes are responsible for this haplo-lethality remains uncertain.

Figure 41. Alignment of uL11 protein sequence among eukaryotes.
The alignment was realized with Clustal Omega v1.2.4. D.m, Drosophila melanogaster; H.s, Homo sapiens; S.c Saccharomyces cerevisiae; S.p, Schizosaccharomyces pombe.

Drosophila uL11 is a highly conserved 165 amino-acids protein with a mildly basic isoelectric point (8.29) and a molecular weight of 17.7 kDa (**Fig. 41**). Its structure off the ribosome has never been solved, but bioinformatic tools predict the existence of several secondary structures. There is otherwise very little structural data available for ribosome-free uL11.

uL11 is imported into the nucleus specifically by importin-11 (Plafker and Macara, 2002). It has been described to bind the pre-60S at late nucleolar/nuclear stages of assembly (de la Cruz et al., 2015). It associates with the GTPase domain of the 28S rRNA, at the base of the P stalk of the ribosome (Uchiumi and Kominami, 1997). Structural data on ribosome-bound eukaryotic uL11 is scarce. Indeed, it is missing from most crystal structures of the ribosome, perhaps due to its labile nature. It was however built as a polyalanine chain in a structure of the yeast ribosome, and was found to align completely on the structure of bL11 (Ben-Shem et al., 2011). Consequently, the data about bL11 ribosomal function may provide insight about its eukaryotic counterpart.

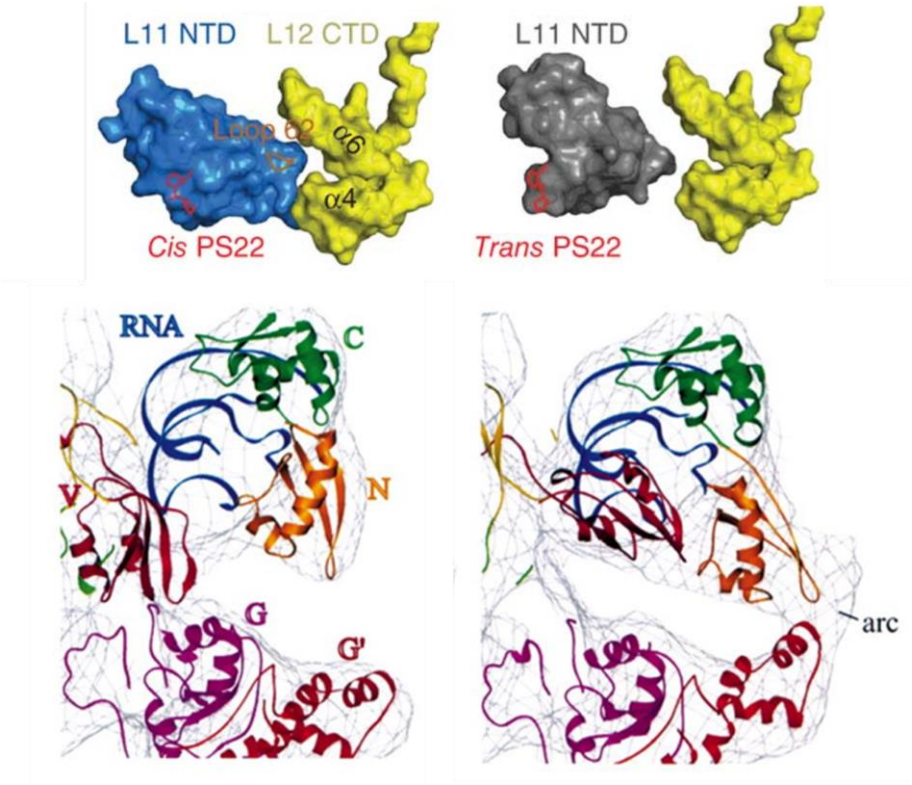

Figure 42. Conformational changes in bL11 during translation elongation.
Top panel: Interplay between the bL11 NTD and the bL12 CTD on the ribosome. Left: The bL11 NTD (blue) and the bL12 CTD (yellow). Proline Switch 22 (PS22, red) is cis and loop 62 (brown) is inserted into the cleft between α4 and α6 of the bL12 CTD. Right: when bL11 from the isolated structure is aligned with bL11 from the ribosome complex, the trans PS22 (red) makes the bL11 NTD too far to connect the bL12 CTD. Taken from (Wang et al., 2012). Lower panel: presentation of the fitting of the X-ray structures of EF-G and bL11-23S rRNA complex into the cryo-EM density of the 70S·EF-G complexes obtained before and after GTP hydrolysis. The cryo-EM densities are shown as grey wire-mesh. (a) 70 S·EF-G·GMPPCP complex; and (b) 70 S·(tRNA)2·EF-G·GDP·fusidic acid complex. (a) Based on the fitting, hairpin portions of three loop structures of domain V (red) of EF-G are facing downward in the GTP state. (b) Following GTP hydrolysis, domain V rotates such that the three loop structures move into the cleft between RNA (blue) and N-terminal domain (NTD) (gold) of protein bL11, thereby inducing a shift of NTD. The lower tip of NTD is brought closer to the G' domain (brown) of EF-G, which also moves upward, helping in the formation of the arc-like connection. Landmarks: RNA, 58 nt RNA; C, CTD of L11; N, NTD of L11; V, domain V of EF-G; G (magenta), portion of G domain of EF-G; and G', portion of G' domain of EF-G. Taken from (Agrawal et al., 2001).

bL11 contains two globular domains separated by a flexible linker. It has been described to bind the 23S rRNA and bacterial uL10 through its C-terminal domain (Wimberly et al., 1999). It is not necessary

to recruit bL10 and the L7/L12 stalk, but increases their binding efficiency a hundred fold (Iben and Draper, 2008). Importantly, it was shown to change conformation at all steps of the elongation cycle (Ilin et al., 2005; Kavran and Steitz, 2007). Indeed, the N-terminal domain of bL11 contains a proline switch that can be found in the *trans* position in factor-free ribosomes. Elongation factor EF-G catalyses its isomerisation to the *cis* position, displacing the bL11 NTD, which subsequently contacts the CTD of bL12. This movement is a pre-requisite for EF-G binding (Wang et al., 2012). Upon GTP hydrolysis, the N-terminal domain of bL11 forms an arc-like connection with EF-G (**Fig. 42** and Agrawal et al., 2001). It was thus proposed that bL11 transmits conformational changes induced by GTP hydrolysis to bL10, bL12 and the 23S rRNA (Diaconu et al., 2005). This mechanism is likely to be shared with other GTPases that bind the same region (EF-Tu, IF2, IF4, RF3) since they both contact bL11 and display peptidyl prolyl isomerase activity (Wang et al., 2012). Importantly, ribosomes lacking bL11 were found to be deficient for EF-G dependent GTP hydrolysis, which is required for elongation (Schrier and Möller, 1975). As eukaryotic uL11 is reported to bind EF-2 and the rRNA at the same location, these roles may be conserved in eukaryotic ribosomes (Uchiumi and Kominami, 1997; Uchiumi et al., 1986).

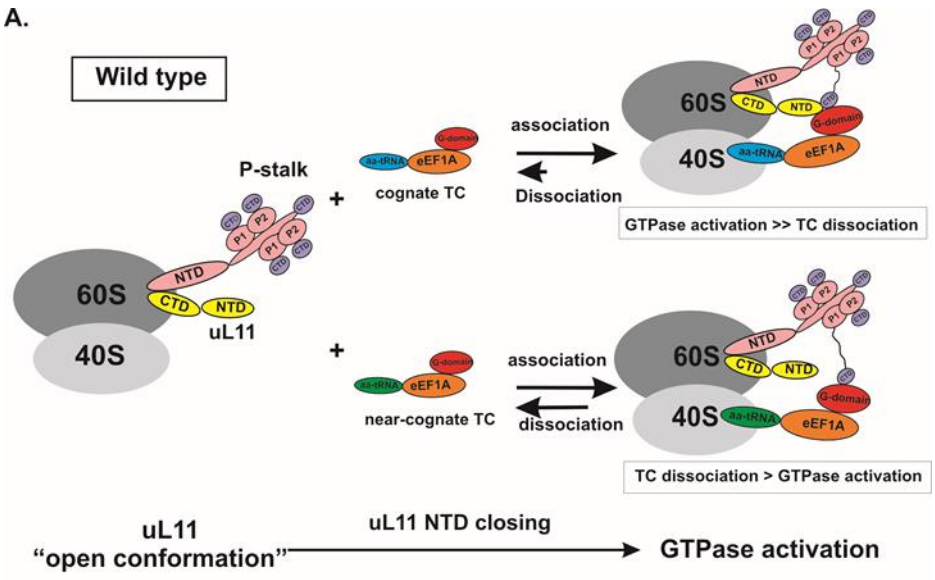

Figure 43. Model of uL11 contribution to translational fidelity.
uL11 is depicted in the form of two C-terminal and N-terminal domains - CTD and -NTD, respectively. The P-stalk is shown as a separate structure, and P1 and P2 proteins with C-terminal domains responsible for G-domain binding of eEF1A are also shown. uL11 is in its basic 'open conformation'. The cognate ternary complex binding is stabilized by allosteric rearrangements within the GAC, involving movement of uL11 CTD into 'close conformation' and probably interacting with the G-domain of eEF1A. uL11 'closing' prevents cognate TC dissociation and leads to 'productive state' stabilization, leading at the same time to GTPase activation. Near-cognate TC does not induce uL11 'closing', which induces TC dissociation before GTPase activation. Taken from (Wawiórka et al., 2016).

Interestingly, uL11 does not seem important for pre-60S maturation since its absence only leads to a mild accumulation of precursor RNA (de la Cruz et al., 2015). It is however necessary for the assembly of the P stalk which occurs in eukaryotes at the onset of translation (cf. **Fig. 12** and Briones et al., 1998). Furthermore, uL11 has been described to be important at many steps of the translation cycle. Indeed, deficiency for uL11 in yeast prevents the release of ribosome associated protein Tif6, which is the last maturation step before 60S subunits become functional. Furthermore, uL11-deficient ribosomes display a decrease in translational fidelity, which may participate in the reduction of translational elongation speed (**Fig. 43** and Wawiórka et al., 2016).

In addition to its role in translation, uL11 was shown to carry extra-ribosomal activities. Indeed, it was shown in *C. elegans* and *M. musculus* that uL11 binds its own messenger RNA and inhibits its splicing (cf III.B.2) (Cuccurese et al., 2005; Mitrovich and Anderson, 2000; Takei et al., 2016). Furthermore, uL11 was shown to be required for the transcription of a subset of PHO pathway genes that are inducible under low phosphate conditions in *S. cerevisiae* (Tu et al., 2011). However, while the authors showed that the observed decrease in mRNA levels was not a result of decreased mRNA stability (which may occur upon translation inhibition), they provided no evidence that uL11 regulates the PHO pathway at the transcriptional level. Indeed, some ribosomal proteins were shown to be required for the translation of specific mRNA (cf III.A.3), and one could argue that uL11 may promote the translation of a PHO pathway transcription factor. For this reason, the involvement of uL11 in transcriptional regulation is still in need of solid evidence.

3. Methylation of uL11

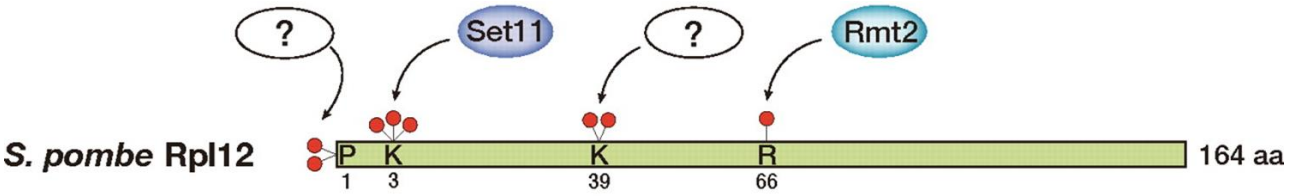

Figure 44. Summary of uL11 post-translational methyl modifications.
The methylation sites and corresponding enzymes are depicted. The red lollipops represent methyl modifications. Taken from (Sadaie et al., 2008).

uL11 is known to be methylated over several residues of its N terminal domain, in a reproducible pattern (**Fig. 44**). The function of these modifications is rather poorly known: mono-methylation of arginine 66 was found to be catalysed by Rmt2 in *S. cerevisiae*, but no physiological role was uncovered yet (Chern et al., 2002). The same applies for lysine methylations, though some lines of data allow to speculate.

Di-methylation of lysine 39 was observed in yeast, as a facultative modification (Sadaie et al., 2008). No enzyme or function was associated to it. It is interesting to note that uL11 lysine 39 is a predicted ubiquitination site. Methylated proteins were shown to have longer half-lives than their unmethylated counterpart, correlating with the fact that nearly half methylation sites overlap ubiquitination sites in *S. cerevisiae*. It was thus postulated that lysine methylation might protect a protein from ubiquitination at the corresponding site (Pang et al., 2010).

Mass-spectrometry analysis allowed to discover that uL11 is di-methylated on its terminal amine function in *S. cerevisiae*, *S. pombe* and *A. thaliana* (Carroll et al., 2008; Sadaie et al., 2008; Webb et al., 2008). While the enzyme responsible for this modification was not uncovered, the study of a similar modification on human RCC1 allowed to describe that a consensus (N-ter-A/S/P-P-K) motif was required. In addition, RCC1 N-terminal di-methylation was shown to improve its binding to dsDNA, stabilizing its presence on chromatin. As N-terminal methylation grants a pH-independent positive charge to the modified amine function, the authors propose that it could enhance the interaction between a protein and the phosphate backbone of nucleic acids (Chen et al., 2007).

Trimethylation of uL11 lysine 3 was also confirmed in *S. cerevisiae*, *S. pombe* and *A. thaliana* (Carroll et al., 2008; Sadaie et al., 2008; Webb et al., 2008). *S. pombe* Set11 and *S. cerevisiae* Rkm2 were found to be responsible for this modification, and uL11 was their only identified substrate. Interestingly, *in vitro* methylation test showed that recombinant Set11 was able to methylate uL11 from *ΔSet11* cell extracts but not from wild-type ones. The authors thus concluded that uL11 lysine 3 must be predominantly methylated in wild-type cells. The physiological role of this modification however remained unclear: deletion of Set11 had little impact on growth rates and uL11 incorporation in ribosomes but its overexpression caused a severe growth defect (Sadaie et al., 2008). It however remains to be demonstrated whether Set11 has other functions than uL11 methylation, or substrates.

Ten ribosomal protein methyltransferases were studied in *S. cerevisiae* for their effect on ribosome biogenesis and functions. Among them, Rkm2 had no effect on ribosome synthesis, UAA codon readthrough, -1 ribosome frameshifting or amino-acids misincorporation. It however increased the level of UAG codon readthrough albeit having the most moderate effect among ribosomal protein methyltransferases (Al-Hadid et al., 2016b).

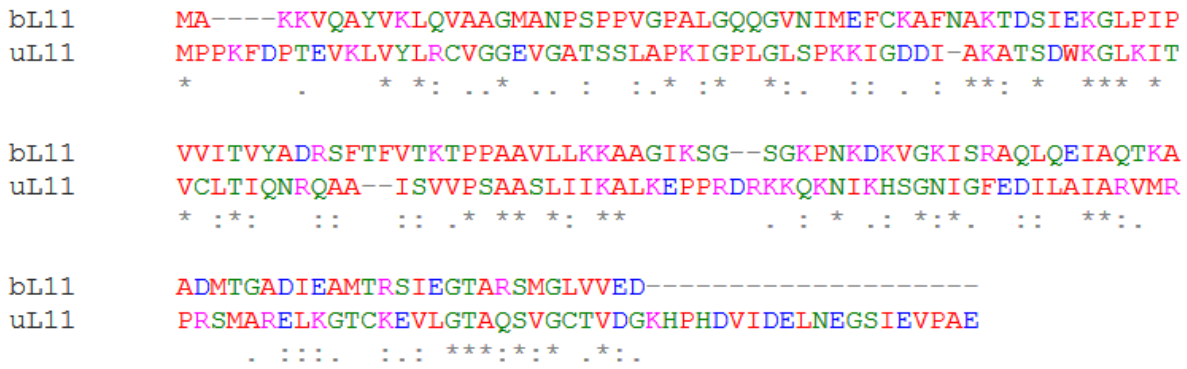

Figure 45. Conservation of uL11 between E. coli and D. melanogaster.
Clustal Omega (v1.2.4) alignment of E. coli uL11 (up, bL11) versus D. melanogaster uL11 (down, uL11).

Interestingly, bL11 is also known to be methylated on lysine 3 and di-methylated on its terminal amine function. It has been referred to as "the most heavily methylated protein from *Escherichia coli* ribosomes" (Dognin and Wittmann-Liebold, 1977). However, while uL11 is structurally conserved, it displays eukaryote-specific extensions in N-ter and C-ter (**Fig. 45**). For this reason, it is debatable whether the methylation pattern of bL11 lysine 3 can be informative for that of uL11.

Recent work in our laboratory has established that *D. melanogaster* uL11 is bound by a chromodomain-like structure of the epigenetic co-factor Corto. Chromodomains are known to recognize specifically trimethylated lysine residues, and the interaction between uL11 and Corto was indeed shown to require uL11 lysine 3 to be trimethylated (Coléno-Costes et al., 2012). Thus, the methylation of uL11 lysine 3 is likely to regulate a potential extra-ribosomal function.

B. The transcription factor corto

As the interactor of methylated uL11, Corto is likely to mediate its extra-ribosomal function. Three lines of evidence suggest a role in the regulation of transcription. 1) uL11 and Corto bind polytene chromosomes at largely overlapping sites. 2) They are found on heatshock genes' body and their presence correlates with transcriptional activity. 3) Their overexpression alters the expression of a same subset of genes, many of which are involved in ribosome biogenesis (Coléno-Costes et al., 2012). While light remains to be shed on the underlying mechanism of this extra-ribosomal activity, the wealth of data about the functions of Corto in gene regulation and metabolism may provide some insight towards its functional implications.

1. General features of Corto

Corto is encoded by a gene located on the right arm of chromosome 3, at cytogenetic position 82E7. Five annotated intron-less transcripts encode a single 550 amino-acids protein. However, northern blot analysis detected only a 3.2kb and a 3.6kb transcript, which are expressed from different TSS. The first one was described to be expressed from the embryonic to the pupal stage. The second is expressed in adult females, and deposited maternally in embryos, where it can be detected until the pupal stage (Kodjabachian et al., 1998).

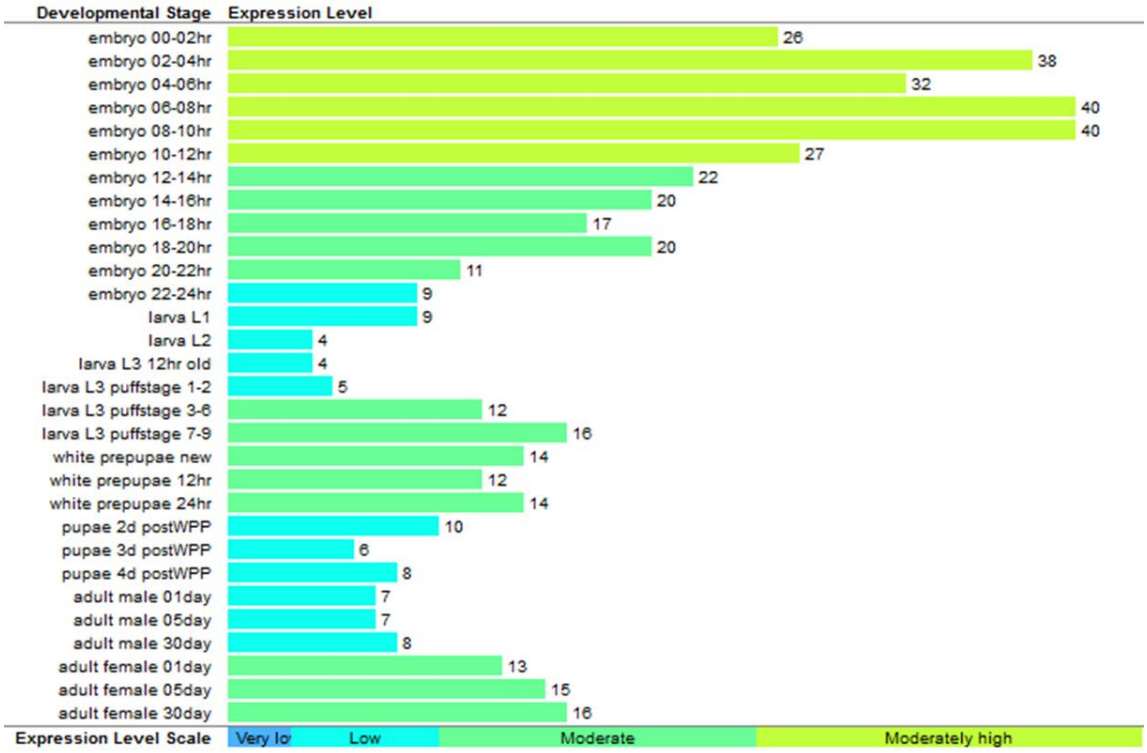

Figure 46. Transcriptomic profile of corto expression during development.
Taken from FlyBase (http://flybase.org/).

Consistently, transcriptomic data show that the expression of *corto* follows a well-defined developmental trajectory, very high in embryos and decreasing gradually until the third larval instar. Corto is then expressed differently between males and female adults. Its expression is seen to increase during the late third instar larvae and pupal stage, but in the absence of sex-specific data, it cannot be determined whether this results from general or female-specific expression (**Fig. 46**).

corto is uncovered in a deletion covering cytological regions 82E to 82F: *Df(3R)6-7*. Furthermore, several loss-of-function alleles have been described. *corto*^{420} is a deletion of the whole *corto* gene obtained by the imprecise excision of a *P* element (Coléno-Costes, 2012; Kodjabachian et al., 1998). *corto*^{L1} contains a premature stop codon allowing but the expression of a 24 amino-acids peptide (Daldalhon-Cuménal et al., submitted; Marenda et al., 2004). Lastly, *corto*^{07128} is a regulatory mutant with a *P* element inserted in the promoter region, and behaves as a null allele (Mouchel-Vielh et al., 2011; Smulders-Srinivasan et al., 2010).

Homozygous mutants for *corto* display 90% lethality, spread from the first larval instar to the pupal stage. They exhibit prolonged development and low activity during larval stages. Survivors carry bristle defects, with some thoracic macrochaetae either duplicated or absent. Furthermore, their wings carry ectopic veins. Half surviving males possess an ectopic sex comb on the second segment of the first pair of legs (Kodjabachian et al., 1998). Germinal clones for the *corto*^{420} allele result in complete first larval instar lethality in homozygous offspring, underlining the importance of the maternal contribution. Heterozygotes for the *corto*^{420} allele display a thoracic bristle defect phenotype with 10% penetrance (Lopez et al., 2001).

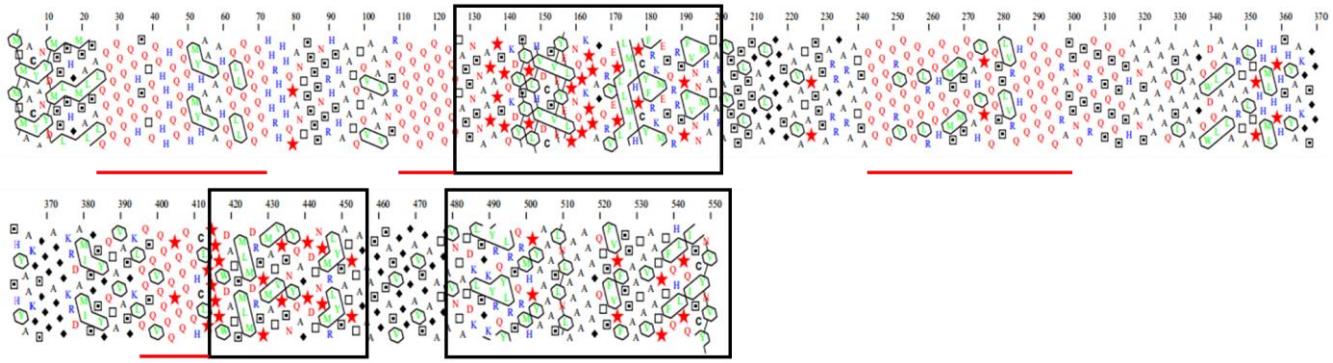

Figure 47. Hydrophobic cluster analysis of Corto.
Each letter represents an amino-acid. Colours represent hydrophobic properties. Blue: alkaline. Red: Polar. Black: neutral. Green: hydrophobic. Amino-acids with specific structural properties are depicted with symbols. Red star: proline. Black diamond: glycine. Square: threonine. Dotted square: serine. The globular domains of Corto, at positions 127-203, 418-455 and 480-550, are shown in black boxes. Homopeptide stretches are underlined in red. The HCA plot was obtained with HCA v1.0.2 (Callebaut et al., 1997).

Corto is a 68 kDa protein showing little homology to any known protein sequence. It contains three structured domains (**Fig. 47**). Among them, the one encompassing amino-acids 127 to 203 was shown to display all the characteristics of a chromodomain: it binds RNA, recruits Corto to chromatin, and recognizes a trimethylated lysine in a sequence-specific manner. This domain is responsible for the interaction between Corto and uL11 over tri-methyl lysine 3. (Coléno-Costes et al., 2012). Corto otherwise displays a very unusual amino-acid composition. Its 118 glutamines, 93 alanines and 67 serines make up more than half of the protein. Interestingly, glutamines form several homopeptide stretches (**Fig. 47**). These have been associated to protein-protein interactions and in particular with the assembly of large multiprotein of nucleic acid complexes (Faux et al., 2005; Hancock and Simon, 2005). Indeed, Corto contains large unstructured domains and specifically interacts with a number of proteins (**Fig. 48**). Thus, it carries all the properties of a hub protein (Krasowski et al., 2008).

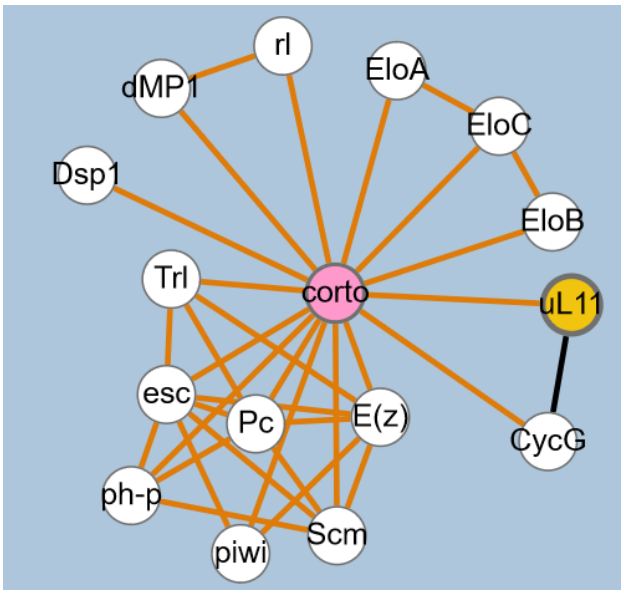

Figure 48. Network representation of the physical interactions of Corto.
EasyN diagram of physical interactions centered on Corto. Golden edges represent a physical interaction. Interactions between Corto and other proteins have been experimentally validated in the following studies: (Coléno-Costes et al., 2012; Mouchel-Vielh et al., 2011; Peng et al., 2016; Rougeot et al., 2013; Salvaing et al., 2003, 2008). A black edge between uL11 and CycG was added to fit the preliminary observation of a physical interaction by co-immunoprecipitation (Delphine Dardalhon-Cumenal, unpublished data). Note that dMP1 stands for the CG5110 gene product, following the nomenclature used in the cited articles. The diagram was adapted from FlyBase (http://flybase.org/).

2. corto participates in epigenetic maintenance of segmental identity during development.

Originally called centrosomal and chromosomal factor (ccf), Corto was shown to bind chromatin and participate in chromosome condensation during mitosis (Kodjabachian et al., 1998). Its loss of function causes the second tarsus (T2) of the first pair of legs to transform into a first tarsus (T1) structure, as evidenced by the presence of ectopic sex combs in males. In addition, the overexpression of *corto* causes a transformation of the aristae into leg structures (*aristapedia* phenotype). These phenotypes correspond to the loss of identity of these segments and its replacement by that of another.

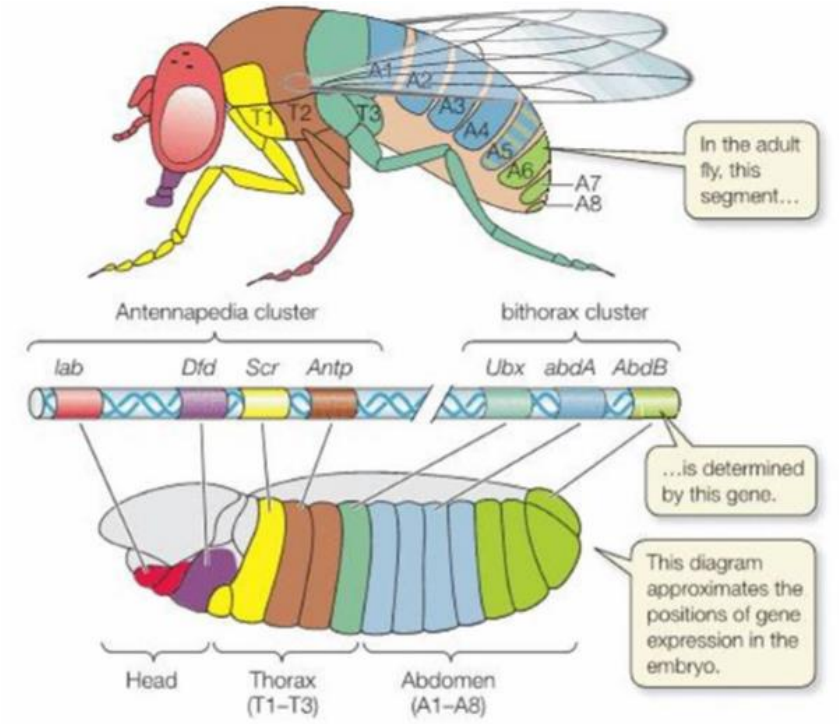

Figure 49. Hox gene expression boundaries in Drosophila melanogaster.
Hox genes form two clusters in Drosophila. Their expression pattern is set during embryogenesis and maintained throughout development to give rise to the adult segments. Taken from (Sadava et al., 2009).

Segment identity is defined by the specific expression of *Hox* genes (**Fig. 49**). Their pattern is first established by transcription factors of the gap and pair-rule gene families during embryogenesis. *Hox* gene expression is maintained during development by the *Polycomb group* (*PcG*) and *trithorax group* (*trxG*) genes (Kennison, 1995). As a general feature, *PcG* genes prevent ectopic expression of *Hox* genes while *trxG* genes maintain their activation in the appropriate segments. Consistently, mutations in *PcG* or *trxG* genes do not prevent the establishment of homeotic territories, but they interfere with the maintenance of their boundaries during development. This typically results in the transformation of a segment into another, a phenotype termed homeotic transformation.

The transformation of leg segment T2 to T1 is typically associated with the loss of repression of the *Sex comb reduced* gene (*Scr*) within this territory (Struhl, 1982). This phenotype is observed upon loss of function of *PcG* genes. Thus, the ectopic sex combs observed in $corto^{420}$ mutants suggest that Corto is involved in epigenetic repression. Indeed, it was found to bind the maintenance element (ME) of *Scr*, suggesting that it is directly involved in its regulation during development. However, the presence of Corto is not sufficient to establish repression of *Scr*: Corto was also found to bind this element in S2

cells where *Scr* is expressed (Salvaing et al., 2006). In addition, *corto* was also shown to repress ectopic expression of the *Hox* genes *Ultrabithorax* in third instar larvae and *Abdominal-B* in embryos (Lopez et al., 2001; Salvaing et al., 2008).

Further evidence suggests the involvement of Corto in epigenetic repression: genetic interaction experiments show that heterozygous mutation of *corto* increases the phenotypes of mutations for PcG genes *Polycomb*, *Enhancer of Zeste*, *Polyhomeotic*, *Polycomblike, multi sex combs* and *Sex comb on midleg* (Kodjabachian et al., 1998; Lopez et al., 2001). However, *corto* was also shown to genetically interact with the *trxG* genes *osa* for the formation of scutellar bristles, and *ash1*, *kohtalo*, *kismeth*, *moira*, and *Vha55* for the patterning of wing veins (Lopez et al., 2001).

These data designate *corto* as a member of the Enhancer of Trithorax and Polycomb (ETP) family, which participates both in epigenetic activation and repression of *Hox* genes during development. While their molecular function is unclear, they are believed to associate alternatively with Polycomb or Trithorax complexes, depending on target genes, tissues, or developmental stages. Interestingly, physical interaction between Corto and several PcG proteins have been established (**Fig. 49**). Among them, PSC, SCM, PC and PH are core components of the Polycomb repressive complex 1 (PRC1). These interactions suggest that Corto may associate with the PRC1 complex. On the contrary, no physical interaction was found with trxG proteins to date.

3. corto may be involved in developmental homeostasis

Although the mechanisms through which *corto* regulates transcription are largely unknown, it was found to interact physically with the Elongin complex, which supresses RNA polymerase II pausing (Bradsher et al., 1993; Takagi et al., 1995). The analysis of *corto* and Elongin complex members dysregulation revealed their antagonistic relationship in wing vein patterning. Furthermore, Corto was found to bind chromatin on the *rhomboid* gene at the expected location of paused RNA polymerase (Rougeot et al., 2013). In addition, Corto co-localizes extensively with paused polymerase (RNAPolIISer5p) on polytene chromosomes, and much less with elongating polymerase (RNAPolIISer2p) (Coléno-Costes et al., 2012). These data suggest that *corto* may regulate transcription at the level of RNA polymerase pausing.

Interestingly, Corto was shown to interact specifically with the MAP kinase ERK (encoded by *rolled*, the homolog of mammalian *ERK*), and the dMP1 scaffold protein. These two proteins were shown to genetically interact with Corto during wing vein specification. Importantly, Corto is phosphorylated by ERK. The effect of this phosphorylation is unknown, but it is likely that it modifies the behaviour of Corto. Since it co-localizes with MP1 and ERK on polytene chromosomes, and their interaction is detected only in the nucleus, it is possible that the transcriptional function of Corto may be affected (Mouchel-Vielh et al., 2011). Three sites meet the criteria for ERK-mediated phosphorylation (Serines 139, 190 and 428). The first two are located within the chromodomain of Corto, while the third one localizes to another globular domain. It is tempting to speculate that phosphorylation of any or a combination of these sites modifies the ability of Corto to bind chromatin, protein partners, or to dimerize. Strikingly, ERK is an effector kinase of the MAPK pathway, while dMP1 is a component of the Tor pathway. Phosphorylation of Corto could thus be regulated by these pathways in response to metabolic cues (cf II.A). Indeed, in serum-starved S2 cells, it is possible to induce phosphorylation of Corto within 15 minutes by addition of serum (Mouchel-Vielh et al., 2011).

Interestingly, Corto also interacts with Cyclin G (CycG), a transcriptional cyclin that genetically behaves as an enhancer of Polycomb for the regulation of *Hox* genes (Dupont et al., 2015). This protein was shown to regulate the specificity of the TOR pathway antagonist PP2A by associating with its subunits

Well rounded (Wrd) and Widerborst (Wdb). Through this interaction, CycG was shown to regulate growth and lipid metabolism throughout development (Fischer et al., 2015, 2016).

Indeed, Corto is at the centre of a nexus of proteins involved either in epigenetic regulation of gene expression, or cell homeostasis. Its interaction with uL11 may also be regulated in such a way: the availability of ribosomal proteins for extra-ribosomal function is heavily dependent on ribosome biogenesis homeostasis (cf III.B.1). Consistently, Corto was shown to regulate the expression of ribosome biogenesis genes, which are known target of the TOR and MAPK pathway (Coléno-Costes et al., 2012). Thus, Corto may behave as a link between epigenetic regulation, cell homeostasis, and ribosome biogenesis.

V. Presentation of the thesis project

At the beginning of my thesis project, our team had extensively studied Corto and its interaction with a number of epigenetic and transcription factors. The study that preceded this project characterized the interaction between Corto and an unexpected partner: uL11. It yielded a number of conclusions that served as foundation for the hypotheses and methodology of this work.

1) Corto contains a domain that displays structural and functional homology to chromodomains (CortoCD). 2) This domain is essential for the function of Corto. 3) This domain binds uL11. 4) This interaction requires uL11 to be tri-methylated on its lysine 3 (uL11K3me3). 5) uL11 and Corto bind chromatin and co-localize on polytene chromosomes. 6) uL11 and Corto are recruited on the *hsp70* gene upon transcriptional activation. 7) Expression of CortoCD or uL11 dysregulate a common set of genes, enriched in ribosome biogenesis components (Coléno-Costes et al., 2012).

This study provided solid evidence that uL11 possesses an extra-ribosomal function, and strongly suggested that it was carried directly on chromatin. We thus hypothesized that the interaction between Corto and uL11K3me3 underlaid a transcriptional function, possibly in the regulation of ribosome biogenesis genes. Thus, the purpose of my work was to further characterize the role of this interaction in the regulation of transcription.

As a first approach, we sought to determine which genomic loci they bound and whether they overlapped. To this end, we generated the genome-wide binding profile of uL11K3me3 and CortoCD by ChIP-seq. In addition, preliminary results from one of my supervisors showed that uL11 interacts with Calypso, the catalytic subunit of the PR-DUB complex (Sébastien Bloyer, unpublished). This complex is known to catalyse the removal of histone H2A lysine 118 mono-ubiquitination (H2AK118ub) Conversely, Corto physically and genetically interacts with components of the PRC1 complex, that ubiquitinate H2A on lysine 118. These data suggested that there may be an interplay between Corto, uL11 and the Polycomb complexes that control the ubiquitination of H2AK118. Thus, we also described the genome-wide distribution of H2AK118ub by ChIP-seq. The analysis of these data will be presented in the first chapter of results.

To study the extra-ribosomal function of *uL11*, we needed tools to disrupt it without affecting its ribosomal function. Since Corto interacts specifically with uL11 methylated on lysine 3, we decided to replace that amino-acid with an alanine. However, mutating *uL11* turned out to be more challenging than we originally thought: *uL11* is part of a haplo-lethal locus with very little intergenic sequences. Therefore, we designed a CRISPR/Cas9-mediated one-step homologous recombination strategy and refrained from inserting a phenotypic marker at the *uL11* locus. The latter part implied that we set up a phenotype-independent screening protocol. To this end, we combined an allele-specific amplification strategy with real-time PCR. We improved its robustness by using tetramethylammonium chloride buffer and inserting locked nucleic acid bases into the screening primers. Our method achieved sufficient sensitivity and specificity to be used in a high-throughput manner. Furthermore, we generated a bacterial artificial chromosome (BAC) carrying a similar mutation by using a one-step recombination protocol. We also showed that our screening method permits to quickly recover a recombinant BAC in spite of the absence of a phenotypic marker. These results are presented in the second chapter of results.

We hypothesized that this mutation affecting but the lysine 3 of *uL11*, should disrupt its interaction with Corto, but not its ribosomal function. To validate this hypothesis, we depleted uL11 in flies, and rescued it by expressing of a variant of uL11 whose lysine 3 is replaced by an alanine ($uL11^{K3A}$). We found that it partially rescues the growth defects resulting from the loss of wild-type uL11 ($uL11^{WT}$),

suggesting that the mutated form keeps at least a part of uL11 functions. Furthermore, we showed that uL11^{K3A} is distributed in ribosomal fractions with the same profile as uL11^{WT}, showing that the loss of lysine 3 does not hinder its assembly into ribosomes nor the ability of uL11^{K3A}-containing ribosomes to commit to translation. These results validated the use of uL11^{K3A} to study the specific loss of the extra-ribosomal function of uL11. Thus, we studied the phenotypes of the uL11^{K3A} flies, and those of a uL11$^{\Delta K3}$ mutant which displays milder phenotypes. Strikingly, uL11 lysine 3 mutations generate minute-like phenotypes, but while uL11$^{\Delta K3}$ is recessive, uL11^{K3A} behaves as a dominant negative. The fact that different mutations deleting uL11 lysine 3 exhibit different phenotypes suggests that the N-terminal part of uL11 likely interacts with other partners in addition to Corto. These results are presented in the third chapter of results.

Over the course of my thesis, I have been involved with another project that focused on another interacting partner of Corto: Cyclin G. Indeed, our team produced RNA-seq and ChIP-seq data to study its transcriptional function. I performed the analysis of these data. Strikingly, it revealed that CycG binds and regulates a number of genes involved in ribosome biogenesis. Correlation of its binding sites with those of PcG genes strongly suggested an interaction with both the PRC1 and PR-DUB complexes. These results corroborated the observations that: 1) CycG physically binds Asx, which is part of the PR-DUB complex. 2) CycG is an enhancer of Polycomb (Dupont et al., 2015). 3) CycG-induced fluctuating asymmetry phenotype is enhanced by mutations in PR-DUB and PRC1 complexes members. 4) Corto physically interacts with PRC1 complex core members (Salvaing et al., 2003). 5) Corto enhances the penetrance of PcG gene mutants phenotypes (Kodjabachian et al., 1998; Lopez et al., 2001). These data will be presented in the appendix.

Results

I. Ribosomal protein uL11 tri-methylated on lysine 3 binds broad genomic regions and displays an exclusion pattern with Corto on chromatin.

Several lines of evidence place the interaction between Corto and uL11K3me3 on chromatin. Indeed, the chromodomain of Corto autonomously binds chromatin and reproduces the binding sites of the full-length protein. Furthermore, its overexpression causes the retention of uL11 but not uL11^{K3A} in the nucleus. Both Corto and uL11 bind polytene chromosomes where they share binding sites, and they are recruited to the *hsp70* gene upon transcriptional activation (Coléno-Costes et al., 2012). Thus, in order to understand what function this interaction could underlie on chromatin, we set to determine their genome-wide binding pattern by ChIP-seq.

Importantly, our lab had been using third instar female larvae wing discs as a source of chromatin for such experiments. Indeed, this material offers the advantage of containing relatively few cell types and displays little cell death while still being a developing tissue. However, the expression of ribosomal protein genes is described to decrease four-fold between the second larval instar and the pupal stage. Furthemore, the mechanisms that regulate ribosome biogenesis are extremely sensitive to environmental fluctuations such as food condition or even temperature. Thus, we reasoned that the amount of time required to gather sufficient biological material from larvae dissections would likely compromise consistency between replicates. In addition, we expected that describing the genomic targets of uL11K3me3 and Corto would benefit from comparison with known epigenetic marks. The amount of ChIP-seq data available in third instar female larvae wing discs is somewhat limited, prompting us to choose another source of material. Thus, we worked with S2 cells, for they carry the double advantage of allowing fast collection of a large quantity of material, and to be the material source for a number of ChIP-seq datasets available on GEO.

Among histone marks, we were particularly interested in the genome-wide distribution of histone H2A ubiquitination on lysine 118. Indeed, evidences of physical interactions between Corto and PRC1 components, as well as between uL11 and Calypso, hinted towards a function in the regulation of H2AK118ub. A ChIP-seq dataset is available for this mark, but it was obtained from a cell line derived from a mutant carrying a thermosensitive mutation for E(Z) (Lee et al., 2015). Thus, to ensure that our comparisons would be relevant, we decided to generate our own genome-wide profile for H2AK118ub.

Importantly, there was no available antibody that could immunoprecipitate endogenous Corto. In addition, stable expression of the latter is deleterious to cells, and it is difficult to reliably express a tagged version of this protein (Emmanuèle Mouchel-Viehl, personal communication). In contrast, it is possible to stably express the chromodomain of Corto alone (CortoCD). Previously obtained data showed that CortoCD reproduces most of the binding sites of full length Corto on polytene chromosomes, suggesting that their binding profile would be similar (Coléno-Costes et al., 2012). We thus decided to immunoprecipitate CortoCD as a proxy for full length Corto.

A. Results

uL11 associates with the H2AK118 deubiquitinase Calypso.

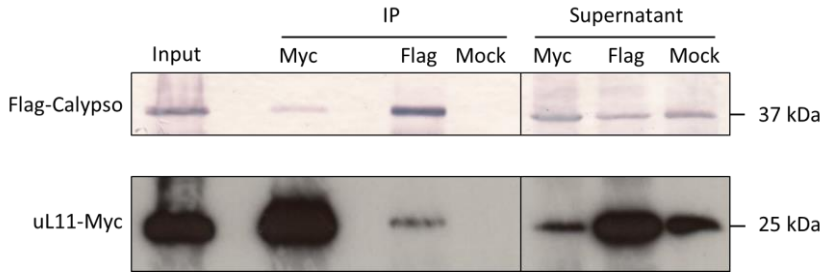

Figure 50. uL11 physically interacts with H2AK118 C-terminal hydrolase Calypso.
S2 cells were co-transfected with expression vectors encoding uL11-Myc and Flag-Calypso. They were fixated in 1% paraformaldehyde before protein extraction. Immunoprecipitations were performed with either anti-Flag, anti-Myc or anti-HA (Mock IP) antibodies. They were revealed with anti-Flag and anti-Myc antibodies. Three replicates were obtained. IP: immunoprecipitation. Vertical lines indicate that different wells from the same gel were juxtaposed in the image for clarity.

A previous study identified uL11 among the proteins that co-immunoprecipitate with Calypso, by mass-spectrometry (Scheuermann et al., 2010). However, ribosomal proteins are often detected in such experiments as contaminants. Thus, we decided to confirm whether this interaction was specific. To this end, we co-transfected S2 cells with *pAct-Flag-Calypso* and *pAct-uL11-Myc* vectors, and performed co-immunoprecipitations with anti-Myc and anti Flag antibodies. Co-immunoprecipitation between uL11-Myc and Flag-Calypso was detected with either protein as bait, confirming that this interaction is specific (**Fig. 50**). As Calypso is known to deubiquitinate H2AK118 in *Drosophila*, these results prompted us to determine the genome-wide distribution of this mark in addition to that of uL11K3me3 and Corto.

Characterisation of the uL11 antibodies.

Polyclonal antibodies were generated in rabbits by injection of a peptide corresponding to the N-terminal domain of uL11, tri-methylated on lysine 3. To obtain an antibody that recognizes specifically the tri-methylated lysine of uL11, one of these antibodies underwent differential purification. The antibodies retained on a column loaded with the tri-methylated uL11 peptide were further purified on a similar column loaded with the same peptide, though unmethylated. The flow-through was recovered and is referred to as the uL11K3me3 antibody, while the retained fraction is referred to as the uL11 antibody. Both were shown to recognize a single band in western blot, at the approximate molecular weight of uL11 (17.7kDa) (Anne Coléno-costes, Sébastien Bloyer).

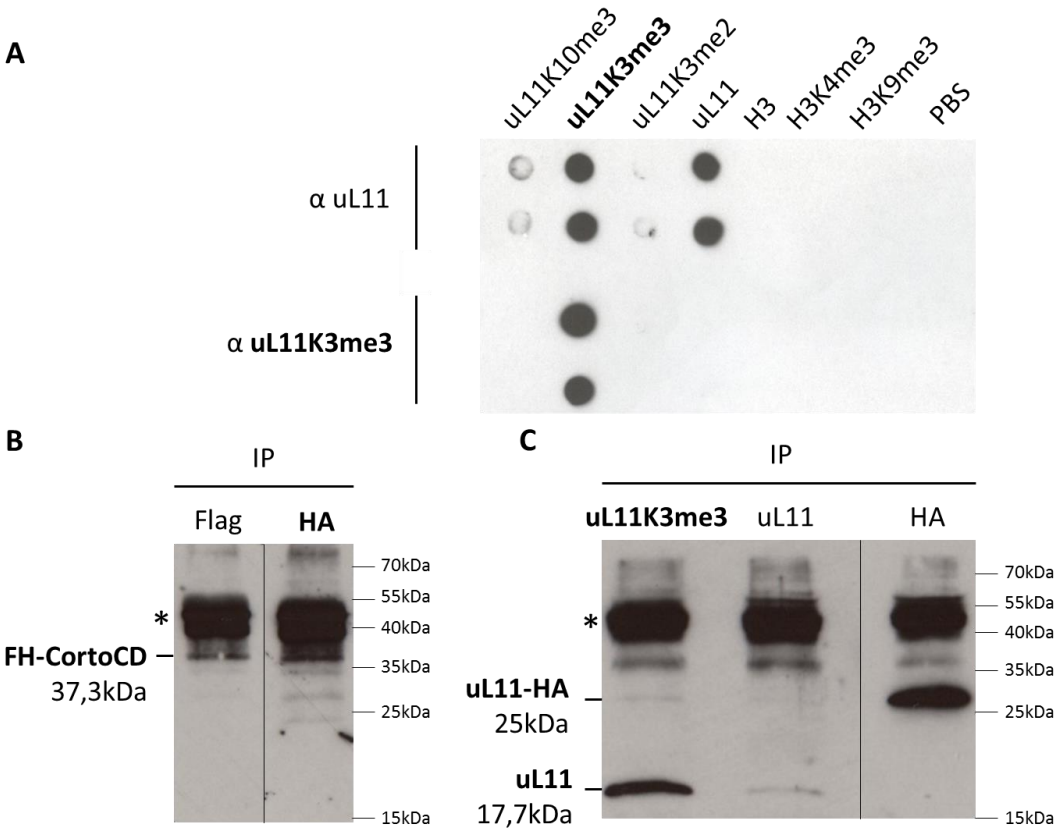

Figure 51. Characterisation of ChIP-seq antibodies.
A) Dot-blot showing the reactivity of the uL11 and uL11K3me3 antibodies for a variety of peptides containing lysines in different methylation states. B) and C) Chromatin from stable S2 cells lines expressing Flag-HA-CortoCD (B) or uL11-HA (C) was crosslinked and sonicated according to our ChIP-seq protocol (cf. Materials and methods). It was then used as material for immunoprecipitation with uL11, uL11K3me3, HA or Flag antibodies. Immuno-precipitates were denatured by heating and separated by SDS-PAGE. Shown are western blot revelation for HA (B) or all forms of uL11 (C). Vertical lines indicate that different wells from the same gel were juxtaposed in the image for clarity. Asterisks: IgG.

To determine the specificity of these antibodies, their reactivity towards a range of methylated and unmethylated peptides was tested by dot-blotting (Anne Coléno-Costes, Hélène Thomassin, **Fig. 51A**). The results show that while the uL11 antibody recognizes all uL11 peptides, the uL11K3me3 antibody specifically reacts with tri-methylated lysine 3 of uL11.

I adapted a protocol previously used by our team to perform ChIP, for use in S2 cells. To validate it, I immunoprecipitated chromatin from stable cells expressing the chromodomain of Corto tagged with Flag and HA in N-ter (FH-CortoCD), with either anti-HA or anti-Flag antibodies, which had already been validated for ChIP experiments. Both antibodies yielded a band corresponding to the expected molecular weight of FH-CortoCD, thus validating the adapted ChIP protocol (**Fig. 51B**).

To determine whether the uL11K3me3 antibody may be used to produce ChIp-seq data, I tested its ability to immunoprecipitate uL11 from chromatin preparations. To this end, I generated a vector to express uL11 with a HA tag in C-ter. A stable S2 cell line was generated by transfection with this plasmid (Hélène Thomassin). I then precipitated chromatin from these cells with either the anti-uL11, anti-uL11K3me3 or an anti-HA antibody. Western blot revealed that the anti-uL11K3me3 antibody immunoprecipitated two bands, corresponding to uL11-HA and endogenous uL11 (**Fig. 51C**). Strikingly, the band corresponding to uL11-HA was very faint as compared to endogenous uL11. This suggests

that either uL11-HA is expressed at much lower levels than uL11, or that it is methylated less efficiently. These results however validate the use of the uL11K3me3 antibody for ChIP experiments.

ChIP-seq analysis.

In order to compare the distribution of FH-CortoCD, uL11K3me3 and H2AK118ub within the same sample, we decided to perform all chromatin immunoprecipitations within a single cell line expressing FH-CortoCD. Three sub-lines were established, and maintained independently for two weeks. Cells from each sub-line were then collected at the same time, and their chromatin purified for ChIP experiments. Each preparation was split in three parts to immunoprecipitate H2AK118, FH-CortoCD and uL11K3me3. Immunoprecipitated chromatin was then sent to the "transcriptome and epigenome" platform at the Pasteur institute for library preparation and sequencing (Caroline Proux).

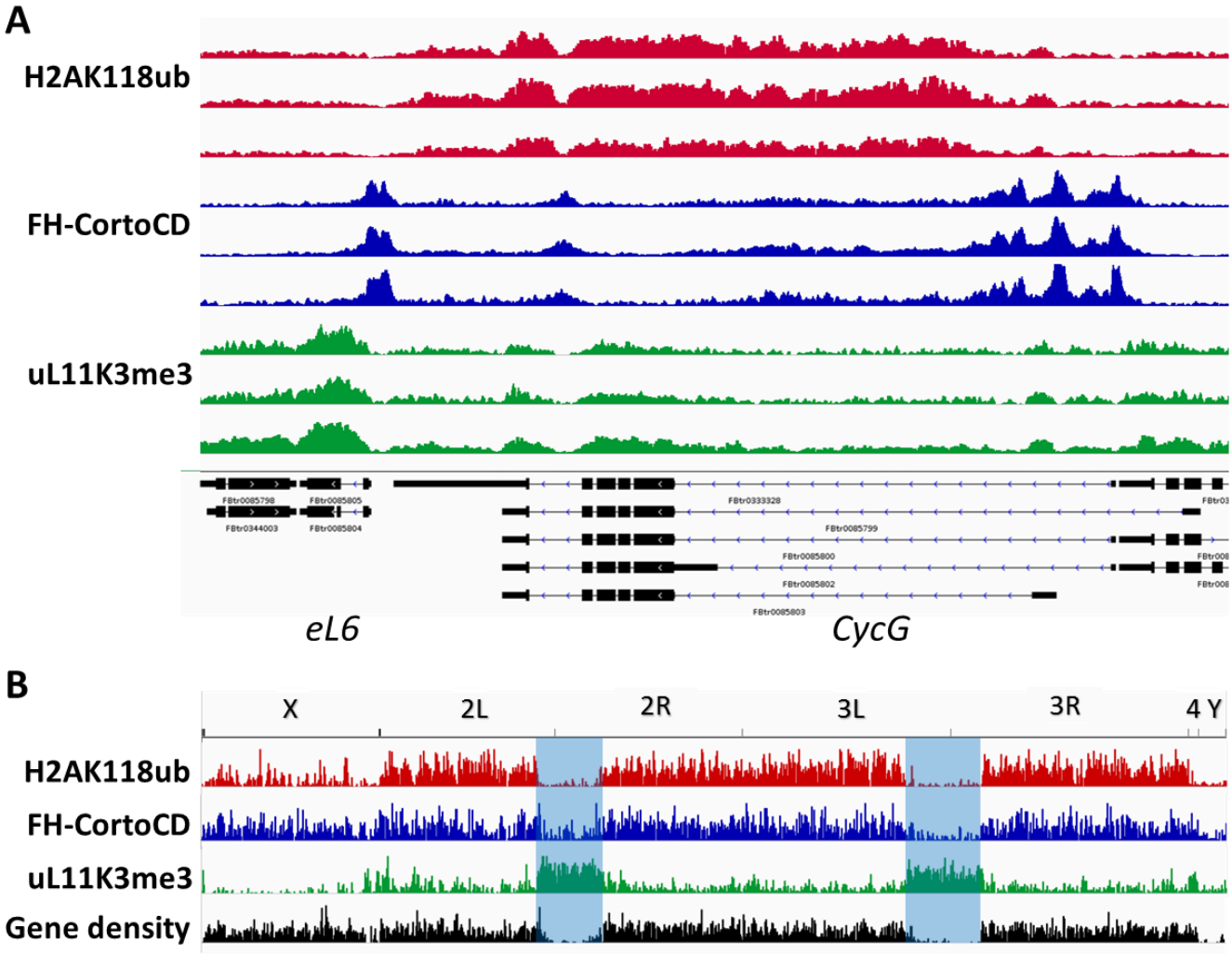

Figure 52. Overview of the ChIP-seq profiles for H2AK118ub, FH-CortoCD and uL11K3me3.
A) Zoomed-in view of the tag density for H2AK118, FH-CortoCD and uL11K3me3 replicates over the eL6-CycG region. Transcript models are provided for comparison. Black boxes: exons. Dotted lines: introns. Note the high similarity of the tag distribution between replicates. B) Genome-wide view of the density of regions enriched for H2AK118ub (red), FH-CortoCD (blue) and uL11K3me3 (green) as obtained with MACS 2.0. Gene density (black) is provided for comparison. Note the high density of regions enriched for uL11K3me3 corresponds to areas of low gene density. Two of them encompass the centromeres of second and third chromosomes (highlighted in blue).

All three immunoprecipitations produced clear enrichment signals with very high reproducibility between samples (**Fig. 52A**). Strikingly, FH-CortoCD was enriched over sharp regions, mostly located

at the TSS of annotated genes. In contrast, both H2AK118ub and uL11K3me3 displayed broad enrichment profiles.

Regions significantly enriched in regard to the input were determined with the MACS 2.0 software. Computation of the Irreproducible Discovery Rate (IDR) showed that the called regions were highly reproducible for FH-CortoCD, and moderately for uL11K3me3 and H2AK118ub (cf. Materials and Methods). The latter may be explained by the lower detection accuracy of the MACS software for broad enrichment profiles. Strikingly, uL11K3me3 was found to be enriched both within coding genes and large regions devoid of them. Indeed, the genome-wide distribution of uL11K3me3-enriched sites displayed an unusual bias towards regions of low gene density (**Fig. 52B**). Two of them encompass the centromeres of the second and third chromosome. A third one may correspond to the centromeric region of the X chromosome. This suggests that uL11K3me3 may bind within heterochromatin domains.

Analysis of the gene-wise binding pattern of FH-CortoCD, uL11K3me3 and H2AK118.

The TSS bound by FH-CortoCD could be reliably identified, and 7588 genes were identified for the presence of Corto in all replicates. However, they proved to be too numerous to perform a Gene Ontology analysis. On the opposite, while many regions enriched for uL11K3me3 and H2AK118ub could be detected, their large binding domains were detected as multiple enriched regions clustering next to each other. The large number of those enrichment regions and their approximative placement in regard to enrichment domains caused the IDR method to eliminate most of them. We were thus concerned that the selected regions would thus not be representative of the general enrichment pattern of uL11K3me3 and H2AK118ub.

To circumvent those issues, and describe their target genes, I decided to characterize their binding patterns over all coding genes in the genome. By clustering together genes that display the same enrichment profiles, it is possible to describe the general binding patterns of uL11K3me3, FH-CortoCD and H2AK118ub. Furthermore, to gain insight into the transcriptional state of their target genes, I included in the clustering analysis some ChIP-seq data generated in S2 cells for RNAPolII, H3K4me3 and H3K27me3. For ease of reading, the results of this clustering are split between genes enriched or depleted for RNAPolII, as a proxy for transcriptional competence.

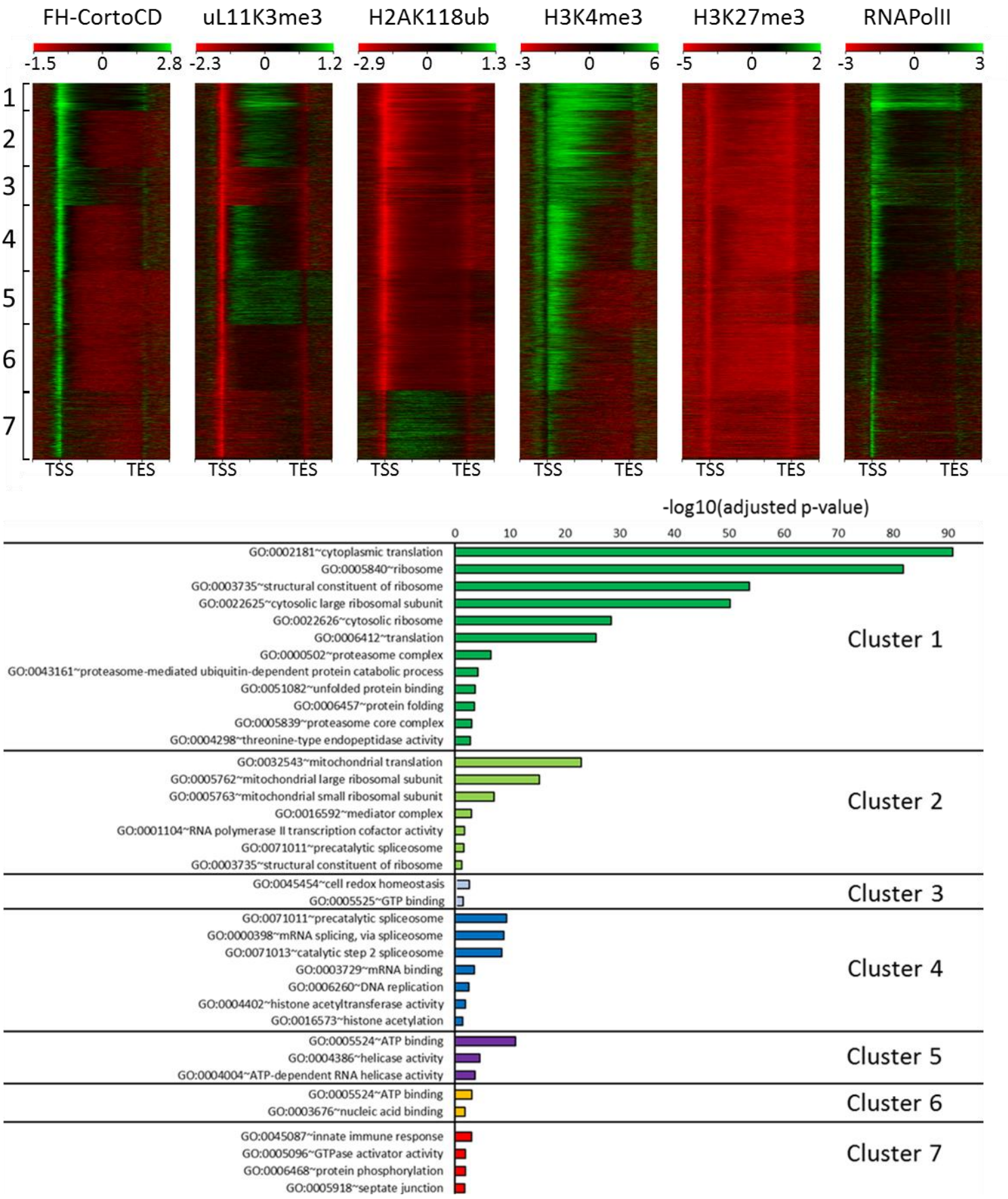

Figure 53. Hierarchical clustering of genes enriched for RNAPolII.

Upper panel: Heatmap showing the relative enrichment of FH-CortoCD, uL11K3me3, H2AK118ub, H3K4me3,

H27K3me3 and RNAPolII over their respective input, along the transcribed regions of coding genes enriched for RNAPolII. Unsupervised hierarchical clustering was performed using the enrichment signal for all six datasets. After an initial round of clustering, each cluster was submitted to further clustering until no new patterns could be discovered. Resulting clusters that shared the same patterns were then merged. The colour keys display the log2(Fold change over input) and its translation into the colour code. Genes are aligned over their Transcription start site (TSS) and Transcription end sites (TES). A 2000 base pair region is displayed 5' of the TSS and 3' of the TES. Lower panel: Gene ontology analysis of the enrichment for Cellular Compartment, Molecular Function and Biological Process GO terms within each identified cluster.

Strikingly, FH-CortoCD localizes at the TSS and correlates with the enrichment for RNAPolII. Gene clustering reached saturation without identifying a cluster that contained RNAPolII but not FH-CortoCD. This suggests that FH-CortoCD can bind every transcribed or paused TSS.

In contrast, uL11K3me3 was found on the gene bodies. While it covered the whole gene bodies in clusters 1 and 2, it displayed a preference for the 5' region in cluster 4. Interestingly, it was not contained within the gene body and extended 3' of the TES in cluster 5. Remarkably, uL11K3me3 was locally depleted within all the TSS bound by FH-CortoCD.

H2AK118ub was found within the bodies of a single cluster of RNAPolII-enriched genes. Strikingly, this cluster displayed the least enrichment for RNAPolII and H3K4me3, suggesting that those genes are weakly transcribed or transcriptionally paused in S2 cells.

It is interesting to note that unlike FH-CortoCD, gene clusters were found that are devoid of uL11K3me3 (clusters 3, 6 and 7) or H2AK118ub (clusters 1 to 6). This suggests that their binding is specific to certain genes either regarding their ontology or their transcriptional status. I thus performed a Gene Ontology analysis to determine whether these clusters were enriched for functional categories. While the cluster enriched for H2AK118ub did not show any striking gene ontology, all four clusters that contained uL11K3me3 displayed functional term enrichment. Notably, clusters 1 and 2 were highly enriched for cytoplasmic and mitochondrial translation, respectively. On the other hand, cluster 4 and 5 displayed milder enrichment for spliceosome components, ATP-binding and helicase ativity.

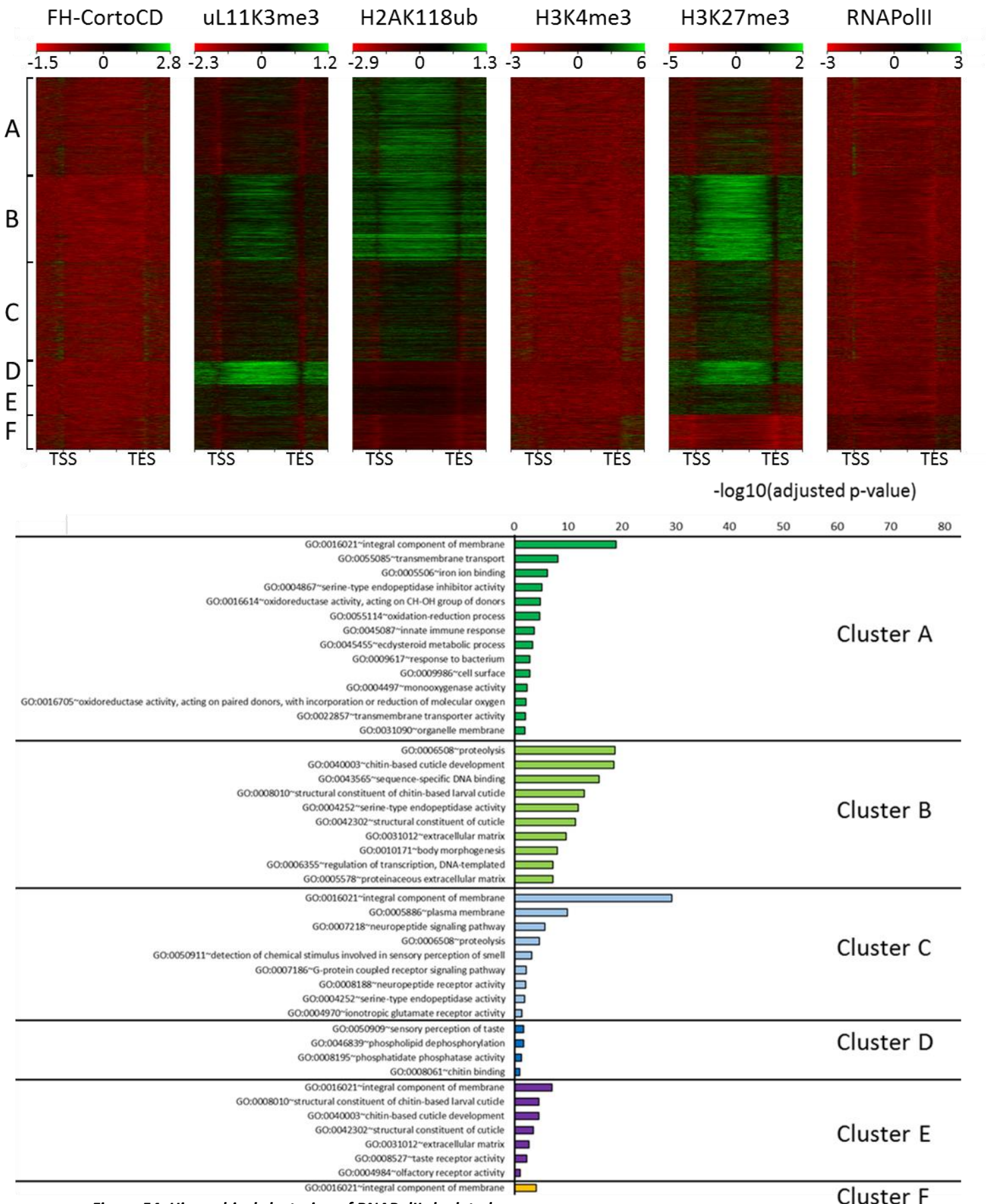

Figure 54. Hierarchical clustering of RNAPolII-depleted genes.

Upper panel: Heatmap showing the relative enrichment of FH-CortoCD, uL11K3me3, H2AK118ub, H3K4me3, H27K3me3 and RNAPolII over their respective input, along the transcribed regions of coding genes depleted for RNAPolII. Unsupervised hierarchical clustering was performed using the enrichment signal for all six datasets. After an initial round of clustering, each cluster was submitted to further clustering until no new patterns could be discovered. Resulting clusters that shared the same patterns were then merged. The colour keys display the log2(Fold change over input) and its translation into the colour code. Genes are aligned over their Transcription start site (TSS) and Transcription end sites (TES). A 2000 base pair region is displayed 5' of the TSS and 3' of the TES. Lower panel: Gene ontology analysis of the enrichment for Cellular Compartment, Molecular Function and Biological Process GO terms within each identified cluster.

No enrichment for FH-CortoCD was detected over genes devoid of RNAPolII. In contrast, both uL11K3me3 and H2AK118ub displayed strong enrichment over many such genes. Interestingly, uL11K3me3 enrichment was strongest within the clusters marked by H3K27me3 (clusters B, C, D and E). It spanned across gene bodies and visual inspection on a genome browser confirmed that in many cases, it covered broad regions that corresponded to H3K27me3 domains. Similarly, H2AK118ub spanned across gene bodies and formed broad domains. It however seemed to localize indifferently over genes either depleted or enriched for uL11K3me3 and H3K27me3.

Gene ontology analysis revealed no specific enrichment within these clusters, with the exception of the term proteolysis in cluster B. Membrane components were also found to be enriched, but as this ontology appeared in most of these clusters, it is likely that this enrichment is rather a feature of RNAPolII-depleted genes in general.

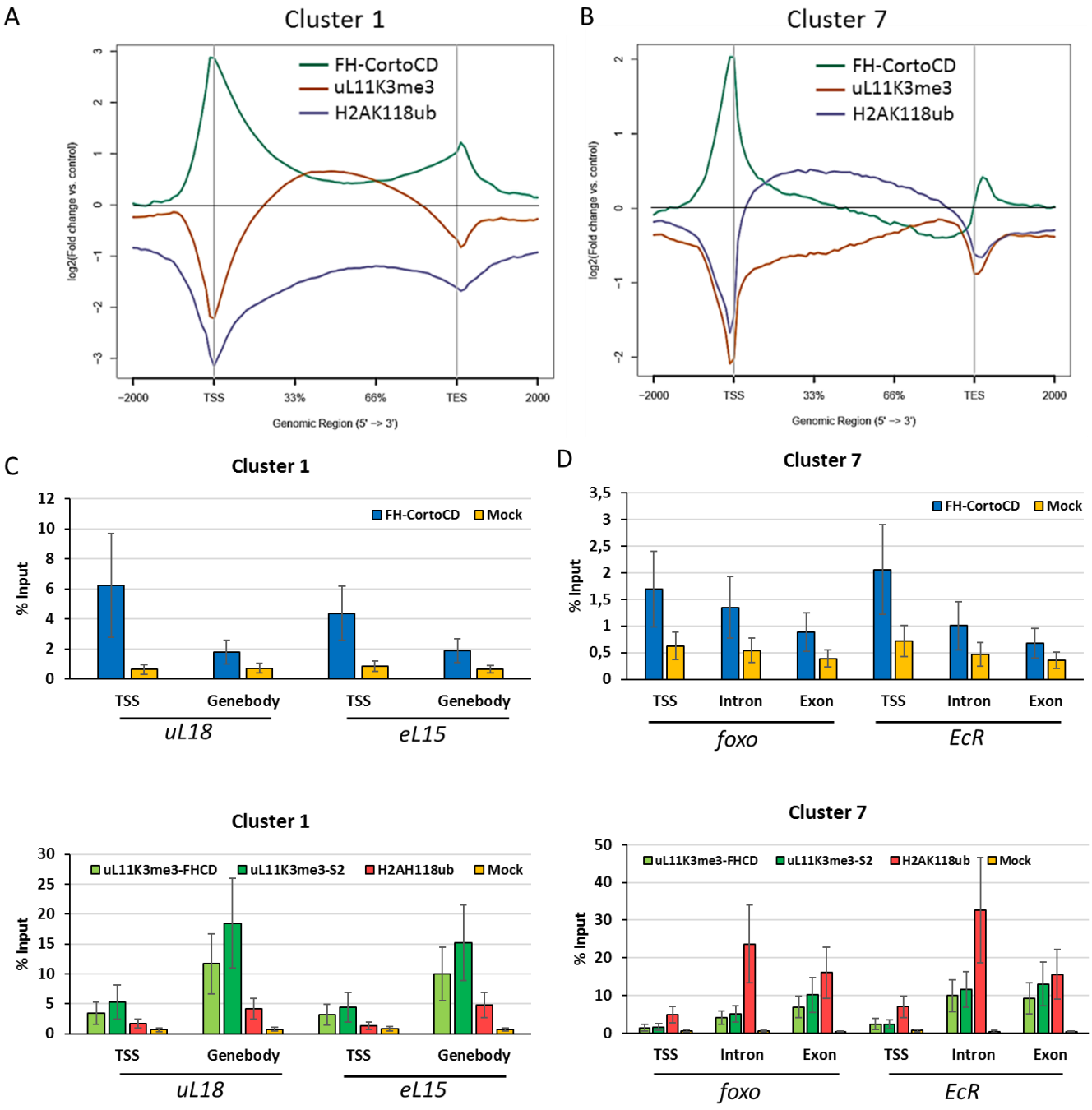

Figure 55. ChIP-qPCR validation of the binding profiles of FH-CortoCD, uL1K3me3 and H2AK118ub over cluster 1 and 7 genes.

A) and B) Average profiles of the enrichment for FH-CortoCD, uL11K3me3 and H2AK118ub over all genes from clusters 1 and 7. Genes were aligned over their TSS and TES (vertical lines). C) and D) ChIP-qPCR analysis of genes from clusters 1 and from cluster 7. IPs were performed with anti-HA antibody in cells expressing FH-CortoCD (blue) or in wild-type cells as a mock control (yellow). Tri-methylated uL11 was immunoprecipitated with the described uL11K3me3 antibody in cells expressing FH-CortoCD (light green, uL11K3me3-FHCD) or wild-type cells (dark green, uL11K3me3-S2). H2AK118ub was immunoprecipitated from FH-CortoCD cells (red). Note the difference in scale of the y-axis, justifying the double representation for a given set of genes. Error bars represent the standard error mean over two replicates. TSS: Transcription start site. The list of primers used and their genomic coordinates can be found in table 2.

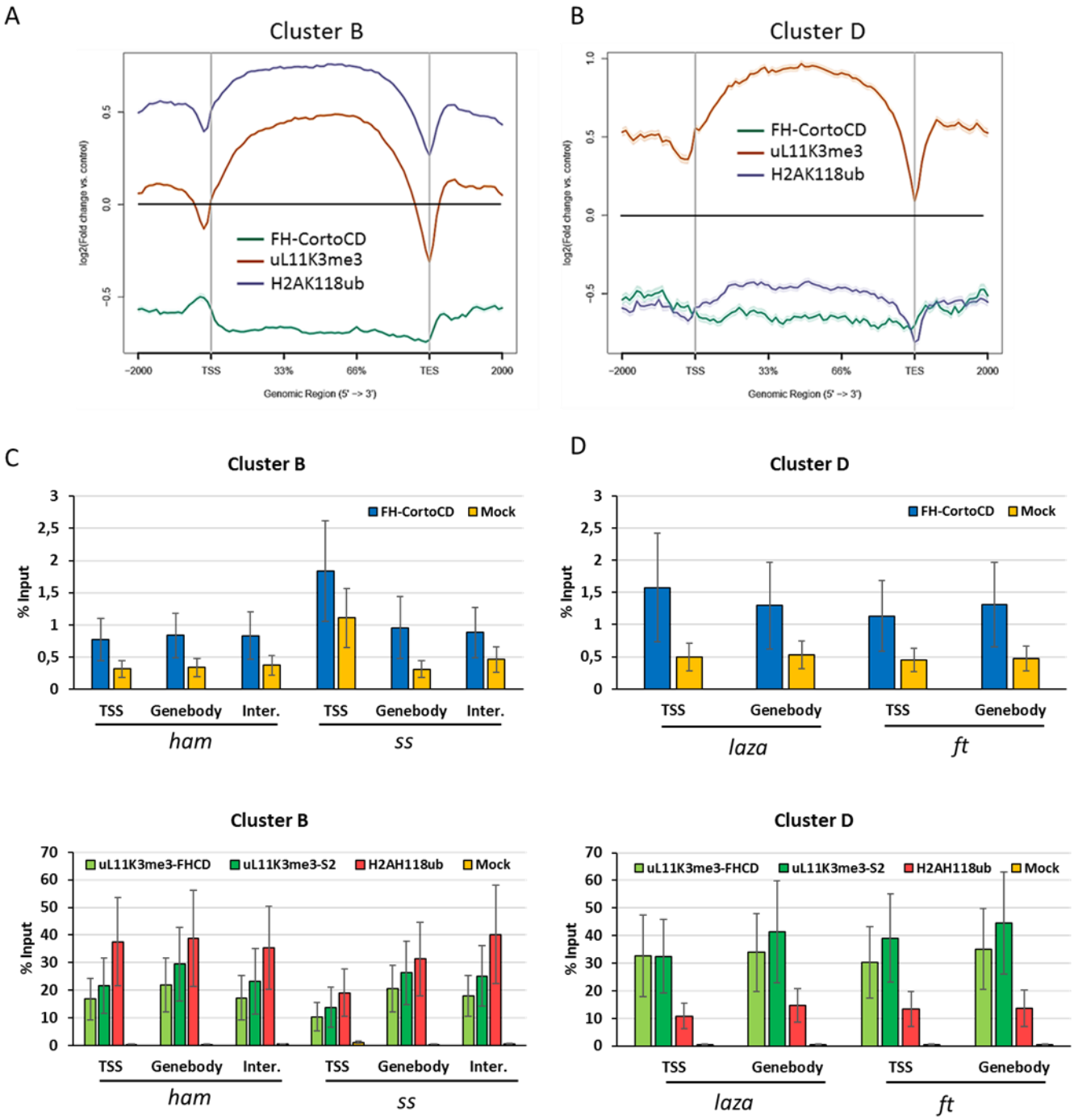

Figure 56. ChIP-qPCR validation of the binding profiles of FH-CortoCD, uL11K3me3 and H2AK118ub over cluster B and D genes.

A) and B) Average profiles of the enrichment for FH-CortoCD, uL11K3me3 and H2AK118ub over all genes from clusters B and D. Genes were aligned over their TSS and TES (vertical lines). C) and D) ChIP-qPCR analysis of genes from clusters B and from cluster D. IPs were performed with anti-HA antibody in cells expressing FH-CortoCD (blue) or in wild-type cells as a mock control (yellow). Tri-methylated uL11 was immunoprecipitated with the described uL11K3me3 antibody in cells expressing FH-CortoCD (light green, uL11K3me3-FHCD) or wild-type cells (dark green, uL11K3me3-S2). H2AK118ub was immunoprecipitated from FH-CortoCD cells (red). Note the difference in scale of the y-axis, justifying the double representation for a given set of genes. Error bars represent the standard error mean over two replicates. TSS: Transcription start site. Inter.: intergenic region. The list of primers used and their genomic coordinates can be found in table 2.

Validation of the described binding patterns by ChIP-qPCR

The enrichment of uL11K3me3, FH-CortoCD and H2AK118ub was tested by ChIP-qPCR over two genes from clusters 1 and 7 (**Fig. 55**), and two genes from clusters B and D (**Fig. 56**). Since the expression of FH-CortoCD was previously shown to modify the localization of uL11 in S2 cells (Coléno-Costes et al., 2012), we also decided to verify whether the uL11K3me3 binding pattern was similar in wild type cells.

FH-CortoCD was detected specifically at the TSS of cluster 1 genes *uL18* and *eL15*, and to a lesser extent at those of cluster 7 genes *foxo* and *Ecdysone Receptor* (*EcR),* in accordance to the heatmap data. Furthermore, it showed no noteworthy enrichment at the TSS of cluster B gene *hamlet* (*ham*) and cluster genes *lazaro* (*laza*) and *fat* (*ft*). Some enrichment was detected at the TSS of cluster B gene *spineless* (*ss*), but its specificity is questionable, considering that the mock IP also displayed stronger signal at this location.

The binding patterns of uL11K3me3 was also consistent with the heatmap data: it was specifically enriched over the gene body in regard to the TSS in cluster 1 genes *uL18* and *eL15*. Some signal could however be detected over the gene bodies of cluster 7 genes *foxo* and *EcR*, though it was weaker than in cluster 1 genes. In addition, uL11K3me3 displayed a monotonous enrichment over cluster B and D genes *ham*, *ss*, *laza* and *ft*, confirming the binding pattern observed in the heatmap. Strikingly, the signal strength was very high in those genes, ranging between 20 and 40% of input recovery, a range reminiscent of histone ChIP signal. The binding pattern of uL11K3me3 obtained from wild type cells was similar over all tested genes, suggesting that expression of FH-CortoCD does not qualitatively change it. However, it was subtly, but consistently higher at all tested locations. These data suggest that FH-CortoCD expression reduce the overall amount of uL11K3me3 bound on chromatin.

As expected, H2AK118ub was detected in a monotonous pattern over cluster B and D genes *ham*, *ss*, *laza* and *ft* and was depleted in cluster 1 genes *uL18* and *eL15*. Furthermore, it was indeed detected over the gene bodies of cluster 7 *foxo* and *EcR*. Interestingly, it distribution was not homogenous throughout these genes, displaying stronger signal within introns than exons in both cases.

H2AK118ub displays a preference for genes containing large introns.

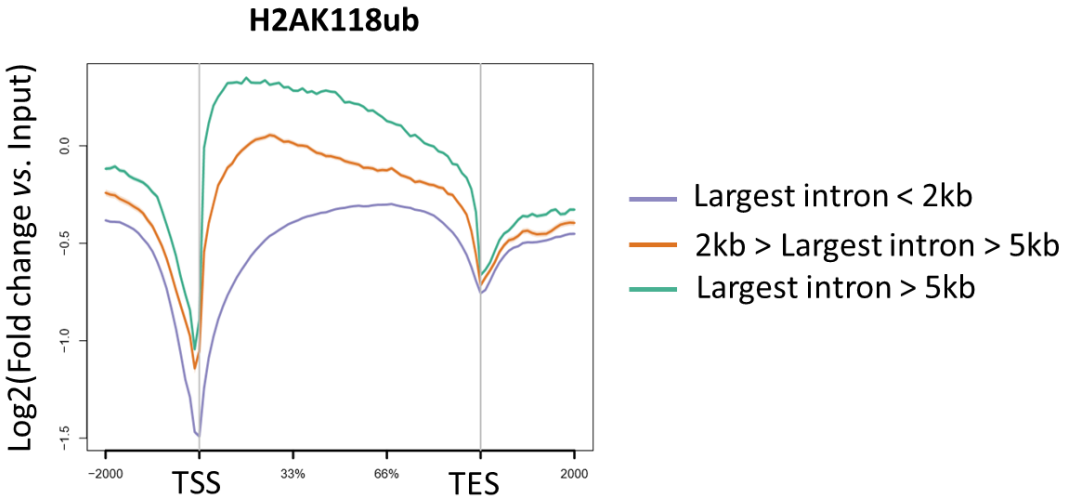

Figure 57. Average profile of H2AK118ub signal over all genes classified according to the size of their largest intron.
Coding genes were separated into three categories depending on the size of their largest intron. The average enrichment for H2AK118ub over the gene body is represented for each category.

The enrichment pattern of H2AK118ub appeared different within cluster 7 genes than within RNAPolII-depleted genes. Indeed, it was contained within gene bodies, and was not monotonous. Thus, we looked whether they shared a common feature that might explain such a pattern.

Strikingly, upon visual inspection on a genome browser, many of these genes appeared to contain very large introns. Indeed, 38,4% of cluster 7 genes contained introns larger than 5kb, while these are found in only 11,4% of all genes (binomial p-value < 10^{-6}). To determine whether H2AK118ub displayed enrichment over such genes genome-wide, we separated all coding genes in three categories based on the size of their largest intron. Computing the average profile of H2AK118ub enrichment over these gene categories revealed its preference for genes containing introns larger than 5 kilobases. Furthermore, H2AK118ub enrichment was skewed towards the 5' of those genes (**Fig. 57**). This oriented profile further suggests that there may be a structural feature within those genes that correlates with H2AK118ub enrichment.

B. Discussion

FH-CortoCD binds the same TSS as RNAPolII

Genome-wide analysis of the pattern of FH-CortoCD enrichment revealed its presence at all TSS enriched for RNAPolII (Clusters 1 to 7, **Fig. 53**). Conversely, FH-CortoCD was not detected at TSS lacking RNAPolII (Clusters A to F, **Fig. 54**). Hierarchical clustering attained saturation without identifying any cluster of genes containing one but not the other. These results suggest that FH-CortoCD may be recruited onto TSS by associating with the RNAPolII complex. Consistently, previous work showed that FH-CortoCD was recruited onto the *hsp70* gene upon heatshock induced activation of transcription (Coléno-Costes et al., 2012).

Interestingly, that work also showed that FH-CortoCD co-localized with paused RNAPolII (Ser5p) on polytene chromosomes, to a greater extent than with elongating RNAPolII (Ser2p). Furthermore, another study showed that Corto specifically interacts with the elongin complex, and antagonizes its function in wing vein specification (Rougeot et al., 2013). Since the elongin complex is known to promote RNAPolII elongation, it suggests that Corto may regulate RNAPolII pausing at the TSS. The observed binding profile is consistent with this hypothesis. Indeed, FH-CortoCD signal sharply localizes at the TSS, and does not spread towards the gene body as much as RNAPolII signal does over the most active gene clusters (1 to 4).

It should however be noted that FH-CortoCD peaks can be found at other sites than TSS (**Fig. 52** shows several such peaks within the introns of the *CycG* gene). It would be interesting to analyse whether these sites correspond to regulatory elements. Additionally, Corto has been described to associate with several Polycomb-group proteins and Enhancers of Polycomb and Trithorax (cf **Fig.48**), It would be thus interesting to determine whether it co-localizes with PRC1 components genome-wide.

uL11 binds both active genes and repressed chromatin domains

The genome-wide distribution of uL11K3me3 revealed that it binds broad chromatin domains. Interestingly, significantly enriched regions detected by the MACS 2.0 software clustered near the centromeres of the second and third chromosomes. These data suggest that uL11K3me3 may associate with heterochromatin. Consistently, high enrichment density is also detected over the fourth chromosome, which is mostly heterochromatic in *Drosophila*. In contrast, the Y chromosome that is also heterochromatic, shows no such enrichment. It should however be noted that this chromosome is frequently lost in S2 cells, and fails to produce reads for DNA-seq (Lee et al., 2014). The observation that uL11 binds to both gene bodies and heterochromatin is reminiscent of the binding pattern of uL5, uL23 and uL30 described in *S. pombe*. Indeed, these three r-proteins were found by ChIP-on-chip to bind genes and pericentromeric chromatin (De et al., 2011).

Indeed, uL11K3me3 was also found to be enriched over the gene bodies of both active and repressed coding genes. In repressed chromatin, it formed broad enrichment domains that spanned across gene bodies and correlated with H3K27me3 enrichment. In contrast, it was mainly found contained within gene bodies in RNAPolII-enriched genes. In that aspect, its pattern on cluster 5 genes was an exception: uL11K3me3 enrichment could be detected within the gene body, but it also extended 3’ of the TES. While this warrants further investigation, it is possible that those genes are located at the borders of repressed chromatin domains. Indeed, the heatmap representation displays RNAPolII and H3K4me3 signal 5’ of the TSS and 3’ of the TES of most active genes, which likely correspond to the presence of neighbouring active genes. In the case of Cluster 5, RNAPolII and H3K4me3 signal were depleted 3’ of the TES in comparison to other clusters. Furthermore, subtle signal could be detected for H2AK118ub and H3K27me3, suggesting the presence of neighbouring repressed chromatin domains.

Thus, we conclude that uL11 displays at least two different binding patterns, which suggests that it may be recruited to chromatin by different mechanisms. Notably, we found that the intensity of uL11K3me3 signal in ChIP-qPCR is on par with that of histone ChIP. A previous study showed that several r-proteins bind chromatin though interaction with histone H1 in *Drosophila* and mediate gene repression (Ni et al., 2006). Such an interaction could explain the broad distribution of uL11K3me3 on chromatin. Alternatively, r-proteins have been shown to bind coding genes and pericentromeric chromatin in an RNA-dependent manner (De et al., 2011; Schroder and Moore, 2005). It was thus proposed that r-proteins associated with nascent transcripts on chromatin. Consistently, uL11 was recruited to the *hsp70* gene upon transcription activation (Coléno-Costes et al., 2012). While this may explain a part of the binding pattern of uL11K3me3, it should be noted that at least one cluster was identified that displayed all the characteristics of actively transcribed genes, but did not contain uL11K3me3 (cluster 3). While this should be confirmed by analysing transcriptomic data, it suggests that transcription of a gene is not sufficient to recruit uL11K3me3. Thus, its binding appears specific to a subset of genes, which are most enriched for cytoplasmic and mitochondrial ribosome biogenesis ontologies.

uL11K3me3 and FH-CortoCD are mutually exclusive over coding genes.

uL11K3me3 was sharply depleted at the TSS that were bound by FH-CortoCD, but not at other TSS. This is surprising considering that FH-CortoCD specifically interacts with the tri-methylated lysine of uL11. Several hypotheses may explain this exclusion. 1) The binding of FH-CortoCD to uL11K3me3 may prevent the antibodies from accessing the trimethylated lysine 3 epitope, especially after paraformaldehyde fixation. This would be consistent with the observation that FH-CortoCD colocalizes with uL11 on polytene chromosomes (Coléno-Costes et al., 2012). This hypothesis could be tested by doing ChIP experiments with an antibody that recognizes a tagged version of uL11, though it will not allow to determine its methylation state. 2) FH-CortoCD may antagonize the binding of uL11K3me3. While they do interact, it is possible that FH-CortoCD relocalizes uL11 away from chromatin, or that it induces its degradation or demethylation. This would be consistent with the fact that FH-CortoCD expression in S2 cells decreases the signal for uL11K3me3 over all the genomic loci we tested by ChIP-qPCR. uL11K3me3 was found to be also depleted at the TSS in wild type cells, but this may reflect the same effect from endogenous Corto. Thus, to test that hypothesis, the chromatin binding profile uL11K3me3 should be compared to that of a variant whose lysine 3 is replaced or deleted, preventing its interaction with Corto. 3) As RNAPolII binds the TSS of active genes, it displaces nucleosomes, resulting in a local depletion of histone ChIP signals. The deficit of uL11K3me3 signal at the TSS of active genes is reminiscent of this effect. Indeed, H2AK118ub displays the very same depletion pattern as uL11K3me3 in all described clusters. Since FH-CortoCD signal greatly correlates with that of RNAPolII, this exclusion pattern could be explained if uL11K3me3 were to bind chromatin by associating with histones.

H2AK118ub is enriched in repressed chromatin and a specific cluster of RNAPolII-enriched genes.

Similarly, H2AK118ub displayed two binding patterns. It covered repressed genes in a monotonous manner, and extended across the limits of those genes. Conversely, H2AK118ub localized within the gene body of specific RNAPolII-enriched genes. Interestingly, H2AK118ub enrichment within genes seemed to correlate with the presence of large introns. This correlation does not necessarily mean that H2AK118ub binds large introns. It could be that the genes that contain large introns share specific features that correlate with H2AK118 ubiquitination. Notably, large introns are known to frequently contain regulatory elements, and cryptic TSS or exons (Sibley et al., 2015). It would thus be interesting to determine if H2AK118ub specifically correlates with any such feature. To this end, average profiles could be computed over a set of features, and compared to the enrichment for nucleosomes, as obtained with a pan H2A or H3 ChIP.

Relationship between H2AK118 and uL11

No obvious co-localization or exclusion pattern could be observed between uL11K3me3 and H2AK118ub. There is thus no evidence that the interaction between uL11 and Calypso may regulate H2AK118 ubiquitination over coding genes. Several possibilities however remain to be tested. 1) This interaction may occur away from chromatin. 2) It might occur away from coding genes, for instance at PREs, which have not yet been analysed. 3) This interaction could be specific of unmethylated uL11, which may display a different localization than uL11K3me3.

C. Materials and methods

Cell culture and transfections

The uL11 and Calypso CDS were cloned into the *pAWM and pAFW* Gateway® *Drosophila* vectors allowing expression of uL11 with a Myc tag in C-ter or Calypso with a Flag tag in N-ter, respectively. S2 cells were cultured at 25°C in Schneider's *Drosophila* medium supplemented with 10%, heat inactivated foetal bovine serum and 100 units.mL^{-1} of penicillin and streptomycin. S2 cells were cultured at 25°C in Schneider's *Drosophila* medium supplemented with 10%, heat inactivated foetal bovine serum and 100 units.mL^{-1} of penicillin and streptomycin. For transfection, a mix of *pAWM-uL11* and *pAFW-Calypso* expression vectors was prepared in a 1:1 molar ratio. Cells were transfected with 2µg DNA of this mix using Effecten® transfection reagent (Qiagen) according to the manufacturer's instructions (1:10 DNA/Effecten® ratio). For stable expression of FH-CortoCD, a mix of the expression vector *pAFHW-CortoCD-NLS* (Coléno-Costes et al., 2012) and the *pCoBlast* selection plasmid was prepared in a 5:1 molar ratio. Cells were transfected with 2 µg DNA of this mix according to the same procedure as described above. Selection was performed by addition of 10 µg.mL^{-1} of blasticidin after 48 hours. After initial selection, stable cell lines were cultured with 2 µg.mL^{-1} blasticidin.

Co-Immunoprecipitations

48 hours after transfection, protein crosslinking was realised by treating cells with 1% paraformaldehyde for 10 minutes on ice, followed by neutralization with 1.3M Glycine on ice. Protein lysates were extracted in RIPA buffer (50mM Tris-HCl pH 7.5, 150mM NaCl, 25mM $NaVO_4$, 25mM NaF, 0.1% SDS, 0.5% NP40) supplemented with protease inhibitor cocktail and phosphatase inhibitor cocktail (Roche Diagnostics, Meylan, France). 500µg of protein exctract were immunoprecipitated with 3 µg of either anti-Myc (ab9132), anti-Flag (FC3165) or anti-HA (ab9110) antibodies, using magnetic protein G-agarose beads (Ademtech). Immunoprecipitates were dissociated from the beads by heating 5 minutes at 95°C and loaded onto 12% SDS gels. Western blot was performed according to standard protocols. Anti-Flag (FC3165, 1/5000) and Anti-Myc (ab9132, 1/5000) antibodies were used for revelation.

Dot-Blot

50 and 200 ng of H3K9me3, H3K4me3, uL11K3me3, uL11K3me2, uL11K10me3, unmethylated uL11 or unmethylated histone3 peptides, previously described in (Coléno-Costes et al., 2012), were deposited on a wet nitrocellulose membrane. The membrane was left to dry 5 minutes at room temperature before saturation for 3 hours in TBS-Tween (20 mM Tris-HCl pH 7.4, 150 mM NaCl, 0.2 % Tween 20) supplemented with 5 % Régilait. The membrane was washed twice in TBS-Tween and incubated with uL11 (1/14000) or uL11K3me3 (1/2000) antibodies at 4°C overnight. The membrane then underwent classical Western blot protocols.

Chomatin Immunoprecipitation

2*10^7 S2 cells stably expressing FH-CortoCD were harvested at 50% confluence and washed in Schneider's medium to remove foetal bovine serum. Cross-linking was realised in 1% paraformaldehyde for 10 minutes at room temperature, followed by neutralization with 1.3 M glycine. Cells were then washed in ice-cold PBS and resuspended in 3 mL hypotonic buffer (20 mM HEPES pH 7.9, 10 mM KCl, 1 mM EDTA, 10% glycerol, 1 mM DTT) supplemented with EDTA-free protease inhibitor cocktail (Roche Diagnostics). Cells were lysed in a dounce tissue grinder (Sigma-Aldrich) by applying 30

strokes of the loose pestle. Nuclei were then pelleted by centrifugation at 600 g for 5 min at 4 °C, and flash frozen in liquid nitrogen after removal of the supernatant. Nuclei were lysed by thawing in 3 mL RIPA buffer (50 mM Tris-HCl pH 8, 150 mM NaCl, 1 % NP-40, 0.5 % sodium deoxycholate, 0.1 % SDS, 1 mM DTT) supplemented with EDTA-free protease inhibitor cocktail (Roche Diagnostics). After incubation on ice for 30 minutes, lysates were separated into 12 microtubes of 200 µL and underwent sonication for 20 cycles (Diagenode Bioruptor sonifier; cycles of 30'' ON, 30'' OFF, high power). They were then pooled and centrifugated twice at 13,000 g for 15 minutes at 4°C to pellet insoluble chromatin. The supernatant was recovered and 24nµL were kept as input. For immunoprecipitation, 120 µL of A protein coated paramagnetic beads (Diagenode) were washed twice in RIPA buffer, and incubated for 4 hours with 12 µg of antibodies in RIPA buffer, on a rotating wheel at 4°C. After washing twice with RIPA buffer to eliminate excess antibody, beads were resuspended in the sonicated chromatin extract and incubated overnight on a rotating wheel at 4 °C. Beads were then washed 3 times for 10 minutes in RIPA buffer, once in LiCl buffer (10 mM Tris-HCl pH 8, 250 mM LiCl, 0.5 % NP-40, 0.5 % sodium deoxycholate, 1 mM EDTA, 1 mM DTT), and twice in TE buffer (10 mM Tris-HCl pH 8, 1 mM EDTA, 1 mM DTT).

For ChIP-Western blot experiments, proteins were dissociated from the beads by heating at 95 °C for 5 minutes, and were loaded onto 15% SDS gels. Western blots were performed according to standard protocols. Anti-uL11 (Santa Cruz sc-82359, 1/1000) and anti-HA (Sigma F2411, 1/1000) were used to reveal uL11 and FH-CortoCD, respectively.

For qPCR and sequencing, immunoprecipitated DNA was purified with the IPure kit following the manufacturer's instructions (Diagenode). Elution was realized in 70 µL buffer C. Antibodies used for immunoprecipitation were: anti-uL11K3me3, anti-H2AK118ub (Cell signalling D27C4), and anti-HA (ab9110).

ChIP-seq analysis

Library reparation and sequencing were performed at the "Transcriptome and Epigenome" platform of the Pasteur institute, using 50 ng of IP or input DNA. Libraries were multiplexed by 12 on one Illumina flow cell run. A 51 bp single read sequencing provided an average of 45.9 reads per sample. Reads were filtered by the "fastq_quality_filter" command from the "fastx-toolkit" package (http://hannonlab.cshl.edu/fastx_toolkit/), using a threshold of 90 % bases with mapping quality ≥ 20. Reads that successfully passed the filtering step were aligned to the *Drosophila* genome (dm6, r6.13) using Bowtie 2 (http://bowtie-bio.sourceforge.net/bowtie2/) (v2.1.0) with default parameters (Langmead and Salzberg, 2012). Peaks were called by MACS2 (v2.1.0) by comparing each ChIP to its input library with default parameters (Zhang et al., 2008). Alignment files from replicates were merged by using the Samtools suite command "merge". Datasets for histones marks and RNAPolII, and their inputs obtained from S2 cells were recovered from GEO: H3K4me3 (IP: GSM1017409, Input: GSM1017398), H3K27me3 (IP: GSM1017406, Input: GSM1017397), RNAPolII (IP: GSM796331, Input: GSM796332). Heatmaps and aggregation plots of ChIP signal over gene bodies and Transcription Start Sites (TSS) were generated using the ngsplot package. (https://github.com/shenlab-sinai/ngsplot) (Shen et al., 2014). Some genes with spurious signal (such as genes from the histone complex) were excluded from the analysis based on signal uniformity over the full length of the gene. For heatmaps, unsupervised hierarchical clustering was performed over the signal for FH-CortoCD, uL11K3me3, H3K4me3, H3K27me3 and RNAPolII over gene bodies, in a recursive manner: clusters identified from a first step were submitted to further clustering until no new pattern could be discovered. Clusters displaying similar patterns were then merged, and represented as a heatmap.

qPCR

For validations, ChIP were performed similarly with the anti-uL11K3me3, anti-H2AK118ub and anti-HA antibodies. A mock immunoprecipitation was realised with the anti-HA antibody with chromatin extracted from untransfected S2 cells. qPCR experiments were carried out in a CFX96 system (Bio-Rad) using SsoFast EvaGreen Supermix (Bio-Rad). Two biological replicates – three technical replicates per biological replicate - were performed for each condition. Sequences of primer couples are listed in Table 2. Data were normalized against Input chromatin.

ChIP-qPCR primers		**Coordinates**
uL18-TSS-F	5'-agcgtcaaaggcacagcacaac-3'	2L:22536908-22536930
uL18-TSS-R	5'-atcgttcataccgttcacatcgc-3'	2L:22536739-22536760
uL18-genebody-F	5'-ccgaccgagaagaagacaggg-3'	2L:22535850-22535871
uL18-genebody-R	5'-ctcactacaacgatggcaaggc-3'	2L:22535669-22535689
eL15-TSS-F	5'-tatcccaaagcaactctgagc-3'	3L:27267208-27267228
eL15-TSS-R	5'-acaaccaacttacagcacgg-3'	3L:27267277-27267296
eL15-genebody-F	5'-cagtgctattcgtcgtgatccaa-3’	3L:27268199-27268221
eL15-genebody-R	5'-gctcacggttcttgcgcttcc-3’	3L:27268357-27268377
foxo-TSS-F	5'-ggtgaagtgagcggttgtgg-3'	3R:14056802-14056802
foxo-TSS-R	5'-actgattcgccgtcgccttc-3'	3R:14056925-14056944
foxo-intron-F	5'-atgagaggggcaggtacagc-3’	3R:14061742-14061761
foxo-intron-R	5'-aaggtgtccgccagatgctc-3’	3R:14061896-14061915
foxo-exon-F	5'-gccgaactcagtaaccacaac-3'	3R:14081012-14081032
foxo-exon-F	5'-accatcagtgccgcagtgtc-3'	3R:14081115-14081134
EcR-TSS-F	5'-tttactttggtgtgcgtgcc-3’	2R:6131970-6131989
EcR-TSS-R	5'-cgtgcgagcgaacaaccg-3’	2R:6131875-6131892
EcR-intron-F	5'-ctctccgttttctggctcacc-3’	2R:6126017-6126037
EcR-intron-R	5'-gttatccctgttttgtgttctgc-3’	2R:6125822-6125844
EcR-exon-F	5'-gagtgccgcctgaaaaagtg-3’	2R:6094780-6094799
EcR-exon-R	5'-agtggtcattttgtccttctcc-3’	2R:6094677-6094698
ham-TSS-F	5'-aatagtcggcgttctctgct-3’	2L:18792882-18792901
ham-TSS-R	5'-cccacaaagctcctcgaaag-3’	2L:18792977-18792996
ham-genebody-F	5'-ctcgctgtcatccgtgtccg-3'	2L:18765739-18765758
ham-genebody-R	5'-gccttggagcacacctcgc-3’	2L:18765641-18765659
ham-intergenic-F	5'-ggttatttggtcacagtctgc-3’	2L:18761513-18761533
ham-intergenic-R	5'-atcactctcatattcctaacttgg-3’	2L:18761388-18761411
ss-TSS-F	5'-cagtgtagtatgtgtgtgcg-3’	3R:16403972-16403991
ss-TSS-R	5'-acgatgttccactaccaacc-3’	3R:16403841-16403860
ss-genebody-F	5'-tcggtcctaggggtgaatag-3’	3R:16384510-16384529
ss-genebody-R	5'-tacagtgatgggtatgtgcg-3’	3R:16384349-16384368
ss-intergenic-F	5'-tcccctattcaattcgaggc-3’	3R:16408973-16408992
ss-intergenic-R	5'-cattgatcaggatgcagcag-3’	3R:16409123-16409142

laza-TSS-F	5'-aagaccgtagagcgtagagcg-3’	3L:22461196-22461216
laza-TSS-R	5'-ctgcgaccgagaaggcgac-3’	3L:22461085-22461103
laza-genebody-F	5'-gtaacctattgcggcggc-3’	3L:22459880-22459897
laza-genebody-R	5'-ggcgtcgttgtggtcattg-3’	3L:22459729-22459747
ft-TSS-F	5'-acaacaggtatctctctccg-3’	2L:4221907-4221926
ft-TSS-R	5'-ctcgctcagtggtctcaacg-3’	2L:4221772-4221791
ft-genebody-F	5'-gggtcgcctccacttac-3’	2L:4207282-4207299
ft-genebody-R	5'-cgtccttatccgttgctctg-3’	2L:4207139-4207158

Table 2. List of ChIP-qPCR primers.

II. Editing essential genes: a marker independent CRISPR mutagenesis strategy.

A. Overview

A classical way to study the functional importance of a gene is to examine the phenotypes caused by its mutation, inactivation, or overexpression. These approaches seemed however unfit for *uL11*. Indeed, no mutant was available, and its inactivation by RNA interference triggered the loss of nearly any tissue it was performed in (cf. Introduction chapter IV, Coléno-Costes, 2012). In addition, attempts to overexpress *uL11* with the UAS-Gal4 system yielded no obvious phenotype. This would be consistent with the description of *uL11* as resistant to overexpression in nematodes, as a consequence of its ability to regulate its own expression (Mitrovich and Anderson, 2000).

More importantly, uL11 is known to play an important role in translation, and its dysregulation was expected to impact that function. As we aimed to study specifically the biological meaning of its interaction with Corto, we decided to generate a variant of uL11 whose lysine 3 is mutated to an alanine ($uL11^{K3A}$). To this end, we set to generate the first genetic alleles for this gene.

We first considered to use an ends-out homologous recombination method to replace *uL11* with $uL11^{K3A}$. An elegant system allowed both positive and negative selection of mutant flies, at the cost of inserting a selection cassette within a few kilobases of the mutation of interest (Zhou et al., 2012). Unfortunately, the genomic locus of *uL11* contained no suitable location to insert such a sequence without taking the risk of disturbing the regulation of other essential genes (cf. Results chapter II.B).

Coincidentally, a new method was emerging during the first years of my thesis: CRISPR/Cas9-mediated mutagenesis This tool, first developed in bacteria, and later in eukaryotic cells, achieved remarkable efficiency (Jinek et al., 2012; Mali et al., 2013). It did not take much time before *Drosophila* researchers harnessed it for mutagenesis through Non Homologous End Joining (NHEJ) or Homologous Directed Repair (HDR) (Gratz et al., 2013, 2014). The high mutagenesis rates of this method (up to 22% injected flies displaying recombination events, and up to 18 % transmission to their progeny), made it conceivable to recover an HDR event by molecular screening.

B. Article

Marker-independent screen for CRISPR mutations by allele-specific quantitative PCR

Jérôme Deraze[1,2], Hélène Thomassin[1,2], Immane R'Kiki[1,2], Sébastien Bloyer[3] and Frédérique Peronnet[1,2,*].

[1] Sorbonne Universités, UPMC Univ Paris 06, Institut de Biologie Paris-Seine (IBPS), UMR 7622, Developmental Biology, F-75005, Paris, France

[2] CNRS, IBPS, UMR 7622, Developmental Biology, F-75005, Paris, France

[3] Institute for Integrative Biology of the Cell (I2BC), CEA, CNRS, Univ. Paris-Sud, Université Paris-Saclay, 91198, Gif-sur-Yvette cedex, France

* Corresponding author : Frederique.Peronnet@upmc.fr

Abstract

Single step CRISPR/Cas9-mediated generation of small scale nucleotide replacements can sometimes be the only option for mutagenesis, such as when working with essential genes. It can also be used to obtain precise mutation quickly in any gene, since it requires very limited upstream reagents. However, this formidable tool is plagued by lack of options to recover given mutations. Here, we adapted an allele-specific quantitative PCR technology for high-throughput screening of desired mutations in *Drosophila*. We generated a one codon substitution in the essential gene *RpL12/uL11* by CRISPR/Cas9-mediated homologous directed repair, thus obtaining the first allele for this gene. We describe here a high throughput qPCR-based method to quickly recover successful HDR events in *uL11*. Discriminating efficiency is increased by introducing a locked nucleic acid (LNA) at a strategic position in the screening primer. This improved specificity allows to test pools of flies for presence of a single allele copy. Additionally, we describe how this method can be adapted to recover a similar HDR event after BAC recombineering in bacteria. This strategy is a valuable addition to the CRISPR repertoire, as it serves the purpose of both recovering a small-scale HDR in flies, and the recombined BAC to perform rescue experiments.

Introduction

Drosophila melanogaster has been a model of choice for genetics, owing to its large collection of mutants. A hundred years of research on *Drosophila* yielded a number of strategies to alter its genome, from random gene disruption to insertional mutagenesis[1]. The recent advent of CRISPR/Cas9 mediated mutagenesis has now brought further the ability to modify the genome in ever more precise ways[2-5]. Its unprecedented ease of use and efficiency now allows researchers to target virtually any region of the genome.

However, while generating mutations is becoming simpler, such cannot be said of recovering mutants. Indeed, the identification of successful mutational events has always been somewhat tedious, and this step may discourage many researchers from using such approaches. Numerous strategies have emerged to ease the screening for mutants, many of which rely on phenotypic markers[6,7]. These convenient gene markers come with a price though: their insertion in the vicinity of the mutation site is likely to bias the expression of the mutated gene. Such confusing effect is expected to cloud the analysis of the mutant phenotypes, and defeats the purpose of precise gene editing. Recent “pop in/pop out” strategies have been described that elegantly address this caveat[8,9] . These strategies employ a two-step transformation protocol: the locus to be mutated is first replaced by a marker gene. A second mutagenesis is then performed to remove the marker and insert the desired mutation instead.

While these methods constitute a remarkably fool-proof approach to obtain scarless gene modifications, they require extensive preliminary reagent generation by molecular cloning. Additionally, the requirement for two successive rounds of mutagenesis implies a significant delay before mutant recovery.

A more important caveat is that the loss of function mutants that result from the marker integration need to be viable and fertile in order to proceed to the second mutagenesis step. Therefore, some essential genome locations cannot be targeted with these methods. Indeed, many *Drosophila* genes are essential either in development[10], or at the cellular level[11]. Unsurprisingly, genetic alleles are unavailable for many of the latter. Additionally, several genomic regions are described as haplo-lethal[12]. The study of this yet unreachable portion of the genome is a challenge that can now be undertaken with the CRISPR/Cas9 technology. It is indeed possible to study essential genes and loci by introducing a punctual mutation, for instance to replace a specific amino-acid[13]. This method however requires that target genes be left functional at all steps of mutagenesis.

This requirement provides little room for the insertion of a phenotypic marker, leaving no choice but to identify the mutant by molecular screening. In *Drosophila*, it typically requires individually crossing the G1 progeny, and collecting it for genotyping after it mated. The whole screening process must then be completed before the emergence of G2 adults, otherwise the number of mutant candidates becomes unmanageable. This calls for high-throughput screening methods, which can be tedious, for small-scale sequence changes are difficult to detect. A variety of techniques can be used, such as High Resolution Melting Analysis (HRMA)[14], allele-specific PCR[15], endonuclease assays[16], or even Sanger sequencing. However, these come with the draw-back of being time-consuming, labour-intensive, costly, or prone to false negatives.

A second challenge rises from the property of CRISPR/Cas9 to generate rather unpredictable off-target mutations[17,18]. Most of these can be removed by crossing the mutant with a control genetic background over several generations.

However, when the desired mutation has no phenotypic marker and/or causes viability and fertility defects, this process can become very cumbersome. Additionally, off-targets localized close to the target mutation may still be co-purified.

Thus, to indisputably attribute phenotypes to the mutation, the golden standard remains to perform functional rescue experiments. To this end, a Bacterial Artificial Chromosome (BAC) containing the whole gene region and surrounding regulatory sequences can be inserted in the *Drosophila* genome[19]. A similar mutation can be engineered in the BAC to ensure that the observed phenotypes are only rescued by a wild-type copy of the target. To this end, recombineering strategies have been developed, most of which also rely on a “pop in/pop out” strategy[20,21]. Once again, these strategies are very efficient but require a gruelling amount of molecular cloning, and two successive rounds of homologous-directed repair (HDR). In the case of small-scale HDR, an alternative approach removes these caveats: single-stranded DNA templates can catalyse HDR with high efficiency, abolishing the requirement for phenotypic selection[22,23]. They do however require a molecular screening method to recover recombinants.

We generated a one codon substitution in the essential gene *RpL12/uL11* by CRISPR/Cas9 mediated HDR, thus obtaining the first genetic allele for this gene in *Drosophila melanogaster*. It should be noted that we will henceforth follow the new nomenclature proposed to eliminate the confusion caused by the assignment of identical names to ribosomal proteins from different species[24] and use the name *uL11* instead of *RpL12*. We describe here a high throughput quantitative PCR-based method to quickly recover the successful HDR events in *uL11*. Discriminating efficiency is increased by introducing a locked nucleic acid (LNA) at a strategic position in the screening primer. This improved specificity allows to test pools of flies

for the presence of a single allele copy. Combination with real time qPCR makes easy to distinguish specific *versus* artefactual amplification without extensive upstream development. Additionally, we describe how the same method can be adapted to recover a similar HDR event after BAC recombineering in bacteria. By testing a pool of transformed cells, the efficiency of HDR can be verified, and the mutant isolated by a few rounds of dilutions.

Thus, our strategy is a valuable addition to the CRISPR repertoire, as it serves the purpose of both recovering a small-scale HDR in flies, and the recombined BAC to perform rescue experiments.

Results

The uL11 protein (aka RPL12) is a canonical component of the ribosome in all domains of life. Its depletion in flies is lethal, likely due to major ribosome impairments, as shown in yeast[25]. However, uL11 may be involved in other processes than translation. We have previously shown that it interacts through its lysine 3 with the Enhancer of Trithorax and Polycomb Corto and controls transcription [26]. We therefore decided to target this interaction by replacing lysine 3 into an alanine codon in the *uL11* gene.

The latter is located within a cluster of highly transcribed genes, many of which are also essential (*eIF5A*, *RpL39/eL39*, *yki...*)[27,28]. Unsurprisingly, this cluster is part of the 1.6% of haplo-lethal regions of the euchromatic *Drosophila* genome[29]. The immediate neighbourhood of *uL11* contains only two small intergenic sequences (465 and 620 bp, respectively) that might contain regulatory elements (Fig. 1A). Thus, the insertion of a selection cassette at any position inside this locus would be likely to disturb gene expression and impede viability. We therefore opted to edit the *uL11*

lysine 3 to alanine (K3A) by single step CRISPR/Cas9 mediated HDR using a single-strand DNA probe as template (ssODN).

Choice of a guide RNA and cutting tests in S2 cells.

The choice of an appropriate single guide RNA (sgRNA) is crucial to ensure the efficiency of mutagenesis. Indeed, the ability of different sgRNA to mediate Cas9 mediated mutagenesis is known to vary greatly and the cleavage site should be as close as possible to the sequence to be edited. We identified 6 Protospacer Adjacent Motives (PAM) within 25 bp of the target lysine codon (Fig. 1B). We thus cloned the corresponding sgRNAs into *pAc-sgRNA-Cas9* under the control of the *U6* promoter to test their ability to generate insertion and deletion (indel) mutations in *Drosophila* S2 cells. The 6 sgRNA were found to display similar efficiency (data not shown). Hence, sgRNA corresponding to the PAM sequence 4 (sgRNA4) (Supplementary Fig. 1) was chosen for it drives cleavage immediately next to the target codon and its orientation ensures that the target but not the ATG codon is deleted by Cas9 exonuclease activity.

Mutagenesis of the uL11 lysine 3 codon in *Drosophila*.

We next undertook fly mutagenesis. First, we cloned sgRNA4 in *pU6-BbsI-chiRNA* to express it in *Drosophila* embryos[30]. In this plasmid, the sgRNA is expressed together with a tracrRNA (trans-activating CRISPR RNA) that is required for Cas9-mediated DNA interference[31] (Fig. 2). To replace the target codon, we generated a 123 nucleotide ssODN template carrying the lysine (AAA) to alanine (GCC) substitution (K3A) encompassed in two 60 nucleotide-long homology arms. The *uL11* region of the recipient line *vasa-Cas9* (*w^{1118}; PBac{y[+mDint2]=vas-Cas9}VK00027*) was

sequenced before designing the ssODN in order to respect possible polymorphisms. To prevent base pairing with sgRNA4, the ssODN was designed to be homologous to the PAM-carrying strand.

Two-hundred *vasa-Cas9* embryos were injected with a mix of *ssODN* and sgRNA expression vector (Fig. 2). Expressing Cas9 under the control of the germline-specific promoter *vasa* ensured that no mutations would occur in the soma, therefore reducing potential toxicity for the injected individuals. The 44 males and 48 females that emerged from the injected embryos were crossed with the balancer strain *Gla/SM5* (Fig. 3). Among them, only 18 males and 11 females were fertile. We recovered around 10 progenies from each G0, and individually crossed them with *Gla/SM5* strain. After G2 progenies were produced, a total of 294 G1 individuals were genotyped to detect the presence of the mutant allele of *uL11*.

Screen for *uL11* mutations.

To easily detect successful HDR events, we set up a high-throughput qPCR method relying on the use of discriminative primers. Upon recombination, the *uL11* lysine 3 codon (AAA) should be replaced by an alanine one (GCC). We designed allele-specific primers which 3'-ends matching either the wild-type or the recombinant codon. To improve the discriminative power of these oligonucleotides, we included a LNA at the second position of the mismatch codon (Fig. 4A)[32,33]. In addition, we used TMAC (Tetramethyl ammonium chloride) buffer which is known to increase both the specificity of hybridization and the Tm of the primers[34,35]. To quicken processing of large number of samples, we prepared mixtures of genomic DNAs from 4 to 5 individuals. We then amplified the *uL11* locus with either the lysine codon (*LNAWT*, data not shown) or the alanine codon (*LNAK3A*) matching primer. While most

genomic DNA mixtures displayed amplification kinetics close to the level of the negative control, six of them exhibited faster amplification (ΔCt between 2 and 7) (Fig. 4B). We thus repeated the experiment on individual genomic DNAs from these 6 pools. Ten genomic DNA exhibited quicker amplification than the control with the *LNAK3A* forward primer (ΔCt > 5) (Fig. 4C). Sequencing the *uL11* locus confirmed that the ten positive genomic DNA contained the recombinant allele $uL11^{K3A}$ at the heterozygous state (Fig. 4D shows the sequence of one of them). These flies originated from two independent G0 founding males.

Mutagenesis of the uL11 lysine 3 codon in a bacterial artificial chromosome (BAC) by recombineering.

The *attB-P[acman]-CmR-BW:CH322-137O14* BAC (further called BAC*137O14*) contains the *uL11* gene as well as surrounding genomic sequences (22.4 kbp covering *ppk29*, *CG13563, eIF-5A, CR44814, uL11/RpL12, RpL39/eL39, Rap21, yki* genes as well as part of *sei* and *CG3209* genes). This BAC could thus be used to rescue the *uL11* mutants. To verify that the observed phenotypes of the $uL11^{K3A}$ allele were due to this mutation and not to mutation of one surrounding genes, we generated this mutation in *BAC 137O14* by HDR.

In *Escherichia* coli, small mutations are recognized and repaired by the methyl-directed mismatch repair (MMR) pathway, reducing efficiency one hundred-fold[23]. The MMR is however unable to repair large mutations, and the presence of 4 consecutive mismatches is sufficient to reduce its activity. We thus generated ssDNA templates carrying a silent nucleotide substitution directly 5' of the K3A mutation, encompassed in 35 nucleotide-long homology arms (Fig. 5A). Since the orientation of the ssDNA template also affects efficiency of recombination, we generated ssDNA

templates complementary to each strand (*ssODN-sense* and *ssODN-antisense*)[22]. We then performed recombination in the dedicated SW102 bacterial strain and plated the potential recombinants. Since no selection marker was introduced during recombination, we diluted the transformed bacteria until obtaining isolated colonies. To determine whether the recombination was successful, we harvested a plate of bacteria by washing it with LB medium, and purified all BACs together. We then performed allele-specific qPCR (as previously described) to test for the presence of the K3A allele. While it was detected after recombination with both the sense and antisense ssDNA templates, it was amplified faster in the bacteria treated with the sense ssDNA, suggesting that its recombination efficiency was higher (Fig. 5B).

Thus, we focused on the isolation of a recombinant clone from these bacteria. To this end, we transferred isolated colonies to plates of 20 clones. Each plate was then harvested and all colonies tested together (data not shown). The recombinant allele was amplified in the DNA harvested from one plate, suggesting that at least one colony was recombinant. Each clone was then tested individually for the presence of the wild-type allele (Fig. 5C) and the recombinant allele (Fig. 5D). Out of these, only one was containing the recombinant *uL11*^{K3A} allele but not the wild-type one. Sequencing the *uL11* gene in this recombinant BAC confirmed the presence of the desired mutation (Fig. 5E).

Discussion

Single step CRISPR/Cas9-mediated generation of small-scale nucleotide replacements can sometimes be the only option for mutagenesis, such as when working with essential genes. It can also be used to obtain precise mutation quickly in any gene, since it requires very limited upstream reagents. However, this formidable

tool is plagued by the lack of options to recover given mutations. Here, we adapted an allele-specific PCR technology for high-throughput screening of desired mutations in *Drosophila*. This method eases the burden of screening hundreds of flies, by achieving sufficient sensitivity to assay up to 480 individuals within a single 96-well qPCR plate.

Small mutations can be hard to detect, and strategy for molecular screening should be carefully envisioned. Several methods have been developed for this purpose, with different advantages and liabilities (Table1). Undoubtedly, the most unambiguous one is the direct sequencing of the target region in all mutant candidates. However, this method can become very expensive as it requires to purify PCR amplicons and sequence them individually. Furthermore, to detect heterozygous mutations detection requires the examination of each chromatogram and its comparison with the reference sequence. Thus, this method should be used only when the mutation rate is expected to be very high (for instance when looking for any null mutation, or after observing phenotypes in mutant candidates).

In comparison, T7 endonuclease I and HRMA assays allow to detect mutational events in a more economic manner. T7 endonucleases detect mismatches that form upon amplifying heterozygous regions by PCR. It should be noted that T7E1 only recognizes a subset of SNP, depending on the base substitution[36]. Importantly, T7-based assays require multiple steps downstream of PCR, and are known to be very sensitive to DNA:enzyme ratio and incubation time. Robust screening thus requires very careful upstream development. In addition, unspecific PCR products can be readily mistaken for digested amplicons which appear as faint additional bands upon gel electrophoresis. Thus, several protocols advise to add a nested PCR step or to purify PCR products on gel before enzymatic digestion. In contrast, HRMA screening

is quicker, more robust and requires less development. It can detect both substitutions and indels, and its resolution can be pushed to SNP level. However, achieving such precision will require dedicated material: saturating dyes, specialized thermocycler, and most importantly, normalization software. While this method was developed to analyse a temperature shift between the melting curves of different alleles, the most spectacular effect can be seen upon formation of heteroduplexes during PCR, which are denatured much quicker than homoduplexes of any sequence. This property makes HRMA sensitive to the presence of polymorphisms within the amplicon. Therefore, it is a powerful tool for the recovery of random mutations, at the expense of specialized equipment and careful upstream development.

When a punctual mutation is set, the method of choice for screening is allele-specific PCR. Indeed, a primer matching the mutation should only amplify the mutated allele. To achieve sufficient specificity, the mutation should match the 3'-end of the primer, whose base pairing is the most important for polymerase elongation[37]. The draw-back is that only two primers can be designed, their 3' matching the mutation in either orientation, leaving little room for primer optimisation. Furthermore, a few mismatches in the primer binding sequence often delay PCR amplification rather than prevent it, resulting in false positives. Thus, only the reaction conditions can be tweaked to try and achieve specificity. This often implies finding PCR conditions stringent enough so that only the matching primer can amplify. Under such restrictive conditions, PCR may lack robustness and be prone to false negatives. This implies that robust screening requires a very careful upstream optimisation, and tightly controlled PCR conditions.

The method we describe here offers several improvements in that regard. First, by using real time PCR, we analyse the amplification speed rather than the final product of PCR. Even should the primers amplify the wrong allele, the presence of a complete match should result in faster amplification. PCR can thus be performed under permissive conditions, reducing the need for upstream optimisation and the risk of false negatives. Additionally, since visual inspection of qPCR amplification curves is sufficient to identify mutation events, it is possible to read the results directly on the qPCR device monitor (Fig. 4 and 5). Our method thus removes the need for gel electrophoresis or bioinformatical analysis steps.

To increase discrimination efficiency, we included TMAC in the PCR buffer. This salt is commonly used in commercial PCR enhancer solutions to reduce unspecific priming. TMAC generally increases oligonucleotide hybridization temperature and renders it independent of GC content. These properties allow the robust amplification of even impractical regions such as AT-rich promoter sequences or GC-rich islands[33,38]. In addition, it broadens the choice of a satisfactory reverse primer: since there are no composition requirements, the only concern should be to find a unique matching primer. Thus, the use of TMAC buffer allows to deploy our method in most non-repetitive loci in the genome.

The introduction of a LNA also serves to improve discriminative power. Indeed, LNA display very high affinity and specificity for their complementary base, thus improving the discrimination between a match or mismatch allele. They have been used to increase PCR specificity for applications in SNP genotyping[39]. Importantly, LNA bases increase the binding stability of the neighbour DNA bases. Thus, a single LNA can improve the binding efficiency for three nucleotides[40]. Such improved 3' stability is expected to favour robust PCR amplification. For this very reason, it is not

recommended to introduce multiple LNA bases, since unspecific amplification may arise from very stable binding of a short part of the primer 3' region. It should also be noted that mismatches occurring out of the LNA area of influence are unlikely to prevent specific amplification. For instance, the mutated allele was specifically amplified on a BAC despite the introduction of a mismatch two bases 5' of the LNA. It is thus possible that recombined alleles containing an unwanted mutation in the 5' area of the primer would be detected as positive. For this reason, all positive alleles should be sequenced after recovery.

While our method significantly hastens the allele detection step, molecular screening still remains labour-intensive. Specifically, the extraction of individual genomic DNA is a bottleneck for large screens, especially since many detection methods require clean DNA extractions and controlled DNA amounts. Lesser quality extractions may quicken this step but will result in a drastic increase in PCR failure or unspecific amplification. The use of high-throughput DNA extraction methods such as described by Lang *et al.* provide an opportunity to reduce the time spent in extracting DNA[41]. Additionally, commercial kits allow column purification of genomic DNA on plates of 96 samples, allowing for large scale high-quality gDNA preparation.

Generating a BAC carrying the same mutation should be readily considered when working with genes for which genetic tools are unavailable, rendering the interpretation of mutant phenotypes vulnerable to off-target effects (OTEs). OTEs can be eliminated for the most part by backcrossing into a control genetic background, but it requires crossing individual heterozygotes at each generation. In the absence of a phenotypic marker, heterozygotes need to be identified after laying eggs. Thus, they must be crossed blindly, and genotyped at each generation. In addition, mutations in essential genes are expected to have deleterious effects on viability and

fertility in many cases. For instance, *uL11*^{K3A} homozygous flies display almost 50% larval lethality and poor fertility. Therefore, isogenization can be even more tedious than mutant recovery. In contrast, phenotypes can be unambiguously assigned to the mutation if they are rescued by the wild-type BAC but not by the mutated BAC. Engineering such mutation is time-consuming however, for phenotype-based screening methods require two recombination steps. In contrast, our method can not only be used to isolate mutations after single step, marker-less HDR event, but also to verify that the recombination worked before proceeding to the screen. It then allows to test pools of colonies and specifically detects a recombinant within up to 50 clones. Without the requirement for two rounds of recombination, it allows to consider generating both the mutant fly and BAC at the same time.

To conclude, the method described here simplifies the isolation of small CRISPR/Cas9-induced mutations in the absence of phenotypic markers and provides the means to recover a matching mutation on a BAC. Furthermore, this method is cost-efficient and readily usable with limited upstream development. As a complement to CRISPR/Cas9 gene editing, it can thus be a particularly valuable tool in conquering the most reluctant regions of the genome.

Materials and Methods

Construction of *sgRNA* vectors for S2 cells.

Single guide RNAs (sgRNA) were cloned into *pAc-sgRNA-Cas9* (from Dr. Ji-Long Liu's lab; Addgene plasmid # 49330) as described in Bassett *et al.*[42]. Briefly, forward and reverse 5'-phosphorylated oligonucleotides (100 µM) (Supplementary Table S1) were annealed in T4 ligation buffer (NEB) by heating to 95°C and slowly cooling down to 25°C. The annealed oligonucleotides were then ligated to the *pAc-*

sgRNA-Cas9 plasmid linearized with *BspQ1*. The ligation product was introduced into *DH5α* competent cells. Proper insertion was confirmed by Sanger sequencing.

Cell culture and transfection.

S2 cells (*Drosophila* Genomics Resource Center) were cultured at 25°C in Schneider's medium supplemented with 10% fetal bovine serum, 100 units/mL penicillin and 100 µg/mL streptomycin. The day before transfection, 2 mL of medium were seeded with 0.5 10^6 cells. Two µg of DNA were transfected using Effectene transfection reagent (Qiagen) according to the manufacturer's instructions using a 1 :10 DNA to Effectene ratio. Cells were then incubated during 3 days before addition of selective medium containing 5 µg/mL of puromycin (Sigma). They were subsequently maintained for 7 days in selective medium. DNA extraction was performed and analyzed by High Resolution Melting Analysis (HRMA) as described by Bassett *et al.*[14]. Briefly, oligonucleotides *uL11HRMA_F* and *uL11HRMA_R* (Supplementary Table S1) were used to amplify a 173 bp region centred on the *uL11* lysine 3 codon. PCR were performed with *Sso Fast EvaGreen Supermix*^{TM} (Bio-Rad) in 20 µL reactions containing 2 to 15 ng genomic DNA and 0.5 µM each oligonucleotide. Cycles were carried out in a CFX96 system (Bio-Rad): [98°C 3 min, 40 cycles (98°C 2 s; 57,3°C 15 s)]. Thermal melting profiles were obtained in the same device by increasing temperature from 75°C to 95°C using a temperature increment of 0.2°C. They were normalized as described by Wittwer *et al.*[43].

Construction of *sgRNA* vector for fly transgenesis.

The *pU6-chiRNA:sgRNA4* plasmid was obtained by incorporating the *sgRNA*4 sequence (obtained by annealing *pho-sgRNA4_F* and *pho-sgRNA4_R*,

Supplementary Table S1) into *pU6-BbsI-chiRNA* (Addgene plasmid # 45946)[30] following the protocol provided on the flyCRISPR website (http://flycrispr.molbio.wisc.edu/protocols/gRNA). Proper insertion was confirmed by sequencing using the T3 universal primer.

For homologous recombination, a single-strand DNA template of 123 nucleotides (*ssODN*) was used as template (Supplementary Table S1). It was synthetized and purified by standard desalting by Integrated DNA Technologies, Inc.

Fly transgenesis and crosses.

Flies were raised on standard yeast-cornmeal medium (1% agar, 8.25% brewer's yeast, 9.1% cornstarch, 2.5% moldex) at 25°C. Embryos of the *w^{1118}; PBac{y[+mDint2]=vas-Cas9}VK00027* strain (BL-51324) were injected by BestGene Inc. with a mixture containing 100 ng/µL *pU6-chiRNA:sgRNA4* and 100 ng/µL *ssODN*.

Transformant G0 flies were individually crossed to *w^{1118}; In(2LR) Gla, wg^{Gla-1}/SM5* flies (*Gla/SM5*). Curly wing G1 siblings were individually crossed to *Gla/SM5* flies. Once the G2 progeny was born, G1 founding flies were harvested, genomic DNA extracted, and genotyping performed as described below. Curly wing G2 offspring of G1 flies carrying a mutant allele of *uL11* were crossed with each other to establish mutant strains.

Genomic DNA extraction.

Genomic DNA was extracted by crushing single flies in 100 µL SB buffer (10 mM Tris pH 8.0, 1 mM EDTA, 25 mM NaCl, 200 µg/µL Proteinase K), followed by a

30 min incubation at 37°C. DNA was further purified by standard phenol:chloroform extraction followed by ethanol precipitation.

Locked Nucleic Acid (LNA) allele-specific qPCR

Forward allele-specific primers with 3'-end matching either wild-type (*LNAWT*) or mutated 3rd codon (*LNAK3A*) of *uL11* (AAA or GCC, respectively) were used in combination with a reverse primer (*CRISPR1_R*) to amplify a 219 nucleotide region (Supplementary Table S1). 25 µL reactions were set to contain 5 to 15 ng of genomic DNA, 0.5 µM forward and reverse primers, 0.4 nM dNTP, 0.75 µL SYBR green (Diagenode), and 2.5 Units of DreamTaq polymerase (Thermo Fisher Scientific) in TMAC buffer (67 mM Tris pH8.8, 6.7 mM MgCl2, 16.6 mM ammonium sulphate, 0.5 mM tetra-methyl-ammonium chloride, 0.17 mg/mL BSA). qPCR plates were prepared and kept at 4°C until starting PCR cycles. 0.5 ng of plasmid containing the *uL11* coding region in which the AAA lysine 3 codon is replaced by GCC was used as positive control. qPCRs were carried out in a CFX96 system (Bio-Rad): [95°c 3 min, 40 cycles of (95°C 20 s, 64°C 20 s, 72°C 30 s)]. To confirm the presence of the mutated allele, a 1.5 kb region centred on the lysine 3 codon was amplified from positive genomic DNA and sequenced.

Bacterial strains and recombineering.

SW102 bacteria[44] were rendered electro-competent using the Krantz lab's protocol[45]. Briefly, a culture was grown at 30°C until reaching 0.5-0.6 OD at 600 nm. All subsequent steps were carried out at 4°C. Ten mL of culture were pelleted at 500 g for 5 minutes. The pellet was resuspended in 10 mL cold water and pelleted again under the same conditions. This step was repeated once. The pellet was next

resuspended in 1 mL cold water, transferred to a 1.5 mL microtube, and pelleted again under the same conditions. The pellet was then resuspended in 50 µL cold water and transformed by electroporation (Gene Pulser II BioRad, 0.2 cm cuvette, 2.5 kV, 25 µFa, 100 Ω) with 500 ng of *attB-P[acman]-CmR-BW:CH322-137O14* plasmid (further called BAC *137O14*) (obtained from the BACPAC resources Center https://bacpacresources.org)[46]. Bacteria were then plated on chloramphenicol plates, and a clone containing the BAC (as verified by PCR) was selected for amplification at 30°C until 0.5-0.6 OD_{600}. Ten mL of culture were then incubated at 42°C for 15 minutes to induce expression of the bacterial recombination genes. After chilling on ice, bacteria were rendered competent following the protocol described above. They were transformed by electroporation with either no DNA, 0.72 µg of *ssODN-sense* or the same amount of *ssODN-antisense* (Supplementary Table S1) synthesized by Integrated DNA Technologies, Inc. then diluted by a factor 10^6 and plated on chloramphenicol plates to obtain single colonies.

References

1. St Johnston, D. Using mutants, knockdowns, and transgenesis to investigate gene function in *Drosophila*. *Wiley Interdiscip Rev Dev Biol* **2,** 587-613 (2013).
2. Jinek, M., Chylinski, K., Fonfara, I., Hauer, M., *et al.* A programmable dual-RNA-guided DNA endonuclease in adaptive bacterial immunity. *Science* **337,** 816-821 (2012).

3. Gratz, S. J., Wildonger, J., Harrison, M. M. & O'Connor-Giles, K. M. CRISPR/Cas9-mediated genome engineering and the promise of designer flies on demand. *Fly (Austin)* **7,** 249-255 (2013).

4. Ren, X., Yang, Z., Mao, D., Chang, Z., *et al.* Performance of the Cas9 Nickase System in *Drosophila melanogaster*. *G3 (Bethesda)* **4,** 1955-1962 (2014).

5. Bassett, A. R., Kong, L. & Liu, J. L. A genome-wide CRISPR library for high-throughput genetic screening in *Drosophila* cells. *J Genet Genomics* **42,** 301-309 (2015).

6. Klemenz, R., Weber, U. & Gehring, W. J. The white gene as a marker in a new P-element vector for gene transfer in *Drosophila*. *Nucleic Acids Res* **15,** 3947-3959 (1987).

7. Zhou, W., Huang, J., Watson, A. M. & Hong, Y. W::neo: a novel dual-selection marker for high efficiency gene targeting in *Drosophila*. *PLoS One* **7,** e31997 (2012).

8. Kühn, R. & Chu, V. T. Pop in, pop out: a novel gene-targeting strategy for use with CRISPR-Cas9. *Genome Biol* **16,** 244 (2015).

9. Lamb, A. M., Walker, E. A. & Wittkopp, P. J. Tools and strategies for scarless allele replacement in *Drosophila* using CRISPR/Cas9. *Fly (Austin)* **11,** 53-64 (2017).

10. Dietzl, G., Chen, D., Schnorrer, F., Su, K. C., *et al.* A genome-wide transgenic RNAi library for conditional gene inactivation in *Drosophila*. *Nature* **448,** 151-156 (2007).

11. Boutros, M., Kiger, A. A., Armknecht, S., Kerr, K., *et al.* Genome-wide RNAi analysis of growth and viability in *Drosophila* cells. *Science* **303,** 832-835 (2004).

12. Lindsley, D. L., Sandler, L., Baker, B. S., Carpenter, A. T., *et al.* Segmental aneuploidy and the genetic gross structure of the *Drosophila* genome. *Genetics* **71,** 157-184 (1972).

13. McKay, D. J., Klusza, S., Penke, T. J., Meers, M. P., *et al.* Interrogating the function of metazoan histones using engineered gene clusters. *Dev Cell* **32,** 373-386 (2015).

14. Bassett, A. & Liu, J. L. CRISPR/Cas9 mediated genome engineering in *Drosophila*. *Methods* **69,** 128-136 (2014).

15. Kc, R., Srivastava, A., Wilkowski, J. M., Richter, C. E., *et al.* Detection of nucleotide-specific CRISPR/Cas9 modified alleles using multiplex ligation detection. *Sci Rep* **6,** 32048 (2016).

16. Vouillot, L., Thélie, A. & Pollet, N. Comparison of T7E1 and surveyor mismatch cleavage assays to detect mutations triggered by engineered nucleases. *G3 (Bethesda)* **5,** 407-415 (2015).

17. Cho, S. W., Kim, S., Kim, Y., Kweon, J., *et al.* Analysis of off-target effects of CRISPR/Cas-derived RNA-guided endonucleases and nickases. *Genome Res* **24,** 132-141 (2014).

18. Wu, X., Kriz, A. J. & Sharp, P. A. Target specificity of the CRISPR-Cas9 system. *Quant Biol* **2,** 59-70 (2014).

19. Venken, K. J., Carlson, J. W., Schulze, K. L., Pan, H., *et al.* Versatile P[acman] BAC libraries for transgenesis studies in *Drosophila melanogaster*. *Nat Methods* **6,** 431-434 (2009).

20. Hollenback, S. M., Lyman, S. & Cheng, J. Recombineering-based procedure for creating BAC transgene constructs for animals and cell lines. *Curr Protoc Mol Biol* **Chapter 23,** Unit 23.14 (2011).

21. Li, X. T., Thomason, L. C., Sawitzke, J. A., Costantino, N. & Court, D. L. Positive and negative selection using the tetA-sacB cassette: recombineering and P1 transduction in *Escherichia coli*. *Nucleic Acids Res* **41,** e204 (2013).

22. Ellis, H. M., Yu, D., DiTizio, T. & Court, D. L. High efficiency mutagenesis, repair, and engineering of chromosomal DNA using single-stranded oligonucleotides. *Proc Natl Acad Sci U S A* **98,** 6742-6746 (2001).

23. Sawitzke, J. A., Costantino, N., Li, X. -T., Thomason, L. C., *et al.* Probing cellular processes with oligo-mediated recombination and using the knowledge gained to optimize recombineering. *J Mol Biol* **407,** 45-59 (2011).

24. Ban, N., Beckmann, R., Cate, J. H., Dinman, J. D., *et al.* A new system for naming ribosomal proteins. *Curr Opin Struct Biol* **24,** 165-169 (2014).

25. Wawiórka, L., Molestak, E., Szajwaj, M., Michalec-Wawiórka, B., *et al.* Functional analysis of the uL11 protein impact on translational machinery. *Cell Cycle* **15,** 1060-1072 (2016).

26. Coléno-Costes, A., Jang, S. M., de Vanssay, A., Rougeot, J., *et al.* New partners in regulation of gene expression: the Enhancer of Trithorax and

Polycomb Corto interacts with methylated Ribosomal Protein L12 via its chromodomain. *PLoS Genet* **8,** e1003006 (2012).

27. Park, M. H., Nishimura, K., Zanelli, C. F. & Valentini, S. R. Functional significance of eIF5A and its hypusine modification in eukaryotes. *Amino Acids* **38,** 491-500 (2010).

28. Huang, J., Wu, S., Barrera, J., Matthews, K. & Pan, D. The Hippo signaling pathway coordinately regulates cell proliferation and apoptosis by inactivating Yorkie, the *Drosophila* Homolog of YAP. *Cell* **122,** 421-434 (2005).

29. Cook, R. K., Christensen, S. J., Deal, J. A., Coburn, R. A., *et al.* The generation of chromosomal deletions to provide extensive coverage and subdivision of the *Drosophila melanogaster* genome. *Genome Biol* **13,** R21 (2012).

30. Gratz, S. J., Cummings, A. M., Nguyen, J. N., Hamm, D. C., *et al.* Genome engineering of *Drosophila* with the CRISPR RNA-guided Cas9 nuclease. *Genetics* **194,** 1029-1035 (2013).

31. Karvelis, T., Gasiunas, G., Miksys, A., Barrangou, R., *et al.* crRNA and tracrRNA guide Cas9-mediated DNA interference in *Streptococcus thermophilus*. *RNA Biol* **10,** 841-851 (2013).

32. Latorra, D., Campbell, K., Wolter, A. & Hurley, J. M. Enhanced allele-specific PCR discrimination in SNP genotyping using 3' locked nucleic acid (LNA) primers. *Hum Mutat* **22,** 79-85 (2003).

33. Thomassin, H., Kress, C. & Grange, T. MethylQuant: a sensitive method for quantifying methylation of specific cytosines within the genome. *Nucleic Acids Res* **32,** e168 (2004).

34. Hung, T., Mak, K. & Fong, K. A specificity enhancer for polymerase chain reaction. *Nucleic Acids Res* **18,** 4953 (1990).

35. Chevet, E., Lemaître, G. & Katinka, M. D. Low concentrations of tetramethylammonium chloride increase yield and specificity of PCR. *Nucleic Acids Res* **23,** 3343-3344 (1995).

36. Tsuji, T. & Niida, Y. Development of a simple and highly sensitive mutation screening system by enzyme mismatch cleavage with optimized conditions for standard laboratories. *Electrophoresis* **29,** 1473-1483 (2008).

37. Simsek, M. & Adnan, H. Effect of single mismatches at 3'-end of primers on polymerase chain reaction. *J Sci Res Med Sci* **2,** 11-14 (2000).

38. Jacobs, K. A., Rudersdorf, R., Neill, S. D., Dougherty, J. P., *et al.* The thermal stability of oligonucleotide duplexes is sequence independent in tetraalkylammonium salt solutions: application to identifying recombinant DNA clones. *Nucleic Acids Res* **16,** 4637-4650 (1988).

39. Mouritzen, P., Nielsen, A. T., Pfundheller, H. M., Choleva, Y., *et al.* Single nucleotide polymorphism genotyping using locked nucleic acid (LNA). *Expert review of molecular diagnostics* **3,** 27-38 (2003).

40. Petersen, M., Nielsen, C. B., Nielsen, K. E., Jensen, G. A., *et al.* The conformations of locked nucleic acids (LNA). *J Mol Recognit* **13,** 44-53 (2000).

41. Lang, M., Nagy, O., Lang, C. & Orgogozo, V. High throughput preparation of fly genomic DNA in 96-well format using a paint-shaker. *Fly (Austin)* **9,** 138-144 (2015).

42. Bassett, A. R., Tibbit, C., Ponting, C. P. & Liu, J. L. Highly Efficient Targeted Mutagenesis of *Drosophila* with the CRISPR/Cas9 System. *Cell Rep* **4,** 220-228 (2013).

43. Wittwer, C. T., Reed, G. H., Gundry, C. N., Vandersteen, J. G. & Pryor, R. J. High-resolution genotyping by amplicon melting analysis using LCGreen. *Clin Chem* **49,** 853-860 (2003).

44. Warming, S., Costantino, N., Court, D. L., Jenkins, N. A. & Copeland, N. G. Simple and highly efficient BAC recombineering using galK selection. *Nucleic Acids Res* **33,** e36 (2005).

45. Wang, J., Sarov, M., Rientjes, J., Fu, J., *et al.* An improved recombineering approach by adding RecA to lambda Red recombination. *Mol Biotechnol* **32,** 43-53 (2006).

46. Venken, K. J., He, Y., Hoskins, R. A. & Bellen, H. J. P[acman]: a BAC transgenic platform for targeted insertion of large DNA fragments in *D. melanogaster*. *Science* **314,** 1747-1751 (2006).

Acknowledgments

We thank Dr. Jean-Michel Gibert and the team “Epigenetic control of developmental homeostasis and plasticity” for stimulating discussions and critical reading of the manuscript, the Bloomington Stock Center for fly strains, Dr. Allison Bardin for the SW102 bacterial strain, Dr. Melissa Harrison, Kate O'Connor-Giles & Jill Wildonger for the *pU6-BbsI-chiRNA* (Addgene 45946). This work was funded by the Centre National de la Recherche Scientifique (CNRS), Université Pierre et Marie Curie

(UPMC) and Fondation ARC pour la Recherche sur le Cancer (grant PJA20131200314 to FP). JD was funded by a doctoral fellowship from the MESR and by the Fondation pour la Recherche médicale (FDT20160435164).

Author Contributions

Conception of the work : J.D, H.T., S.B., F.P ; Data collection : J.D, H.T., I.R'K. ; Data analysis and interpretation : J.D, H.T., S.B., F.P ; Writing the article : J.D, H.T., S.B., F.P.

Conflict of interest

The authors declare that they have no conflict of interest.

Figure legends

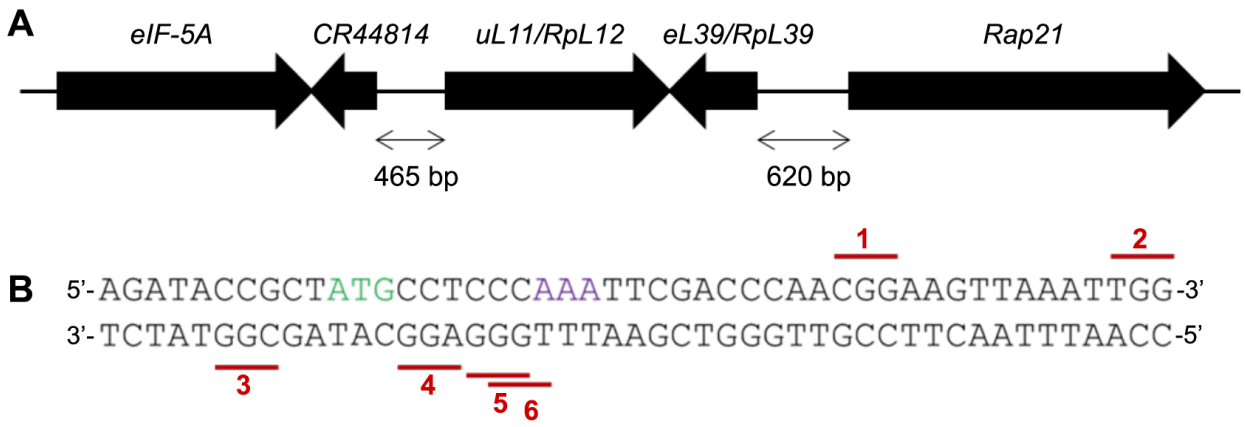

Figure 1: Genomic organization of the *uL11* locus

A - Genomic locus containing the *uL11/RpL12* gene (dm6 2L:24,060,378..24,061, 860).

B - Sequence of the target *uL11* locus. In green the initiation codon, in purple the lysine 3 target codon. Red dashes indicate the PAM sequences corresponding to all possible single guide RNAs.

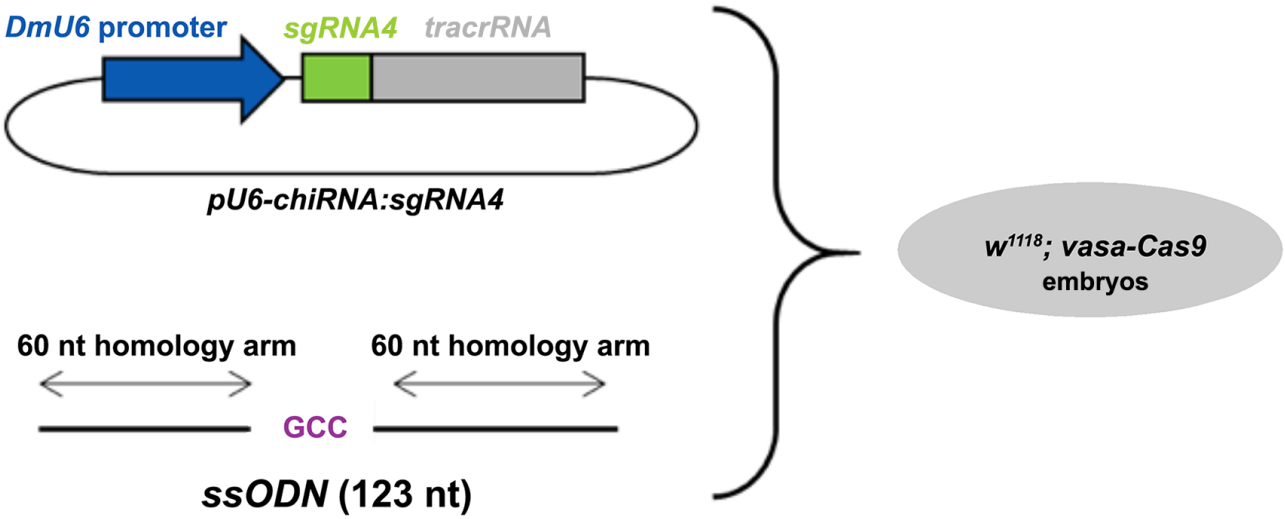

Figure 2: Mutagenesis reagents

CRISPR/Cas9 mediated homologous recombination requires three components: a single guide RNA (sgRNA), a template for recombination (ssODN), and the Cas9 nuclease. The sgRNA corresponding to PAM sequence 4 (sgRNA4) was subcloned into plasmid *pU6-chiRNA* under the control of the *Drosophila* U6 promoter. The *tracrRNA* (trans-activating CRISPR RNA) was shown to be required for Cas9-mediated DNA interference (Karvelis et al., 2013). Recombination template was provided as a 123 nucleotide-long ssODN containing the desired mutation (GCC alanine codon) between two 60 nucleotide-long homology arms (*ssODN-sense*). These two components were injected in embryos from the *vasa-Cas9* strain which expresses Cas9 in the germ-line.

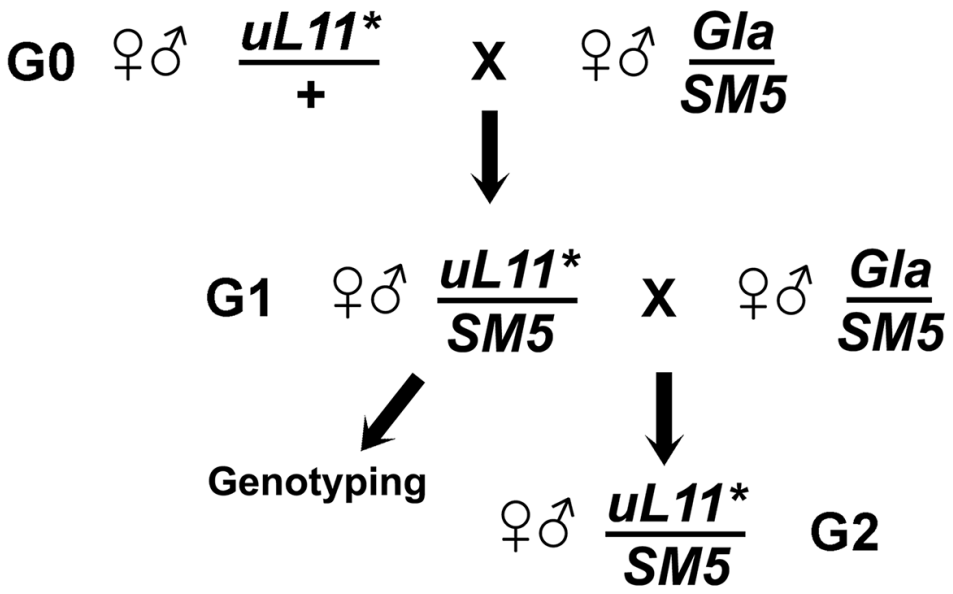

Figure 3: Genetic crosses scheme for mutant recovery

*uL11** designates a potential mutant allele of *uL11*. G0 flies were individually crossed with the *Gla/SM5* balancer strain. Then, G1 flies bearing the *SM5* balancer were individually crossed with the same balancer strain. Once few larvae were present, the G1 parent was collected for genotyping.

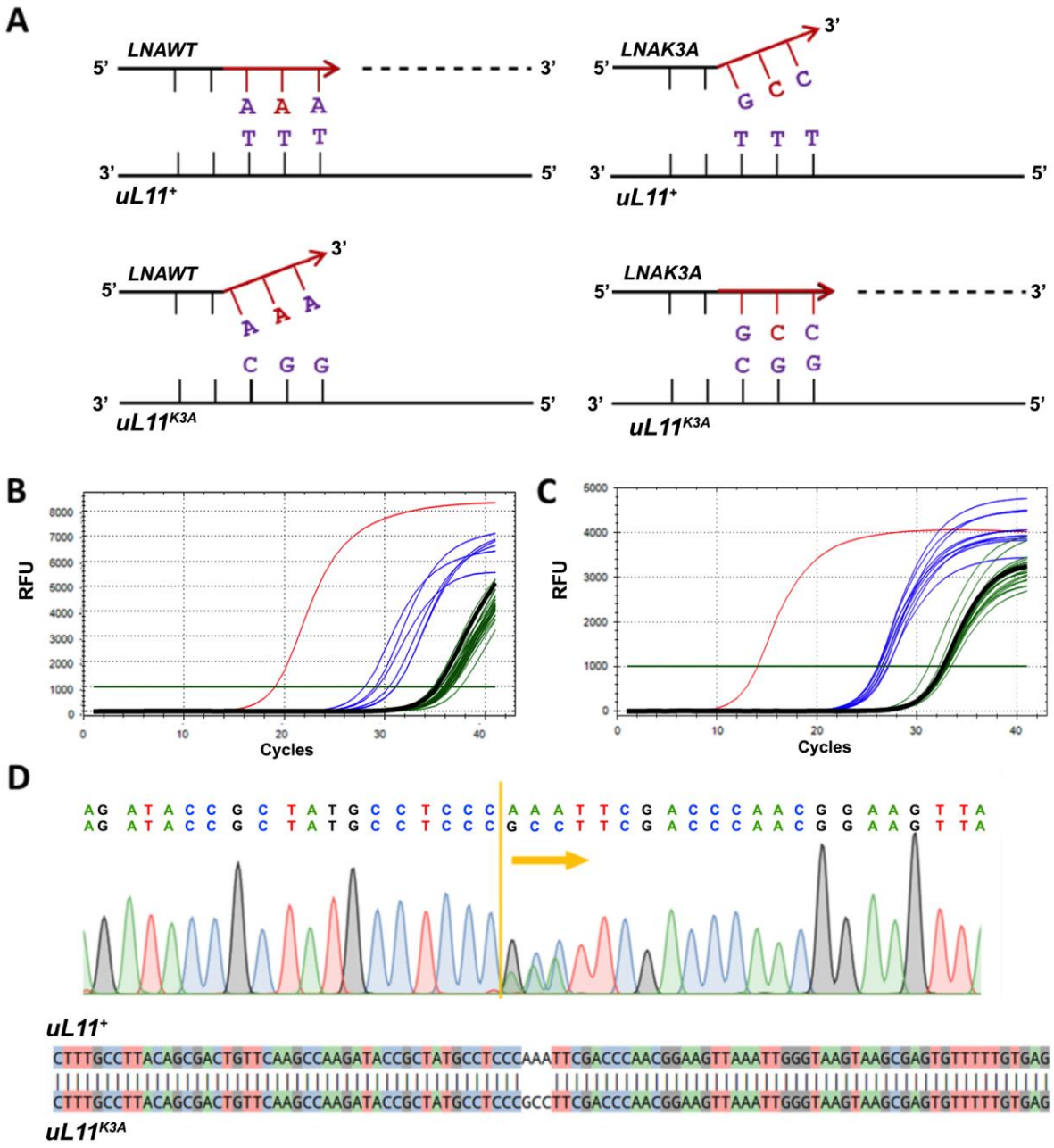

Figure 4. Molecular screening for the *uL11*^{K3A} allele

A - Rationale for the discriminative PCR. Purple bases correspond to the target codon. Red bases stand for locked nucleic acids (LNA). The *LNAWT* primer ended with the lysine AAA codon of the wild-type *uL11* gene whereas the *LNAK3A* primer ended with the alanine GCC codon corresponding to the desired mutation.

B - qPCR were performed with the *LNAK3A* primer matching the *uL11*^{K3A} allele. Red curve: plasmid carrying the *uL11*^{K3A} allele as positive control. Black curve: genomic

DNA from a wild-type fly. Blue curves: pools of up to 5 different genomic DNA from candidate G1 flies considered to be positive. Green curves: pools of up to 5 different genomic DNA from candidate G1 flies considered to be negative.

C - The same qPCR were performed on individual genomic DNA from the pools that were previously found to be positive for the *uL11*^{K3A} allele. Several indivuals wearing the mutation were thus identified (blue curves).

D - Sequencing of the *uL11* locus from one positive individual. Chromatogram analysis and alignment were obtained from http://crispid.gbiomed.kuleuven.be

RFU: Relative Fluorescence Units.

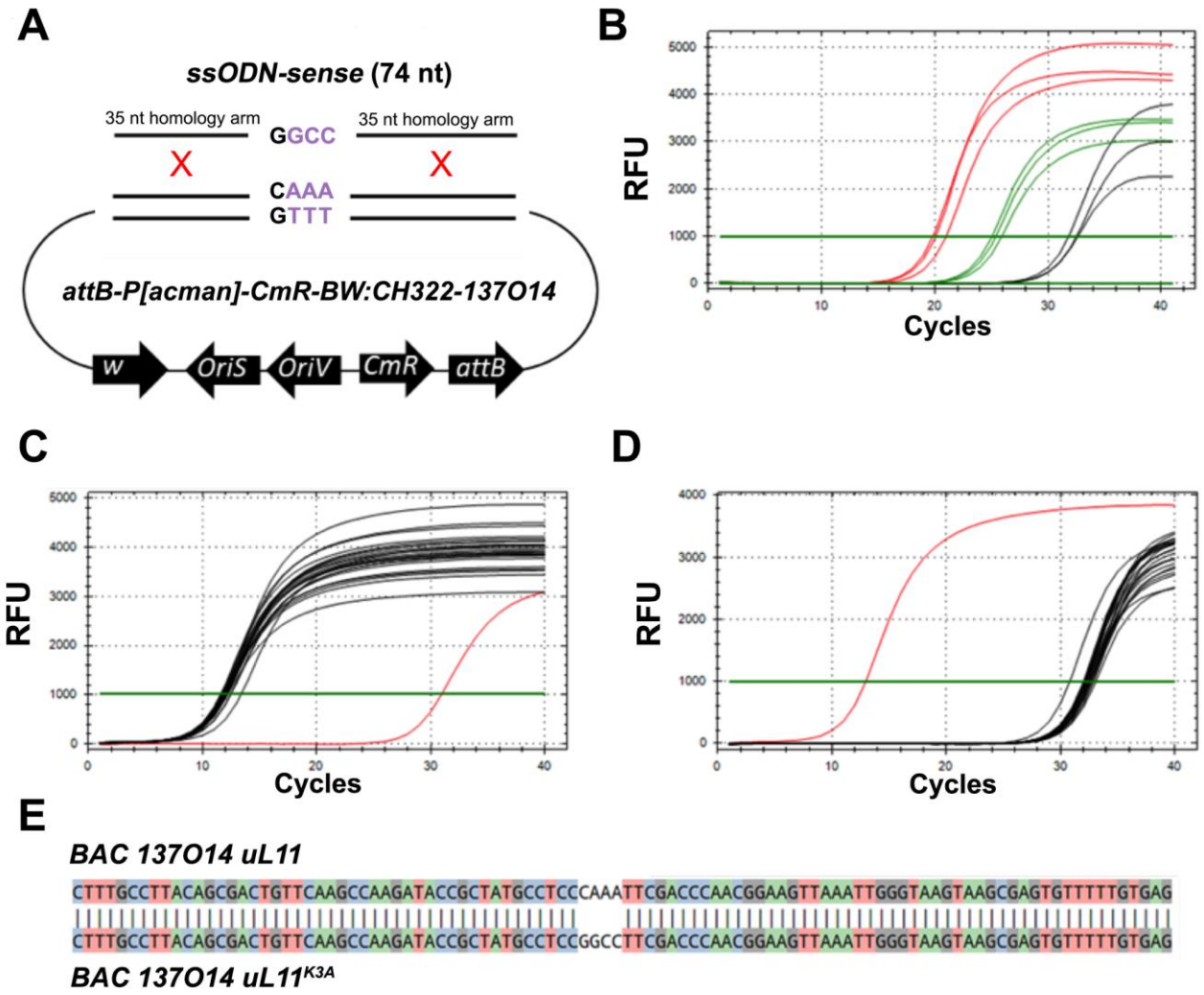

Figure 5. Generation and recovery of a BAC containing the *uL11*^{K3A} allele

A - The desired mutation was introduced by recombination in BAC *125O14* using *ssODN-sense* as template. Purple nucleotides: lysine (AAA) and alanine (GCC) codons. Black nucleotide: a silent fourth nucleotide substitution was added to avoid repair by the MMR pathway.

B - qPCR were performed on plasmids extracted from pools of bacteria obtained after recombination on the *uL11* locus using the *LNAK3A* primer which matches the K3A allele. Black curves: recombination without template; Green curves: recombination with *ssODN-antisense* template; Red curves: recombination with *ssODN-sense* template. Three technical replicates are shown.

C, D - Twenty clones isolated from a positive plate after recombination with the *ssODN-sense* template were tested individually for the presence of the *uL11*^{K3A} allele. BACs from individual clones were analysed by qPCR with the *LNAWT* primer (matching the wild-type *uL11* allele) in C, and with the *LNAK3A* primer (matching the *uL11*^{K3A} allele) in D. The red curves indicate a clone deemed positive.

E - The *uL11* locus from this positive clone was sequenced and aligned with the wild-type *uL11* allele.

RFU: Relative Fluorescence Units.

Method		Allele-specific qPCR	HRMA	Sanger sequencing	T7E1 nuclease
Detection range	Indels	-	+++	+++	++
	Substitution	+++	+++	+++	++
	SNPs	++	++	+++	+/-
Cost		+	++	+++	++
Labor		++	+++	+++	+++
Upstream development		+	++	+	+++
Specificity		+++	+++	+++	+
Sensitivity		+++	+++	+++	+
Polymorphism sensitivity		+	++	-	+/-
Protocol steps	Individual G1 cross	y	y	y	y
	Single fly gDNA extraction	y	y	y	y
	Phenol/column purification	y	y	o	o
	DNA quantification	o	o	o	o
	PCR	y	y	y	y
	Melting curve acquisition	n	y	n	n
	PCR purification	n	n	y	y
	Quantification	n	n	y	y
	Hybridization	n	n	n	y
	Enzymatic digestion	n	n	n	y
	Gel electrophoresis	n	n	n	y
	Bioinformatical analysis	n	y	y	n

Table 1. Comparison of several molecular screening options for CRISPR-mediated HDR. +++: High, ++: Moderate, +: Low, - No, +/- Unreliable, y: yes, n: no, o: optional.

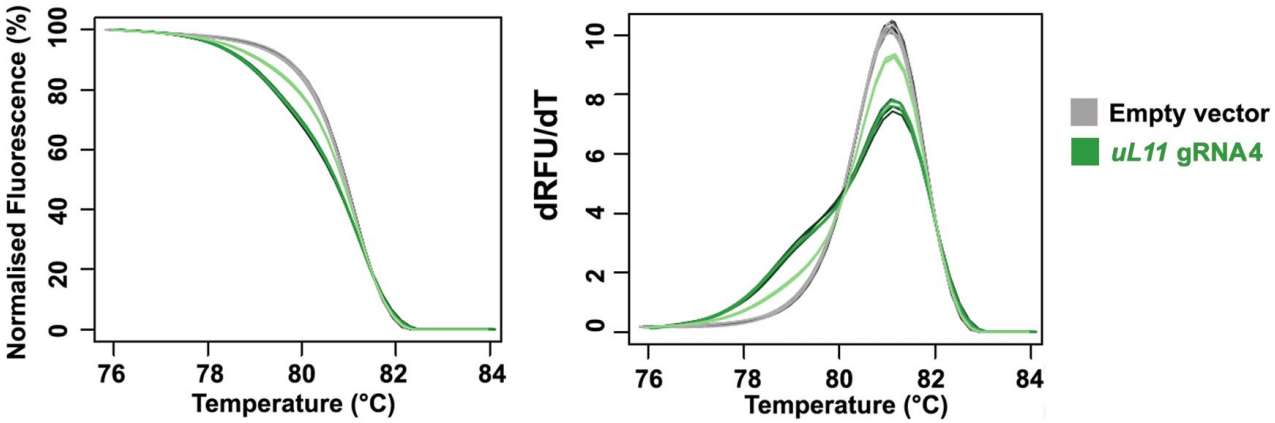

Figure S1: Guide RNA efficiency assay

Melting profile of the *uL11* amplicon after transfection of S2 cells by a *pU6-sgRNA-Cas9* plasmid containing the guide RNA sequence 4 (sgRNA4) (green), or empty (grey). Three biological replicates are represented by different shades of the same colour. Left: melting curves; Right: derivatives. RFU: Relative Fluorescence Units.

High Resolution Melting Analysis	
uL11HRMA_F	5'-tgcggtaaagtacatgagctg-3'
uL11HRMA_R	5'-tcgaagctcaactcctcaca-3'
LNA Primers	
LNAWT_F	5'-gataccgctatgcctccca**A**a-3'
LNAK3A _F	5'-gataccgctatgcctcccg**C**c-3'
CRISPR1_R	5'-gaccgaggggaccgatctt-3'
uL11 Sequencing	
uL11-708_F	5'-cgctactgagctttgctacacccc-3'
uL11+805_R	5'-caataacatcgtgagggtgct-3'
Guide RNA tested	
gRNA1	5'-gcctcccaaattcgacccaa-3'
gRNA2	5'-cgacccaacggaagttaaat-3'
gRNA3	5'-gtcgaatttgggaggcatag-3'
gRNA4	5'-tccgttgggtcgaatttggg-3'
gRNA5	5'-acttccgttgggtcgaattt-3'
gRNA6	5'-aacttccgttgggtcgaatt-3'
Cloning of sgRNA4 in pU6-BbsI-chiRNA	
PHO-sgRNA4_F	5'-CTTC**G**tccgttgggtcgaatttggg-3'
PHO-sgRNA4_R	5'-AAACcccaaattcgacccaacggac-3'
Template for fly mutagenesis	
ssODN	5'-agctcaactcctcacaaaaacactcgcttacttacccaatttaacttccg ttgggtcgaaggcgggaggcatagcggtatcttggcttgaacagtcgctg taaggcaaagattacgttagttt-3'
Templates for BAC recombineering	
ssODN-sense	5'-agcgactgttcaagccaagataccgctatgcctccGGCCttcgacc caacgcaagttaaattgggtataagc-3'
ssODN-antisense	5'-gcttacttacccaatttaacttgcgttgggtcgaaggCCGGaggcat agcggtatcttggcttgaacagtcgct-3'

Table S1: Oligonucleotides used in this study.

In primers LNAWT_F and LNAK3A_F, bold uppercase nucleotides correspond to the LNA bases.In primers PHO-sgRNA4_F and PHO-sgRNA4_R, uppercase nucleotides correspond to the floating sequences used for cloning. The bold guanosine was introduced to increase efficiency of the U6 promoter.

C. Complementary data

CRISPR/Cas9-induced double strand breaks are highly mutagenic, and promote both HDR and NHEJ-induced mutations at the desired locus. While we introduced a template to promote homologous directed repair, it was likely that NHEJ-mediated also occurred in the injected flies. The endonuclease activity of Cas9 generates double strand breaks at predictable sites, and the fortunate placement *sgRNA4* was expected to induce one immediately next to the lysine 3 codon of *uL11*. Importantly, Cas9 also displays exonuclease activity, which was shown to promote insertion/deletion events (indels) stemming from the DSB site, and extending in the 5' direction of the PAM carrying strand (Bassett et al., 2014; Jinek et al., 2012). Therefore, it was conceivable that some G1 flies would harbour indel events deleting this codon.

Such mutated alleles would not be detected with our allele-specific method. Thus, we tested each DNA sample extracted from G1 flies by HRMA, using the protocol we previously used to detect indels in S2 cells. Denaturation kinetics of the *uL11* amplicons were analysed individually for 294 G1 flies. Among them, 36 differed from a wild-type control. Consistently, they included all ten identified uL11^{K3A} mutants. Sequencing those amplicons confirmed the presence of mutations in every one of these samples. Eight different alleles were thus identified that each corresponded to a reproducible HRMA pattern (**Table 3**, **Fig. 58**).

Founder(s)	Allele(s)	Sequence
M-12	K3A-12	ACCGCTATGCCTCCCAAATTCGACCCAACGGAA
M-43	K3A-43	ACCGCTATGCCTCCCGCCTTCGACCCAACGGAA
M-12	ΔK3-12	ACCGCTATGCCTCCCAAATTCGACCCAACGGAA
M-43	ΔK3-43	ACCGCTATGCCTCCC---TTCGACCCAACGGAA
M-5	ΔK3F4	ACCGCTATGCCTCCCAAATTCGACCCAACGGAA
		ACCGCTATGCCTCCC------GACCCAACGGAA
M-31	K3Y	ACCGCTATGCCTCCCAAATTCGACCCAACGGAA
		ACCGCTATGCCTCCCTACTTCGACCCAACGGAA
M-12	P2LK3E	ACCGCTATGCCTCCCAAATTCGACCCAACGGAA
		ACCGCTATGCCTCTTGAATTCGACCCAACGGAA
M-5	P2QK3R	ACCGCTATGCCTCCCAAATTCGACCCAACGGAA
		ACCGCTATGCCTCAACGCTTCGACCCAACGGAA
M-43	F+2	ACCGCTATGCCTCCCAAA--TTCGACCCAACGGAA
		ACCGCTATGCCTCCCTATGCTTCGACCCAACGGAA
F-6	F-4	ACCGCTATGCCTCCCAAATTCGACCCAACGGAA
		ACCGCTATGCCTCC----TTCGACCCAACGGAA

Table 3. Sequence of the uL11 alleles of G0 flies.

Founder G0 flies were named after their sex (M-, male; F-, female) and the order of their recovery. Each allele was recovered in several descendants of the same founders. The $uL11^{K3A}$ and $uL11^{\Delta K3}$ alleles were found in the progeny of two different founders. Substitution alleles were named to reflect the amino-acid change in the uL11 protein, following the amino-acid one-letter code. (K, lysine ; A, alanine ; F, phenylalanine ; Y, tyrosine; P, proline; L, leucine; E, glutamate; Q, glutamine; R, arginine). The lower two alleles are named after the reading frame shift that they introduce in the uL11 gene. The sequence of each allele is provided with a wild-type uL11 sequence as reference. The start codon of uL11 is highlighted in green and the lysine 3 codon in purple. Sequence changes are highlighted in red.

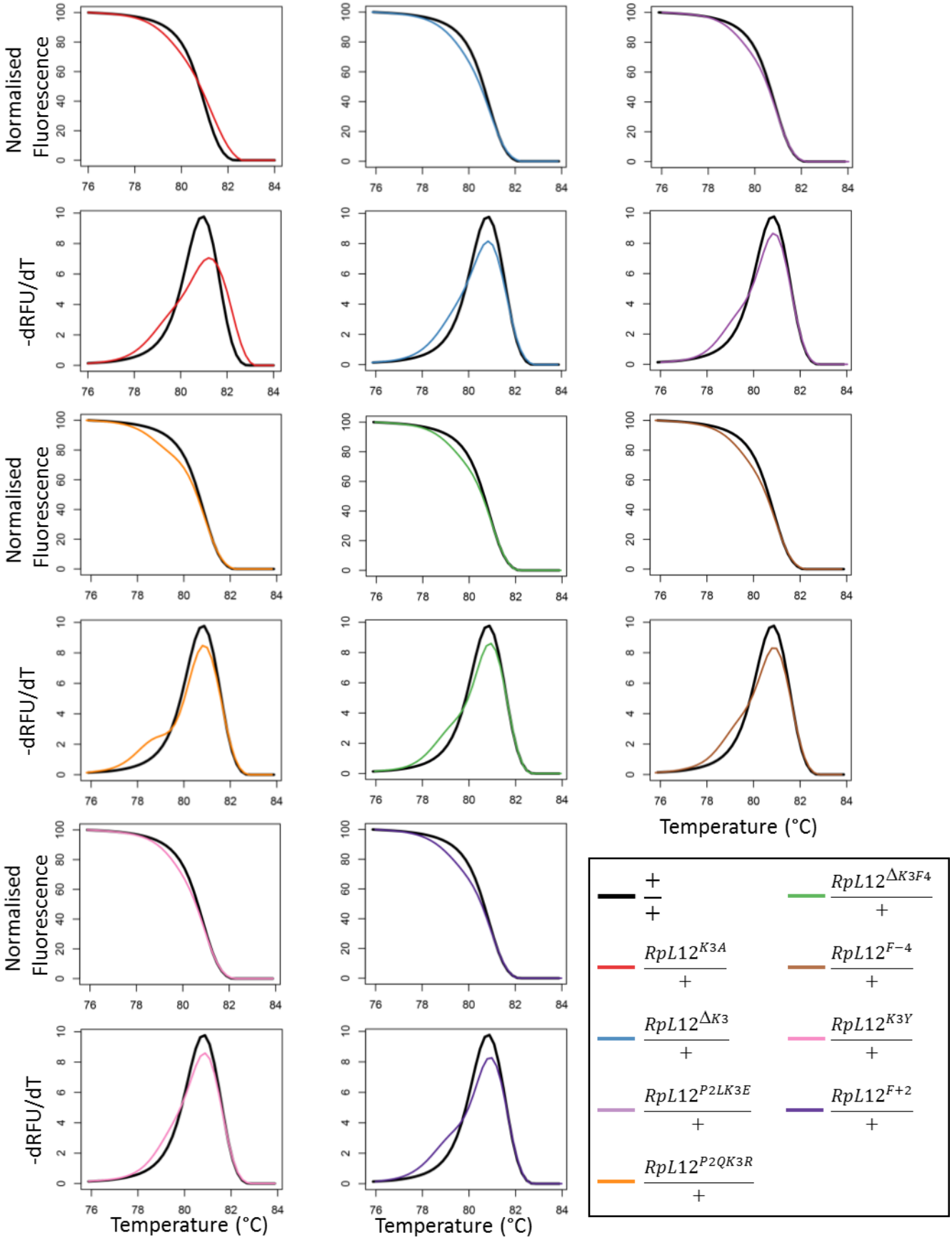
Normalised Fluorescence
-dRFU/dT
Normalised Fluorescence
-dRFU/dT
Normalised Fluorescence
-dRFU/dT
Temperature (°C)
Temperature (°C)
Temperature (°C)
+/+
RpL12^K3A/+
RpL12^ΔK3/+
RpL12^P2LK3E/+
RpL12^P2QK3R/+
RpL12^ΔK3F4/+
RpL12^F−4/+
RpL12^K3Y/+
RpL12^F+2/+

Figure 58. HRMA profiles of the uL11 alleles.
Melting profile of the uL11 amplicons from genomic DNA of G1 flies (gDNA). One example of each discovered allele is provided. Melting peaks flatter and broader than the reference reveal the presence of two different amplicons, indicating that the tested gDNA contains a mutation at the uL11 locus. Melting curves were normalized according to the method described by (Wittwer et al., 2003).

It is interesting to consider that this mutagenesis was not our only attempt at obtaining mutations for *uL11* through CRISPR/Cas9-mediated mutagenesis. Indeed, we concomitantly tried to obtain indel mutants at this locus by injecting the same flies with the same guide RNA at higher concentration (150 ng/µL), but without a HDR template. We however failed to identify any indel event within 516 G1 descendants obtained from 53 fertile G0 flies. Finding multiple indels in this screen was thus surprising. It suggested that the presence of the ssODN template improved indel generation efficiency at this locus. A possible explanation would be that while indels mostly stem from NHEJ-mediated repair, they can also be generated by aberrant recombination with a repair template.

Strikingly, the reading frame of uL11 is intact in five recovered indel mutants out of seven. While there are not enough alleles to draw a firm conclusion, it is higher than the expected one in three in-frame indels. This is however not surprising: considering that uL11 is an essential gene, nonsense mutations are likely to be deleterious. The two frameshift mutants that we recovered (F+2 and F-4) indeed exhibited dire phenotypes (cf. Results chapter III). It should be noted that their mutation introduces a +2 reading frame shift in both cases. While uL11 may no longer be produced from its canonical initiator codon, the frame shift puts its CDS in frame with an ATG codon located in the 5'UTR. It is thus possible that a protein may be expressed, with a 24 amino-acids extension to uL11. Whether these are complete loss-of-function alleles of *uL11* thus remains to be ascertained.

III. Mutation of a single amino-acid on ribosomal protein uL11 generates a *Minute*-like phenotype in *Drosophila*.

The demonstration that ribosomal protein uL11 interacts with the Enhancer of Trithorax and Polycomb Corto suggested that their interaction underlaid an extra-ribosomal function. This interaction occurs only when uL11 lysine 3 is tri-methylated. Thus, mutations that delete or replace that lysine are expected to prevent the association between uL11 and Corto. Importantly, that lysine is not part of a structured domain of uL11. Furthermore, when uL11 is bound to the ribosome, its lysine 3 is located at the surface. It is thus unlikely that it would participle in binding rRNA or other structural components of the ribosome. We thus hypothesized that mutations that remove or replace the lysine 3 of uL11 would not prevent it from assembling into ribosomes, and to carry its ribosomal function. These mutations would however prevent uL11 from interacting with Corto, giving us the opportunity to understand the biological implications of this interaction.

A. Results

uL11^{K3A} assembles into functional ribosomes

To verify whether the lysine 3 is necessary for its ribosomal function, we aimed to determine whether a uL11^{K3A} variant protein would retain the ability of uL11 to associate with translating ribosomes. Typically, several ribosomes can be found carrying translation simultaneously on the same messenger RNA. The complex that they form together is called a polyribosome. Importantly, the presence of several ribosomes over the same mRNA implies that they moved after the initiation step. For this reason, ribosomes that associate into polyribosomes are considered as caught in the act of translation.

To determine whether uL11^{K3A} associated with polyribomes, we generated stable cell lines expressing either uL11^{K3A}-HA or uL11^{WT}-HA under the control of the Actin:5C promoter (cf Materials and Methods). Cytoplasmic extracts were purified from both genotypes for polysomal fractionation. As a control, an extract of each genotype was supplemented with 25mM EDTA, a concentration that disrupts the interaction between ribosomal subunits and mRNA. Lysates were then loaded on a sucrose gradient and centrifuged to allow differential sedimentation of ribosomal complexes. Gradients were then separated in 22 fractions containing complexes of increasing density. Every second fraction was analysed by western blot to reveal the presence of uL11^{K3A}-HA or uL11^{WT}-HA.

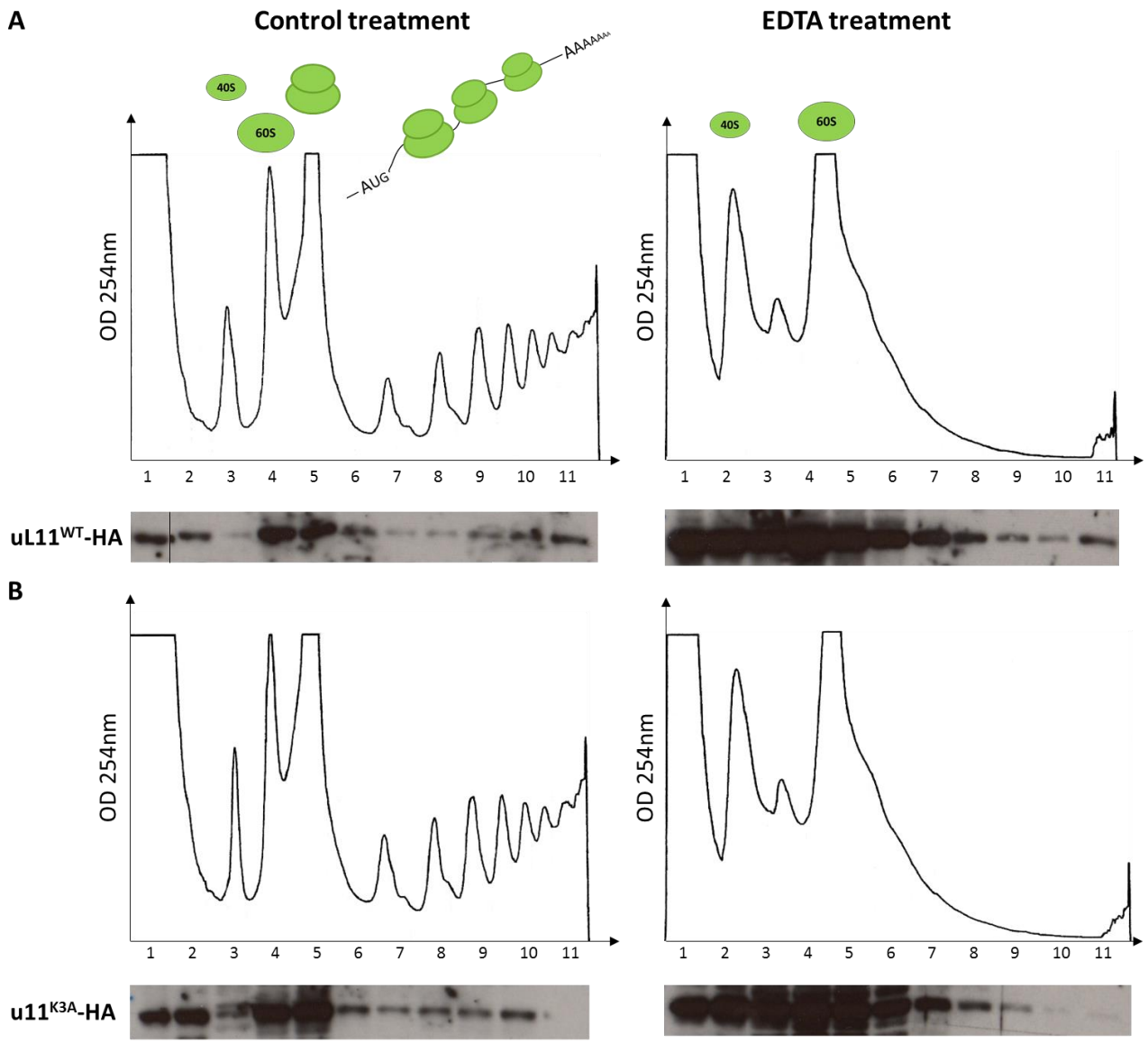

Figure 59. uL11 lysine 3 is not required for integration in active ribosomes.
Cytoplasmic lysates (Left) and EDTA-treated lysates (Right) from S2 cells expressing uL11^{WT}-HA (A) or uL11^{K3A}-HA (B) were separated by centrifugation over a sucrose gradient. Optical density at 254 nm allows to estimate the amount of RNA at any point in the gradient, and was monitored during fractionation (Top panels). The peaks observed in the gradient correspond to the different ribosomal complexes. By increasing order of density: 40S subunit, 60S subunit, 80S monosome, polyribosomes. A schematic representation of these complexes is provided above their respective peaks for clarity. Note that EDTA treatment dissociates ribosomes from mRNA, causing the disappearance of monosomes and polyribosomes from the gradient. Proteins collected from fractions were analysed by Western blotting with anti-HA antibody (Lower panels). A vertical line indicates that different wells from the same gel were juxtaposed in the image for clarity. Images are representative for three obtained replicates.

These experiments revealed the presence of uL11^{K3A}-HA in all ribosomal fractions. Furthermore, EDTA treatment triggered its relocalisation towards lighter fractions, confirming that uL11^{K3A}-HA sedimentated into heavy fractions by association with polyribosomes (**Fig. 59**). Thus, ribosomes that contain uL11^{K3A}-HA are competent for translation initiation and elongation. Furthermore, its distribution among fractions was not biased towards inactive ribosomal fractions when compared to the distribution of uL11^{WT}-HA. Thus, 60S subunits containing uL11^{K3A} displayed no obvious defect in 40S binding or initiation rates. We thus concluded that the loss of uL11 lysine 3 had no critical impact

on its ribosomal function, thus validating the use of lysine 3 deletion or replacement variant to study the extra-ribosomal function of uL11.

Characterization of the *uL11^{K3A}* and *uL11$^{\Delta K3}$* alleles

Using CRISPR/Cas9-mediated HDR, we obtained 8 alleles, among which 6 deleted or replaced lysine 3 without disrupting the *uL11* gene (cf results section chapter II, Table 3). We reasoned that phenotypes caused by the loss of interaction between uL11 and Corto should be observed with different alleles removing uL11 lysine 3. We thus decided to study both the uL11^{K3A} and the uL11$^{\Delta K3}$ allele.

CRISPR/Cas9-mediated mutagenesis is known to cause off-target mutations. Those may generate phenotypes that can be mistakenly attributed to the mutation of interest. To eliminate this risk, we introduced the *uL11* alleles into a controlled genetic background (*w^{1118}*) to separate them from most off-target mutations. To this end, we crossed heterozygous females with *w^{1118}* males for eight generations (Hélène Thomassin and Héloïse Grunchec). Since the *uL11* alleles are not associated to a phenotypic marker, 10 females were crossed individually at each generation, then genotyped by HRMA after laying eggs.

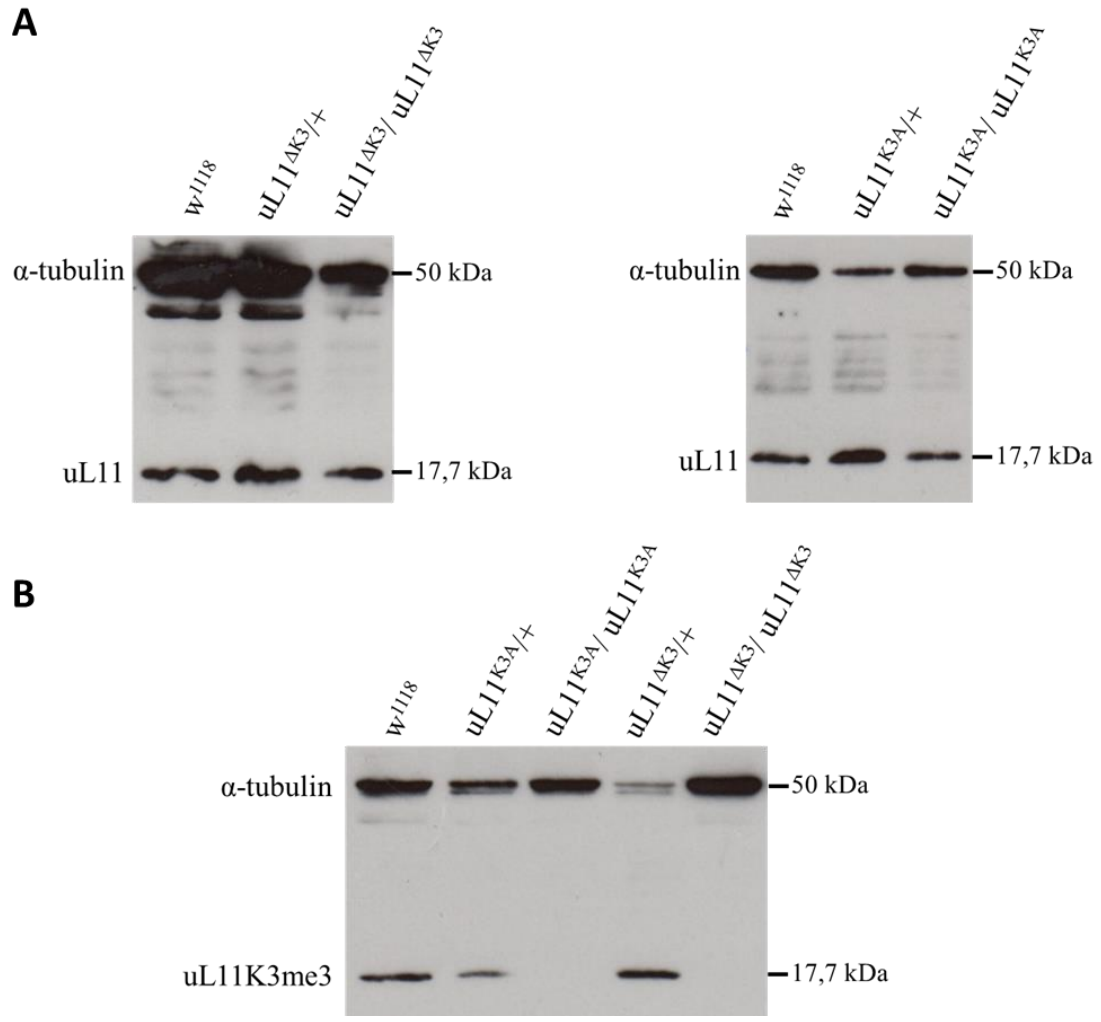

Figure 60. Characterisation of the expression of the uL11 $^{\Delta K3}$ and uL11^{K3A} alleles.
Total proteins were extracted from third instar larvae heterozygous or homozygous for the uL11$^{\Delta K3}$ and uL11^{K3A} mutations or from wild-type larvae. 30 µg proteins were loaded onto SDS-PAGE gels. uL11 was revealed with an anti-uL11 antibody that recognizes an internal epitope (A), or the anti-uL11K3me3 antibody that specifically reacts with uL11 tri-methylated on lysine 3 (B). α-tubulin was revealed as a loading control.

We then analysed their expression by Western blotting (**Fig. 60A**). As expected, uL11 could be detected in all lines with an antibody that recognizes all forms of uL11 through an internal epitope. In contrast, uL11 could no longer be detected in homozygotes with the anti-uL11K3me3 antibody (**Fig. 60B**). These results show that both the uL11^{K3A} and the uL11$^{\Delta K3}$ allele express an unmethylable version of uL11 (Heloïse Grunchec).

Viability of the *uL11* alleles

Both alleles generated obvious phenotypes. The first of those was revealed by our inability to establish homozygous strains. Both the *uL11^{K3A}* and the *uL11$^{\Delta K3}$* alleles produced very little homozygotes. These were mostly males that hatched with a large developmental delay (>2 days) at 25°C. Interestingly, a smaller delay could be observed with *uL11^{K3A}* heterozygotes as compared to wild-type flies (about one day at 25°C). In addition, heterozygous *uL11^{K3A}* females were frequently sterile, and produced less progeny than wild type flies. This phenotype was most apparent when crossing males and females heterozygous for the *uL11^{K3A}* allele, suggesting that both sexes display reduced fertility. While it was possible to keep the *uL11^{K3A}* allele over the *SM5* balancer chromosome for a few generations, it was necessary to regularly cross heterozygous *uL11^{K3A}* males with the *Gla/SM5* balancer strain to maintain the number of individuals. In contrast, the *uL11$^{\Delta K3}$* allele could be established over the *SM5* balancer chromosome, and heterozygotes showed normal developmental time and fertility.

It should be noted that the rate of recovery of *uL11^{K3A}* homozygotes was too low (about 5 per week) to gather enough individuals for robust phenotypic characterisation. However, all their phenotypes could be observed in *uL11^{K3A}* heterozygotes, albeit less severely.

uL11 mutants display *Minute* bristles

One of the most apparent phenotypes that we could observe was a reduction in the size and thickness of the bristles of the *uL11^{K3A}* heterozygotes and homozygotes. We could also visually detect this phenotype in *uL11$^{\Delta K3}$* homozygotes, but not in *uL11$^{\Delta K3}$* heterozygotes (**Fig. 61A**). Scanning electron miscroscopy confirmed the thin bristle phenotype of *uL11^{K3A}* heterozygotes and *uL11$^{\Delta K3}$* homozygotes. In contrast, it revealed no thickness difference between the bristle of control and heterozygous *uL11$^{\Delta K3}$* flies (**Fig.61B**).

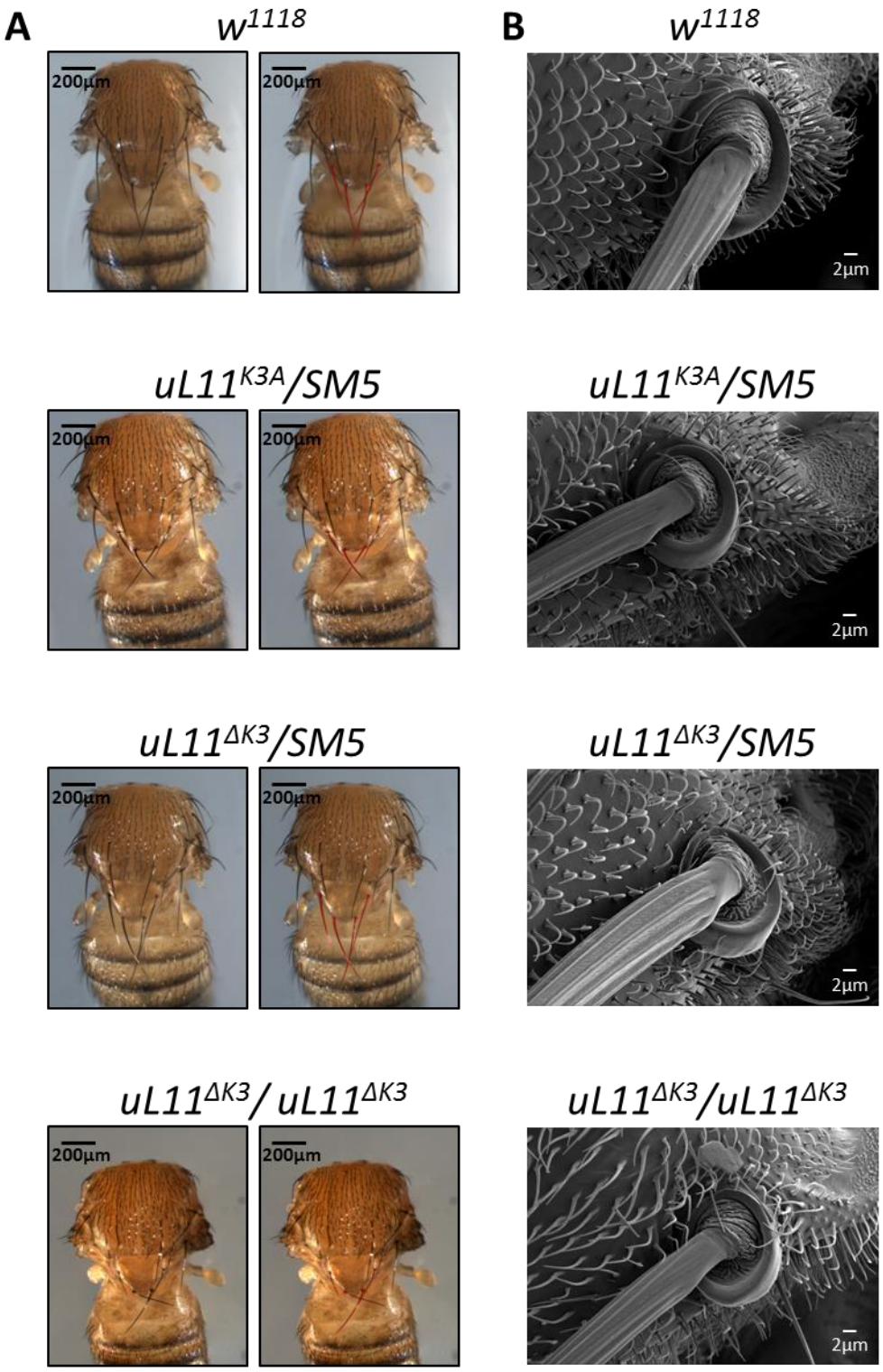

Figure 61. uL11 mutants display Minute bristles.

Left and middle panels: Light microscopy pictures of the uL11 mutants. Fly bodies were disposed on gelose after their wings and heads were cut. Images were then captured using a Leica Model MZ FLIII microscope equipped with a Leica Model DC480 camera. For clarity, scutellar bristles were pseudocolored in red with Photoshop (Middle panels). Note the reduced size and thickness of the scutellar bristles in heterozygous uL11^{K3A} and homozygous uL11$^{\Delta K3}$ mutants. Pictures are representative of 5 imaged individuals. Right panels: Scanning electron micrography of the post-alar bristles of uL11 mutants (cf. Materials and methods). 5 males per genotype were pictured. Note the decreased thickness of the bristle in heterozygous uL11^{K3A} and homozygous uL11$^{\Delta K3}$ mutants. Images were obtained by Heloïse Grunchec and Hélène Thomassin.

The *uL11* mutants exhibit bristle duplications

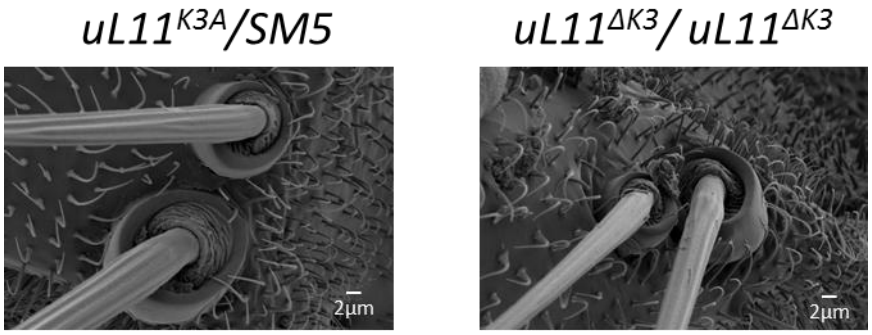

Figure 62. uL11 mutants display bristle duplication phenotypes.
Scanning electron micrography of duplicated post-alar bristles in uL11 mutants. Images were obtained by Heloïse Grunchec and Hélène Thomassin.

The uL11 mutants displayed another bristle phenotype. The anterior post-alar macrochaete was frequently duplicated in both *uL11^{K3A}* heterozygotes and homozygotes (a schematic representation of the thoracic macrochaetes can be found on **Fig. S1** in appendix). Once again, this phenotype could be observed in *uL11$^{\Delta K3}$* homozygotes but not in heterozygotes.

In *Drosophila*, each macrochaete stems from a socket cell. Duplication phenotypes can be observed when two bristles emerge from a single socket, but also when both structures are duplicated. Scanning electron microscopy allowed us to determine that the phenotype of the *uL11* mutants belonged to the second category (**Fig. 62**).

The *uL11^{K3A}* mutation is responsible for the bristle duplication phenotype.

To confirm whether the bristle duplication phenotypes were caused by the mutation of *uL11*, we set to perform functional rescue experiments. To this end, we recovered a bacterial artificial chromosome that contained the entire *uL11* locus - *BAC(uL11^{WT})*. We then introduced a *uL11^{K3A}* mutation by recombineering - *BAC(uL11^{K3A})*, as described in chapter II. We inserted both at the same genomic locus on the third chromosome (VK00027), by ϕC31-mediated integration (BestGene Inc.). Recovered flies were then crossed with balancer strains to replace the first and second chromosomes by those of the *w^{1118}* genetic background. Both transgenes were homozygous lethal, and the lines were established over the *TM6c* balancer chromosome. We then crossed *uL11^{K3A}* flies with each BAC strain to determine whether they would rescue the bristle duplication phenotype (**Table 4**).

	AVERAGE NUMBER OF ANTERIOR POST-ALAR BRISTLES	
	Males	Females
w^{1118}	2	2,02
ul11^{K3A}/+	2,54	2,8
BAC(ul11^{WT}) /+	2	2,02
ul11^{K3A}/+ ; BAC(ul11^{WT}) /+	2,49	2,8
BAC(ul11^{K3A}) /+	2,28	2,53

Table 4. analysis of the anterior post-alar bristle phenotype of the uL11^{K3A} mutant.
The number of anterior post-alar bristles of 40 individuals per genotype was determined. Statistical analysis was performed on R. As variances were not homogeneous Scheirer-Ray-Hare tests were performed. The effects on the phenotype of the uL11^{K3A} mutation, the BAC(uL11^{WT}), the BAC(uL11^{K3A}) and that of the interaction between the uL11^{K3A} mutation and the BAC(uL11^{WT}) were tested.
*For males: uL11^{K3A} mutation, p=3*10^{-4}; BAC(uL11^{WT}), NS; BAC(uL11^{K3A}), p=0,02; Interaction between the uL11^{K3A} mutation and BAC(uL11^{WT}), NS.*
*For females: uL11^{K3A} mutation, p=9*10^{-6}; BAC(uL11^{WT}), NS; BAC(uL11^{K3A}), p=4*10^{-6}; Interaction between the uL11^{K3A} mutation and BAC(uL11^{WT}), NS.*
NS, Not significant. Data were obtained by Hélène Thomassin and Héloïse Grunchec.

As previously observed, surnumerary anterior post-alar bristles were detected in *uL11^{K3A}* heterozygotes. Strikingly, the BAC transgene carrying a wild-type copy of *uL11* had no effect on bristle number on its own, and failed to rescue this phenotype. In contrast, the *BAC(uL11^{K3A})* transgene induced post-alar bristle duplications in an otherwise control genetic background. We were so far unable to recover enough *uL11^{K3A}/+; BAC(uL11^{K3A})* flies to assess whether this association modifies the penetrance of the bristle duplication phenotype.

These data confirm that the bristle duplication phenotype can be attributed to the *uL11^{K3A}* mutation, since it is the only difference between the *BAC(uL11^{K3A})* and the *BAC(uL11^{WT})* transgenes.

The *uL11^{K3A}*, but not the *uL11$^{\Delta K3}$* mutations cause the appearance of ectopic wing veins.

Drosophila melanogaster flies display a very stereotyped wing vein pattern (**Fig. 63**, left). In contrast, both heterozygous and homozygous *uL11^{K3A}* mutants exhibited ectopic veins and cross-veins (**Fig. 63**, right). Surprisingly, this phenotype could not be detected in either heterozygous or homozygous *uL11$^{\Delta K3}$* mutants.

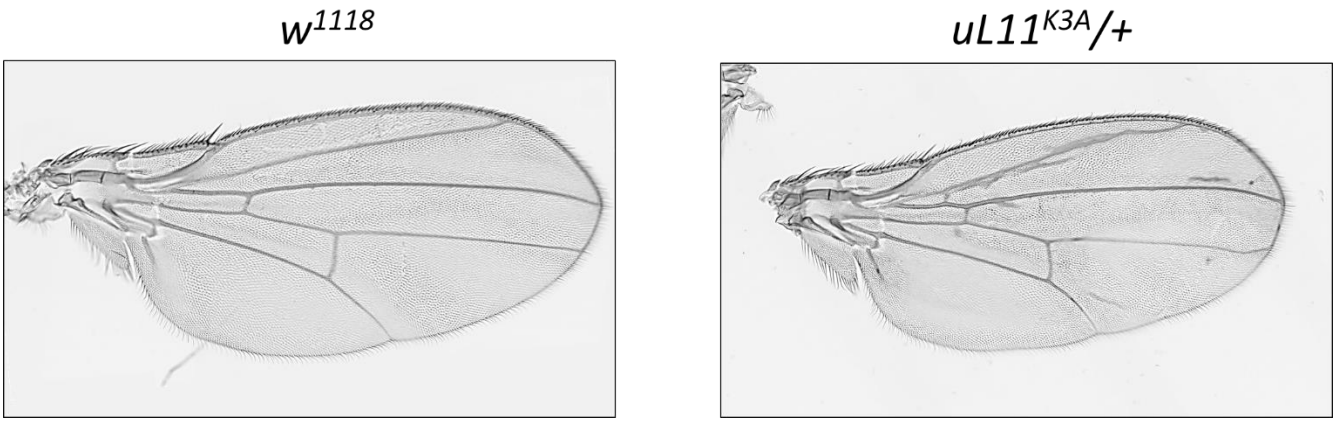

Figure 63. uL11^{K3A} mutant wings display ectopic veins.
Left: wing from a control fly. Right: wings from uL11^{K3A} heterozygotes display ectopic veins and crossveins. Representative pictures of 60 wings collected on 30 females of each genotype.

B. Discussion

Mutations of the lysine 3 of *uL11* generate *Minute*-like phenotypes

The phenotypes of *uL11*^{K3A} and *uL11*$^{\Delta K3}$ mutants, reduced viability and fertility, small and thin bristles, are signature phenotypes of the *Minute* mutants (cf. Introduction chapter II.B.3). Furthermore, ectopic wing veins and alar bristle duplications have also been described in some *Minute* mutants (Marygold et al., 2005; Schultz, 1929). While the other alleles of *uL11* have not been introduced in a controlled genetic background, it is interesting to note that we observed similar phenotypes in several of them (a summary of phenotypes and preliminary observations can be found in Table S4 in appendix). *Minute* mutations have been associated to the loss of function of ribosomal proteins, and their phenotypes are thought to reflect a decreased capacity for protein synthesis (Marygold et al., 2007). Under that hypothesis, tissues that are the most dependent on translation are likely to be the most affected. For instance, high ribosome biogenesis intensity was suggested to be necessary for the maintenance of germinal stem cells in the *Drosophila* ovarium, which could explain the reduced fertility of *Minute* females (Zhang et al., 2014). Similarly, macrochaetes are described to require a very high amount of protein synthesis over a short developmental period (Marygold et al., 2007). The *Minute*-like phenotypes that we observed suggest that translation rates may also be altered in the *uL11* lysine 3 mutants.

Minute mutations however display characteristic genetic features: they are all dominant, and homozygous lethal. Furthermore, they are recessive to two doses of a wild-type allele (Schultz, 1929). In contrast, *uL11*$^{\Delta K3}$ was recessive over all phenotypes. *uL11*^{K3A} was dominant over two copies of the wild-type gene for the bristle duplication phenotypes. In addition, other alleles of *uL11* could be maintained as homozygous strains (K3Y, P2LK3E, P2QK3R). We thus conclude that they are not *Minute* mutations.

Reduction in translation capacity may arise from other mechanisms than r-protein gene loss of functions. For instance, loss of function of *diminutive*, the *Drosophila* gene that encodes Myc, results in small body size, *Minute* bristles and female sterility (Lindsley and Zimm, 1992). Myc is a transcription factor that activates the expression of ribosome biogenesis genes (cf. Introduction chapter II.A.1). This suggests that *Minute*-like phenotypes may result from a dysregulation of this category of genes. By analogy, *uL11* may regulate the transcription of ribosome biogenesis genes. This would be consistent with a previous report that overexpression of *uL11* increases the transcription of r-protein genes (Coléno-Costes et al., 2012), and the fact that uL11K3me3 binds the bodies of these genes (cf. Results chapter I).

uL11 mutations disturb the establishment of the anterior post-alar bristle

In *Drosophila*, the macrochaetes are composed of four cells that originate from a single Sensory Organ Precursor (SOP) cell, following a well-establish differentiation program. The SOP cell (also called pI) divides into the pIIa and pIIb cells. Then, pIIa gives rise to the shaft and socket cells, while pIIb divides into pIIIb and a glial precursor. Finally, pIIIb divides into the sheath and neurone cells while the glial precursor undergoes apoptosis (a schematic representation of the mechanosensory bristle organization and lineage can be found in **Figure S2** in appendix). Both the *uL11*$^{\Delta K3}$ and *uL11*^{K3A} alleles were associated with duplication of the anterior post-alar bristle. Furthermore, scanning electron microscopy allowed to determine that both the bristle and the socket cells were duplicated. Therefore, the duplication event occurs prior to pIIa division. Preliminary neural tracking experiments were realised (Michel Gho), where neuronal cells (identified by anti-Elav staining), could be observed to be duplicated in *uL11* mutants. This would suggest that duplication arises before the asymmetrical division of the SOP.

During development, proneural clusters of 20 to 30 cells segregate from the undifferentiated cells of the wing disc. Each of them carries the potential to become a SOP cell. One of them, that expresses the highest level of the Notch ligand Delta, triggers the Notch signalling cascade in the neighbouring cells, resulting in the repression of proneural genes in all of them (Koch et al., 2013). This lateral inhibition phenomenon ensures that only one SOP cell is specified in each proneural cluster. Interestingly, mutations in ribosome biogenesis components were shown in zebrafish to induce ectopic expression of proneural genes, correlating with a neuronal expansion phenotype (Essers, 2013). It was thus proposed that Notch-mediated inhibition of neuronal differentiation requires a minimum level of ribosomal activity. In addition, many reports have linked mutations in ribosome biogenesis factors with stem cell renewal failure or premature differentiation (for review: Brombin et al., 2015). Thus, the duplication phenotypes we observe could also be a consequence of ribosome biogenesis impairment.

uL11^{K3A} may be a neomorphic or antimorphic allele.

The dominant bristle duplication phenotype generated by the *uL11*^{K3A} allele displayed very peculiar genetic properties. Indeed, it was not rescued by a bacterial artificial chromosome carrying a copy of the *uL11* gene, arguing against haploinsufficiency. Furthermore, the same transgene carrying a *uL11*^{K3A} allele generated bristle duplications in a control genetic background. These data suggest that the *uL11*^{K3A} allele genetically behaves like an antimorph or a neomorph since both the *uL11*^{K3A} mutation or the overexpression of *uL11*^{K3A} result in the same bristle duplication phenotype. It would be very interesting to determine whether these dominance patterns also apply to its other phenotypes.

uL11 has been demonstrated to regulate its own expression by interfering with the splicing of its mRNA in nematodes and mammals (Cuccurese et al., 2005; Mitrovich and Anderson, 2000). If this mechanism were to be conserved in *Drosophila*, expression of a mutant *uL11* gene copy may reduce the expression of the wild type copies by inhibiting the splicing of their messenger. This would make *uL11*^{K3A} a dominant negative allele. This hypothesis could be tested by adapting the allele-specific qPCR method we described in chapter II for RNA quantification.

Mutations of the uL11 lysine 3 display different phenotypes.

We obtained six different alleles that remove or replace the lysine 3 of *uL11*. All of them should prevent the association between uL11 and Corto. We expected that this would result in the same phenotypes in all these mutants. However, the phenotypes that we identified displayed different severity and dominance properties among *uL11* alleles. So far none was identified in all mutants, as the P2QK3R allele displayed no apparent phenotypes (though bristle size and number still need to be studied). It is thus very likely that some of these phenotypes are not directly related to Corto.

To further study the role of the interaction between uL11K3me3 and Corto, it will thus be necessary to first verify that none of these mutants retained the ability to bind Corto. Then, phenotypes common to all mutants should be sought. Since none could be easily identified, it would be informative to combine these mutants with a gain of function for the chromodomain of Corto (CortoCD). Indeed, overexpression of the latter in flies with the UAS-Gal4 system was described to cause high lethality, bristle duplications, partial transformation of the aristae into leg structures and reduction of the number of sex comb teeth (Coléno-Costes et al., 2012). If some of those phenotypes were to result from the interaction between CortoCD and uL11K3me3, they should no longer be observed in *uL11* lysine 3 mutants.

The *uL11* mutant phenotypes may reveal a new function of the N-terminal extension of uL11

While they have different properties, all described phenotypes could be observed in several alleles of *uL11* lysine 3 (Table S4). This argues that they are indeed linked to the N-terminal part of uL11. Notably, the bristle duplication phenotype could be reproduced by a bacterial artificial chromosome containing

a *uL11*^{K3A}, but not a wild-type gene copy. It is thus very likely that these phenotypes reflect the loss of function of the N-terminal extension of *uL11*.

One explanation would be that these mutations may affect the ribosomal function of *uL11*. Indeed, structural modifications could differentially impede the function of the N-terminal domain of uL11 within the ribosome. The phenotypes of the *uL11*^{K3A} mutants were among the most severe, but uL11^{K3A}-HA was found to associate with the same ribosomal fractions as uL11-HA, suggesting that the lysine 3 to alanine mutation does not compromise its general ribosomal function. It is still possible that the ribosomes that contain uL11^{K3A} may have altered translation accuracy or speed, as these phenotypes were associated to the loss of function of *uL11* in yeast (Wawiórka et al., 2016). These could be tested respectively by performing STOP codon readthrough and polysome "run-off" experiments. Another possibility would be that the ribosomes that contain uL11^{K3A} may display altered affinity for specific mRNA, as has been described for ribosomes lacking eS26 in yeast (Ferretti, 2015, 10th EMBO conference on ribosome synthesis, unpublished data), or uL38 in mice (Xue et al., 2015). This hypothesis could be tested by ribosome profiling. These phenotypes may also result from a yet undescribed function of the N-terminal part of uL11, on or off the ribosome. Purifying and comparing the interactome of each of the *uL11* lysine 3 mutants would surely provide insight about the nature of this function.

In any case, the high lethality of several *uL11* lysine 3 mutants suggest that some essential function requires its integrity. Interestingly, subtle changes in its sequence greatly affect the severity of these phenotypes. For instance, ΔK3 is recessive while ΔK3F4 is dominant. Similarly, K3A causes high lethality but K3Y is homozygous viable. This suggests that the activity of the N-terminal part of uL11 is highly dependent on its structure, charge or hydrophobicity. In this context, one could readily imagine that Corto - a 68 kDa protein with a chromodomain and RNA binding properties and a propension to dimerize - would interfere with uL11 activity when bound to trimethylated lysine 3. This could be one of the biological functions of the interaction between uL11K3me3 and Corto.

C. Materials and methods

Plasmids and S2 cells transfection

The *uL11* and *uL11^{K3A}* coding sequences were cloned into the *pAWH* Gateway® *Drosophila* vector allowing expression of fusion proteins with a HA tag in C-ter (Dardalhon-Cuménal et al., submitted). S2 cells were cultured at 25°C in Schneider's *Drosophila* medium supplemented with 10%, heat inactivated foetal bovine serum and 100 units.mL^{-1} of penicillin and streptomycin. For transfection, a mix containing a 5:1 molar ratio of either expression vector and the selection plasmid *pCoBlast* was prepared. 10^6 cells were then transfected with 2µg DNA using Effecten® transfection reagent (Qiagen) according to the manufacturer's instructions (1:10 DNA/Effecten® ratio). Selection was performed by addition of 10 µg.mL^{-1} of blasticidin after 48 hours. After initial selection, stable cell lines were cultured with 2 µg.mL^{-1} blasticidin.

Polyribosome fractionation

Cells were harvested at 50% confluence and washed in Schneider medium at room temperature to remove the foetal bovine serum. They were then resuspended in ice-cold lysis buffer (20 mM HEPES pH 7.5, 250 mM KCl, 10 mM $MgCl_2$, 5 mM DTT, 1 mM EDTA, 0.5 % NP-40) supplemented with EDTA-free protease inhibitor cocktail (Roche Diagnostics, Meylan, France) and 40 U.mL^{-1} Ribolock RNAse Inhibitor (ThermoFisher). For EDTA treatment, the lysis buffer was replaced with (20 mM HEPES pH 7.5, 250 mM KCl, 5 mM DTT, 25 mM EDTA, 0.5 % NP-40). After centrifugation at 500g for 5 min to pellet nuclei, supernatants were layered onto 10-50% sucrose gradients in polyribosome buffer (20 mM HEPES pH7.5, 250 mM KCl, 20 mM $MgCl_2$, 2 mM DTT), supplemented with EDTA-free protease inhibitor cocktail (Roche Diagnostics, Meylan, France) and 40 U.mL^{-1} Ribolock RNAse Inhibitor (ThermoFisher). Gradients were centrifugated at 39,000 rpm for 2 hours and 45 minutes at 4°C in a Beckman SW41-Ti rotor. Optical density at 254 nm was monitored using a density gradient fractionator (Teledyne Isco, Lincoln, NE).

Protein extraction and Western Blotting

Total proteins were extracted from third instar larvae in RIPA buffer (150 mM sodium chloride, 1% NP-40, 0,5% sodium deoxycholate, 0,1% SDS, 50 mM Tris-HCl pH 8,0) supplemented with phosphatase and protease inhibitors (Roche). 30 µg of protein extracts were resolved on a 15 % acrylamide gel. For polyribosomal fractions, proteins were purified by precipitation in two volumes of 100 % ethanol, followed by incubation overnight at -20°C and centrifugation for 30 minutes at 13,000 g at 4°c. Fractions 1 and 2 protein pellets were resuspended in 200 µL 1X Laemmli buffer, while other fractions were resuspended in 50 µL. 15 µL were loaded onto 15% acrylamide gels. Western-blot analysis was performed according to standard protocols. Antibodies used were: anti-uL11 (Santa-Cruz sc-82359, 1/1,000), anti-uL11K3me3 (described in Results chapter I, 1/6,000), anti-α-tubulin (gift from M.H. Verlhac, 1/10,000), anti-HA (Sigma F2411, 1/1,000).

Drosophila stocks and culture

The *uL11*^{K3A} and *uL11*$^{\Delta K3}$ alleles were obtained by CRISPR/Cas9-mediated mutagenesis as described in chapter II. They were introduced in the *w*^{1118} genetic background by backcrossing heterozygous females with *w*^{1118} males for eight generations. *BAC*(*uL11*) and *BAC*(*uL11*^{K3A}) were obtained by recombineering as described in chapter II. *BAC*(*uL11*) and *BAC*(*uL11*^{K3A}) were inserted at the *VK00027* site by ϕC31 -mediated integration, using the BL-9744 strain (BestGene Inc.). The recovered transgenes were crossed with balancer strains to replace the first and second chromosomes by those of the *w*^{1118} genetic background. Other fly strains were obtained from the Bloomington Stock Center. *D. melanogaster* stocks and crosses were kept on standard medium (1 % agar, 8.25 % brewer's yeast, 9.1 % cornstarch, 2.5 % methyl hydroxy-4 benzoate) at 25°C.

Name	Genotype
w	*w*^{1118}
***uL11*$^{\Delta K3}$*/SM5**	*w*^{1118}; *uL11*$^{\Delta K3}$/*SM5*
***uL11*^{K3A}*/SM5**	*w*^{1118}; *uL11*^{K3A}/*SM5*
BAC (uL11*^{wt}*)	*w*^{1118}; *Pbac{y[+]-attR-wBAC(CH322-137O14)-w[+]-attL}VK00027/TM6c*
BAC (uL11*^{K3A}*)	*w*^{1118}; *Pbac{y[+]-attR-BAC(CH322-137O14-uL11*^{K3A}*)-w[+]-attL}VK00027/TM6c*
Gla/CyO, GFP	*w*^{1118}; *Gla/CyO, P{w[+mC]=3xP3-EGFP}2*
BL-9744	*y*^{1} *w*^{1118}; *PBac{y[+]-attP}VK00027*

Table 5. Fly strain genotypes.

Scanning Electron Microscopy (SEM)

Adult flies were kept overnight in 70% ethanol after their wings and legs were cut. They were next dehydrated by immersion in increasing concentrations of alcohol (2x in 95% ethanol, and 2x in 100% ethanol, 20 min each). The samples were dried (by the critical point of CO_2 method). They were mounted on aluminium stubs with double-sided sticky tapes and coated with a layer of platinum (5 nm). Observation was realised with a Zeiss ULTRA55 SEM.

Rescue experiments

The ability of the *BAC(uL11*^{WT}*)* to rescue post-alar bristle duplication phenotype of observed in *uL11*^{K3A} mutants was tested by crossing *BAC(uL11*^{WT}*)/TM6c* or *BAC(uL11*^{K3A}*)/TM6c* females with *uL11*^{K3A}*/SM5* males. Post-alar bristles were quantified in the progeny and a Scheirer-Ray-Hare test (as variances were non-homogeneous) was performed using the R software.

Wing imaging

Adult flies were kept in 70% ethanol for 48 h and transferred into 1:1 (v/v) PBS/glycerol. Wings were then dissected and mounted on glass slides, dorsal side up, in Hoyer's medium. Slides were scanned with a Hamamatsu Nanozoomer Digital Slide scanner, running the Nanozoomer software with a 20 x objective and an 8-bit camera. Wing pictures were separately exported into tif format using NDP.view and the 5 x lens.

Discussion and perspectives

Previous work demonstrated that Corto interacts specifically with uL11 tri-methylated on lysine 3, and suggested that they both have a role in activating the transcription of ribosome biogenesis genes (Coléno-Costes et al., 2012). The fact that both proteins would bind chromatin on largely overlapping sites further suggested a direct regulation of transcription. In addition, Corto had been extensively characterized as an Enhancer of Trithorax and Polycomb (ETP), which can both activate or repress genes, by associating with different epigenetic complexes. Thus, we hypothesized that the association between Corto and uL11K3me3 underlaid a function in regulation of transcription directly on chromatin.

What is the function of uL11K3me3 and CortoCD on chromatin?

The chromodomain of Corto (CortoCD) reproduces the binding sites of the full-length protein on polytene chromosomes, and its overexpression causes the same phenotypes, though less severely. It is thus likely that its genome-wide binding pattern represents that of Corto. Strikingly, it displays a very sharp enrichment at the transcription start site (TSS) of coding genes. The large amount of TSS it binds – 7588 – are also enriched for RNAPolII. In contrast, it cannot be found in TSS lacking RNAPolII (cf. Results chapter I.A). These data suggest that Corto might physically interact with either the pre-initiation complex or RNAPolII itself. On polytene chromosomes, Corto preferentially co-localized with paused RNA polymerase (RNAPolIISer5p) rather than with elongating polymerase (RNAPolIISer2p). This is consistent with its sharp enrichment at the TSS of coding genes. In addition, Corto was shown to antagonize the elongin complex in *Drosophila* vein patterning (Rougeot et al., 2013). Since the elongin complex is known to regulate RNAPolII elongation, these data would suggest a role for Corto in the regulation of transcriptional pausing.

However, the overexpression of CortoCD disturbs the expression of but a subset of genes. It is thus likely that the Corto does not have trans-activator or trans-repressor properties by itself. That would be coherent with its description as an ETP: these transcription factors are thought to be bridge together proteins and allow the assembly of diverse epigenetic complexes. Indeed, Polycomb and Trithorax complexes do not display strong DNA sequence specificity. Their recruitment to specific sites on chromatin has been postulated to depend on their interaction with other factors, among which ETPs (Déjardin et al., 2005). Corto itself possesses all the properties of a hub protein: it contains large unstructured domains with aggregative properties and specifically interacts with more than ten proteins (Krasowski et al., 2008). Thus, its function in transcription may be to bridge together different transcription factors and epigenetic complexes. Indeed, uL11K3me3 may be part of one of those complexes.

The genome-wide binding profile of uL11K3me3 however displays little similarity with that of CortoCD. The ribosomal protein is detected on broad domains, and within gene bodies. Interestingly, the binding of many r-proteins to chromatin has been observed in *Drosophila*. Several of them associate to histone H1, and localize to condensed chromatin (Ni et al., 2006). Other observations reported that a number of r-proteins bind transcribed regions in an RNA-dependent manner (Brogna et al., 2002; Rugjee et al., 2013). In yeast, transcriptional activation correlates with recruitment of r-proteins over the gene body, suggesting an association with nascent RNA (Schroder and Moore, 2005). It is possible that uL11K3me3 is recruited to chromatin through similar mechanisms. Notably, it was shown to be recruited to the *hsp70* gene upon heatshock induction (Coléno-Costes et al., 2012). This would also correlate with the fact that uL11 co-localizes with elongating RNAPolII more than with paused RNAPolII on polytene chromosomes. Interestingly, uL11K3me3 is not enriched in all transcribed gene bodies, suggesting that it displays gene-specific recruitment. Importantly, it is detected in clusters of genes enriched for

cytoplasmic and mitochondrial translation. It is thus possible that it participates in the regulation of their transcription.

Intriguingly, uL11K3me3 was found to be enriched in many regions clustering near the centromeres of chromosomes II and III. It also forms broad enrichment domains that cover inactive genes, and preliminary observation suggests that these correspond to H3K27me3 domains. The binding of r-proteins to heterochromatin has been described in yeast, and was also found to be RNA-dependent (De et al., 2011). While no mechanism or function for this phenomenon has been proposed yet, it may be worthy to consider that ribosomal proteins aggregate around chromosomes during mitosis (Van Hooser et al., 2005), and that *Minute* mutants share a propension to lose chromosomes in somatic cells (Schultz, 1929). It could thus suggest a role for r-proteins in genome stability.

Strikingly, uL11K3me3 was depleted at the TSS bound by CortoCD. Several hypotheses may explain this exclusion. The binding of Corto may prevent antibodies from accessing the K3me3 epitope, or Corto may remove uL11K3me3 from chromatin. Alternatively, CortoCD correlates with the presence of RNApolII, which is known to displace nucleosomes from the TSS, resulting in sharp depletion of histone signal. This could affect uL11K3me3 if its recruitment to chromatin were to occur through histone binding. While this remains to be elucidated, it appears that the TSS of active genes are the only genomic loci where uL11K3me3 and CortoCD are found in close proximity. These loci are further restricted to the genes bound by uL11K3me3*, i.e.* a subset of genes among which ribosome biogenesis components are enriched. This is consistent with the hypothesis that their interaction underlies a function in direct regulation of transcription. Importantly, since each protein displays a specific binding pattern, it is unlikely that their interaction serves the purpose of addressing them to chromatin. An exciting possibility would be that the recognition of uL11K3me3 by the Corto chromodomain triggers a molecular event such as a change in conformation, affinity or a post-translational modification of either protein. Indeed, such mechanism was proposed for eEF3 in yeast: this translational elongation factor contains a chromodomain-like domain that is thought to interact with several ribosomal proteins. Mutation of critical residues of this domain does not impede the binding of eEF3 to the ribosome, but compromises its ATPase activity (Sasikumar and Kinzy, 2014).

Interestingly, preliminary results from our team show that uL11 co-immunoprecipitates with CycG, which also physically interacts with Corto. CycG is a transcriptional cycline, and the analysis of its binding sites revealed that it binds the TSS of genes enriched for ribosome biogenesis genes in *Drosphila* wing imaginal discs (cf. Appendix). In addition, its overexpression also increases the transcription of these genes. These data suggest that there is an interplay between Corto, uL11 and CycG in the regulation of ribosome biogenesis genes. Most interestingly, CycG interacts with Cyclin-dependent kinase 2 (CDK2), which has been shown to phosphorylate uL11 on Serine38 (Chi et al., 2008). Interestingly, CDK2 was also shown to promote the transcription of HIV-1 by phosphorylating the C-terminal domain (CTD) of RNAPolII on Serine 2, at the onset of transcriptional elongation.

Altogether, these data suggest that the interaction between Corto and uL11K3me3 may enhance the transcription of ribosome biogenesis genes at the level of RNAPolII pausing. Notably, the distribution of uL11K3me3 would be consistent with the idea that it binds nascent RNA and promotes transcriptional elongation. A possibility would be that uL11K3me3 may interact with the short transcripts that emerge from paused polymerases. Transient association with Corto could trigger an allosteric effect with other transcription factors, such as CycG or the elongin complex, as has been proposed for eEF3. This could result in RNAPolII release from pause, allowing transcription of ribosome biogenesis genes. Binding of uL11 to the nascent mRNA would result in its ChIP signal spreading across the gene body, without being enriched at the TSS or spreading further than the TES.

Is uL11K3me3 involved in epigenetic regulation of gene expression?

Chromodomains usually bind tri-methylated lysines on the tails of histones. Furthermore, Corto is a known co-factor of the Polycomb complexes (Kodjabachian et al., 1998; Lopez et al., 2001; Salvaing et al., 2003, 2006). It was thus tempting to hypothesize that epigenetic complexes would participate in the uL11K3me3-mediated regulation of transcription.

Indeed, we found that uL11 interacts physically with the Polycomb-group protein Calypso. Interestingly, CycG was shown previously to interact with Additional Sex Combs (ASX) in both S2 cells and embryos (Dupont et al., 2015). Calypso and ASX are part of the PR-DUB complex, and are both necessary to deubiquitinate histone H2A (Scheuermann et al., 2010). In contrast, Corto is known to physically interact with PRC1 complex core components PC and PH (Salvaing et al., 2003). As the PRC1 complex ubiquitinates histone H2A on lysine 118, these data suggest that the interaction between uL11K3me3 and Corto could play a role in the establishment and removal of this mark. However, there is no obvious correlation between the distribution of H2AK118ub and the genomic localization of Corto and uL11K3me3.

Several other functions can be proposed for the interaction between uL11 and Calypso. Indeed, it could occur away from coding genes, or from chromatin. Additionally, it remains to be tested whether uL11-bound Calypso is always complexed with ASX, which is required for its deubiquitinase activity. For instance, the association of Caypso and ASX could be promoted by the interaction between uL11 and CycG. On chromatin, this would amount to the TSS of active genes.

Importantly, a study demonstrated that the promoters of a subset of active genes are ubiquitinated during mitosis in human cells. These genes are silenced during that phase, but their transcription resumes in G1 phase. Strikingly, that ubiquitination was dependent on PRC1 components BMI1 and RING1A, though its substrate was not histone H2A. Depletion of RING1A prevents this ubiquitination, blocks cell proliferation, and reduces the G1 phase transcription of those genes, among which *Myc*, *uS11*, *eL8* and *eL19*. It was thus proposed that PRC1 "bookmarks" during mitosis a subset of genes whose expression is required for proliferation in early G1 phase (Arora et al., 2012, 2016).

An exciting hypothesis would be that instead of uL11 recruiting Calypso to target genes, it may rather be Calypso that targets uL11 to bookmarked promoters, through recognition of this ubiquitinated substrate. Indeed, ribosomal biogenesis genes are typically silenced in mitosis and re-expressed in G1 phase. Furthermore, they are required for cell growth and proliferation (cf. Introduction chapter II.A.2). It would thus be very interesting to determine whether the subset of active genes bound by uL11K3me3 correspond to bookmarked promoters.

The N-terminal domain of uL11 carries a critical function in Drosophila

Several lines of evidence suggest that the methylation of lysine 3 is not required for the translational activity of uL11. First, its position in the ribosome leaves the lysine 3 residue at the surface, where it is unlikely to engage in interactions with core ribosomal components. Second, deletion of the enzyme responsible for uL11 lysine 3 methylation in *S. cerevisiae* and *S. pombe* has little impact on ribosome assembly and function or on cell viability (Porras-Yakushi et al., 2006; Sadaie et al., 2008).

We thus generated mutant alleles of *uL11* that remove or replace that residue. These alleles are expected to disrupt the ability of uL11 to bind Corto. Strikingly, these mutants displayed phenotypes akin to those of *Minute* mutants. Their viability is reduced, they display sterility, minute and duplicated bristles, and ectopic veins. However, these phenotypes display different dominance properties between alleles, and none is common to all mutants. This inconsistency strongly argues that most of these phenotypes are linked to something else than the loss of interaction between uL11 and Corto. Rather, it shows that the N-terminal domain of uL11 is involved into something very important during

development. Indeed, several of these alleles are sub-viable, suggesting that this function is essential. Furthermore, their *Minute*-like phenotypes suggest a reduction in translation capacity.

One of the most parsimonious explanations would be that the N-terminal extension of uL11 is critical for translation. The diverse sequence modifications in the uL11 alleles could produce proteins with more or less severe impairments for their ribosomal function, explaining the difference in phenotype strength. Interestingly, while the *uL11*^{K3A} allele displays phenotypes amongst the most severe, we observed that a uL11^{K3A} fusion protein associates to the same ribosomal fractions as its wild-type counterpart. *uL11* loss of function was shown in yeast to impede inter-subunit joining, and to halve translation speed (Wawiórka et al., 2016). If uL11^{K3A} were non-functional in translation, we would expect it to display bias for lighter ribosomal fractions, which is not the case. While this argues against mutations of the N-terminal part of uL11 impeding its ribosomal function, it is likely that much more sensitive assays will be required to obtain such certitude. Indeed, we cannot exclude that the ribosomes which contain mutated versions of uL11 display altered properties. For instance, *uL11* loss of function causes increased amino-acid misincorporation and termination codon readthrough in yeast (Wawiórka et al., 2016). Such phenotypes could be assayed by performing polysome run-off and STOP codon readthrough assays.

Another explanation for these phenotypes would be that the N-terminal extension of uL11 is involved in other extra-ribosomal functions. For instance, uL11K3me3 was detected over many broad chromatin domains devoid of CortoCD. It would be conceivable that uL11 carries functions that do not require the trimethylation of lysine 3. The N-terminal domain of uL11 is an unstructured extension composed of hydrophilic aminoacids. It could be a hub for protein interactions. Indeed, one of the phenotypes that we observed, *i.e.* ectopic wing veins, do not seem to correlate with the others. Indeed, this phenotype can be observed in *uL11*^{P2LK3E} and *uL11*^{K3Y} homozygous mutants, but not in *uL11*$^{\Delta K3}$ homozygotes, even though this allele displays more severe phenotypes. In contrast, it can be observed in *uL11*^{K3A} heterozygotes and homozygotes, which respectively display lesser and stronger phenotypes than *uL11*$^{\Delta K3}$ homozygotes. While these observations are still at the preliminary stage, it could suggest that the wing vein phenotype is caused by something else than the other phenotypes.

While these potential functions are unlikely to reflect the role of the interaction between Corto and uL11K3me3, it should be considered that they may be related. Indeed, whichever function is carried by the N-terminal extension of uL11 appears to be critically sensitive to its sequence, structure or charge. The binding of Corto to tri-methylated lysine 3 could easily affect these parameters, and promote or antagonize other functions of the N-terminal domain of uL11. It would thus be very interesting to investigate the existence of such functions. For instance, the protein-protein interactions of each version of uL11 could be compared to identify which partners correlate with the observed phenotypes.

The methylation of uL11 lysine 3 is not essential in Drosophila.

In the midst of these mutant phenotypes, consequences of the loss of uL11K3me3 interaction with Corto remain undetected. One possible, though unlikely explanation would be that this interaction is actually inconsequential. A few lines of evidence suggest otherwise. Notably, the overexpression of the uL11 methyltransferase Set11 in *S. pombe* causes severe growth defects (Sadaie et al., 2008). Although it is not known whether Set11 carries other functions, it suggests that the methylation of uL11 has a biological function. In addition, most of the phenotypes of the overexpression of Corto could be reproduced by the expression of its chromodomain (CortoCD) in flies. While CortoCD likely associates with other proteins than uL11K3me3, it is plausible that some of these phenotypes result from this interaction. For this reason, it should be very informative to determine whether each *uL11* mutation rescues these phenotypes.

Another explanation for the lack of obvious phenotypes is that this function may not be required under permissive growth conditions. Indeed, many extra-ribosomal functions are triggered under stress conditions, and participate in the coordination between ribosome biogenesis and cell homeostasis (cf. Introduction chapter III.B). It would thus be interesting to test whether the *uL11* mutants display altered resistance to stresses that affect ribosome biogenesis, for instance by raising them with specific food diets.

Is the function of uL11 lysine 3 methylation strictly transcriptional?

The prevalence of uL11 lysine 3 methylation was not quantified, but it is thought to be high. Indeed, in *S. pombe*, the methyltransferase that catalyses this modification is unable to methylate uL11 from wild-type cell extracts. Its activity could only be detected by incubating it with extracts from *ΔSet11* mutants. It was thus proposed that most, if not all uL11, is methylated in *S. pombe* under steady-state conditions (Sadaie et al., 2008). Consistently, we could detect the presence of uL11K3me3 in all ribosomal fractions. It is worthy to consider that Corto is found both in the nucleus and in the cytoplasm, enabling the possibility that it would interact with ribosome-bound uL11.

As mentioned previously, the lysine 3 of ribosome-bound uL11 is exposed at the surface of the ribosome (Fig. 33). The whole N-terminal domain of uL11 is located at the base of the P stalk of the ribosome. It is known to be labile and to change its conformation at all steps of the elongation cycle. Importantly, it is bound by elongation and termination factors during translation (cf. Introducton chapter IV.A.2). It is likely that the binding of Corto to methylated lysine 3 would sterically interfere with the binding of elongation or termination factors. While the binding of Corto to the ribosome remains but a possibility, our team observed that CycG associates to the same ribosomal fractions as uL11 in S2 cells. It is not known whether this association occurs through physical interaction with uL11, but suggests that there is merit in investigating the possibility.

Indeed, a recent study demonstrated that the ribosome is bound by numerous proteins, which are likely to affect its properties (Simsek et al., 2017). Several roles could be proposed: Corto or CycG may repress translation by excluding elongation factors from the GTPase centre of the ribosome. Alternatively, they might promote or repress the translation of specific mRNA. Noteworthily, the P stalk of the ribosome binds only at the onset of translation elongation. Thus, the immediate neighbourhood of uL11 in free 60S subunits is remarkably accessible for protein-protein interactions. In addition, the lysine 3 of uL11 is located near the intersubunit interface. In addition, Corto was shown to bind specific regions of both the 18S and 28S rRNA. One could thus imagine that CycG, Corto or other factors may bind to uL11 and promote the association of free 60S subunits to a subset of 43S initiation complexes. Performing ribosome profiling experiments in the *uL11* mutants would likely be very informative about this possibility.

uL11 as an amplifier of ribosome biogenesis?

Many extra-ribosomal functions have been identified to regulate ribosome biogenesis. However, most of them are involved in its repression. Metabolic stresses, or cues that impair ribosome biogenesis trigger the release of r-proteins, which in turn supress the production of surnumerary ribosome components. An extra-ribosomal function of uL11 in activation of ribosome biogenesis implies the existence of an amplification loop, and goes against this paradigm. Indeed, uL11K3me3 is expected to increase its own abundance together with ribosome components. Specifically, it implies that the release of uL11 from the nucleolus or the ribosome, unlike other r-proteins, is not a sign of metabolic distress.

Several layers of safety are dedicated to preventing r-proteins from accumulating out of the ribosomal component. They are often escorted to the nucleolus, where they are retained. Additionally, they are quickly degraded in the nucleoplasm (cf. Introduction chapter III.B.1). Not much is known about the

peculiar case of uL11, though. Because it is hardly ever present in crystal structures of the eukaryotic ribosome, data about its incorporation are very indirect. The situation has been emphatetically summarized: "*Data on the assembly of [uL11] ... are both scarce and contradictory …*" (Francisco-Velilla et al., 2013). A few peculiarities have been discovered though. Unlike other r-proteins, uL11 is imported into the nucleolus by the importin-11 pathway (Plafker and Macara, 2002). In addition, its depletion only causes a minor delay in the maturation of the 60S subunit (de la Cruz et al., 2015). Thus, it is possible that uL11 would be less constrained to assemble into the ribosome than other r-proteins. If it were to be the case, ribosome-free uL11 could accumulate under normal conditions.

However, it seems very likely that the extra-ribosomal function of uL11 would be the target of regulatory events. Indeed, our lab demonstrated that Corto is phosphorylated in response to the activation of the MAPK pathway (Mouchel-Vielh et al., 2011). Three potential phosphorylation sites have been predicted, two of which are located within the chromodomain. Such phosphorylations could regulate the localization, conformation, or protein interactions of Corto. The MAPK pathway is activated in response to growth signals, and is a positive regulator of ribosome biogenesis (cf. Introduction chapter II.A.1). Thus, one could expect this post-translational modification to enhance its function in activating ribosome biogenesis gene transcription. Such a mechanism would couple the regulation of ribosome biogenesis and the sensing of metabolic cues, through the extra-ribosomal function of uL11.

Bibliography

Abreu, R. de S., Penalva, L.O., Marcotte, E.M., and Vogel, C. (2009). Global signatures of protein and mRNA expression levels. Mol. Biosyst. *5*, 1512–1526.

Adhikary, S., and Eilers, M. (2005). Transcriptional regulation and transformation by Myc proteins. Nat. Rev. Mol. Cell Biol. *6*, 635–645.

Adilakshmi, T., Ramaswamy, P., and Woodson, S.A. (2005). Protein-independent folding pathway of the 16S rRNA 5' domain. J. Mol. Biol. *351*, 508–519.

Agrawal, R.K., Linde, J., Sengupta, J., Nierhaus, K.H., and Frank, J. (2001). Localization of L11 protein on the ribosome and elucidation of its involvement in EF-G-dependent translocation1. J. Mol. Biol. *311*, 777–787.

Akopian, D., Shen, K., Zhang, X., and Shan, S. (2013). Signal Recognition Particle: An essential protein targeting machine. Annu. Rev. Biochem. *82*, 693–721.

Al-Hadid, Q., Roy, K., Chanfreau, G., and Clarke, S.G. (2016a). Methylation of yeast ribosomal protein Rpl3 promotes translational elongation fidelity. RNA *22*, 489–498.

Al-Hadid, Q., White, J., and Clarke, S. (2016b). Ribosomal Protein Methyltransferases in the Yeast Saccharomyces cerevisiae: Roles in Ribosome Biogenesis and Translation. Biochem. Biophys. Res. Commun. *470*, 552–557.

Al-Jubran, K., Wen, J., Abdullahi, A., Chaudhury, S.R., Li, M., Ramanathan, P., Matina, A., De, S., Piechocki, K., Rugjee, K.N., et al. (2013). Visualization of the joining of ribosomal subunits reveals the presence of 80S ribosomes in the nucleus. RNA *19*, 1669.

Andersen, C.B.F., Becker, T., Blau, M., Anand, M., Halic, M., Balar, B., Mielke, T., Boesen, T., Pedersen, J.S., Spahn, C.M.T., et al. (2006). Structure of eEF3 and the mechanism of transfer RNA release from the E-site. Nature *443*, 663–668.

Anderson, P., and Kedersha, N. (2009). Stress granules. Curr. Biol. *19*, R397–R398.

Anderson, J., Phan, L., Cuesta, R., Carlson, B.A., Pak, M., Asano, K., Björk, G.R., Tamame, M., and Hinnebusch, A.G. (1998). The essential Gcd10p–Gcd14p nuclear complex is required for 1-methyladenosine modification and maturation of initiator methionyl-tRNA. Genes Dev. *12*, 3650–3662.

Angelier, N., Tramier, M., Louvet, E., Coppey-Moisan, M., Savino, T.M., De Mey, J.R., and Hernandez-Verdun, D. (2005). Tracking the interactions of rRNA processing proteins during nucleolar assembly in living cells. Mol. Biol. Cell *16*, 2862–2871.

Anger, A.M., Armache, J.-P., Berninghausen, O., Habeck, M., Subklewe, M., Wilson, D.N., and Beckmann, R. (2013). Structures of the human and Drosophila 80S ribosome. Nature *497*, 80–85.

Aoufouchi, S., Yélamos, J., and Milstein, C. (1996). Nonsense mutations inhibit RNA splicing in a cell-free system: recognition of mutant codon is independent of protein synthesis. Cell *85*, 415–422.

Apcher, S., Millot, G., Daskalogianni, C., Scherl, A., Manoury, B., and Fåhraeus, R. (2013). Translation of pre-spliced RNAs in the nuclear compartment generates peptides for the MHC class I pathway. Proc. Natl. Acad. Sci. U. S. A. *110*, 17951–17956.

Arabi, A., Wu, S., Ridderstråle, K., Bierhoff, H., Shiue, C., Fatyol, K., Fahlén, S., Hydbring, P., Söderberg, O., Grummt, I., et al. (2005). c-Myc associates with ribosomal DNA and activates RNA polymerase I transcription. Nat. Cell Biol. *7*, 303–310.

Araujo, P.R., Yoon, K., Ko, D., Smith, A.D., Qiao, M., Suresh, U., Burns, S.C., and Penalva, L.O.F. (2012). Before It Gets Started: Regulating Translation at the 5′ UTR. Int. J. Genomics *2012*, e475731.

Arora, M., Zhang, J., Heine, G.F., Ozer, G., Liu, H., Huang, K., and Parvin, J.D. (2012). Promoters active in interphase are bookmarked during mitosis by ubiquitination. Nucleic Acids Res. *40*, 10187–10202.

Arora, M., Packard, C.Z., Banerjee, T., and Parvin, J.D. (2016). RING1A and BMI1 bookmark active genes via ubiquitination of chromatin-associated proteins. Nucleic Acids Res. *44*, 2136–2144.

Aström, S.U., and Byström, A.S. (1994). Rit1, a tRNA backbone-modifying enzyme that mediates initiator and elongator tRNA discrimination. Cell *79*, 535–546.

Audas, T.E., Jacob, M.D., and Lee, S. (2012). Immobilization of proteins in the nucleolus by ribosomal intergenic spacer noncoding RNA. Mol. Cell *45*, 147–157.

Baker, N.E. (2017). Mechanisms of cell competition emerging from Drosophila studies. Curr. Opin. Cell Biol. *48*, 40–46.

Baltz, A.G., Munschauer, M., Schwanhäusser, B., Vasile, A., Murakawa, Y., Schueler, M., Youngs, N., Penfold-Brown, D., Drew, K., Milek, M., et al. (2012). The mRNA-Bound Proteome and Its Global Occupancy Profile on Protein-Coding Transcripts. Mol. Cell *46*, 674–690.

Ban, N., Nissen, P., Hansen, J., Moore, P.B., and Steitz, T.A. (2000). The Complete Atomic Structure of the Large Ribosomal Subunit at 2.4 Å Resolution. Science *289*, 905–920.

Ban, N., Beckmann, R., Cate, J.H.D., Dinman, J.D., Dragon, F., Ellis, S.R., Lafontaine, D.L.J., Lindahl, L., Liljas, A., Lipton, J.M., et al. (2014). A new system for naming ribosomal proteins. Curr. Opin. Struct. Biol. *24*, 165–169.

Barbet, N.C., Schneider, U., Helliwell, S.B., Stansfield, I., Tuite, M.F., and Hall, M.N. (1996). TOR controls translation initiation and early G1 progression in yeast. Mol. Biol. Cell *7*, 25–42.

Barna, M., Pusic, A., Zollo, O., Costa, M., Kondrashov, N., Rego, E., Rao, P.H., and Ruggero, D. (2008). Suppression of Myc oncogenic activity by ribosomal protein haploinsufficiency. Nature *456*, 971–975.

Barnum, K.J., and O'Connell, M.J. (2014). Cell Cycle Regulation by Checkpoints. Methods Mol. Biol. Clifton NJ *1170*, 29–40.

Baronas-Lowell, D.M., and Warner, J.R. (1990). Ribosomal protein L30 is dispensable in the yeast Saccharomyces cerevisiae. Mol. Cell. Biol. *10*, 5235–5243.

Bassett, A.R., Tibbit, C., Ponting, C.P., and Liu, J.-L. (2014). Mutagenesis and homologous recombination in Drosophila cell lines using CRISPR/Cas9. Biol. Open *3*, 42–49.

Beckmann, H., Chen, J.L., O'Brien, T., and Tjian, R. (1995). Coactivator and promoter-selective properties of RNA polymerase I TAFs. Science *270*, 1506–1509.

Ben-Shem, A., Loubresse, N.G. de, Melnikov, S., Jenner, L., Yusupova, G., and Yusupov, M. (2011). The Structure of the Eukaryotic Ribosome at 3.0 Å Resolution. Science *334*, 1524–1529.

Berger, A.B., Decourty, L., Badis, G., Nehrbass, U., Jacquier, A., and Gadal, O. (2007). Hmo1 is required for TOR-dependent regulation of ribosomal protein gene transcription. Mol. Cell. Biol. *27*, 8015–8026.

Bermudez-Santana, C., Attolini, C.S.-O., Kirsten, T., Engelhardt, J., Prohaska, S.J., Steigele, S., and Stadler, P.F. (2010). Genomic organization of eukaryotic tRNAs. BMC Genomics *11*, 270.

Bernstein, K.A., Bleichert, F., Bean, J.M., Cross, F.R., and Baserga, S.J. (2007). Ribosome Biogenesis Is Sensed at the Start Cell Cycle Checkpoint. Mol. Biol. Cell *18*, 953–964.

Bhargava, P., and Kassavetis, G.A. (1999). Abortive initiation by Saccharomyces cerevisiae RNA polymerase III. J. Biol. Chem. *274*, 26550–26556.

Bhavsar, R.B., Makley, L.N., and Tsonis, P.A. (2010). The other lives of ribosomal proteins. Hum. Genomics *4*, 327.

Bierhoff, H., Dundr, M., Michels, A.A., and Grummt, I. (2008). Phosphorylation by casein kinase 2 facilitates rRNA gene transcription by promoting dissociation of TIF-IA from elongating RNA polymerase I. Mol. Cell. Biol. *28*, 4988–4998.

Birch, J.L., and Zomerdijk, J.C.B.M. (2008). Structure and function of ribosomal RNA gene chromatin. Biochem. Soc. Trans. *36*.

Blackwell, T.K., Huang, J., Ma, A., Kretzner, L., Alt, F.W., Eisenman, R.N., and Weintraub, H. (1993). Binding of myc proteins to canonical and noncanonical DNA sequences. Mol. Cell. Biol. *13*, 5216–5224.

Blander, G., and Guarente, L. (2004). The Sir2 family of protein deacetylases. Annu. Rev. Biochem. *73*, 417–435.

Blank, M.F., and Grummt, I. (2017). The seven faces of SIRT7. Transcription *8*, 67–74.

Bloom, J., and Pagano, M. (2004). To be or not to be ubiquitinated? Cell Cycle Georget. Tex *3*, 138–140.

Bobrow, M., Pearson, P.L., and Collacott, H.E. (1971). Para-nucleolar position of the human Y chromosome in interphase nuclei. Nature *232*, 556–557.

Bogenhagen, D.F., Wormington, W.M., and Brown, D.D. (1982). Stable transcription complexes of Xenopus 5S RNA genes: a means to maintain the differentiated state. Cell *28*, 413–421.

Boisvert, F.-M., van Koningsbruggen, S., Navascués, J., and Lamond, A.I. (2007). The multifunctional nucleolus. Nat. Rev. Mol. Cell Biol. *8*, 574–585.

Boria, I., Garelli, E., Gazda, H.T., Aspesi, A., Quarello, P., Pavesi, E., Ferrante, D., Meerpohl, J.J., Kartal, M., Da Costa, L., et al. (2010). The Ribosomal Basis of Diamond-Blackfan Anemia: Mutation and Database Update. Hum. Mutat. *31*, 1269–1279.

Bortoluzzi, S., d'Alessi, F., Romualdi, C., and Danieli, G.A. (2001). Differential expression of genes coding for ribosomal proteins in different human tissues. Bioinforma. Oxf. Engl. *17*, 1152–1157.

Bouchard, C., Marquardt, J., Brás, A., Medema, R.H., and Eilers, M. (2004). Myc-induced proliferation and transformation require Akt-mediated phosphorylation of FoxO proteins. EMBO J. *23*, 2830–2840.

Boulon, S., Westman, B.J., Hutten, S., Boisvert, F.-M., and Lamond, A.I. (2010). The Nucleolus under Stress. Mol. Cell *40*, 216–227.

Bradsher, J.N., Jackson, K.W., Conaway, R.C., and Conaway, J.W. (1993). RNA polymerase II transcription factor SIII. I. Identification, purification, and properties. J. Biol. Chem. *268*, 25587–25593.

Bravo, R., Parra, V., Gatica, D., Rodriguez, A.E., Torrealba, N., Paredes, F., Wang, Z.V., Zorzano, A., Hill, J.A., Jaimovich, E., et al. (2013). Endoplasmic Reticulum and the Unfolded Protein Response: Dynamics and Metabolic Integration. Int. Rev. Cell Mol. Biol. *301*, 215–290.

Brehme, K.S. (1939). A Study of the Effect on Development of "Minute" Mutations in Drosophila Melanogaster. Genetics *24*, 131–161.

Breitschopf, K., and Gross, H.J. (1994). The exchange of the discriminator base A73 for G is alone sufficient to convert human tRNA(Leu) into a serine-acceptor in vitro. EMBO J. *13*, 3166.

Brenner, C., Deplus, R., Didelot, C., Loriot, A., Viré, E., De Smet, C., Gutierrez, A., Danovi, D., Bernard, D., Boon, T., et al. (2005). Myc represses transcription through recruitment of DNA methyltransferase corepressor. EMBO J. *24*, 336–346.

Briones, E., Briones, C., Remacha, M., and Ballesta, J.P. (1998). The GTPase center protein L12 is required for correct ribosomal stalk assembly but not for Saccharomyces cerevisiae viability. J. Biol. Chem. *273*, 31956–31961.

Brogna, S., Sato, T.-A., and Rosbash, M. (2002). Ribosome Components Are Associated with Sites of Transcription. Mol. Cell *10*, 93–104.

Brombin, A., Joly, J.-S., and Jamen, F. (2015). New tricks for an old dog: ribosome biogenesis contributes to stem cell homeostasis. Curr. Opin. Genet. Dev. *34*, 61–70.

Bursać, S., Brdovčak, M.C., Pfannkuchen, M., Orsolić, I., Golomb, L., Zhu, Y., Katz, C., Daftuar, L., Grabušić, K., Vukelić, I., et al. (2012). Mutual protection of ribosomal proteins L5 and L11 from degradation is essential for p53 activation upon ribosomal biogenesis stress. Proc. Natl. Acad. Sci. U. S. A. *109*, 20467–20472.

Bussiere, C., Hashem, Y., Arora, S., Frank, J., and Johnson, A.W. (2012). Integrity of the P-site is probed during maturation of the 60S ribosomal subunit. J. Cell Biol. *197*, 747–759.

Cai, X., Gao, L., Teng, L., Ge, J., Oo, Z.M., Kumar, A.R., Gilliland, D.G., Mason, P.J., Tan, K., and Speck, N.A. (2015). Runx1 Deficiency Decreases Ribosome Biogenesis and Confers Stress Resistance to Hematopoietic Stem and Progenitor Cells. Cell Stem Cell *17*, 165–177.

Callebaut, I., Labesse, G., Durand, P., Poupon, A., Canard, L., Chomilier, J., Henrissat, B., and Mornon, J.P. (1997). Deciphering protein sequence information through hydrophobic cluster analysis (HCA): current status and perspectives. Cell. Mol. Life Sci. CMLS *53*, 621–645.

Calvo, S.E., Pagliarini, D.J., and Mootha, V.K. (2009). Upstream open reading frames cause widespread reduction of protein expression and are polymorphic among humans. Proc. Natl. Acad. Sci. U. S. A. *106*, 7507.

Carroll, A.J., Heazlewood, J.L., Ito, J., and Millar, A.H. (2008). Analysis of the Arabidopsis Cytosolic Ribosome Proteome Provides Detailed Insights into Its Components and Their Post-translational Modification. Mol. Cell. Proteomics *7*, 347–369.

Carron, C., Balor, S., Delavoie, F., Plisson-Chastang, C., Faubladier, M., Gleizes, P.-E., and O'Donohue, M.-F. (2012). Post-mitotic dynamics of pre-nucleolar bodies is driven by pre-rRNA processing. J. Cell Sci. *125*, 4532–4542.

Castello, A., Fischer, B., Eichelbaum, K., Horos, R., Beckmann, B.M., Strein, C., Davey, N.E., Humphreys, D.T., Preiss, T., Steinmetz, L.M., et al. (2012). Insights into RNA biology from an atlas of mammalian mRNA-binding proteins. Cell *149*, 1393–1406.

Castle, J.C., Armour, C.D., Löwer, M., Haynor, D., Biery, M., Bouzek, H., Chen, R., Jackson, S., Johnson, J.M., Rohl, C.A., et al. (2010). Digital genome-wide ncRNA expression, including SnoRNAs, across 11 human tissues using polyA-neutral amplification. PloS One *5*, e11779.

Cavaillé, J., Buiting, K., Kiefmann, M., Lalande, M., Brannan, C.I., Horsthemke, B., Bachellerie, J.P., Brosius, J., and Hüttenhofer, A. (2000). Identification of brain-specific and imprinted small nucleolar RNA genes exhibiting an unusual genomic organization. Proc. Natl. Acad. Sci. U. S. A. *97*, 14311–14316.

Cebollero, E., Reggiori, F., and Kraft, C. (2012). Reticulophagy and Ribophagy: Regulated Degradation of Protein Production Factories. Int. J. Cell Biol. *2012*.

Challagundla, K.B., Sun, X.-X., Zhang, X., DeVine, T., Zhang, Q., Sears, R.C., and Dai, M.-S. (2011). Ribosomal Protein L11 Recruits miR-24/miRISC To Repress c-Myc Expression in Response to Ribosomal Stress □. Mol. Cell. Biol. *31*, 4007–4021.

Chang, F.N., Navickas, I.J., Au, C., and Budzilowicz, C. (1978). Identification of the methylated ribosomal proteins in HeLa cells and the fluctuation of methylation during the cell cycle. Biochim. Biophys. Acta *518*, 89–94.

Chen, D., and Huang, S. (2001). Nucleolar Components Involved in Ribosome Biogenesis Cycle between the Nucleolus and Nucleoplasm in Interphase Cells. J. Cell Biol. *153*, 169–176.

Chen, C., Stevens, B., Kaur, J., Smilansky, Z., Cooperman, B.S., and Goldman, Y.E. (2011). Allosteric vs. spontaneous exit-site (E-site) tRNA dissociation early in protein synthesis. Proc. Natl. Acad. Sci. U. S. A. *108*, 16980.

Chen, T., Muratore, T.L., Schaner-Tooley, C.E., Shabanowitz, J., Hunt, D.F., and Macara, I.G. (2007). N-terminal α-methylation of RCC1 is necessary for stable chromatin association and normal mitosis. Nat. Cell Biol. *9*, 596–603.

Cherkasov, V., Grousl, T., Theer, P., Vainshtein, Y., Glässer, C., Mongis, C., Kramer, G., Stoecklin, G., Knop, M., Mogk, A., et al. (2015). Systemic control of protein synthesis through sequestration of translation and ribosome biogenesis factors during severe heat stress. FEBS Lett. *589*, 3654–3664.

Chern, M.-K., Chang, K.-N., Liu, L.-F., Tam, T.-C.S., Liu, Y.-C., Liang, Y.-L., and Tam, M.F. (2002). Yeast ribosomal protein L12 is a substrate of protein-arginine methyltransferase 2. J. Biol. Chem. *277*, 15345–15353.

Cheung, M., Sharma, A., Madhunapantula, S.V., and Robertson, G.P. (2008). Akt3 and Mutant V600EB-Raf Cooperate to Promote Early Melanoma Development. Cancer Res. *68*, 3429–3439.

Chi, Y., Welcker, M., Hizli, A.A., Posakony, J.J., Aebersold, R., and Clurman, B.E. (2008). Identification of CDK2 substrates in human cell lysates. Genome Biol. *9*, R149.

Chu, D., Barnes, D.J., and von der Haar, T. (2011). The role of tRNA and ribosome competition in coupling the expression of different mRNAs in Saccharomyces cerevisiae. Nucleic Acids Res. *39*, 6705–6714.

Chung, S., Yao, H., Caito, S., Hwang, J., Arunachalam, G., and Rahman, I. (2010). Regulation of SIRT1 in cellular functions: role of polyphenols. Arch. Biochem. Biophys. *501*, 79–90.

Clarke, S.G. (2013). Protein methylation at the surface and buried deep: thinking outside the histone box. Trends Biochem. Sci. *38*, 243–252.

Clavería, C., Giovinazzo, G., Sierra, R., and Torres, M. (2013). Myc-driven endogenous cell competition in the early mammalian embryo. Nature *500*, 39–44.

Clemens, K.R., Liao, X., Wolf, V., Wright, P.E., and Gottesfeld, J.M. (1992). Definition of the binding sites of individual zinc fingers in the transcription factor IIIA-5S RNA gene complex. Proc. Natl. Acad. Sci. U. S. A. *89*, 10822–10826.

Coléno-Costes, A. (2012). Rôle de l'ETP Corto et de la protéine ribosomique RPL12 dans la régulation transcriptionnelle chez Drosophila melanogaster. phdthesis. Université Pierre et Marie Curie - Paris VI.

Coléno-Costes, A., Jang, S.M., de Vanssay, A., Rougeot, J., Bouceba, T., Randsholt, N.B., Gibert, J.-M., Le Crom, S., Mouchel-Vielh, E., Bloyer, S., et al. (2012). New partners in regulation of gene expression: the enhancer of Trithorax and Polycomb Corto interacts with methylated ribosomal protein l12 via its chromodomain. PLoS Genet. *8*, e1003006.

Cook, R.K., Christensen, S.J., Deal, J.A., Coburn, R.A., Deal, M.E., Gresens, J.M., Kaufman, T.C., and Cook, K.R. (2012). The generation of chromosomal deletions to provide extensive coverage and subdivision of the Drosophila melanogaster genome. Genome Biol. *13*, R21.

Cooper, S.J. (2008). From Claude Bernard to Walter Cannon. Emergence of the concept of homeostasis. Appetite *51*, 419–427.

Corsi, A.K., and Schekman, R. (1996). Mechanism of polypeptide translocation into the endoplasmic reticulum. J. Biol. Chem. *271*, 30299–30302.

Covington, J.D., and Bajpeyi, S. (2016). The sirtuins: Markers of metabolic health. Mol. Nutr. Food Res. *60*, 79–91.

Cozzarelli, N.R., Gerrard, S.P., Schlissel, M., Brown, D.D., and Bogenhagen, D.F. (1983). Purified RNA polymerase III accurately and efficiently terminates transcription of 5S RNA genes. Cell *34*, 829–835.

de la Cruz, J., Karbstein, K., and Woolford, J.L. (2015). Functions of ribosomal proteins in assembly of eukaryotic ribosomes in vivo. Annu. Rev. Biochem. *84*, 93–129.

Cuccurese, M., Russo, G., Russo, A., and Pietropaolo, C. (2005). Alternative splicing and nonsense-mediated mRNA decay regulate mammalian ribosomal gene expression. Nucleic Acids Res. *33*, 5965.

Dabeva, M.D., and Warner, J.R. (1993). Ribosomal protein L32 of Saccharomyces cerevisiae regulates both splicing and translation of its own transcript. J. Biol. Chem. *268*, 19669–19674.

Dahlberg, J., and Lund, E. (2012). Nuclear translation or nuclear peptidyl transferase? Nucl. Austin Tex *3*, 320–321.

DAHLBERG, J.E., LUND, E., and GOODWIN, E.B. (2003). Nuclear translation: What is the evidence? RNA *9*, 1–8.

Dai, M.-S., Arnold, H., Sun, X.-X., Sears, R., and Lu, H. (2007). Inhibition of c-Myc activity by ribosomal protein L11. EMBO J. *26*, 3332.

Danilova, N., and Gazda, H.T. (2015). Ribosomopathies: how a common root can cause a tree of pathologies. Dis. Model. Mech. *8*, 1013–1026.

David, A., Dolan, B.P., Hickman, H.D., Knowlton, J.J., Clavarino, G., Pierre, P., Bennink, J.R., and Yewdell, J.W. (2012). Nuclear translation visualized by ribosome-bound nascent chain puromycylation. J. Cell Biol. *197*, 45–57.

Davuluri, R.V., Suzuki, Y., Sugano, S., and Zhang, M.Q. (2000). CART Classification of Human 5′ UTR Sequences. Genome Res. *10*, 1807.

De, S., and Brogna, S. (2010). Are ribosomal proteins present at transcription sites on or off ribosomal subunits? Biochem. Soc. Trans. *38*, 1543–1547.

De, S., Varsally, W., Falciani, F., and Brogna, S. (2011). Ribosomal proteins' association with transcription sites peaks at tRNA genes in Schizosaccharomyces pombe. RNA *17*, 1713–1726.

Debat, V., Bloyer, S., Faradji, F., Gidaszewski, N., Navarro, N., Orozco-Terwengel, P., Ribeiro, V., Schlötterer, C., Deutsch, J.S., and Peronnet, F. (2011). Developmental stability: a major role for cyclin G in drosophila melanogaster. PLoS Genet. *7*, e1002314.

Decatur, W.A., and Fournier, M.J. (2002). rRNA modifications and ribosome function. Trends Biochem. Sci. *27*, 344–351.

DeLabre, M.L., Kessl, J., Karamanou, S., and Trumpower, B.L. (2002). RPL29 codes for a non-essential protein of the 60S ribosomal subunit in Saccharomyces cerevisiae and exhibits synthetic lethality with mutations in genes for proteins required for subunit coupling. Biochim. Biophys. Acta *1574*, 255–261.

Denissov, S., Lessard, F., Mayer, C., Stefanovsky, V., Driel, M. van, Grummt, I., Moss, T., and Stunnenberg, H.G. (2011). A model for the topology of active ribosomal RNA genes. EMBO Rep. *12*, 231.

Dever, T.E., and Green, R. (2012). The Elongation, Termination, and Recycling Phases of Translation in Eukaryotes. Cold Spring Harb. Perspect. Biol. *4*.

DeYoung, M.P., Horak, P., Sofer, A., Sgroi, D., and Ellisen, L.W. (2008). Hypoxia regulates TSC1/2-mTOR signaling and tumor suppression through REDD1-mediated 14-3-3 shuttling. Genes Dev. *22*, 239–251.

Dez, C., Houseley, J., and Tollervey, D. (2006). Surveillance of nuclear-restricted pre-ribosomes within a subnucleolar region of Saccharomyces cerevisiae. EMBO J. *25*, 1534.

Dharia, A.P., Obla, A., Gajdosik, M.D., Simon, A., and Nelson, C.E. (2014). Tempo and mode of gene duplication in mammalian ribosomal protein evolution. PloS One *9*, e111721.

Diaconu, M., Kothe, U., Schlünzen, F., Fischer, N., Harms, J.M., Tonevitsky, A.G., Stark, H., Rodnina, M.V., and Wahl, M.C. (2005). Structural Basis for the Function of the Ribosomal L7/12 Stalk in Factor Binding and GTPase Activation. Cell *121*, 991–1004.

Dieci, G., Preti, M., and Montanini, B. (2009). Eukaryotic snoRNAs: A paradigm for gene expression flexibility. Genomics *94*, 83–88.

Dognin, M.J., and Wittmann-Liebold, B. (1977). The primary structure of L11, the most heavily methylated protein from Escherichia coli ribosomes. FEBS Lett. *84*, 342–346.

Donati, G., Bertoni, S., Brighenti, E., Vici, M., Treré, D., Volarevic, S., Montanaro, L., and Derenzini, M. (2011). The balance between rRNA and ribosomal protein synthesis up- and downregulates the tumour suppressor p53 in mammalian cells. Oncogene *30*, 3274–3288.

Douet, J., and Tourmente, S. (2007). Transcription of the 5S rRNA heterochromatic genes is epigenetically controlled in Arabidopsis thaliana and Xenopus laevis. Heredity *99*, 5–13.

Drygin, D., Rice, W.G., and Grummt, I. (2010). The RNA Polymerase I Transcription Machinery: An Emerging Target for the Treatment of Cancer. Annu. Rev. Pharmacol. Toxicol. *50*, 131–156.

Dubey, R.N., and Gartenberg, M.R. (2007). A tDNA establishes cohesion of a neighboring silent chromatin domain. Genes Dev. *21*, 2150–2160.

Dupont, C. (2015). Cycline G et le maintien de l'homéostasie des tissus au cours du développement chez drosophila melanogaster (Paris 6).

Dupont, C.A., Dardalhon-Cuménal, D., Kyba, M., Brock, H.W., Randsholt, N.B., and Peronnet, F. (2015). Drosophila Cyclin G and epigenetic maintenance of gene expression during development. Epigenetics Chromatin *8*, 18.

DuRose, J.B., Scheuner, D., Kaufman, R.J., Rothblum, L.I., and Niwa, M. (2009). Phosphorylation of eukaryotic translation initiation factor 2alpha coordinates rRNA transcription and translation inhibition during endoplasmic reticulum stress. Mol. Cell. Biol. *29*, 4295–4307.

Eberhardy, S.R., and Farnham, P.J. (2001). c-Myc mediates activation of the cad promoter via a post-RNA polymerase II recruitment mechanism. J. Biol. Chem. *276*, 48562–48571.

Edfors, F., Danielsson, F., Hallström, B.M., Käll, L., Lundberg, E., Pontén, F., Forsström, B., and Uhlén, M. (2016). Gene-specific correlation of RNA and protein levels in human cells and tissues. Mol. Syst. Biol. *12*, 883.

Eickbush, T.H., and Eickbush, D.G. (2007). Finely Orchestrated Movements: Evolution of the Ribosomal RNA Genes. Genetics *175*, 477–485.

Eilers, M., and Eisenman, R.N. (2008). Myc's broad reach. Genes Dev. *22*, 2755–2766.

Eisenberg, E., and Levanon, E.Y. (2013). Human housekeeping genes, revisited. Trends Genet. *29*, 569–574.

Elkon, K., Skelly, S., Parnassa, A., Moller, W., Danho, W., Weissbach, H., and Brot, N. (1986). Identification and chemical synthesis of a ribosomal protein antigenic determinant in systemic lupus erythematosus. Proc. Natl. Acad. Sci. U. S. A. *83*, 7419.

Emmott, E., and Hiscox, J.A. (2009). Nucleolar targeting: the hub of the matter. EMBO Rep. *10*, 231–238.

Esguerra, J., Warringer, J., and Blomberg, A. (2008). Functional importance of individual rRNA 2'-O-ribose methylations revealed by high-resolution phenotyping. RNA N. Y. N *14*, 649–656.

Essers, P. (2013). In profile: models of ribosome biogenesis defects and regulation of protein synthesis.

Fairley, J.A., Scott, P.H., and White, R.J. (2003). TFIIIB is phosphorylated, disrupted and selectively released from tRNA promoters during mitosis in vivo. EMBO J. *22*, 5841–5850.

Faux, N.G., Bottomley, S.P., Lesk, A.M., Irving, J.A., Morrison, J.R., de la Banda, M.G., and Whisstock, J.C. (2005). Functional insights from the distribution and role of homopeptide repeat-containing proteins. Genome Res. *15*, 537–551.

Fermi, B., Bosio, M.C., and Dieci, G. (2016). Promoter architecture and transcriptional regulation of Abf1-dependent ribosomal protein genes in Saccharomyces cerevisiae. Nucleic Acids Res. *44*, 6113–6126.

Fernandez, P.C., Frank, S.R., Wang, L., Schroeder, M., Liu, S., Greene, J., Cocito, A., and Amati, B. (2003). Genomic targets of the human c-Myc protein. Genes Dev. *17*, 1115–1129.

Ferreira-Cerca, S., Pöll, G., Gleizes, P.-E., Tschochner, H., and Milkereit, P. (2005). Roles of eukaryotic ribosomal proteins in maturation and transport of pre-18S rRNA and ribosome function. Mol. Cell *20*, 263–275.

Ferreira-Cerca, S., Pöll, G., Kühn, H., Neueder, A., Jakob, S., Tschochner, H., and Milkereit, P. (2007). Analysis of the In Vivo Assembly Pathway of Eukaryotic 40S Ribosomal Proteins. Mol. Cell *28*, 446–457.

Fichelson, P., Moch, C., Ivanovitch, K., Martin, C., Sidor, C.M., Lepesant, J.-A., Bellaiche, Y., and Huynh, J.-R. (2009). Live-imaging of single stem cells within their niche reveals that a U3snoRNP component segregates asymmetrically and is required for self-renewal in Drosophila. Nat. Cell Biol. *11*, 685–693.

Filbin, M.E., and Kieft, J.S. (2009). Towards a structural understanding of IRES RNA function. Curr. Opin. Struct. Biol. *19*, 267.

Filipowicz, W., Pelczar, P., Pogacic, V., and Dragon, F. (1999). Structure and biogenesis of small nucleolar RNAs acting as guides for ribosomal RNA modification. Acta Biochim. Pol. *46*, 377–389.

Fischer, P., La Rosa, M.K., Schulz, A., Preiss, A., and Nagel, A.C. (2015). Cyclin G Functions as a Positive Regulator of Growth and Metabolism in Drosophila. PLoS Genet. *11*, e1005440.

Fischer, P., Preiss, A., and Nagel, A.C. (2016). A triangular connection between Cyclin G, PP2A and Akt1 in the regulation of growth and metabolism in Drosophila. Fly (Austin) *10*, 11–18.

Francisco-Velilla, R., Remacha, M., and Ballesta, J.P.G. (2013). Carboxy terminal modifications of the P0 protein reveal alternative mechanisms of nuclear ribosomal stalk assembly. Nucleic Acids Res. *41*, 8628.

French, S.L., Santangelo, T.J., Beyer, A.L., and Reeve, J.N. (2007). Transcription and Translation are Coupled in Archaea. Mol. Biol. Evol. *24*, 893–895.

Friedrich, J.K., Panov, K.I., Cabart, P., Russell, J., and Zomerdijk, J.C.B.M. (2005). TBP-TAF complex SL1 directs RNA polymerase I pre-initiation complex formation and stabilizes upstream binding factor at the rDNA promoter. J. Biol. Chem. *280*, 29551–29558.

Friend, K., Campbell, Z.T., Cooke, A., Kroll-Conner, P., Wickens, M.P., and Kimble, J. (2012). A conserved PUF/Ago/eEF1A complex attenuates translation elongation. Nat. Struct. Mol. Biol. *19*, 176–183.

Fuchs, M., Gerber, J., Drapkin, R., Sif, S., Ikura, T., Ogryzko, V., Lane, W.S., Nakatani, Y., and Livingston, D.M. (2001). The p400 complex is an essential E1A transformation target. Cell *106*, 297–307.

Fumagalli, S., Ivanenkov, V.V., Teng, T., and Thomas, G. (2012). Suprainduction of p53 by disruption of 40S and 60S ribosome biogenesis leads to the activation of a novel G2/M checkpoint. Genes Dev. *26*, 1028–1040.

García-Gómez, J.J., Fernández-Pevida, A., Lebaron, S., Rosado, I.V., Tollervey, D., Kressler, D., and de la Cruz, J. (2014). Final pre-40S maturation depends on the functional integrity of the 60S subunit ribosomal protein L3. PLoS Genet. *10*, e1004205.

Gautier, T., Robert-Nicoud, M., Guilly, M.N., and Hernandez-Verdun, D. (1992). Relocation of nucleolar proteins around chromosomes at mitosis. A study by confocal laser scanning microscopy. J. Cell Sci. *102 (Pt 4)*, 729–737.

Gautier, T., Fomproix, N., Masson, C., Azum-Gélade, M.C., Gas, N., and Hernandez-Verdun, D. (1994). Fate of specific nucleolar perichromosomal proteins during mitosis: cellular distribution and association with U3 snoRNA. Biol. Cell *82*, 81–93.

Gébrane-Younès, J., Fomproix, N., and Hernandez-Verdun, D. (1997). When rDNA transcription is arrested during mitosis, UBF is still associated with non-condensed rDNA. J. Cell Sci. *110 (Pt 19)*, 2429–2440.

Geiduschek, E.P., and Tocchini-Valentini, G.P. (1988). Transcription by RNA polymerase III. Annu. Rev. Biochem. *57*, 873–914.

George, R., Walsh, P., Beddoe, T., and Lithgow, T. (2002). The nascent polypeptide-associated complex (NAC) promotes interaction of ribosomes with the mitochondrial surface in vivo. FEBS Lett. *516*, 213–216.

Gerbasi, V.R., Weaver, C.M., Hill, S., Friedman, D.B., and Link, A.J. (2004). Yeast Asc1p and mammalian RACK1 are functionally orthologous core 40S ribosomal proteins that repress gene expression. Mol. Cell. Biol. *24*, 8276–8287.

Gerber, A.P., and Keller, W. (1999). An adenosine deaminase that generates inosine at the wobble position of tRNAs. Science *286*, 1146–1149.

Gersappe, A., Burger, L., and Pintel, D.J. (1999). A premature termination codon in either exon of minute virus of mice P4 promoter-generated pre-mRNA can inhibit nuclear splicing of the intervening intron in an open reading frame-dependent manner. J. Biol. Chem. *274*, 22452–22458.

Ghalei, H., Schaub, F.X., Doherty, J.R., Noguchi, Y., Roush, W.R., Cleveland, J.L., Stroupe, M.E., and Karbstein, K. (2015). Hrr25/CK1δ-directed release of Ltv1 from pre-40S ribosomes is necessary for ribosome assembly and cell growth. J. Cell Biol. *208*, 745–759.

Goberdhan, D.C.I., Wilson, C., and Harris, A.L. (2016). Amino Acid Sensing by mTORC1: Intracellular Transporters Mark the Spot. Cell Metab. *23*, 580–589.

Gomez-Roman, N., Grandori, C., Eisenman, R.N., and White, R.J. (2003). Direct activation of RNA polymerase III transcription by c-Myc. Nature *421*, 290–294.

Goodfellow, S.J., and Zomerdijk, J.C.B.M. (2012). Basic Mechanisms in RNA Polymerase I Transcription of the Ribosomal RNA Genes. Subcell. Biochem. *61*.

Görlach, A., Bertram, K., Hudecova, S., and Krizanova, O. (2015). Calcium and ROS: A mutual interplay. Redox Biol. *6*, 260–271.

Grandori, C., Gomez-Roman, N., Felton-Edkins, Z.A., Ngouenet, C., Galloway, D.A., Eisenman, R.N., and White, R.J. (2005). c-Myc binds to human ribosomal DNA and stimulates transcription of rRNA genes by RNA polymerase I. Nat. Cell Biol. *7*, 311–318.

Gratz, S.J., Cummings, A.M., Nguyen, J.N., Hamm, D.C., Donohue, L.K., Harrison, M.M., Wildonger, J., and O'Connor-Giles, K.M. (2013). Genome engineering of Drosophila with the CRISPR RNA-guided Cas9 nuclease. Genetics *194*, 1029–1035.

Gratz, S.J., Ukken, F.P., Rubinstein, C.D., Thiede, G., Donohue, L.K., Cummings, A.M., and O'Connor-Giles, K.M. (2014). Highly specific and efficient CRISPR/Cas9-catalyzed homology-directed repair in Drosophila. Genetics *196*, 961–971.

Gray, N.K., and Hentze, M.W. (1994). Regulation of protein synthesis by mRNA structure. Mol. Biol. Rep. *19*, 195–200.

Grummt, I. (2003). Life on a planet of its own: regulation of RNA polymerase I transcription in the nucleolus. Genes Dev. *17*, 1691–1702.

Grummt, I. (2010). Wisely chosen paths--regulation of rRNA synthesis: delivered on 30 June 2010 at the 35th FEBS Congress in Gothenburg, Sweden. FEBS J. *277*, 4626–4639.

Gu, S., Jin, L., Zhang, F., Sarnow, P., and Kay, M.A. (2009). Biological basis for restriction of microRNA targets to the 3' untranslated region in mammalian mRNAs. Nat. Struct. Mol. Biol. *16*, 144–150.

Guetg, C., Lienemann, P., Sirri, V., Grummt, I., Hernandez-Verdun, D., Hottiger, M.O., Fussenegger, M., and Santoro, R. (2010). The NoRC complex mediates the heterochromatin formation and stability of silent rRNA genes and centromeric repeats. EMBO J. *29*, 2135–2146.

Gunasekaran, K., Tsai, C.-J., and Nussinov, R. (2004). Analysis of ordered and disordered protein complexes reveals structural features discriminating between stable and unstable monomers. J. Mol. Biol. *341*, 1327–1341.

Haeusler, R.A., and Engelke, D.R. (2006). Spatial organization of transcription by RNA polymerase III. Nucleic Acids Res. *34*, 4826–4836.

Hancock, J.M., and Simon, M. (2005). Simple sequence repeats in proteins and their significance for network evolution. Gene *345*, 113–118.

Hannan, K.M., Brandenburger, Y., Jenkins, A., Sharkey, K., Cavanaugh, A., Rothblum, L., Moss, T., Poortinga, G., McArthur, G.A., Pearson, R.B., et al. (2003). mTOR-dependent regulation of ribosomal gene transcription requires S6K1 and is mediated by phosphorylation of the carboxy-terminal activation domain of the nucleolar transcription factor UBF. Mol. Cell. Biol. *23*, 8862–8877.

Hansen, K.D., Lareau, L.F., Blanchette, M., Green, R.E., Meng, Q., Rehwinkel, J., Gallusser, F.L., Izaurralde, E., Rio, D.C., Dudoit, S., et al. (2009). Genome-Wide Identification of Alternative Splice Forms Down-Regulated by Nonsense-Mediated mRNA Decay in Drosophila. PLoS Genet. *5*.

Harding, H.P., Zhang, Y., Bertolotti, A., Zeng, H., and Ron, D. (2000). Perk is essential for translational regulation and cell survival during the unfolded protein response. Mol. Cell *5*, 897–904.

Haupt, Y., Maya, R., Kazaz, A., and Oren, M. (1997). Mdm2 promotes the rapid degradation of p53. Nature *387*, 296–299.

Heix, J., Vente, A., Voit, R., Budde, A., Michaelidis, T.M., and Grummt, I. (1998). Mitotic silencing of human rRNA synthesis: inactivation of the promoter selectivity factor SL1 by cdc2/cyclin B-mediated phosphorylation. EMBO J. *17*, 7373–7381.

Helm, M. (2006). Post-transcriptional nucleotide modification and alternative folding of RNA. Nucleic Acids Res. *34*, 721–733.

Hemmings-Mieszczak, M., Hohn, T., and Preiss, T. (2000). Termination and Peptide Release at the Upstream Open Reading Frame Are Required for Downstream Translation on Synthetic Shunt-Competent mRNA Leaders. Mol. Cell. Biol. *20*, 6212–6223.

Henras, A.K., Plisson-Chastang, C., O'Donohue, M.-F., Chakraborty, A., and Gleizes, P.-E. (2015). An overview of pre-ribosomal RNA processing in eukaryotes. Wiley Interdiscip. Rev. RNA *6*, 225–242.

Hentze, M.W., and Kühn, L.C. (1996). Molecular control of vertebrate iron metabolism: mRNA-based regulatory circuits operated by iron, nitric oxide, and oxidative stress. Proc. Natl. Acad. Sci. U. S. A. *93*, 8175.

Hernandez-Verdun, D. (2006). The nucleolus: a model for the organization of nuclear functions. Histochem. Cell Biol. *126*, 135.

Hernandez-Verdun, D., Roussel, P., Thiry, M., Sirri, V., and Lafontaine, D.L.J. (2010). The nucleolus: structure/function relationship in RNA metabolism. Wiley Interdiscip. Rev. RNA *1*, 415–431.

Higgins, R., Gendron, J.M., Rising, L., Mak, R., Webb, K., Kaiser, S.E., Zuzow, N., Riviere, P., Yang, B., Fenech, E., et al. (2015). The unfolded protein response triggers site-specific regulatory ubiquitylation of 40S ribosomal proteins. Mol. Cell *59*, 35–49.

Hinnebusch, A.G. (2017). Structural Insights into the Mechanism of Scanning and Start Codon Recognition in Eukaryotic Translation Initiation. Trends Biochem. Sci.

Hoof, A. van, Lennertz, P., and Parker, R. (2000). Three conserved members of the RNase D family have unique and overlapping functions in the processing of 5S, 5.8S, U4, U5, RNase MRP and RNase P RNAs in yeast. EMBO J. *19*, 1357.

Hoppe, S., Bierhoff, H., Cado, I., Weber, A., Tiebe, M., Grummt, I., and Voit, R. (2009). AMP-activated protein kinase adapts rRNA synthesis to cellular energy supply. Proc. Natl. Acad. Sci. U. S. A. *106*, 17781–17786.

Hopper, A.K. (2013). Transfer RNA Post-Transcriptional Processing, Turnover, and Subcellular Dynamics in the Yeast *Saccharomyces cerevisiae*. Genetics *194*, 43–67.

Horos, R., IJspeert, H., Pospisilova, D., Sendtner, R., Andrieu-Soler, C., Taskesen, E., Nieradka, A., Cmejla, R., Sendtner, M., Touw, I.P., et al. (2012). Ribosomal deficiencies in Diamond-Blackfan anemia impair translation of transcripts essential for differentiation of murine and human erythroblasts. Blood *119*, 262–272.

Houseley, J., and Tollervey, D. (2006). Yeast Trf5p is a nuclear poly(A) polymerase. EMBO Rep. *7*, 205–211.

Høyer-Hansen, M., and Jäättelä, M. (2007). Connecting endoplasmic reticulum stress to autophagy by unfolded protein response and calcium. Cell Death Differ. *14*, 1576–1582.

Huang, J., Wu, S., Barrera, J., Matthews, K., and Pan, D. (2005). The Hippo Signaling Pathway Coordinately Regulates Cell Proliferation and Apoptosis by Inactivating Yorkie, the Drosophila Homolog of YAP. Cell *122*, 421–434.

Hughes, M.E., Grant, G.R., Paquin, C., Qian, J., and Nitabach, M.N. (2012). Deep sequencing the circadian and diurnal transcriptome of Drosophila brain. Genome Res. *22*, 1266–1281.

Hussey, G.S., Chaudhury, A., Dawson, A.E., Lindner, D.J., Knudsen, C.R., Wilce, M.C.J., Merrick, W.C., and Howe, P.H. (2011). Identification of an mRNP complex regulating tumorigenesis at the translational elongation step. Mol. Cell *41*, 419–431.

Iben, J.R., and Draper, D.E. (2008). Specific interactions of the L10(L12)4 ribosomal protein complex with mRNA, rRNA, and L11. Biochemistry (Mosc.) *47*, 2721–2731.

Ilin, S., Hoskins, A., Ohlenschläger, O., Jonker, H.R.A., Schwalbe, H., and Wöhnert, J. (2005). Domain Reorientation and Induced Fit upon RNA Binding: Solution Structure and Dynamics of Ribosomal Protein L11 from Thermotoga maritima. ChemBioChem *6*, 1611–1618.

Jackman, J.E., Gott, J.M., and Gray, M.W. (2012). Doing it in reverse: 3′-to-5′ polymerization by the Thg1 superfamily. RNA *18*, 886–899.

Jackson, R.J., Hellen, C.U.T., and Pestova, T.V. (2010). The mechanism of eukaryotic translation initiation and principles of its regulation. Nat. Rev. Mol. Cell Biol. *11*, 113–127.

Jacob, M.D., Audas, T.E., Uniacke, J., Trinkle-Mulcahy, L., and Lee, S. (2013). Environmental cues induce a long noncoding RNA-dependent remodeling of the nucleolus. Mol. Biol. Cell *24*, 2943–2953.

Jäkel, S., Mingot, J.-M., Schwarzmaier, P., Hartmann, E., and Görlich, D. (2002). Importins fulfil a dual function as nuclear import receptors and cytoplasmic chaperones for exposed basic domains. EMBO J. *21*, 377–386.

Jannot, G., Bajan, S., Giguère, N.J., Bouasker, S., Banville, I.H., Piquet, S., Hutvagner, G., and Simard, M.J. (2011). The ribosomal protein RACK1 is required for microRNA function in both C. elegans and humans. EMBO Rep. *12*, 581–586.

Jewell, J.L., Russell, R.C., and Guan, K.-L. (2013). Amino acid signalling upstream of mTOR. Nat. Rev. Mol. Cell Biol. *14*, 133.

Jinek, M., Chylinski, K., Fonfara, I., Hauer, M., Doudna, J.A., and Charpentier, E. (2012). A programmable dual-RNA-guided DNA endonuclease in adaptive bacterial immunity. Science *337*, 816–821.

Jonas, S., and Izaurralde, E. (2015). Towards a molecular understanding of microRNA-mediated gene silencing. Nat. Rev. Genet. *16*, 421–433.

Jordan, P., Mannervik, M., Tora, L., and Carmo-Fonseca, M. (1996). In vivo evidence that TATA-binding protein/SL1 colocalizes with UBF and RNA polymerase I when rRNA synthesis is either active or inactive. J. Cell Biol. *133*, 225–234.

Jorjani, H., Kehr, S., Jedlinski, D.J., Gumienny, R., Hertel, J., Stadler, P.F., Zavolan, M., and Gruber, A.R. (2016). An updated human snoRNAome. Nucleic Acids Res. *44*, 5068–5082.

Kalashnikova, A.A., Winkler, D.D., McBryant, S.J., Henderson, R.K., Herman, J.A., DeLuca, J.G., Luger, K., Prenni, J.E., and Hansen, J.C. (2013). Linker histone H1.0 interacts with an extensive network of proteins found in the nucleolus. Nucleic Acids Res. *41*, 4026–4035.

Kantidakis, T., Ramsbottom, B.A., Birch, J.L., Dowding, S.N., and White, R.J. (2010). mTOR associates with TFIIIC, is found at tRNA and 5S rRNA genes, and targets their repressor Maf1. Proc. Natl. Acad. Sci. U. S. A. *107*, 11823–11828.

Kassavetis, G.A., Braun, B.R., Nguyen, L.H., and Geiduschek, E.P. (1990). S. cerevisiae TFIIIB is the transcription initiation factor proper of RNA polymerase III, while TFIIIA and TFIIIC are assembly factors. Cell *60*, 235–245.

Kavran, J.M., and Steitz, T.A. (2007). Structure of the Base of the L7/L12 Stalk of the Haloarcula marismortui Large Ribosomal Subunit: Analysis of L11 Movements. J. Mol. Biol. *371*, 1047–1059.

Kearse, M.G., Chen, A.S., and Ware, V.C. (2011). Expression of ribosomal protein L22e family members in Drosophila melanogaster: rpL22-like is differentially expressed and alternatively spliced. Nucleic Acids Res. *39*, 2701–2716.

Kellis, M., Birren, B.W., and Lander, E.S. (2004). Proof and evolutionary analysis of ancient genome duplication in the yeast Saccharomyces cerevisiae. Nature *428*, 617–624.

Kenneth, N.S., Ramsbottom, B.A., Gomez-Roman, N., Marshall, L., Cole, P.A., and White, R.J. (2007). TRRAP and GCN5 are used by c-Myc to activate RNA polymerase III transcription. Proc. Natl. Acad. Sci. U. S. A. *104*, 14917–14922.

Kennison, J.A. (1995). The Polycomb and trithorax group proteins of Drosophila: trans-regulators of homeotic gene function. Annu. Rev. Genet. *29*, 289–303.

Kim, I.R.& Y.K. (2017). Translation initiation mediated by nuclear cap-binding protein complex. BMB Rep. *50*, 186–193.

Kim, K., Choi, J., Heo, K., Kim, H., Levens, D., Kohno, K., Johnson, E.M., Brock, H.W., and An, W. (2008). Isolation and Characterization of a Novel H1.2 Complex That Acts as a Repressor of p53-mediated Transcription. J. Biol. Chem. *283*, 9113–9126.

Kim, T.-H., Leslie, P., and Zhang, Y. (2014). Ribosomal proteins as unrevealed caretakers for cellular stress and genomic instability. Oncotarget *5*, 860.

Kim, T.-S., Jang, C.-Y., Kim, H.D., Lee, J.Y., Ahn, B.-Y., and Kim, J. (2006). Interaction of Hsp90 with Ribosomal Proteins Protects from Ubiquitination and Proteasome-dependent Degradation. Mol. Biol. Cell *17*, 824–833.

King, T.H., Liu, B., McCully, R.R., and Fournier, M.J. (2003). Ribosome structure and activity are altered in cells lacking snoRNPs that form pseudouridines in the peptidyl transferase center. Mol. Cell *11*, 425–435.

Klein, C., and Struhl, K. (1994). Protein kinase A mediates growth-regulated expression of yeast ribosomal protein genes by modulating RAP1 transcriptional activity. Mol. Cell. Biol. *14*, 1920–1928.

Klein, J., and Grummt, I. (1999). Cell cycle-dependent regulation of RNA polymerase I transcription: The nucleolar transcription factor UBF is inactive in mitosis and early G1. Proc. Natl. Acad. Sci. U. S. A. *96*, 6096.

Klinge, S., Voigts-Hoffmann, F., Leibundgut, M., Arpagaus, S., and Ban, N. (2011). Crystal Structure of the Eukaryotic 60S Ribosomal Subunit in Complex with Initiation Factor 6. Science *334*, 941–948.

Knight, J.R.P., Bastide, A., Roobol, A., Roobol, J., Jackson, T.J., Utami, W., Barrett, D.A., Smales, C.M., and Willis, A.E. (2015). Eukaryotic elongation factor 2 kinase regulates the cold stress response by slowing translation elongation. Biochem. J. *465*, 227–238.

Knight, J.R.P., Bastide, A., Peretti, D., Roobol, A., Roobol, J., Mallucci, G.R., Smales, C.M., and Willis, A.E. (2016). Cooling-induced SUMOylation of EXOSC10 down-regulates ribosome biogenesis. RNA N. Y. N *22*, 623–635.

Koberna, K., Malínský, J., Pliss, A., Masata, M., Vecerova, J., Fialová, M., Bednár, J., and Raska, I. (2002). Ribosomal genes in focus: new transcripts label the dense fibrillar components and form clusters indicative of “Christmas trees” in situ. J. Cell Biol. *157*, 743–748.

Koch, U., Lehal, R., and Radtke, F. (2013). Stem cells living with a Notch. Development *140*, 689–704.

Kodjabachian, L., Delaage, M., Maurel, C., Miassod, R., Jacq, B., and Rosset, R. (1998). Mutations in ccf, a novel Drosophila gene encoding a chromosomal factor, affect progression through mitosis and interact with Pc-G mutations. EMBO J. *17*, 1063–1075.

Koenig, E., and Martin, R. (1996). Cortical plaque-like structures identify ribosome-containing domains in the Mauthner cell axon. J. Neurosci. Off. J. Soc. Neurosci. *16*, 1400–1411.

Komili, S., Farny, N.G., Roth, F.P., and Silver, P.A. (2007). Functional specificity among ribosomal proteins regulates gene expression. Cell *131*, 557–571.

Kondrashov, N., Pusic, A., Stumpf, C.R., Shimizu, K., Hsieh, A.C., Ishijima, J., Shiroishi, T., and Barna, M. (2011). Ribosome mediated specificity in Hox mRNA translation and vertebrate tissue patterning. Cell *145*, 383.

Kos, M., and Tollervey, D. (2010). Yeast pre-rRNA processing and modification occur cotranscriptionally. Mol. Cell *37*, 809–820.

Koussounadis, A., Langdon, S.P., Um, I.H., Harrison, D.J., and Smith, V.A. (2015). Relationship between differentially expressed mRNA and mRNA-protein correlations in a xenograft model system. Sci. Rep. *5*.

Kozak, M. (1986). Point mutations define a sequence flanking the AUG initiator codon that modulates translation by eukaryotic ribosomes. Cell *44*, 283–292.

Kozak, M. (2002). Pushing the limits of the scanning mechanism for initiation of translation. Gene *299*, 1–34.

Kraft, C., Deplazes, A., Sohrmann, M., and Peter, M. (2008). Mature ribosomes are selectively degraded upon starvation by an autophagy pathway requiring the Ubp3p/Bre5p ubiquitin protease. Nat. Cell Biol. *10*, 602–610.

Krasowski, M.D., Reschly, E.J., and Ekins, S. (2008). Intrinsic disorder in nuclear hormone receptors. J. Proteome Res. *7*, 4359–4372.

Kressler, D., Bange, G., Ogawa, Y., Stjepanovic, G., Bradatsch, B., Pratte, D., Amlacher, S., Strauß, D., Yoneda, Y., Katahira, J., et al. (2012). Synchronizing nuclear import of ribosomal proteins with ribosome assembly. Science *338*, 666–671.

Krogh, N., Jansson, M.D., Häfner, S.J., Tehler, D., Birkedal, U., Christensen-Dalsgaard, M., Lund, A.H., and Nielsen, H. (2016). Profiling of 2'-O-Me in human rRNA reveals a subset of fractionally modified positions and provides evidence for ribosome heterogeneity. Nucleic Acids Res. *44*, 7884–7895.

Kruse, J.-P., and Gu, W. (2009). Modes of p53 Regulation. Cell *137*, 609–622.

Kubbutat, M.H., Jones, S.N., and Vousden, K.H. (1997). Regulation of p53 stability by Mdm2. Nature *387*, 299–303.

LaCava, J., Houseley, J., Saveanu, C., Petfalski, E., Thompson, E., Jacquier, A., and Tollervey, D. (2005). RNA degradation by the exosome is promoted by a nuclear polyadenylation complex. Cell *121*, 713–724.

Lafontaine, D.L., Bousquet-Antonelli, C., Henry, Y., Caizergues-Ferrer, M., and Tollervey, D. (1998). The box H + ACA snoRNAs carry Cbf5p, the putative rRNA pseudouridine synthase. Genes Dev. *12*, 527–537.

Lai, K., Amsterdam, A., Farrington, S., Bronson, R.T., Hopkins, N., and Lees, J.A. (2009). Many Ribosomal Protein Mutations Are Associated With Growth Impairment and Tumor Predisposition in Zebrafish. Dev. Dyn. Off. Publ. Am. Assoc. Anat. *238*, 76–85.

Lam, Y.W., and Trinkle-Mulcahy, L. (2015). New insights into nucleolar structure and function. F1000Prime Rep. *7*.

Lam, Y.W., Lamond, A.I., Mann, M., and Andersen, J.S. (2007). Analysis of Nucleolar Protein Dynamics Reveals the Nuclear Degradation of Ribosomal Proteins. Curr. Biol. *17*, 749–760.

Landry, D.M., Hertz, M.I., and Thompson, S.R. (2009). RPS25 is essential for translation initiation by the Dicistroviridae and hepatitis C viral IRESs. Genes Dev. *23*, 2753–2764.

Lechertier, T., Sirri, V., Hernandez-Verdun, D., and Roussel, P. (2007). A B23-interacting sequence as a tool to visualize protein interactions in a cellular context. J. Cell Sci. *120*, 265–275.

Lee, H., McManus, C.J., Cho, D.-Y., Eaton, M., Renda, F., Somma, M.P., Cherbas, L., May, G., Powell, S., Zhang, D., et al. (2014). DNA copy number evolution in Drosophila cell lines. Genome Biol. *15*.

Lee, H.-G., Kahn, T.G., Simcox, A., Schwartz, Y.B., and Pirrotta, V. (2015). Genome-wide activities of Polycomb complexes control pervasive transcription. Genome Res. *25*, 1170.

Lee, S.-W., Berger, S.J., Martinović, S., Paša-Tolić, L., Anderson, G.A., Shen, Y., Zhao, R., and Smith, R.D. (2002). Direct mass spectrometric analysis of intact proteins of the yeast large ribosomal subunit using capillary LC/FTICR. Proc. Natl. Acad. Sci. U. S. A. *99*, 5942–5947.

Liang, X.-H., Liu, Q., and Fournier, M.J. (2009). Loss of rRNA modifications in the decoding center of the ribosome impairs translation and strongly delays pre-rRNA processing. RNA N. Y. N *15*, 1716–1728.

Liao, J.-M., Zhou, X., Gatignol, A., and Lu, H. (2014). Ribosomal Proteins L5 and L11 Cooperatively Inactivate c-Myc via RNA-induced Silencing Complex. Oncogene *33*, 4916–4923.

Lindsley, D.L., and Zimm, G.G. (1992). The Genome of Drosophila Melanogaster.

Lindsley, D.L., Sandler, L., Baker, B.S., Carpenter, A.T., Denell, R.E., Hall, J.C., Jacobs, P.A., Miklos, G.L., Davis, B.K., Gethmann, R.C., et al. (1972). Segmental aneuploidy and the genetic gross structure of the Drosophila genome. Genetics *71*, 157–184.

Ling, J., and Söll, D. (2010). Severe oxidative stress induces protein mistranslation through impairment of an aminoacyl-tRNA synthetase editing site. Proc. Natl. Acad. Sci. U. S. A. *107*, 4028–4033.

Lo, K.-Y., Li, Z., Wang, F., Marcotte, E.M., and Johnson, A.W. (2009). Ribosome stalk assembly requires the dual-specificity phosphatase Yvh1 for the exchange of Mrt4 with P0. J. Cell Biol. *186*, 849.

Lo, K.-Y., Li, Z., Bussiere, C., Bresson, S., Marcotte, E.M., and Johnson, A.W. (2010). Defining the pathway of cytoplasmic maturation of the 60S ribosomal subunit. Mol. Cell *39*, 196–208.

Lopez, A., Higuet, D., Rosset, R., Deutsch, J., and Peronnet, F. (2001). corto genetically interacts with Pc-G and trx-G genes and maintains the anterior boundary of Ultrabithorax expression in Drosophila larvae. Mol. Genet. Genomics *266*, 572–583.

Lupas, A.N., and Alva, V. (2017). Ribosomal proteins as documents of the transition from unstructured (poly)peptides to folded proteins. J. Struct. Biol. *198*, 74–81.

Madalena, C.R.G., Díez, J.L., and Gorab, E. (2012). Chromatin structure of ribosomal RNA genes in dipterans and its relationship to the location of nucleolar organizers. PloS One *7*, e44006.

Mali, P., Esvelt, K.M., and Church, G.M. (2013). Cas9 as a versatile tool for engineering biology. Nat. Methods *10*, 957–963.

Malygin, A.A., Parakhnevitch, N.M., Ivanov, A.V., Eperon, I.C., and Karpova, G.G. (2007). Human ribosomal protein S13 regulates expression of its own gene at the splicing step by a feedback mechanism. Nucleic Acids Res. *35*, 6414.

Mangiarotti, G. (2002). Synthesis of ribosomal proteins in developing Dictyostelium discoideum cells is controlled by the methylation of proteins S24 and S31. Biochem. Cell Biol. Biochim. Biol. Cell. *80*, 261–270.

Maraia, R.J., and Lamichhane, T.N. (2011). 3′ processing of eukaryotic precursor tRNAs. Wiley Interdiscip. Rev. RNA *2*, 362–375.

Marenda, D.R., Zraly, C.B., and Dingwall, A.K. (2004). The Drosophila Brahma (SWI/SNF) chromatin remodeling complex exhibits cell-type specific activation and repression functions. Dev. Biol. *267*, 279–293.

Marion, R.M., Regev, A., Segal, E., Barash, Y., Koller, D., Friedman, N., and O'Shea, E.K. (2004). Sfp1 is a stress- and nutrient-sensitive regulator of ribosomal protein gene expression. Proc. Natl. Acad. Sci. U. S. A. *101*, 14315–14322.

Martin, D.E., Soulard, A., and Hall, M.N. (2004). TOR regulates ribosomal protein gene expression via PKA and the Forkhead transcription factor FHL1. Cell *119*, 969–979.

Marygold, S.J., Coelho, C.M.A., and Leevers, S.J. (2005). Genetic Analysis of RpL38 and RpL5, Two Minute Genes Located in the Centric Heterochromatin of Chromosome 2 of Drosophila melanogaster. Genetics *169*, 683.

Marygold, S.J., Roote, J., Reuter, G., Lambertsson, A., Ashburner, M., Millburn, G.H., Harrison, P.M., Yu, Z., Kenmochi, N., Kaufman, T.C., et al. (2007). The ribosomal protein genes and Minute loci of Drosophila melanogaster. Genome Biol. *8*, R216.

Mathonnet, G., Fabian, M.R., Svitkin, Y.V., Parsyan, A., Huck, L., Murata, T., Biffo, S., Merrick, W.C., Darzynkiewicz, E., Pillai, R.S., et al. (2007). MicroRNA inhibition of translation initiation in vitro by targeting the cap-binding complex eIF4F. Science *317*, 1764–1767.

Mayer, C., Zhao, J., Yuan, X., and Grummt, I. (2004). mTOR-dependent activation of the transcription factor TIF-IA links rRNA synthesis to nutrient availability. Genes Dev. *18*, 423.

Mazumder, B., Sampath, P., Seshadri, V., Maitra, R.K., DiCorleto, P.E., and Fox, P.L. (2003). Regulated Release of L13a from the 60S Ribosomal Subunit as A Mechanism of Transcript-Specific Translational Control. Cell *115*, 187–198.

McMahon, S.B., Wood, M.A., and Cole, M.D. (2000). The essential cofactor TRRAP recruits the histone acetyltransferase hGCN5 to c-Myc. Mol. Cell. Biol. *20*, 556–562.

Meares, G.P., Hughes, K.J., Naatz, A., Papa, F.R., Urano, F., Hansen, P.A., Benveniste, E.N., and Corbett, J.A. (2011). IRE1-Dependent Activation of AMPK in Response to Nitric Oxide □. Mol. Cell. Biol. *31*, 4286–4297.

Mekhail, K., Rivero-Lopez, L., Khacho, M., and Lee, S. (2006). Restriction of rRNA synthesis by VHL maintains energy equilibrium under hypoxia. Cell Cycle Georget. Tex *5*, 2401–2413.

Mélèse, T., and Xue, Z. (1995). The nucleolus: an organelle formed by the act of building a ribosome. Curr. Opin. Cell Biol. *7*, 319–324.

Mellacheruvu, D., Wright, Z., Couzens, A.L., Lambert, J.-P., St-Denis, N., Li, T., Miteva, Y.V., Hauri, S., Sardiu, M.E., Low, T.Y., et al. (2013). The CRAPome: a Contaminant Repository for Affinity Purification Mass Spectrometry Data. Nat. Methods *10*, 730–736.

Mendoza, M.C., Er, E.E., and Blenis, J. (2011). The Ras-ERK and PI3K-mTOR Pathways: Cross-talk and Compensation. Trends Biochem. Sci. *36*, 320–328.

Merret, R., Carpentier, M.-C., Favory, J.-J., Picart, C., Descombin, J., Bousquet-Antonelli, C., Tillard, P., Lejay, L., Deragon, J.-M., and Charng, Y.-Y. (2017). Heat Shock Protein HSP101 Affects the Release of Ribosomal Protein mRNAs for Recovery after Heat Shock. Plant Physiol. *174*, 1216–1225.

Meyuhas, O., and Kahan, T. (2015). The race to decipher the top secrets of TOP mRNAs. Biochim. Biophys. Acta *1849*, 801–811.

Mihaylova, M.M., and Shaw, R.J. (2011). The AMP-activated protein kinase (AMPK) signaling pathway coordinates cell growth, autophagy, & metabolism. Nat. Cell Biol. *13*, 1016–1023.

Mitrovich, Q.M., and Anderson, P. (2000). Unproductively spliced ribosomal protein mRNAs are natural targets of mRNA surveillance in C. elegans. Genes Dev. *14*, 2173–2184.

Moll, U.M., and Petrenko, O. (2003). The MDM2-p53 Interaction. Mol. Cancer Res. *1*, 1001–1008.

Montanaro, L., Calienni, M., Bertoni, S., Rocchi, L., Sansone, P., Storci, G., Santini, D., Ceccarelli, C., Taffurelli, M., Carnicelli, D., et al. (2010). Novel Dyskerin-Mediated Mechanism of p53 Inactivation through Defective mRNA Translation. Cancer Res. *70*, 4767–4777.

Morata, G., and Ripoll, P. (1975). Minutes: mutants of drosophila autonomously affecting cell division rate. Dev. Biol. *42*, 211–221.

Moreno, E., and Basler, K. (2004). dMyc transforms cells into super-competitors. Cell *117*, 117–129.

Moschall, R., Gaik, M., and Medenbach, J. (2017). Promiscuity in post-transcriptional control of gene expression: Drosophila sex-lethal and its regulatory partnerships. FEBS Lett. *591*, 1471–1488.

Moss, T., and Stefanovsky, V.Y. (2002). At the Center of Eukaryotic Life. Cell *109*, 545–548.

Mouchel-Vielh, E., Rougeot, J., Decoville, M., and Peronnet, F. (2011). The MAP kinase ERK and its scaffold protein MP1 interact with the chromatin regulator Corto during Drosophila wing tissue development. BMC Dev. Biol. *11*, 17.

Murayama, A., Ohmori, K., Fujimura, A., Minami, H., Yasuzawa-Tanaka, K., Kuroda, T., Oie, S., Daitoku, H., Okuwaki, M., Nagata, K., et al. (2008). Epigenetic control of rDNA loci in response to intracellular energy status. Cell *133*, 627–639.

Nader, G.A., McLoughlin, T.J., and Esser, K.A. (2005). mTOR function in skeletal muscle hypertrophy: increased ribosomal RNA via cell cycle regulators. Am. J. Physiol. Cell Physiol. *289*, C1457-1465.

Nakhoul, H., Ke, J., Zhou, X., Liao, W., Zeng, S.X., and Lu, H. (2014). Ribosomopathies: mechanisms of disease. Clin. Med. Insights Blood Disord. *7*, 7–16.

Nalabothula, N., Indig, F.E., and Carrier, F. (2010). The Nucleolus Takes Control of Protein Trafficking Under Cellular Stress. Mol. Cell. Pharmacol. *2*, 203–212.

Németh, A., and Längst, G. (2011). Genome organization in and around the nucleolus. Trends Genet. *27*, 149–156.

Ni, J.-Q., Liu, L.-P., Hess, D., Rietdorf, J., and Sun, F.-L. (2006). Drosophila ribosomal proteins are associated with linker histone H1 and suppress gene transcription. Genes Dev. *20*, 1959–1973.

Noma, K., Cam, H.P., Maraia, R.J., and Grewal, S.I.S. (2006). A Role for TFIIIC Transcription Factor Complex in Genome Organization. Cell *125*, 859–872.

Nomura, M., Nogi, Y., and Oakes, M. (2013). Transcription of rDNA in the Yeast Saccharomyces cerevisiae (Landes Bioscience).

Nottrott, S., Simard, M.J., and Richter, J.D. (2006). Human let-7a miRNA blocks protein production on actively translating polyribosomes. Nat. Struct. Mol. Biol. *13*, 1108–1114.

Oakhill, J.S., Steel, R., Chen, Z.-P., Scott, J.W., Ling, N., Tam, S., and Kemp, B.E. (2011). AMPK is a direct adenylate charge-regulated protein kinase. Science *332*, 1433–1435.

Ohmayer, U., Gamalinda, M., Sauert, M., Ossowski, J., Pöll, G., Linnemann, J., Hierlmeier, T., Perez-Fernandez, J., Kumcuoglu, B., Leger-Silvestre, I., et al. (2013). Studies on the Assembly Characteristics of Large Subunit Ribosomal Proteins in S. cerevisae. PLOS ONE *8*, e68412.

Oliver, E.R., Saunders, T.L., Tarlé, S.A., and Glaser, T. (2004). Ribosomal protein L24 defect in Belly spot and tail (Bst), a mouse Minute. Development *131*, 3907–3920.

Ong, S.-E., and Mann, M. (2005). Mass spectrometry-based proteomics turns quantitative. Nat. Chem. Biol. *1*, 252–262.

Orford, K.W., and Scadden, D.T. (2008). Deconstructing stem cell self-renewal: genetic insights into cell-cycle regulation. Nat. Rev. Genet. *9*, 115–128.

Orian, A., van Steensel, B., Delrow, J., Bussemaker, H.J., Li, L., Sawado, T., Williams, E., Loo, L.W.M., Cowley, S.M., Yost, C., et al. (2003). Genomic binding by the Drosophila Myc, Max, Mad/Mnt transcription factor network. Genes Dev. *17*, 1101–1114.

Osheim, Y.N., French, S.L., Keck, K.M., Champion, E.A., Spasov, K., Dragon, F., Baserga, S.J., and Beyer, A.L. (2004). Pre-18S ribosomal RNA is structurally compacted into the SSU processome prior to being cleaved from nascent transcripts in Saccharomyces cerevisiae. Mol. Cell *16*, 943–954.

Ostareck, D.H., Ostareck-Lederer, A., Shatsky, I.N., and Hentze, M.W. (2001). Lipoxygenase mRNA silencing in erythroid differentiation: The 3'UTR regulatory complex controls 60S ribosomal subunit joining. Cell *104*, 281–290.

Ozcan, U., Ozcan, L., Yilmaz, E., Düvel, K., Sahin, M., Manning, B.D., and Hotamisligil, G.S. (2008). Loss of the Tuberous Sclerosis Complex Tumor Suppressors Triggers the Unfolded Protein Response to Regulate Insulin Signaling and Apoptosis. Mol. Cell *29*, 541.

Padeken, J., Mendiburo, M.J., Chlamydas, S., Schwarz, H.-J., Kremmer, E., and Heun, P. (2013). The Nucleoplasmin Homolog NLP Mediates Centromere Clustering and Anchoring to the Nucleolus. Mol. Cell *50*, 236–249.

Pang, C.N.I., Gasteiger, E., and Wilkins, M.R. (2010). Identification of arginine- and lysine-methylation in the proteome of Saccharomyces cerevisiae and its functional implications. BMC Genomics *11*, 92.

Pang, Y.L.J., Poruri, K., and Martinis, S.A. (2014). tRNA synthetase: tRNA Aminoacylation and beyond. Wiley Interdiscip. Rev. RNA *5*, 461–480.

Panov, K.I., Friedrich, J.K., and Zomerdijk, J.C. (2001). A step subsequent to preinitiation complex assembly at the ribosomal RNA gene promoter is rate limiting for human RNA polymerase I-dependent transcription. Mol. Cell. Biol. *21*, 2641–2649.

Panov, K.I., Friedrich, J.K., Russell, J., and Zomerdijk, J.C.B.M. (2006). UBF activates RNA polymerase I transcription by stimulating promoter escape. EMBO J. *25*, 3310–3322.

Panse, V.G., and Johnson, A.W. (2010). Maturation of Eukaryotic Ribosomes: Acquisition of Functionality. Trends Biochem. Sci. *35*, 260.

Parenteau, J., Lavoie, M., Catala, M., Malik-Ghulam, M., Gagnon, J., and Abou Elela, S. (2015). Preservation of Gene Duplication Increases the Regulatory Spectrum of Ribosomal Protein Genes and Enhances Growth under Stress. Cell Rep. *13*, 2516–2526.

Park, M.H., Nishimura, K., Zanelli, C.F., and Valentini, S.R. (2010). Functional significance of eIF5A and its hypusine modification in eukaryotes. Amino Acids *38*, 491–500.

Patursky-Polischuk, I., Stolovich-Rain, M., Hausner-Hanochi, M., Kasir, J., Cybulski, N., Avruch, J., Rüegg, M.A., Hall, M.N., and Meyuhas, O. (2009). The TSC-mTOR pathway mediates translational activation of TOP mRNAs by insulin largely in a raptor- or rictor-independent manner. Mol. Cell. Biol. *29*, 640–649.

Pausch, P., Singh, U., Ahmed, Y.L., Pillet, B., Murat, G., Altegoer, F., Stier, G., Thoms, M., Hurt, E., Sinning, I., et al. (2015). Co-translational capturing of nascent ribosomal proteins by their dedicated chaperones. Nat. Commun. *6*, 7494.

Pavlakis, G.N., Jordan, B.R., Wurst, R.M., and Vournakis, J.N. (1979). Sequence and secondary structure of Drosophila melanogaster 5.8S and 2S rRNAs and of the processing site between them. Nucleic Acids Res. *7*, 2213–2238.

Pederson, T. (1998). The plurifunctional nucleolus. Nucleic Acids Res. *26*, 3871–3876.

Peisker, K., Braun, D., Wölfle, T., Hentschel, J., Fünfschilling, U., Fischer, G., Sickmann, A., and Rospert, S. (2008). Ribosome-associated complex binds to ribosomes in close proximity of Rpl31 at the exit of the polypeptide tunnel in yeast. Mol. Biol. Cell *19*, 5279–5288.

Peng, J.C., Valouev, A., Liu, N., and Lin, H. (2016). Piwi maintains germline stem cells and oogenesis in Drosophila through negative regulation of Polycomb group proteins. Nat. Genet. *48*, 283–291.

Pestova, T.V., Lomakin, I.B., Lee, J.H., Choi, S.K., Dever, T.E., and Hellen, C.U. (2000). The joining of ribosomal subunits in eukaryotes requires eIF5B. Nature *403*, 332–335.

Petersen, C.P., Bordeleau, M.-E., Pelletier, J., and Sharp, P.A. (2006). Short RNAs repress translation after initiation in mammalian cells. Mol. Cell *21*, 533–542.

Petibon, C., Parenteau, J., Catala, M., and Elela, S.A. (2016). Introns regulate the production of ribosomal proteins by modulating splicing of duplicated ribosomal protein genes. Nucleic Acids Res. *44*, 3878.

Phizicky, E.M., and Hopper, A.K. (2010). tRNA biology charges to the front. Genes Dev. *24*, 1832–1860.

Piekna-Przybylska, D., Decatur, W.A., and Fournier, M.J. (2008). The 3D rRNA modification maps database: with interactive tools for ribosome analysis. Nucleic Acids Res. *36*, D178.

Piir, K., Tamm, T., Kisly, I., Tammsalu, T., and Remme, J. (2014). Stepwise Splitting of Ribosomal Proteins from Yeast Ribosomes by LiCl. PLOS ONE *9*, e101561.

Pillai, R.S., Bhattacharyya, S.N., Artus, C.G., Zoller, T., Cougot, N., Basyuk, E., Bertrand, E., and Filipowicz, W. (2005). Inhibition of translational initiation by Let-7 MicroRNA in human cells. Science *309*, 1573–1576.

Pillet, B., García-Gómez, J.J., Pausch, P., Falquet, L., Bange, G., Cruz, J. de la, and Kressler, D. (2015). The Dedicated Chaperone Acl4 Escorts Ribosomal Protein Rpl4 to Its Nuclear Pre-60S Assembly Site. PLOS Genet. *11*, e1005565.

Piñol-Roma, S. (1999). Association of nonribosomal nucleolar proteins in ribonucleoprotein complexes during interphase and mitosis. Mol. Biol. Cell *10*, 77–90.

Pisarev, A.V., Kolupaeva, V.G., Pisareva, V.P., Merrick, W.C., Hellen, C.U.T., and Pestova, T.V. (2006). Specific functional interactions of nucleotides at key −3 and +4 positions flanking the initiation codon with components of the mammalian 48S translation initiation complex. Genes Dev. *20*, 624.

Plafker, S.M., and Macara, I.G. (2002). Ribosomal protein L12 uses a distinct nuclear import pathway mediated by importin 11. Mol. Cell. Biol. *22*, 1266–1275.

Planta, R.J., and Mager, W.H. (1998). The list of cytoplasmic ribosomal proteins of Saccharomyces cerevisiae. Yeast *14*, 471–477.

Pöll, G., Braun, T., Jakovljevic, J., Neueder, A., Jakob, S., Woolford, J.L., Tschochner, H., and Milkereit, P. (2009). rRNA maturation in yeast cells depleted of large ribosomal subunit proteins. PloS One *4*, e8249.

Polymenis, M., and Schmidt, E.V. (1997). Coupling of cell division to cell growth by translational control of the G1 cyclin CLN3 in yeast. Genes Dev. *11*, 2522–2531.

Pombo, A., Jackson, D.A., Hollinshead, M., Wang, Z., Roeder, R.G., and Cook, P.R. (1999). Regional specialization in human nuclei: visualization of discrete sites of transcription by RNA polymerase III. EMBO J. *18*, 2241.

Pontvianne, F., Carpentier, M.-C., Durut, N., Pavlištová, V., Jaške, K., Schořová, Š., Parrinello, H., Rohmer, M., Pikaard, C.S., Fojtová, M., et al. (2016). Identification of Nucleolus-Associated Chromatin Domains Reveals a Role for the Nucleolus in 3D Organization of the A. thaliana Genome. Cell Rep. *16*, 1574–1587.

Porras-Yakushi, T.R., Whitelegge, J.P., and Clarke, S. (2006). A novel SET domain methyltransferase in yeast: Rkm2-dependent trimethylation of ribosomal protein L12ab at lysine 10. J. Biol. Chem. *281*, 35835–35845.

Qu, J., and Bishop, J.M. (2012). Nucleostemin maintains self-renewal of embryonic stem cells and promotes reprogramming of somatic cells to pluripotency. J Cell Biol *197*, 731–745.

Raab, J.R., Chiu, J., Zhu, J., Katzman, S., Kurukuti, S., Wade, P.A., Haussler, D., and Kamakaka, R.T. (2012). Human tRNA genes function as chromatin insulators. EMBO J. *31*, 330–350.

Ramagopal, S. (1991). Covalent modifications of ribosomal proteins in growing and aggregation-competent dictyostelium discoideum: phosphorylation and methylation. Biochem. Cell Biol. Biochim. Biol. Cell. *69*, 263–268.

Rangaraju, V., Dieck, S. tom, and Schuman, E.M. (2017). Local translation in neuronal compartments: how local is local? EMBO Rep. *18*, 693–711.

Raveh, A., Margaliot, M., Sontag, E.D., and Tuller, T. (2016). A model for competition for ribosomes in the cell. J. R. Soc. Interface *13*.

Reid, D.W., and Nicchitta, C.V. (2015). Diversity and selectivity in mRNA translation on the endoplasmic reticulum. Nat. Rev. Mol. Cell Biol. *16*, 221–231.

Remacha, M., Jimenez-Diaz, A., Bermejo, B., Rodriguez-Gabriel, M.A., Guarinos, E., and Ballesta, J.P. (1995). Ribosomal acidic phosphoproteins P1 and P2 are not required for cell viability but regulate the pattern of protein expression in Saccharomyces cerevisiae. Mol. Cell. Biol. *15*, 4754–4762.

van Riggelen, J., Yetil, A., and Felsher, D.W. (2010). MYC as a regulator of ribosome biogenesis and protein synthesis. Nat. Rev. Cancer *10*, 301–309.

Roberts, D.N., Wilson, B., Huff, J.T., Stewart, A.J., and Cairns, B.R. (2006). Dephosphorylation and Genome-Wide Association of Maf1 with Pol III-Transcribed Genes during Repression. Mol. Cell *22*, 633.

Rodnina, M.V., Beringer, M., and Wintermeyer, W. (2007). How ribosomes make peptide bonds. Trends Biochem. Sci. *32*, 20–26.

Rodrigues, A.B., Zoranovic, T., Ayala-Camargo, A., Grewal, S., Reyes-Robles, T., Krasny, M., Wu, D.C., Johnston, L.A., and Bach, E.A. (2012). Activated STAT regulates growth and induces competitive interactions independently of Myc, Yorkie, Wingless and ribosome biogenesis. Dev. Camb. Engl. *139*, 4051–4061.

Romeo, Y., Moreau, J., Zindy, P.-J., Saba-El-Leil, M., Lavoie, G., Dandachi, F., Baptissart, M., Borden, K.L.B., Meloche, S., and Roux, P.P. (2013). RSK regulates activated BRAF signalling to mTORC1 and promotes melanoma growth. Oncogene *32*, 2917–2926.

Rougeot, J., Renard, M., Randsholt, N.B., Peronnet, F., and Mouchel-Vielh, E. (2013). The elongin complex antagonizes the chromatin factor Corto for vein versus intervein cell identity in Drosophila wings. PloS One *8*, e77592.

Rout, M.P., Blobel, G., and Aitchison, J.D. (1997). A distinct nuclear import pathway used by ribosomal proteins. Cell *89*, 715–725.

Rugjee, K.N., Chaudhury, S.R., Al-Jubran, K., Ramanathan, P., Matina, T., Wen, J., and Brogna, S. (2013). Fluorescent protein tagging confirms the presence of ribosomal proteins at Drosophila polytene chromosomes. PeerJ *1*.

Sadaie, M., Shinmyozu, K., and Nakayama, J. (2008). A Conserved SET Domain Methyltransferase, Set11, Modifies Ribosomal Protein Rpl12 in Fission Yeast. J. Biol. Chem. *283*, 7185–7195.

Sadava, Hillis, D.M., Heller, H.C., and Berenbaum, M. (2009). Life: the science of biology.

Salas-Marco, J., and Bedwell, D.M. (2004). GTP Hydrolysis by eRF3 Facilitates Stop Codon Decoding during Eukaryotic Translation Termination. Mol. Cell. Biol. *24*, 7769.

Salvaing, J., Lopez, A., Boivin, A., Deutsch, J.S., and Peronnet, F. (2003). The Drosophila Corto protein interacts with Polycomb-group proteins and the GAGA factor. Nucleic Acids Res. *31*, 2873.

Salvaing, J., Decoville, M., Mouchel-Vielh, E., Bussière, M., Daulny, A., Boldyreva, L., Zhimulev, I., Locker, D., and Peronnet, F. (2006). Corto and DSP1 interact and bind to a maintenance element of the Scr Hox gene: understanding the role of Enhancers of trithorax and Polycomb. BMC Biol. *4*, 9.

Salvaing, J., Nagel, A.C., Mouchel-Vielh, E., Bloyer, S., Maier, D., Preiss, A., and Peronnet, F. (2008). The Enhancer of Trithorax and Polycomb Corto Interacts with Cyclin G in Drosophila. PLoS ONE *3*.

Sancho, M., Di-Gregorio, A., George, N., Pozzi, S., Sánchez, J.M., Pernaute, B., and Rodríguez, T.A. (2013). Competitive interactions eliminate unfit embryonic stem cells at the onset of differentiation. Dev. Cell *26*, 19–30.

Sanij, E., Poortinga, G., Sharkey, K., Hung, S., Holloway, T.P., Quin, J., Robb, E., Wong, L.H., Thomas, W.G., Stefanovsky, V., et al. (2008). UBF levels determine the number of active ribosomal RNA genes in mammals. J. Cell Biol. *183*, 1259.

Sasikumar, A.N., and Kinzy, T.G. (2014). Mutations in the Chromodomain-like Insertion of Translation Elongation Factor 3 Compromise Protein Synthesis through Reduced ATPase Activity. J. Biol. Chem. *289*, 4853.

Saveanu, C., Namane, A., Gleizes, P.-E., Lebreton, A., Rousselle, J.-C., Noaillac-Depeyre, J., Gas, N., Jacquier, A., and Fromont-Racine, M. (2003). Sequential protein association with nascent 60S ribosomal particles. Mol. Cell. Biol. *23*, 4449–4460.

Scheuermann, J.C., Alonso, A.G. de A., Oktaba, K., Ly-Hartig, N., McGinty, R.K., Fraterman, S., Wilm, M., Muir, T.W., and Müller, J. (2010). Histone H2A deubiquitinase activity of the Polycomb repressive complex PR-DUB. Nature *465*, 243.

Schmidt, E.V. (1999). The role of c-myc in cellular growth control. Oncogene *18*, 2988–2996.

Schrier, P. i., and Möller, W. (1975). The involvement of 50S ribosomal protein L11 in the EF-G dependent GTP hydrolysis of E. coli ribosomes. FEBS Lett. *54*, 130–134.

Schroder, P.A., and Moore, M.J. (2005). Association of ribosomal proteins with nascent transcripts in S. cerevisiae. RNA *11*, 1521–1529.

Schultz, J. (1929). The Minute Reaction in the Development of DROSOPHILA MELANOGASTER. Genetics *14*, 366–419.

Schütz, S., Fischer, U., Altvater, M., Nerurkar, P., Peña, C., Gerber, M., Chang, Y., Caesar, S., Schubert, O.T., Schlenstedt, G., et al. (2014). A RanGTP-independent mechanism allows ribosomal protein nuclear import for ribosome assembly. ELife *3*, e03473.

Sears, R., Nuckolls, F., Haura, E., Taya, Y., Tamai, K., and Nevins, J.R. (2000). Multiple Ras-dependent phosphorylation pathways regulate Myc protein stability. Genes Dev. *14*, 2501–2514.

Semenza, G.L. (2014). Oxygen sensing, hypoxia-inducible factors, and disease pathophysiology. Annu. Rev. Pathol. *9*, 47–71.

Shcherbik, N., Wang, M., Lapik, Y.R., Srivastava, L., and Pestov, D.G. (2010). Polyadenylation and degradation of incomplete RNA polymerase I transcripts in mammalian cells. EMBO Rep. *11*, 106–111.

Shor, B., Wu, J., Shakey, Q., Toral-Barza, L., Shi, C., Follettie, M., and Yu, K. (2010). Requirement of the mTOR Kinase for the Regulation of Maf1 Phosphorylation and Control of RNA Polymerase III-dependent Transcription in Cancer Cells. J. Biol. Chem. *285*, 15380–15392.

Si, K., and Maitra, U. (1999). The Saccharomyces cerevisiae homologue of mammalian translation initiation factor 6 does not function as a translation initiation factor. Mol. Cell. Biol. *19*, 1416–1426.

Sibley, C.R., Emmett, W., Blazquez, L., Faro, A., Haberman, N., Briese, M., Trabzuni, D., Ryten, M., Weale, M.E., Hardy, J., et al. (2015). Recursive splicing in long vertebrate genes. Nature *521*, 371–375.

Silva, G.M., and Vogel, C. (2016). Quantifying gene expression: the importance of being subtle. Mol. Syst. Biol. *12*, 885.

Simms, T.A., Dugas, S.L., Gremillion, J.C., Ibos, M.E., Dandurand, M.N., Toliver, T.T., Edwards, D.J., and Donze, D. (2008). TFIIIC Binding Sites Function as both Heterochromatin Barriers and Chromatin Insulators in Saccharomyces cerevisiae. Eukaryot. Cell *7*, 2078–2086.

Simsek, D., Tiu, G.C., Flynn, R.A., Byeon, G.W., Leppek, K., Xu, A.F., Chang, H.Y., and Barna, M. (2017). The Mammalian Ribo-interactome Reveals Ribosome Functional Diversity and Heterogeneity. Cell *169*, 1051–1065.e18.

Singh, S.A., Goldberg, T.A., Henson, A.L., Husain-Krautter, S., Nihrane, A., Blanc, L., Ellis, S.R., Lipton, J.M., and Liu, J.M. (2014). p53-Independent Cell Cycle and Erythroid Differentiation Defects in Murine Embryonic Stem Cells Haploinsufficient for Diamond Blackfan Anemia-Proteins: RPS19 versus RPL5. PLoS ONE *9*.

Sirri, V., Roussel, P., and Hernandez-Verdun, D. (1999). The mitotically phosphorylated form of the transcription termination factor TTF-1 is associated with the repressed rDNA transcription machinery. J. Cell Sci. *112 (Pt 19)*, 3259–3268.

Sirri, V., Hernandez-Verdun, D., and Roussel, P. (2002). Cyclin-dependent kinases govern formation and maintenance of the nucleolus. J. Cell Biol. *156*, 969.

Sirri, V., Urcuqui-Inchima, S., Roussel, P., and Hernandez-Verdun, D. (2008). Nucleolus: the fascinating nuclear body. Histochem. Cell Biol. *129*, 13–31.

Slavov, N., Semrau, S., Airoldi, E., Budnik, B., and van Oudenaarden, A. (2015). Differential stoichiometry among core ribosomal proteins. Cell Rep. *13*, 865–873.

Sloan, K.E., Warda, A.S., Sharma, S., Entian, K.-D., Lafontaine, D.L.J., and Bohnsack, M.T. (2016). Tuning the ribosome: The influence of rRNA modification on eukaryotic ribosome biogenesis and function. RNA Biol. 1–16.

Smirnov, E., Cmarko, D., Mazel, T., Hornáček, M., and Raška, I. (2016). Nucleolar DNA: the host and the guests. Histochem. Cell Biol. *145*, 359–372.

Smulders-Srinivasan, T.K., Szakmary, A., and Lin, H. (2010). A Drosophila chromatin factor interacts with the Piwi-interacting RNA mechanism in niche cells to regulate germline stem cell self-renewal. Genetics *186*, 573–583.

Somers, J., Pöyry, T., and Willis, A.E. (2013). A perspective on mammalian upstream open reading frame function. Int. J. Biochem. Cell Biol. *45*, 1690–1700.

Spriggs, K.A., Stoneley, M., Bushell, M., and Willis, A.E. (2008). Re-programming of translation following cell stress allows IRES-mediated translation to predominate. Biol. Cell *100*, 27–38.

Sriskanthadevan-Pirahas, S., Deshpande, R., Lee, B., and Grewal, S. (2016). Ras/ERK-signalling promotes tRNA synthesis and growth via the RNA polymerase III repressor Maf1 in Drosophila. BioRxiv 092114.

Staller, P., Peukert, K., Kiermaier, A., Seoane, J., Lukas, J., Karsunky, H., Möröy, T., Bartek, J., Massagué, J., Hänel, F., et al. (2001). Repression of p15INK4b expression by Myc through association with Miz-1. Nat. Cell Biol. *3*, 392–399.

Steffen, K.K., McCormick, M.A., Pham, K.M., MacKay, V.L., Delaney, J.R., Murakami, C.J., Kaeberlein, M., and Kennedy, B.K. (2012). Ribosome deficiency protects against ER stress in Saccharomyces cerevisiae. Genetics *191*, 107–118.

Struhl, G. (1982). Genes controlling segmental specification in the Drosophila thorax. Proc. Natl. Acad. Sci. U. S. A. *79*, 7380–7384.

Strunk, B.S., and Karbstein, K. (2009). Powering through ribosome assembly. RNA *15*, 2083–2104.

Strunk, B.S., Loucks, C.R., Su, M., Vashisth, H., Cheng, S., Schilling, J., Brooks, C.L., Karbstein, K., and Skiniotis, G. (2011). Ribosome assembly factors prevent premature translation initiation by 40S assembly intermediates. Science *333*, 1449–1453.

Strunk, B.S., Novak, M.N., Young, C.L., and Karbstein, K. (2012). Joining of 60S subunits and a translation-like cycle in 40S ribosome maturation. Cell *150*, 111.

Sung, M.-K., Reitsma, J.M., Sweredoski, M.J., Hess, S., and Deshaies, R.J. (2016a). Ribosomal proteins produced in excess are degraded by the ubiquitin–proteasome system. Mol. Biol. Cell *27*, 2642–2652.

Sung, M.-K., Porras-Yakushi, T.R., Reitsma, J.M., Huber, F.M., Sweredoski, M.J., Hoelz, A., Hess, S., and Deshaies, R.J. (2016b). A conserved quality-control pathway that mediates degradation of unassembled ribosomal proteins. ELife *5*, e19105.

Szostak, E., and Gebauer, F. (2013). Translational control by 3'-UTR-binding proteins. Brief. Funct. Genomics *12*, 58–65.

Takagi, M., Absalon, M.J., McLure, K.G., and Kastan, M.B. (2005). Regulation of p53 Translation and Induction after DNA Damage by Ribosomal Protein L26 and Nucleolin. Cell *123*, 49–63.

Takagi, Y., Conaway, J.W., and Conaway, R.C. (1995). A novel activity associated with RNA polymerase II elongation factor SIII. SIII directs promoter-independent transcription initiation by RNA polymerase II in the absence of initiation factors. J. Biol. Chem. *270*, 24300–24305.

Takei, S., Togo-Ohno, M., Suzuki, Y., and Kuroyanagi, H. (2016). Evolutionarily conserved autoregulation of alternative pre-mRNA splicing by ribosomal protein L10a. Nucleic Acids Res.

Taoka, M., Nobe, Y., Yamaki, Y., Yamauchi, Y., Ishikawa, H., Takahashi, N., Nakayama, H., and Isobe, T. (2016). The complete chemical structure of Saccharomyces cerevisiae rRNA: partial pseudouridylation of U2345 in 25S rRNA by snoRNA snR9. Nucleic Acids Res. *44*, 8951–8961.

Taylor, D.J., Nilsson, J., Merrill, A.R., Andersen, G.R., Nissen, P., and Frank, J. (2007). Structures of modified eEF2·80S ribosome complexes reveal the role of GTP hydrolysis in translocation. EMBO J. *26*, 2421–2431.

Tcherkezian, J., Brittis, P.A., Thomas, F., Roux, P.P., and Flanagan, J.G. (2010). Transmembrane receptor DCC associates with protein synthesis machinery and regulates translation. Cell *141*, 632–644.

Tchórzewski, M., Boldyreff, B., and Grankowski, N. (1999). Extraribosomal function of the acidic ribosomal P1-protein YP1alpha from Saccharomyces cerevisiae. Acta Biochim. Pol. *46*, 901–910.

Terzian, T., and Box, N. (2013). Genetics of Ribosomal Proteins: “Curiouser and Curiouser.” PLoS Genet. *9*.

Thapa, M., Bommakanti, A., Shamsuzzaman, M., Gregory, B., Samsel, L., Zengel, J.M., and Lindahl, L. (2013). Repressed synthesis of ribosomal proteins generates protein-specific cell cycle and morphological phenotypes. Mol. Biol. Cell *24*, 3620–3633.

Thompson, M., Haeusler, R.A., Good, P.D., and Engelke, D.R. (2003). Nucleolar Clustering of Dispersed tRNA Genes. Science *302*, 1399.

Tofaris, G.K., Layfield, R., and Spillantini, M.G. (2001). alpha-synuclein metabolism and aggregation is linked to ubiquitin-independent degradation by the proteasome. FEBS Lett. *509*, 22–26.

Tollervey, D., Lehtonen, H., Jansen, R., Kern, H., and Hurt, E.C. (1993). Temperature-sensitive mutations demonstrate roles for yeast fibrillarin in pre-rRNA processing, pre-rRNA methylation, and ribosome assembly. Cell *72*, 443–457.

Tsang, C.K., Liu, H., and Zheng, X.F.S. (2010). mTOR binds to the promoters of RNA polymerase I- and III-transcribed genes. Cell Cycle Georget. Tex *9*, 953–957.

Tsvetkov, P., Reuven, N., and Shaul, Y. (2009). The nanny model for IDPs. Nat. Chem. Biol. *5*, 778–781.

Tu, W.-Y., Huang, Y.-C., Liu, L.-F., Chang, L.-H., and Tam, M.F. (2011). Rpl12p affects the transcription of the PHO pathway high-affinity inorganic phosphate transporters and repressible phosphatases. Yeast *28*, 481–493.

Tudge, C. (2006). The Tree: A Natural History of What Trees Are, How They Live, And Why They Matter (Crown Publishers).

Tyers, M., Tokiwa, G., Nash, R., and Futcher, B. (1992). The Cln3-Cdc28 kinase complex of S. cerevisiae is regulated by proteolysis and phosphorylation. EMBO J. *11*, 1773–1784.

Uchida, N., Hoshino, S., Imataka, H., Sonenberg, N., and Katada, T. (2002). A Novel Role of the Mammalian GSPT/eRF3 Associating with Poly(A)-binding Protein in Cap/Poly(A)-dependent Translation. J. Biol. Chem. *277*, 50286–50292.

Uchiumi, T., and Kominami, R. (1997). Binding of Mammalian Ribosomal Protein Complex P0·P1·P2 and Protein L12 to the GTPase-associated Domain of 28 S Ribosomal RNA and Effect on the Accessibility to Anti-28 S RNA Autoantibody. J. Biol. Chem. *272*, 3302–3308.

Uchiumi, T., Kikuchi, M., Terao, K., Iwasaki, K., and Ogata, K. (1986). Cross-linking of elongation factor 2 to rat-liver ribosomal proteins by 2-iminothiolane. Eur. J. Biochem. *156*, 37–48.

Van Hooser, A.A., Yuh, P., and Heald, R. (2005). The perichromosomal layer. Chromosoma *114*, 377–388.

Vervoorts, J., Lüscher-Firzlaff, J.M., Rottmann, S., Lilischkis, R., Walsemann, G., Dohmann, K., Austen, M., and Lüscher, B. (2003). Stimulation of c-MYC transcriptional activity and acetylation by recruitment of the cofactor CBP. EMBO Rep. *4*, 484–490.

Vincent, J.-P., Kolahgar, G., Gagliardi, M., and Piddini, E. (2011). Steep differences in wingless signaling trigger Myc-independent competitive cell interactions. Dev. Cell *21*, 366–374.

Vogel, C., and Marcotte, E.M. (2012). Insights into the regulation of protein abundance from proteomic and transcriptomic analyses. Nat. Rev. Genet. *13*, 227–232.

Volmer, R., and Ron, D. (2015). Lipid-dependent regulation of the unfolded protein response. Curr. Opin. Cell Biol. *33*, 67–73.

Wallace, E.W.J., Kear-Scott, J.L., Pilipenko, E.V., Schwartz, M.H., Laskowski, P.R., Rojek, A.E., Katanski, C.D., Riback, J.A., Dion, M.F., Franks, A.M., et al. (2015). Reversible, Specific, Active Aggregates of Endogenous Proteins Assemble upon Heat Stress. Cell *162*, 1286–1298.

Wan, F., Anderson, D.E., Barnitz, R.A., Snow, A., Bidere, N., Zheng, L., Hegde, V., Lam, L.T., Staudt, L.M., Levens, D., et al. (2007). Ribosomal protein S3: a KH domain subunit in NF-kappaB complexes that mediates selective gene regulation. Cell *131*, 927–939.

Wang, M., and Pestov, D.G. (2011). 5'-end surveillance by Xrn2 acts as a shared mechanism for mammalian pre-rRNA maturation and decay. Nucleic Acids Res. *39*, 1811–1822.

Wang, X., and Proud, C.G. (2008). A novel mechanism for the control of translation initiation by amino acids, mediated by phosphorylation of eukaryotic initiation factor 2B. Mol. Cell. Biol. *28*, 1429–1442.

Wang, L., Haeusler, R.A., Good, P.D., Thompson, M., Nagar, S., and Engelke, D.R. (2005). Silencing Near tRNA Genes Requires Nucleolar Localization. J. Biol. Chem. *280*, 8637–8639.

Wang, L., Yang, F., Zhang, D., Chen, Z., Xu, R.-M., Nierhaus, K.H., Gong, W., and Qin, Y. (2012). A conserved proline switch on the ribosome facilitates the recruitment and binding of trGTPases. Nat. Struct. Mol. Biol. *19*, 403–410.

Wang, S., Sakai, H., and Wiedmann, M. (1995). NAC covers ribosome-associated nascent chains thereby forming a protective environment for regions of nascent chains just emerging from the peptidyl transferase center. J. Cell Biol. *130*, 519–528.

Ware, V.C., Renkawitz, R., and Gerbi, S.A. (1985). rRNA processing: removal of only nineteen bases at the gap between 28S alpha and 28S beta rRNAs in Sciara coprophila. Nucleic Acids Res. *13*, 3581–3597.

Warner, J.R., and McIntosh, K.B. (2009). How Common are Extra-ribosomal Functions of Ribosomal Proteins? Mol. Cell *34*, 3–11.

Watanabe-Susaki, K., Takada, H., Enomoto, K., Miwata, K., Ishimine, H., Intoh, A., Ohtaka, M., Nakanishi, M., Sugino, H., Asashima, M., et al. (2014). Biosynthesis of ribosomal RNA in nucleoli regulates pluripotency and differentiation ability of pluripotent stem cells. Stem Cells Dayt. Ohio *32*, 3099–3111.

Wawiórka, L., Molestak, E., Szajwaj, M., Michalec-Wawiórka, B., Boguszewska, A., Borkiewicz, L., Liudkovska, V., Kufel, J., and Tchórzewski, M. (2016). Functional analysis of the uL11 protein impact on translational machinery. Cell Cycle Georget. Tex *15*, 1060–1072.

Webb, K.J., Laganowsky, A., Whitelegge, J.P., and Clarke, S.G. (2008). Identification of Two SET Domain Proteins Required for Methylation of Lysine Residues in Yeast Ribosomal Protein Rpl42ab. J. Biol. Chem. *283*, 35561.

Wery, M., Ruidant, S., Schillewaert, S., Leporé, N., and Lafontaine, D.L.J. (2009). The nuclear poly(A) polymerase and Exosome cofactor Trf5 is recruited cotranscriptionally to nucleolar surveillance. RNA *15*, 406.

Wilczynska, A., and Bushell, M. (2015). The complexity of miRNA-mediated repression. Cell Death Differ. *22*, 22–33.

Williamson, N.A., Raliegh, J., Morrice, N.A., and Wettenhall, R.E. (1997). Post-translational processing of rat ribosomal proteins. Ubiquitous methylation of Lys22 within the zinc-finger motif of RL40 (carboxy-terminal extension protein 52) and tissue-specific methylation of Lys4 in RL29. Eur. J. Biochem. *246*, 786–793.

Wilson, D.N., and Cate, J.H.D. (2012). The Structure and Function of the Eukaryotic Ribosome. Cold Spring Harb. Perspect. Biol. *4*, a011536.

Wimberly, B.T., Guymon, R., McCutcheon, J.P., White, S.W., and Ramakrishnan, V. (1999). A Detailed View of a Ribosomal Active Site: The Structure of the L11–RNA Complex. Cell *97*, 491–502.

Wimberly, B.T., Brodersen, D.E., Clemons, W.M., Morgan-Warren, R.J., Carter, A.P., Vonrhein, C., Hartsch, T., and Ramakrishnan, V. (2000). Structure of the 30S ribosomal subunit. Nature *407*, 327–339.

Wittwer, C.T., Reed, G.H., Gundry, C.N., Vandersteen, J.G., and Pryor, R.J. (2003). High-resolution genotyping by amplicon melting analysis using LCGreen. Clin. Chem. *49*, 853–860.

Wood, M.A., McMahon, S.B., and Cole, M.D. (2000). An ATPase/helicase complex is an essential cofactor for oncogenic transformation by c-Myc. Mol. Cell *5*, 321–330.

Woodson, S.A. (2011). RNA folding pathways and the self-assembly of ribosomes. Acc. Chem. Res. *44*, 1312–1319.

Wool, I.G. (1996). Extraribosomal functions of ribosomal proteins. Trends Biochem. Sci. *21*, 164–165.

Xiao, B., Sanders, M.J., Underwood, E., Heath, R., Mayer, F.V., Carmena, D., Jing, C., Walker, P.A., Eccleston, J.F., Haire, L.F., et al. (2011). Structure of mammalian AMPK and its regulation by ADP. Nature *472*, 230–233.

Xiong, Y., and Steitz, T.A. (2004). Mechanism of transfer RNA maturation by CCA-adding enzyme without using an oligonucleotide template. Nature *430*, 640–645.

Xue, S., Tian, S., Fujii, K., Kladwang, W., Das, R., and Barna, M. (2015). RNA regulons in Hox 5' UTRs confer ribosome specificity to gene regulation. Nature *517*, 33–38.

Yamamoto, T. (2000). Molecular mechanism of monocyte predominant infiltration in chronic inflammation: mediation by a novel monocyte chemotactic factor, S19 ribosomal protein dimer. Pathol. Int. *50*, 863–871.

Yang, L., and Chen, J. (2014). SirT1 and rRNA in the nucleolus: regulating the regulator. Oncoscience *1*, 111–112.

Yanofsky, C. (1981). Attenuation in the control of expression of bacterial operons. Nature *289*, 751–758.

Yelick, P.C., and Trainor, P.A. (2015). Ribosomopathies: Global process, tissue specific defects. Rare Dis. Austin Tex *3*, e1025185.

Yoon, A., Peng, G., Brandenburg, Y., Zollo, O., Xu, W., Rego, E., and Ruggero, D. (2006). Impaired Control of IRES-Mediated Translation in X-Linked Dyskeratosis Congenita. Science *312*, 902–906.

Yoshihama, M., Uechi, T., Asakawa, S., Kawasaki, K., Kato, S., Higa, S., Maeda, N., Minoshima, S., Tanaka, T., Shimizu, N., et al. (2002). The Human Ribosomal Protein Genes: Sequencing and Comparative Analysis of 73 Genes. Genome Res. *12*, 379–390.

You, K.T., Park, J., and Kim, V.N. (2015). Role of the small subunit processome in the maintenance of pluripotent stem cells. Genes Dev. *29*, 2004–2009.

Yu, L., Castillo, L.P., Mnaimneh, S., Hughes, T.R., and Brown, G.W. (2006). A Survey of Essential Gene Function in the Yeast Cell Division Cycle. Mol. Biol. Cell *17*, 4736–4747.

Yu, Y., Ji, H., Doudna, J.A., and Leary, J.A. (2005). Mass spectrometric analysis of the human 40S ribosomal subunit: Native and HCV IRES-bound complexes. Protein Sci. Publ. Protein Soc. *14*, 1438.

Zhang, H., and Wang, Z.Z. (2008). Mechanisms that mediate stem cell self-renewal and differentiation. J. Cell. Biochem. *103*, 709–718.

Zhang, Y., and Lu, H. (2009). Signaling to p53: ribosomal proteins find their way. Cancer Cell *16*, 369–377.

Zhang, L.-F., Huynh, K.D., and Lee, J.T. (2007). Perinucleolar targeting of the inactive X during S phase: evidence for a role in the maintenance of silencing. Cell *129*, 693–706.

Zhang, Q., Shalaby, N.A., and Buszczak, M. (2014). Changes in rRNA transcription influence proliferation and cell fate within a stem cell lineage. Science *343*, 298–301.

Zhao, J., Yuan, X., Frödin, M., and Grummt, I. (2003). ERK-dependent phosphorylation of the transcription initiation factor TIF-IA is required for RNA polymerase I transcription and cell growth. Mol. Cell *11*, 405–413.

Zhao, Z., Dammert, M.A., Hoppe, S., Bierhoff, H., and Grummt, I. (2016). Heat shock represses rRNA synthesis by inactivation of TIF-IA and lncRNA-dependent changes in nucleosome positioning. Nucleic Acids Res. *44*, 8144–8152.

Zhimulev, I.F., Belyaeva, E.S., Semeshin, V.F., Koryakov, D.E., Demakov, S.A., Demakova, O.V., Pokholkova, G.V., and Andreyeva, E.N. (2004). Polytene chromosomes: 70 years of genetic research. Int. Rev. Cytol. *241*, 203–275.

Zhou, C., Slaughter, B.D., Unruh, J.R., Guo, F., Yu, Z., Mickey, K., Narkar, A., Ross, R.T., McClain, M., and Li, R. (2014). Organelle-Based Aggregation and Retention of Damaged Proteins in Asymmetrically Dividing Cells. Cell *159*, 530–542.

Zhou, W., Huang, J., Watson, A.M., and Hong, Y. (2012). W::Neo: A Novel Dual-Selection Marker for High Efficiency Gene Targeting in Drosophila. PLoS ONE *7*.

Zhou, X., Hao, Q., Liao, J., Liao, P., and Lu, H. (2013). Ribosomal Protein S14 Negatively Regulates c-Myc Activity. J. Biol. Chem. *288*, 21793–21801.

Zhou, X., Liao, W.-J., Liao, J.-M., Liao, P., and Lu, H. (2015). Ribosomal proteins: functions beyond the ribosome. J. Mol. Cell Biol. *7*, 92–104.

Zhu, J., Blenis, J., and Yuan, J. (2008). Activation of PI3K/Akt and MAPK pathways regulates Myc-mediated transcription by phosphorylating and promoting the degradation of Mad1. Proc. Natl. Acad. Sci. U. S. A. *105*, 6584–6589.

Appendix

Cyclin G and the Polycomb Repressive Complexes PRC1 and PR-DUB cooperate for developmental stability.

A. Overview

Among the protein partners of Corto, Cyclin G met particular attention from our team. Indeed, the expression of a short version lacking its C-terminal PEST-rich sequence (*CycG$^{\Delta P}$*) generates a very unusual phenotype in flies: fluctuating asymmetry (FA). Indeed, while a low level of stochastic asymmetry can be detected in any population, the expression of *CycG$^{\Delta P}$* was shown to increase it nearly forty-fold (Debat et al., 2011).

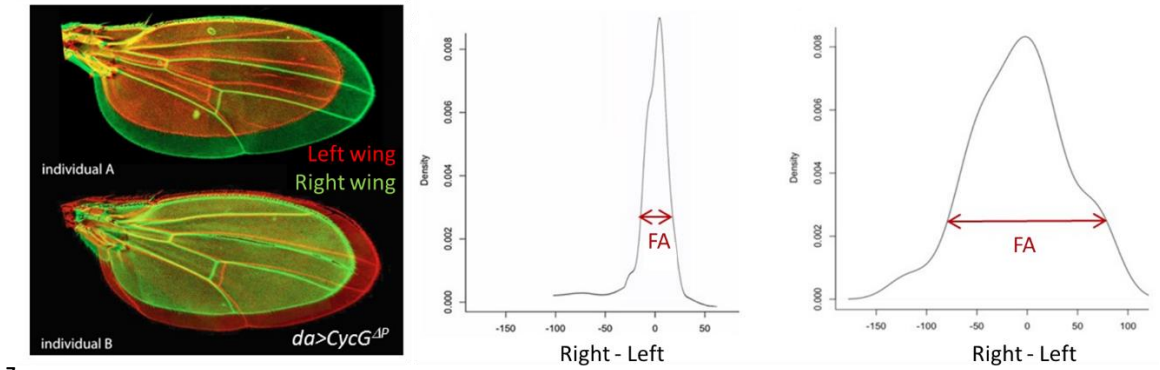

z

Figure 64. The fluctuating asymmetry phenotype.
Left panel: Overexpression of a version of CycG$^{\Delta P}$ induces extreme asymmetry of the wings, as can be seen by the superposition of the left and right wings of an individual. Adapted from (Debat et al., 2011). Middle and right panels: examples of the distribution of the wing size difference (right minus left) in a population with low fluctuating asymmetry (middle) and one where it is higher (right). The values of the (right minus left) wing size differences follow a normal distribution within a population. Fluctuating asymmetry is quantified as the variance of this distribution. Adapted from (Dupont, 2015).

Since fluctuating asymmetry measures the organ size variation within individuals (albeit at the level of a population), it cannot be attributed to environmental or genetic variations. Rather, it results from the intrinsic stochasticity of development. Indeed, generation of an adult organ such as the wing requires a myriad of biological reactions. Whether it is the binding of a ligand to a receptor, the transcription of a gene, or the death of a cell, all of them are subject to a level of randomness. The fact that the final organs are so consistent in spite of all this stochasticity betrays the existence of a system that buffers developmental noise. While the exact nature of this system remains unclear, it is called developmental stability. The observed surge of fluctuating asymmetry suggests that ectopic expression of *CycG$^{\Delta P}$* interferes with developmental stability, providing a unique opportunity to investigate its genetic bases.

Our team observed that the deletion of the N-terminal domain of CycG$^{\Delta P}$ reduces its ability to generate FA by half. This domain underlies the interaction between CycG$^{\Delta P}$ and Corto. Thus, our team asked whether Corto and other epigenetic factors would be instrumental to CycG$^{\Delta P}$-mediated induction of fluctuating asymmetry. Indeed, genetic interaction experiments showed that CycG$^{\Delta P}$-induced FA is significantly increased by mutations of the PRC1 and PR-DUB complexes, but not by that of PRC2. Since CycG was shown to behave as an enhancer of Polycomb-group genes, it was

hypothesized that its role in the regulation of transcription could underlie the fluctuating asymmetry phenotype (Dupont et al., 2015).

To further characterize this role in transcription, our team generated RNA-seq data for the expression of *CycG*$^{\Delta P}$, from the wing discs of third instar female larvae. I then analysed it to find genes that were differentially expressed as compared to a control genotype (*w*^{1118}). A set of 530 de-regulated genes was identified, whose analysis by gene ontology revealed its enrichment in genes involved in translation and energy production.

To determine whether their regulation was directly mediated by CycG, our team produced ChIP-seq data for Myc-CycG$^{\Delta P}$ from third instar female larvae wing discs. I analysed these data and established that CycG is significantly enriched over 889 target genes, where it binds at the TSS. Gene ontology analysis showed that they are enriched in GO terms “translation” and “phosphorylation”. To determine whether CycG could cooperate with Polycomb-group genes in the regulation of transcription, I recovered ChIP-seq data sets generated in the same tissue for Calypso, ASX, PC, PH, PSC, RNAPolII and H3K27me3. and analysed whether these are associated with CycG over the whole genome. To this end, I updated the coordinates of the author-designated enrichment regions to the current genome coordinates. I then assessed the significance of their overlap with CycG-enriched regions with a genomic association test (GAT software). This analysis found that CycG significantly co-localized with ASX, PC, PH, PSC, and RNAPolII, but was significantly excluded from H3K27me3-enriched regions. To confirm whether these conclusions also apply to gene regions, I then assessed the significance of the overlap between the lists of genes enriched for CycG and for other factors. Consistently, CycG-bound genes were found to significantly overlap with ASX, PC, PH, PSC, and RNAPolII bound genes.

Altogether, these results suggest that CycG directly regulates a set of genes among which translation-related genes are enriched. Interestingly, many of these are described as targets of members of the PRC1 and PR-DUB complexes. Since CycG associates with those over the whole genome, and genetically behaves as an Enhancer of PcG gene, it is tempting to speculate that they cooperate in the regulation of gene expression. Furthermore, mutations for members of PRC1 and PR-DUB complexes significantly increase the fluctuating asymmetry phenotype, which suggests that indeed, the transcriptional regulation of these genes plays a role in developmental stability.

B. Article

Cyclin G and the Polycomb Repressive Complexes PRC1 and PR-DUB cooperate for developmental stability.

Delphine Dardalhon-Cuménal[1,2], Jérôme Deraze[1,2], Camille A Dupont[1,2], Valérie Ribeiro[1,2], Anne Coléno-Costes[1,2], Juliette Pouch[4], Stéphane Le Crom [4,5], Hélène Thomassin[1,2], Vincent Debat[3], Neel B Randsholt[1,2] and Frédérique Peronnet[1,2].

[1] Sorbonne Universités, UPMC Univ Paris 06, Institut de Biologie Paris-Seine (IBPS), UMR 7622, Developmental Biology, F-75005, Paris, France

[2] CNRS, IBPS, UMR 7622, Developmental Biology, F-75005, Paris, France

[3] Museum national d'Histoire naturelle, Institut de Systématique, Évolution, Biodiversité, ISYEB UMR 7205, CNRS-MNHN-UPMC-EPHE, Sorbonne Universités, 45 rue Buffon, 75005 Paris, France

[4] IBENS, Département de Biologie, Ecole Normale Supérieure, CNRS, Inserm, PSL Research University, F‐75005 Paris, France

[5] Sorbonne Universités, UPMC Univ Paris 06, Univ Antilles, Univ Nice Sophia Antipolis, CNRS, Evolution Paris Seine - Institut de Biologie Paris Seine (EPS - IBPS), 75005 Paris, France

Keywords : *Drosophila melanogaster*, Developmental Stability, Fluctuating Asymmetry, Developmental noise, Polycomb, Cyclin G

ABSTRACT

In *Drosophila*, ubiquitous expression of a short Cyclin G isoform generates extreme developmental noise estimated by fluctuating asymmetry (FA), providing a model to tackle developmental stability. This transcriptional cyclin interacts with chromatin regulators of the Enhancer of Trithorax and Polycomb (ETP) and Polycomb families. This led us to investigate the importance of these interactions in developmental stability. Deregulation of Cyclin G highlights an organ intrinsic control of developmental noise, linked to the ETP-interacting domain, and enhanced by mutations in genes encoding members of the Polycomb Repressive complexes PRC1 and PR-DUB. Deep-sequencing of wing imaginal discs deregulating *CycG* reveals that high developmental noise correlates with up-regulation of genes involved in translation and down-regulation of genes involved in energy production. Most Cyclin G direct transcriptional targets are also direct targets of PRC1 and RNAPolII in the developing wing. Altogether, our results suggest that Cyclin G, PRC1 and PR-DUB cooperate for developmental stability.

INTRODUCTION

Developmental stability has been described as the set of processes that buffer disruption of developmental trajectories for a given genotype within a particular environment (Palmer, 1994). In other words, developmental stability compensates the random stochastic variation of processes at play during development. Many mechanisms working from the molecular to the whole organism levels contribute to developmental stability (Nijhout and Davidowitz, 2003). For example, chaperones, such as heat-shock proteins, participate in developmental stability in a large variety of developmental processes by protecting misfolded proteins from denaturation (Feder and Hofmann, 1999; Queitsch et al., 2002; Rutherford et al., 2007). In *Drosophila melanogaster*, adjustment of cell growth to cell proliferation is essential to developmental stability by allowing to achieve a consistant organ size (*e.g.* wing size) in spite of variation in cell size or cell number (Debat et al., 2011; Debat and Peronnet, 2013).

Developmental noise, the “sum” of the stochastic part of each developmental process, can be observed macroscopically for morphological traits. In bilaterians, quantification of departure from perfect symmetry, the so-called fluctuating asymmetry (FA), is the most commonly used index to estimate developmental noise (Van Valen, 1962; Palmer and Strobeck, 1992). Indeed, the two sides of bilaterally symmetrical traits are influenced by the same genotype and environmental conditions, and differences between them are thus only due to developmental noise. The use of FA as an index of developmental noise makes analysis of the mechanistic and genetic bases of developmental stability compatible with custom genetic and molecular approaches of developmental biology.

The evolutionary role of developmental stability is subject to many speculations (*e.g.* Dongen, 2006) as its genetic bases remain unclear (for reviews see Leamy and Klingenberg, 2005; Debat and Peronnet, 2013). Experiments showing the role of *Hsp90* in buffering genetic variation led to the idea that developmental stability could be ensured by specific genes (Rutherford and Lindquist, 1998; Milton et al., 2003; Debat et al., 2006; Yeyati et al., 2007; Sangster et al., 2008). On the other hand, both theory and experiments show that complex genetic networks can become intrinsically robust to perturbations, notably through negative and positive feedbacks, suggesting that the topology of gene networks is of paramount importance for developmental stability (Barabasi and Albert, 1999; Siegal and Bergman, 2002; Newman, 2003; Kitano, 2004). Several authors have further suggested that hubs, *i.e.* the most connected genes in these networks, might be particularly important for developmental stability (Rutherford et al., 2007; Levy and Siegal, 2008).

In *Drosophila*, mutants for *dILP8* and *hid*, two genes involved in the control of systemic growth and apoptosis respectively, have been reported to display high FA as compared to wild type flies from the same genetic background (Garelli et al., 2012; Colombani et al., 2012; Neto-Silva et al., 2009), suggesting that these genes are important for developmental stability. Two studies have scanned the *Drosophila* genome for regions involved in developmental stability using FA as an estimator of developmental noise (Breuker et al., 2006; Takahashi et al., 2011). Several deletions increased FA but the genes responsible for this effect inside the deletions were not identified. Nevertheless, these studies confirm that the determinism of developmental stability could well be polygenic, as suggested by Quantitative Trait Loci analyses in mouse (Leamy et al., 2002; Leamy et al., 2005; Leamy et al., 2015). Together, these data reinforce the idea that developmental stability depends on gene networks.

We have shown that the gene *Cyclin G* (*CycG*) of *Drosophila melanogaster*, which encodes a protein involved in transcriptional regulation and in the cell cycle, is important for developmental stability (Salvaing et al., 2008a; Faradji et al., 2011; Debat et al., 2011; Dupont et al., 2015). Indeed, ubiquitous expression of a short Cyclin G version lacking the C-terminal PEST-rich domain ($CycG^{\Delta P}$) generates a very high FA in several organs, notably in the wing. Interestingly, FA induced by $CycG^{\Delta P}$ expression correlates with high variability in cell size and loss of correlation between cell size and cell number, suggesting that the noisy process would somehow be connected to cell cycle related cell growth (Debat et al., 2011). Hence, *CycG* deregulation provides a convenient sensitized system to tackle the impact of cell growth variability on developmental stability.

We previously showed that *CycG* encodes a transcriptional cyclin and interacts with genes of the *Polycomb-group* (*PcG*), *trithorax-group* (*trxG*), and *Enhancer of Trithorax and Polycomb* (*ETP*) families (Salvaing et al., 2008a; Salvaing et al., 2008b; Dupont et al., 2015) . These genes encode evolutionary conserved proteins assembled into large multimeric complexes that bind chromatin. They ensure maintenance of gene expression patterns during development (for recent reviews see Grossniklaus and Paro, 2014; Kingston and Tamkun, 2014; Geisler and Paro, 2015). *PcG* genes are involved in long-term gene repression, whereas *trxG* genes maintain gene activation and counteract *PcG* action. *ETP* genes encode co-factors of both *trxG* and *PcG* genes, and behave alternatively as repressors or activators of target genes (Gildea et al., 2000; Grimaud et al., 2006; Beck et al., 2010). More recently, we discovered that *CycG* behaves as an *Enhancer of Polycomb* regarding homeotic gene regulation suggesting that it is involved in the silencing of these genes (Dupont et al., 2015). Importantly, Cyclin G physically interacts with the ETP proteins Additional Sex Comb (ASX) and Corto *via* its N-terminal ETP-interacting domain, and co-localizes with them on polytene chromosomes at many sites (Salvaing et al., 2008a; Dupont et al., 2015) . Hence, Cyclin G

and these ETPs might share many transcriptional targets and might in particular control cell growth *via* epigenetic regulation of genes involved in growth pathways.

Here, we investigate in depth the role of *CycG* in developmental stability. We first show that localized expression of $CycG^{\Delta P}$ in wing imaginal discs is necessary and sufficient to induce high FA of adult wings. Furthermore, this organ-autonomous effect increases when the ETP-interacting domain of Cyclin G is removed. We show that several mutations for *PcG* or *ETP* genes, notably those encoding members of the PRC1 and PR-DUB complexes, substantially increase *CycG*-induced FA. Next, we report analysis of the transcriptome of wing imaginal discs expressing $CycG^{\Delta P}$ by RNA-seq and find that transcriptional deregulation of genes involved in translation and energy production correlates with high FA of adult wings. By ChIP-seq, we identify Cyclin G binding sites on the whole genome in wing imaginal discs. Strikingly, we observe a significant overlap with genes also bound by ASX, by the Polycomb Repressive complex PRC1, and by RNAPolII in the same tissue. We identify a sub-network of 222 genes centred on Cyclin G showing simultaneous up-regulation of genes involved in translation and down-regulation of genes involved in mitochondrial activity and metabolism. Taken together, our data suggest that Cyclin G and the Polycomb complexes PRC1 and PR-DUB cooperate in sustaining developmental stability. Precise regulation of genes involved in translation and energy production might be important for developmental stability.

RESULTS

Expression of $CycG^{\Delta P}$ in wing precursors is necessary and sufficient to induce high wing FA

We previously reported that expression of *CycG* deleted of the PEST-rich C-terminal domain (amino-acids 541 to 566) ($CycG^{\Delta P}$) under control of ubiquitous drivers (*da-Gal4* or *Actin-Gal4*) generated extremely high FA, notably in wings (Debat et al., 2011) (Figure 1). The strength of this effect was unprecedented in any system or trait. Expression of $CycG^{\Delta P}$ thus provides a unique tool to investigate developmental stability in depth. To determine whether wing FA was due to local or systemic expression of $CycG^{\Delta P}$, we tested a panel of Gal4 drivers specific for wing imaginal discs or neurons. A brain circuit which relays information for bilateral growth synchronization was recently identified (Vallejo et al., 2015). It notably involves a pair of neurons expressing the dILP8 receptor that connects with the insulin-producing cells (IPCs)

and the prothoracicotropic hormone (PTTH) neurons. This circuit was particularly appropriate to test the existence of a remote effect of *CycG$^{\Delta P}$* expression in generating high FA in the wing. Expression of *CycG$^{\Delta P}$* in this circuit (using *dilp3-*, *NPF-*, *pdf-, per-, phm-* and *R19B09-Gal4* drivers) did not increase FA of adult wings (Figure 2 and Table 1). Furthermore, expression of *CycG$^{\Delta P}$* in cells of the future wing hinge using the *ts-Gal4* driver did not affect wing FA either. By contrast, expressing *CycG$^{\Delta P}$* with 5 different wing pouch drivers (*nub-, omb-, rn-, sd-* and *vg-Gal4*) induced high FA. We thus concluded that *CycG$^{\Delta P}$*-induced wing FA was due to an intrinsic response of the growing wing tissue.

The Cyclin G ETP interacting domain sustains developmental stability

The 566 amino-acid Cyclin G protein exhibits 3 remarkable domains: the ETP-interacting domain (amino-acids 1 to 130) that physically interacts with the ETPs Corto and ASX, a cyclin domain (amino-acids 287 to 360) that presents high similarity with the cyclin domain of vertebrate G-type cyclins, and a PEST-rich domain (amino-acids 541 to 566) (Salvaing et al., 2008a; Faradji et al., 2011; Dupont et al., 2015). To test whether the interaction with ETPs (and thus transcriptional regulation by Cyclin G) could be important to control FA, we generated new transgenic lines enabling to express different versions of the *CycG* cDNA: *CycG^{FL}* (encoding the full-length protein), *CycG$^{\Delta E}$* (encoding an ETP-interacting domain deleted protein), *CycG$^{\Delta P}$* (encoding a PEST domain deleted protein), and *CycG$^{\Delta E\Delta P}$* (encoding an ETP-interacting plus PEST domain deleted protein). In order to express these different cDNAs at the same level and compare the amounts of FA induced, all transgenes were integrated at the same site using the *PhiC31* integrase system (at position 51C on the second chromosome). Expression of these transgenic lines was ubiquitously driven by *da-Gal4*. We first confirmed that expression of *CycG$^{\Delta P}$* induced very high FA as compared to *yw* and *da-Gal4/+* controls. Furthermore, expression of *CycG^{FL}* also significantly increased FA, although to a much lesser extent. Interestingly, expression of either *CycG$^{\Delta E}$* or *CycG$^{\Delta E\Delta P}$* significantly increased FA as compared to *CycG^{FL}* or *CycG$^{\Delta P}$*, respectively (Figure 3 and Table 2). These results show that the ETP interacting domain tends to limit Cyclin G-induced FA and suggest that the interaction between Cyclin G and chromatin regulators sustains developmental stability.

CycG and *PcG* or *ETP* genes interact for developmental stability

We next addressed genetic interactions between *CycG* and *PcG* or *ETP* genes for developmental stability. The alleles used are listed in Table 3. FA of flies heterozygous for *PcG* and *ETP* loss of function alleles was not significantly different from that of control flies. However, when combined with a *da-Gal4, UAS-CycG$^{\Delta P}$* chromosome, many of these mutations significantly increased wing FA as compared to *da-Gal4, UAS-CycG$^{\Delta P}$* flies (Figure 4 and Table S1). This was notably the case for alleles for PRC1 and PR-DUB encoding genes, the *PcG* genes *Sex comb extra* (*Sce^{1}*, *Sce^{33M2}* and *Sce^{KO4}*), *calypso* (*caly^{1}* and *caly^{2}*), *Sex comb on midleg* (*Scm^{D1}*), *Polycomb* (*Pc^{1}*), and *polyhomeotic* (*ph-p^{410}* and *ph-d^{401}ph-p^{602}*). No modification of *CycG$^{\Delta P}$*-induced FA was observed with the *Psc^{1}* allele. However, this allele has been described as a complex mutation with both loss and gain of function features (Adler et al., 1989).

Opposite effects were observed for different alleles of the ETPs *Asx* and *corto. Asx^{22P4}* increased *da-Gal4, UAS-CycG$^{\Delta P}$* FA whereas *Asx^{XF23}* decreased it. *Asx^{XF23}* behaves genetically as a null allele but has not been molecularly characterized (Simon et al., 1992), whereas the *Asx^{22P4}* allele does not produce any protein and thus likely reflects the effect of loss of ASX (Scheuermann et al., 2010). Similarly, the *corto^{L1}* allele increased *CycG$^{\Delta P}$*-induced FA whereas the *corto^{420}* allele had no effect. In order to characterize these *corto* alleles, we combined them with the *Df(3R)6-7* deficiency that uncovers the *corto* locus, amplified the region by PCR and sequenced it. The *corto^{420}* allele corresponds to a substitution of 14,209 nucleotides starting at position -59 upstream of the *corto* Transcriptional Start Site (TSS) by a 30-nucleotide sequence. Hence, this allele does not produce any truncated protein. By contrast, *corto^{L1}* corresponds to a C towards T substitution that introduces a stop codon at position +73 downstream the TSS, generating a 24 amino-acid polypeptide. *corto^{L1}* might then behave as a dominant-negative mutation. Lastly, no modification of *CycG$^{\Delta P}$*-induced FA was observed for *E(z)^{63}* and *esc^{21}*.

Interestingly, *Asx* and *caly* encode proteins of the Polycomb Repressive complex PR-DUB whereas *Pc*, *ph*, *Sce* and *Scm* encode proteins of the Polycomb Repressive complex PRC1, and *E(z)* and *esc* encode proteins of the Polycomb Repressive complex PRC2. Taken together, these results indicate that Cyclin G interacts with the Polycomb complexes PRC1 and PR-DUB, but not with PRC2, for developmental stability.

Expression of *CycG$^{\Delta P}$* or *CycG$^{\Delta E\Delta P}$* does not modify the bulk of H2AK118ub

Cyclin G binds polytene chromosomes at many sites and co-localizes extensively with PH and

ASX suggesting a potential interaction with the PRC1 and PR-DUB complexes on chromatin (Salvaing et al., 2008a; Dupont et al., 2015). The two genes *Sce* and *caly* encode antagonistic enzymes of the PRC1 and PR-DUB complexes, respectively. SCE, aka dRing, ubiquitinates histone H2A on lysine 118 (H2AK118ub) whereas Calypso, aka dBap1, is the major deubiquitinase of the same H2A residue (Scheuermann et al., 2010; Scheuermann et al., 2012). To investigate whether Cyclin G was related to these ubiquitin ligase/deubiquitinase activities, we immunostained polytene chromosomes from w^{1118} larvae with anti-Cyclin G and anti-human H2AK119ub antibodies (homologous to *Drosophila* H2AK118ub) (Pengelly et al., 2015). Cyclin G and H2AK118ub co-localized extensively on chromosome arms suggesting that Cyclin G transcriptional activity might somehow be connected to the presence of this histone mark (Figure 5A). However, when either $CycG^{\Delta P}$ or $CycG^{\Delta E \Delta P}$ was expressed in the posterior compartment of wing imaginal discs using the *en-Gal4* driver, the global amount of H2AK118ub was not markedly modified (Figure 5B, Figure 5C). We thus concluded that high FA was not related to a global perturbation of H2AK118 ubiquitination level.

Cyclin G controls the expression of genes involved in translation and energy production

Cyclin G controls the transcription of the homeotic gene *Abdominal-B* and more specifically behaves as an *Enhancer of PcG* gene in the regulation of homeotic gene expression (Salvaing et al., 2008b; Dupont et al., 2015). However, the high number of Cyclin G binding sites on polytene chromosomes suggests that this cyclin has many other transcriptional targets. We thus hypothesized that the high FA induced by expression of $CycG^{\Delta P}$ might be related to the deregulation of Cyclin G transcriptional targets. To further address the role of Cyclin G in transcriptional regulation, we deep-sequenced the transcripts from wing imaginal discs of *da-Gal4, UAS-*$CycG^{\Delta P}$/+ and *da-Gal4*/+ third instar larvae. Sequence reads were aligned with the *Drosophila melanogaster* genome to generate global gene expression profiles. We performed differential analyses to obtain expression changes for *da-Gal4, UAS-*$CycG^{\Delta P}$/+ as compared to the *da-Gal4*/+ control. With an adjusted p-value threshold of 0.05, we retrieved 530 genes whose expression was significantly different between the two genotypes (Table S2). Surprisingly, expression of *CycG* was only weakly induced in *da-Gal4, UAS-*$CycG^{\Delta P}$/+ imaginal discs as compared to *da-Gal4*/+ imaginal discs (1.3 fold). In order to test the hypothesis that Cyclin G could directly or not, induce its own repression, we designed primers in the 3'UTR to measure expression of the endogenous *CycG* gene. Indeed, expression of endogenous *CycG* was significantly decreased when $CycG^{\Delta P}$ was expressed (Figure 6A and Table S3). Among the 530 genes deregulated in *da-Gal4, UAS-*$CycG^{\Delta P}$/+ imaginal discs, 216 were up-regulated and 314 down-regulated. Analysis of Gene Ontology (GO) revealed that up-regulated genes

were enriched in the categories *cytoplasmic translation* and *translational initiation* whereas down-regulated genes were enriched in the category *mitochondrial respiratory chain complex* (Figure 6B and Table S4). By RT-qPCR, we verified that several ribosomal protein genes (*RpL15, RpL7* and *Rack1*) were over-expressed in *da-Gal4, UAS-CycG$^{\Delta P}$*/+ imaginal discs (Figure 6C and Table S5).

In conclusion, *CycG*-induced fluctuating asymmetry correlates with activation of genes involved in translation and repression of genes involved in energy production.

Cyclin G binds the Transcriptional Start Sites of many genes also bound by PRC1 and ASX

In order to determine the direct transcriptional targets of Cyclin G, we analysed by ChIP-seq the genome-wide binding sites of Cyclin G in +/ *UAS-Myc-CycG$^{\Delta P}$; da-Gal4/*+ imaginal discs. 889 genes with significant peaks at the transcriptional start site (TSS) were recovered (Table S6 and Figures 7A and 7B). ChIP-qPCR analysis of Cyclin G binding on *RPL7, RPL5,* and *Rack1* confirmed that Cyclin peaked on the TSS of these genes and decreased on the gene body (7C and Table S7). Furthermore, Cyclin G bound its own TSS almost significantly. We then analysed the binding of Cyclin G on its own gene by ChIP-qPCR and verified the presence of Cyclin G on its TSS (Figure 7C and Table S7). As endogenous *CycG* was down-regulated when *CycG$^{\Delta P}$* was expressed, this suggests that Cyclin G represses its own promoter.

The 889 Cyclin G-bound genes were enriched in GO categories *cytoplasmic translation* and *protein phosphorylation* (Figure 7D). Comparison of the 530 genes deregulated in imaginal discs expressing *CycG$^{\Delta P}$* with the 889 genes presenting a peak at the TSS showed that only 62 genes were both deregulated (39 up- and 23 down-regulated) and bound by Cyclin G (Table S8). Strikingly, the 39 up-regulated genes were significantly enriched in the GO category *translation* (GO:0002181~cytoplasmic translation, 14 genes, enrichment score: 11.84, adjusted p-value 2.07E-16).

Using published datasets, we analysed the correlation between regions bound by Cyclin G in +/*UAS-Myc-CycG$^{\Delta P}$; da-Gal/*+ imaginal discs and those bound by PRC1, PR-DUB or RNAPolII, or enriched in H3K27me3, in wild type wing imaginal discs (Table S9). Cyclin G-bound regions were significantly exclusive from H3K27me3, corroborating polytene chromosome immunostainings (Dupont et al., 2015). The same comparisons were performed gene-wise and gave the same results. Notably, 80% of Cyclin G-bound genes were bound by RNAPolII (Figure 8). Considering RNAPolII as a proxy for transcriptional activity, we concluded that Cyclin G-bound genes were located in open chromatin and were either paused or

transcribed. However, Cyclin G-bound genes were also significantly enriched in PRC1 target genes. Given that PRC1 has the ability to block transcriptional initiation (Dellino et al., 2004), it suggests that Cyclin G-bound genes were most probably paused. Cyclin G also shared many target genes with ASX but, though ASX and Calypso belong to the PR-DUB complex, Cyclin G did not share binding sites with Calypso. This indicates either that the interaction between Cyclin G and ASX destabilizes the PR-DUB complex or that it takes place outside PR-DUB.

Cyclin G is central in the wing imaginal disc network

These genome-wide analyses indicate that Cyclin G coordinates the expression of genes involved in translation and energy production. However, only a few Cyclin G-bound genes were deregulated in *da-Gal4, UAS-CycG$^{\Delta P}$*/+ imaginal discs. To better understand how Cyclin G orchestrates target gene expression, we developed a systems biology approach. We first built an interactome based on genes expressed in control *da-Gal4*/+ wing imaginal discs (with a cutoff of 10 reads). Edges corresponding to protein-protein interactions (PPI) and transcription factor-gene interactions (PDI) were integrated into this interactome through DroID (Murali et al., 2011). The resulting wing imaginal disc interactome, further called the WID network, was composed of 9,966 nodes (proteins or genes) connected *via* 56,133 edges (interactions) (WID.xmml file). We then examined the position of Cyclin G in this network. Betweenness centrality - *i.e.* the total number of non-redundant shortest paths going through a certain node – is a measure of centrality in a network (Yu et al., 2007). A node with a high betweenness centrality could control the flow of information across the network (Yamada and Bork, 2009). With 8.32E-03, Cyclin G had one of the highest value of betweenness centrality of the network, ranking at the 30th position among the 9,966 nodes. This suggests that Cyclin G represents a hub in the WID network.

In order to isolate a connected component of the WID network that showed significant expression change when *CycG$^{\Delta P}$* is expressed, we introduced the expression matrix describing expression of the 530 significantly deregulated genes in the WID network. We next used JactiveModules to identify sub-networks of co-deregulated genes (Ideker et al., 2002). A significant sub-network of 222 nodes and 1069 edges centred on Cyclin G was isolated (Z score 48.53). This sub-network was laid out according to functional categories (Figure 9A, CycG_subnetwork.xmml). Four modules composed of genes respectively involved in transcription, mitochondrial activity, translation, and metabolism, were found to be highly connected to Cyclin G. Strikingly, the “translation” module was mainly composed of genes up-regulated in *da-Gal4, UAS-CycG$^{\Delta P}$*/+ wing imaginal discs. On the contrary, the “mitochondrion” and “metabolism” modules were mainly composed of genes down-regulated in *da-Gal4, UAS-*

CycG$^{\Delta P}$/+ wing imaginal discs. Hence, high fluctuating asymmetry of *da-Gal4, UAS-CycG*$^{\Delta P}$/+ flies correlated positively with the expression of genes involved in translation and negatively with the expression of genes involved in energy production and metabolism. Interestingly, Cyclin G-bound genes in this sub-network were enriched in genes bound by the PRC1 proteins PC, PH and PSC, as well as by RNAPolII, and to a lesser extent by ASX (Figure 9B).

DISCUSSION

The *CycG* gene of *Drosophila melanogaster* encodes a cyclin involved in transcriptional control, cell growth and the cell cycle (Salvaing et al., 2008; Faradji et al., 2011). Mild overexpression of a cDNA encoding Cyclin G deleted of a short C-terminal sequence potentially involved in Cyclin G degradation (a PEST-rich domain; *da-Gal4, UAS-CycG*$^{\Delta P}$/+) induces high fluctuating asymmetry (FA), notably of wings (Debat et al., 2011). Under laboratory conditions (*i.e.* low environmental variation combined with near isogenic lines), this FA should mainly result from developmental noise (Debat and Peronnet, 2013). Thus, *da-Gal4, UAS-CycG*$^{\Delta P}$ flies provide a unique tool to investigate the genetic bases of developmental stability. Cyclin G interacts physically with two chromatin regulators of the Enhancers of Trithorax and Polycomb family (ETP), and genetically with many *Polycomb-group* (*PcG*) and *trithorax-group* (*trxG*) genes (Dupont et al., 2015). This prompted us to re-examine *CycG*-induced developmental stability, notably by testing the effect of chromatin regulator mutations, and to investigate deeply the role of Cyclin G in transcriptional regulation.

Cyclin G maintains developmental stability through an organ-autonomous process that involves the PRC1 and PR-DUB complexes

In *Drosophila* very few mutations have been shown to induce an abnormally high FA. Among them are mutations of the gene encoding the *Drosophila* insulin-like peptide 8 (*Dilp8*). Dilp8 participates in systemic coordination of growth. Being produced in growing tissues, it is secreted into the haemolymph and regulates hormone production *via* a well-identified neuronal circuit (Parker and Shingleton, 2011; Garelli et al., 2012; Colombani et al., 2012). Notably, the neurons that produce Lgr3, the Dilp8 receptor, have been identified, and inactivation of *Lgr3* in these neurons also induces high FA. We investigated here the role of *CycG* in this process by deregulating it in the different modules of the circuit. *CycG*-induced wing FA only occured when the deregulation was local, *i.e.* in wing imaginal discs. More particularly, deregulation of *CycG* in the *Lgr3* neurons did not increase FA. We cannot exclude that Cyclin G induces expression of a systemic factor that is dumped into the haemolymph. However, neither *Dilp8*

nor any other insulin-like peptide gene were found deregulated in *da-Gal4, UAS-CycG$^{\Delta P}$* wing imaginal discs. Altogether, these observations suggest that *CycG* maintains developmental stability through an autonomous mechanism which would not involve the systemic *Dilp8/Lgr3* pathway. Such a mechanism recalls Garcia-Bellido's Entelechia model which proposes that local interactions between wing imaginal disc cells, or populations of these cells, orchestrate their own proliferation in order to generate an adult organ of constant size and shape, independently of global cues (García-Bellido and García-Bellido,1998; García-Bellido 2009).

Expression of Cyclin G deleted of the ETP interacting domain doubles FA as compared to expression of Cyclin G with this domain, irrespective of whether the PEST domain is present or not. Hence, the interaction between Cyclin G and chromatin regulators might somehow participate in developmental stability. To test this hypothesis, we combined the *da-Gal4, UAS-CycG$^{\Delta P}$* chromosome and *ETP* or *PcG* mutations. We observed that mutations of the PRC1 and PR-DUB encoding genes strongly increase FA. Moreover, many of the genes that are bound by Cyclin G in wing imaginal discs are also bound by PRC1 and by ASX. Altogether these observations suggest that transcriptional regulation of target genes shared by Cyclin G, PRC1 and ASX is of paramount importance for developmental stability. We did not observe any significant overlap between Cyclin G-bound genes and binding sites for Calypso, the second component of PR-DUB. Yet, *caly* mutations strongly increase *CycG*-induced FA. Thus, the role of PR-DUB in this context remains to be clarified.

PRC1 and PR-DUB contain antagonistic enzymes (SCE/dRing and Calypso) that respectively ubiquitinates and deubiquitinates H2A on lysine 118 in *Drosophila* (lysine 119 in human). Cyclin G co-localizes extensively with H2AK118ub on polytene chromosomes. However, no modification in the global level of H2AK118 ubiquitination was detected in tissues where Cyclin G isoforms were expressed. It was recently shown that canonical PRC1 accounts for only a small fraction of global H2AK118ub, most of this ubiquitination being due to L(3)73Ah, a homolog of mammalian PCGF3 (Lee et al., 2015). Altogether, our data suggest that H2AK118ub is not involved in developmental stability and rather support the importance of the interaction between Cyclin G and canonical PRC1 in this process. It is tempting to speculate that PRC1 and PR-DUB are partners in the ubiquitination/deubiquitination of an unknown protein important for developmental stability.

Regulation of growth during the cell cycle might be a factor of developmental stability

Additional evidence further connects developmental stability to growth regulation during the cell cycle. Indeed, *CycG*-induced developmental noise is associated with high variance in cell

size along with loss of correlation between cell size and cell number (Debat et al., 2011). As Cyclin G is involved in the control of growth in G1 phase of the cell cycle (Faradji et al., 2011), this supports the hypothesis that a mechanism linked to the regulation of cell cycle-dependent growth is essential for developmental stability (Debat et al., 2011). The fact that genes deregulated in wing imaginal discs deregulating *CycG* are involved mainly in translation, energy production and metabolism, strengthens this hypothesis.

It was shown that promoters of actively transcribed genes, notably *GAPDH* and several ribosomal protein genes, are bookmarked by ubiquitination during mitosis (Arora et al., 2012; Arora et al., 2015). This mechanism would allow post-mitotic resumption of their transcription at the very beginning of the G1 phase. Ubiquitination of these genes correlates with active histone marks such as H3K4me3 and H3K36me3 but not with the repressive histone mark H3K27me3. The enzymes responsible for this ubiquitination are the vertebrate PSC homolog BMI1, and Ring1A, one of the SCE/dRing homologs (Arora et al., 2015). In vertebrates, the major PRC1 component that catalyzes H2A ubiquitination is not Ring1A but its homolog Ring1B suggesting that the role of BMI1 and Ring1A in molecular bookmarking are independent of PRC1, and that BMI1 and Ring1A ubiquitinate another chromatin protein (Arora et al., 2015). In *Drosophila,* this role might be played by PRC1 and SCE/dRing. Cyclin G is exclusive of H3K27me3, and binds the promoter of many ribosomal protein genes (Dupont et al., 2015 and the present work). Furthermore, *CycG* deregulation impairs G1 phase progression and cell growth (Faradji et al., 2011). Lastly, the highest FA is observed when Cyclin G lacking the PEST domain, a potential ubiquitination site, is expressed. Hence, an exciting hypothesis would be that Cyclin G is ubiquitinated by PRC1, or PSC and SCE/dRing outside PRC1, thus releasing the transcriptional standby of active genes at the end of mitosis. In agreement with this, we found that genes involved in metabolism and mitochondrial activity are down-regulated in the $CycG^{\Delta P}$ context. However, we observed at the same time that ribosomal protein genes are up-regulated which should rather promote growth. This foreshadows a complex relationship between Cyclin G and the PRC1 and PR-DUB complexes in the cell cycle-dependent regulation of these genes and appeals to the use of a more integrative, systems biology, approach.

Fine-tuned regulation of genes involved in translation, metabolism and mitochondrial activity is necessary for developmental stability

Cyclin G appears central in a small regulatory sub-network that connects genes involved in metabolism, mitochondrial activity and translation. Besides, many of Cyclin G's direct transcriptional targets in this network are also targets of PRC1 and RNAPolII, and to a lesser

extent of ASX. Interestingly, it was recently shown by a large scale analysis of the *Drosophila* wing imaginal disc proteome that wing size correlates with some basic metabolic functions, positively with glucose metabolism and negatively with mitochondrial activity, but not with ribosome biogenesis (Okada et al., 2016). In agreement with this, we report here that many genes involved in basic metabolism, such as for example *Gapdh1, Gapdh2* or *Jafrac1,* are down-regulated in the $CycG^{\Delta P}$ context, which also agrees with the small mean size of $CycG^{\Delta P}$ flies, organs and cells. However, while mitochondrial genes are negatively regulated, ribosomal biogenesis genes are simultaneously positively regulated. Although transcriptome variations are probably not a direct image of proteome variations, our data suggest that robustness of wing size correlates with the fine-tuning of these key functions relative to each other.

Noisiness of gene expression as a source of developmental noise

Cyclin G, PRC1 and PR-DUB are mainly involved in the regulation of transcription. An exciting hypothesis would be that alteration of developmental stability is due to the noisy transcription of their shared targets. *CycG*-induced high FA is associated with high variability of cell size, that might be due to variability in expression of target genes which are mainly involved in growth control. Phenotypic variations in isogenic populations of both prokaryotic and eukaryotic cells may indeed result from stochastic gene expression mechanisms (McAdams and Arkin, 1997). An increasing corpus of data suggests that the process of gene regulation *per se* can strongly affect variability in gene expression among adjacent cells (for a review see Sanchez et al., 2013). Transcriptional noise may arise at all steps of transcription. For example, the architectural features of promoters have clear effects on mRNA and protein fluctuations in a population of genetically identical cells (Sanchez et al., 2013). RNA polymerase II pausing during elongation is also a source of transcriptional noise (Rajala et al., 2010). In particular, H3K36 methylation, that is related to transcriptional elongation, prevents spurious cryptic transcription from within the gene body (Venkatesh et al., 2012). Recently, activity of the Polycomb complex PRC2 was shown to be important to prevent spurious transcription of inactive genes and to suppress pervasive transcription of intergenic regions (Lee et al., 2015). Mutations of *E(z)* and *esc* that encode two PRC2 members had no effect on *CycG*-induced FA. Dysfunction of PRC2-dependent spurious transcription control is thus unlikely to be the cause of any *CycG*-induced developmental noise. Nevertheless, a similar but weaker effect on intergenic transcription was attributed to PRC1 (Lee et al., 2015). The binding of Cyclin G on many TSS is rather in favor of a role in limiting noisy initiation of transcription. Interestingly, in several cases, noise in gene expression specifically concerns a subset of genes (Weinberger

et al., 2012). For example, H3K36 methylation hinders cryptic transcription in a subclass of genes involved in longevity in *S. cerevisiae* and *C. elegans* (Sen et al., 2015). It is thus tempting to speculate that cooperation between Cyclin G and the PRC1 and PR-DUB complexes is important to prevent spurious transcription of genes involved in growth in the broad sense. It will be very interesting to address these points in the future.

MATERIAL AND METHODS

Plasmids

The *pPMW-attB* plasmid was built as follows: Gateway® vector *pPMW* (Invitrogen, a gift from T. Murphy; (Huynh and Zieler, 1999) was linearized by digestion with *NsiI*; the *attB* sequence was amplified from *pUASTattB* (Bischof et al., 2007) using primers *attB-NsiIF* and *attB-NsiIR* (Table S10) and the PCR product was digested with *NsiI*; the digested PCR product and the linearized plasmid were ligated and sequenced. This plasmid was deposited at Addgene (plasmid # 61814).

The full-length *CycG* cDNA (*CycG^{FL}*, encoding the 566 amino-acid protein) was amplified from S2 cell cDNAs using primers *CycGnF* and *CycGnR*. cDNAs encoding truncated forms of Cyclin G (*CycG$^{\Delta P}$*, Cyclin G deleted of the putative PEST domain corresponding to amino-acids 542 to 566; *CycG$^{\Delta E}$*, Cyclin G deleted of the ETP-interacting domain corresponding to amino-acids 1 to 130; *CycG$^{\Delta E\Delta P}$*, Cyclin G deleted of both domains) were amplified from the full-length *CycG* cDNA using primers *CycGnF* and *CycG541R*, *CycG130F* and *CycGnR*, and *CycG130F* and *CycG541R*, respectively (Table S10 and Dupont et al., 2015). The PCR products were cloned into *pENTR/D-TOPO*® (Invitrogen), transferred into *pPMW-attB* and the resulting plasmids *pPMW-attB-CycG^{FL}*, *pPMW-attB-CycG$^{\Delta P}$*, *pPMW-attB-CycG$^{\Delta E}$*, *pPMW-attB-CycG$^{\Delta E\Delta P}$* were sequenced.

Drosophila melanogaster strains and genetics

Flies were raised on standard yeast-cornmeal medium at 25°C.

Myc-CycG transgenic lines were obtained by *PhiC31*-integrase mediated insertion into strain *y^{1}M{vas-int.Dm}ZH-2Aw*;M{3xP3-RFP.attP'}ZH-51C* (stock BL-24482). Plasmids *pPMW-attB-CycG^{FL}*, *pPMW-attB-CycG$^{\Delta P}$*, *pPMW-attB-CycG$^{\Delta E}$* and *pPMW-attB-CycG$^{\Delta E\Delta P}$* were injected into embryos, G0 adults were back-crossed to *yw*, and G1 transformants were crossed

to *yw* again to obtain G2 transformants (BestGene Inc.). Transformants were individually crossed with *yw; Sp/CyO*, and the curly wing siblings were crossed with each other. Homozygous transgenic lines were then obtained by crossing 5 females and 5 males. The resulting lines were named *UAS-Myc-CycG^{FL}, UAS-Myc-CycG$^{\Delta P}$, UAS-Myc-CycG$^{\Delta E}$* and *UAS-Myc-CycG$^{\Delta E\Delta P}$*.

Gal4 drivers used were *daughterless-Gal4* (*da-Gal4*) (Wodarz et al., 1995), *nubbin-Gal4* (*nub-Gal4*), *optomotor-blind-Gal4* (*omb-Gal4*), *rotund-Gal4* (*rn-Gal4*), *scalloped-Gal4* (*sd-Gal4*), *teashirt-Gal4* (*tsh-Gal4*), *vestigial-Gal4* (*vg-Gal4*) (from the Bloomington *Drosophila* stock center), and *Insulin-like peptide 3-Gal4* (*dILP3-Gal4*), *neuropeptide F-Gal4* (*NPF-Gal4), Pigment-dispersing factor-Gal4* (*Pdf-Gal4*), *period-Gal4* (*per-Gal4*), *phantom-Gal4* (*phm-Gal4*), *Prothoracicotropic hormone-Gal4* (*Ptth-Gal4*), *R10B09-Gal4*, kind gifts from Dr Maria Dominguez's lab (Ferres-Marco et al., 2006).

The *da-Gal4, UAS-CycG$^{\Delta P}$* third chromosome, obtained by recombination of *da-Gal4* with the original *UAS-CycG$^{\Delta P}$* transgene (*RCG76*), was used to test genetic interactions between *CycG* and several *PcG* or *ETP* mutations (Dupont et al., 2015). Alleles used are described in (Soto et al., 1995; Beuchle et al., 2001;Salvaing et al., 2006; Gaytán de Ayala Alonso et al., 2007; Fritsch et al., 2003; Gutiérrez et al., 2012) (Table 3).

For fluctuating asymmetry (FA) analyses, five replicate crosses were performed for each genotype, wherein 6 females carrying a Gal4 driver were mated with 5 males carrying a *CycG* transgene. Parents were transferred into a new vial every 48 h (three times) then discarded. Thirty females were sampled from the total offspring of the desired genotype. For genetic interactions with *PcG* or *ETP* mutants, crosses were performed similarly except that 6 *PcG* or *ETP* mutant females were mated either with 5 *da-Gal4, UAS-CycG$^{\Delta P}$* males, or with *da-Gal4* males as control.

Morphometrics

Right and left wings of 30 sampled females were mounted on slides, dorsal side up, in Hoyer's medium. Slides were scanned with a Hamamatsu Nanozoomer Digital Slide scanner, running the Nanozoomer software with a 20x objective and an 8-bit camera. Wing pictures were separately exported into tif format using NDP.view and the 5x lens. All wings were oriented with the hinge to the left. Image J was used to digitize 15 landmarks or only landmarks 3 and 13 when indicated (Figure 1B). All wings were measured twice. Analysis of size FA was performed as described previously using the Rmorph package (Debat et al., 2011). The FA10 index was used as FA estimator, *i.e.* FA corrected for measurement error, directional

asymmetry and inter-individual variation (Palmer and Strobeck, 1992). For all genotypes, the interaction individual*side was significant, indicating that FA was larger than measurement error. F-tests were performed to compare the different genotypes.

RNA-seq experiments and RT-qPCR validations

Wing imaginal discs from *da-Gal4/UAS-CycG*$^{\Delta P}$ and *da-Gal4/+* third instar female larvae were dissected, and total RNAs were extracted as previously described except that 150 discs homogenized by pipetting were used for each extraction (Coléno-Costes et al., 2012). Three biological replicates (wing imaginal discs dissected from three independent crosses) were generated for each genotype. Library preparation and Illumina sequencing were performed at the Ecole Normale Supérieure Genomic Platform (Paris, France). Messenger (polyA+) RNAs were purified from 1 µg of total RNA using oligo(dT). Libraries were prepared using the strand specific RNA-Seq library preparation TruSeq Stranded mRNA kit (Illumina). Libraries were multiplexed by 6 on 2 flowcell lanes. A 50 bp single read sequencing was performed on a HiSeq 1500 device (Illumina). A mean of 38.1 ± 4.8 million reads was obtained for each of the 6 samples (Table S11). They were aligned with the *Drosophila melanogaster* genome (dm6, r6.07) using TopHat 2 (v2.0.10) (Kim et al., 2013). Unambiguously mapping reads (a mean of 24.9 ± 4.9 million reads) were then assigned to genes and exons described by the Ensembl BDGP5 v77 assembly, by using the "summarizeOverlaps" function from the "GenomicAlignments" package (v 1.2.2) in "Union" mode (Lawrence et al., 2013). Library size normalization and differential expression analysis were both performed with DESeq 2 (v 1.6.3) and genes with adjusted p-value below 0.05 were retained as differentially expressed (Love et al., 2014). Gene Ontology analysis was performed using DAVID (Huang et al., 2009; Huang et al., 2009).

For RT-qPCR validations, RNAs were extracted from wing imaginal discs and treated with Turbo DNAse (Ambion), and cDNA were synthesized with SuperScript II Reverse transcriptase (Invitrogen) using random primers. RT-qPCR experiments were carried out in a CFX96 system (Bio-Rad) using SsoFast EvaGreen Supermix (Bio-Rad). Two biological replicates (cDNA from wing imaginal discs of larvae coming from independent crosses) and three technical replicates (same pool of cDNA) per biological replicate were performed for each genotype. Expression levels were quantified with the Pfaffl method (Bustin et al., 2009). The geometric mean of two reference genes, *Lamin* (*Lam*) and *rasputin* (*rin*), the expression of which did not vary when *CycG*$^{\Delta P}$ was expressed, was used for normalization (Vandesompele et al., 2002). Sequences of primer couples are listed in Table S10.

An interactome was built using Cytoscape (v 2.8.3) and the DroID plugin (v 1.5) to introduce protein-protein and transcription factor-gene interactions (Murali et al., 2011). The jActiveModules plugin (v 2.23) was used to find sub-networks of co-deregulated genes in the interactome by using “overlap threshold” 0.8, “score adjusted for size”, and “regional scoring” (Ideker et al., 2002).

ChIP-seq experiments and ChIP-qPCR validations

Wing imaginal discs from *+/UAS-Myc-CycG$^{\Delta P}$; +/da-Gal4* and *+/da-Gal4* third instar female larvae were used for chromatin immunoprecipitation (ChIP).

For ChIP-seq experiments, 600 wing imaginal discs were dissected (taking one disc per larva) in Schneider medium and aliquoted per 50 in 1.5 mL microtubes on ice. The 12 microtubes were treated as described in (Coléno-Costes et al., 2012) with minor modifications. Discs were fixed at 22°C. 12 sonication cycles were performed (Diagenode Bioruptor sonifier; cycles of 30'' ON, 30'' OFF, high power). After centrifugation, the 12 supernatants were pooled, homogenized, and 2% were removed (Input). The remaining fragmented chromatin was redistributed into 12 tubes and each tube was adjusted to 1 mL with 140 mM NaCl, 10 mM Tris-HCl pH 8.0, 1 mM EDTA, 1% Triton X-100, 0.1% sodium deoxycholate, 0.1% BSA, Roche complete EDTA-free protease inhibitor cocktail). For immunoprecipitation, 3 µg of anti-Myc antibody (Abcam 9132) were added per tube. Two biological replicates were performed.

Library preparation and Illumina sequencing were performed at the Ecole normale superieure Genomic Platform (Paris, France). Libraries were prepared using NEXTflex ChIP-Seq Kit (Bioo Scientific), using 38 ng of IP or Input DNA. Libraries were multiplexed by 10 on one flowcell run. A 75 bp single read sequencing was performed on a NextSeq 500 device (Illumina). Reads were filtered by the "fastq_quality_filter" command from the "fastx-Toolkit" package (http://hannonlab.cshl.edu/fastx_toolkit/), using a threshold of 90% bases with mapping quality ≥ 20. A mean of 55.6 ± 15.2 million reads was obtained for each of the 4 samples (Table S12). Reads that successfully passed the filtering step were aligned to the *Drosophila* genome (dm6, r6.07) using Bowtie 2 (http://bowtie-bio.sourceforge.net/bowtie2/) (v2.1.0) with default parameters (Langmead and Salzberg, 2012). Peaks were called by MACS2 (v2.1.0) by comparing each ChIP to its input library, with fragment size fixed at 110 bp and otherwise default parameters (Zhang et al., 2008). Peak reproducibility between the two biological replicates was then analysed with the IDR method (https://www.encodeproject.org/software/idr/) (Li et al., 2011). Briefly, an IDR score was assigned to each peak by the "batch-consistency-analysis" function, using the recommended

parameters for MACS peaks (peak ranking based on p-value). Peaks below the 0.05 threshold were considered reproducible. The overlapping reproducible peaks from both replicates were fused using the BEDtools suite "merge" function (Quinlan and Hall, 2010), resulting in the final list of peaks kept for subsequent analysis. Cyclin G-bound genes were defined as genes from the genome annotation file (dm6, r6.07) which overlapped at least one of these Cyclin G peaks, as obtained by the BEDtools suite "intersect" function (Quinlan and Hall, 2010).

For ChIP-qPCR validations, ChIP were performed similarly with the anti-Myc antibody. Rabbit IgG (Diagenode) were used as a negative control (mock). qPCR experiments were carried out in a CFX96 system (Bio-Rad) using SsoFast EvaGreen Supermix (Bio-Rad). Three biological replicates – three technical replicates per biological replicate - were performed for each antibody and for the Input. Sequences of primer couples are listed in Table S10. Data were normalized against Input chromatin.

Heatmaps and aggregation plots of Cyclin G signal over gene bodies and Transcription Start Sites (TSS) were generated using the ngsplot package. (https://github.com/shenlab-sinai/ngsplot) (Shen et al., 2014). Some genes with spurious signal (such as genes from the histone complex) were excluded from the analysis based on signal uniformity over the full length of the gene (cumulative derivative of Cyclin G signal over gene length = 0).

Data access

High-throughput sequencing data have been submitted to Gene Expression Omnibus.
Accession numbers for RNA-seq data: GSE99462, GSM2644389, GSM2644390, GSM2644391, GSM2644392, GSM2644393, GSM2644394.

Accession number for ChIP-seq data: GSE99461, GSM2644385, GSM2644386, GSM2644387, GSM2644388.

Genomic association

Genomic loci enriched for Polycomb (PC), Posterior Sex Comb (PSC), Polyhomeotic (PH), RNA Polymerase II (RNAPolII) and H3K27me3 in wild type imaginal discs of third instar larvae were retrieved from GEO (GSE42106) (Schaaf et al., 2013) (H3K27me3_WholeWingDisc GSM1032567, PcRJ_AnteriorWingDisc GSM1032571, PcRJ_PosteriorWingDisc GSM1032574, Ph_WholeWingDisc GSM1032576, PolII_WholeWingDisc GSM1032577, Psc_WholeWingDisc GSM1032578. Binding sites for PC in the whole wing disc were defined as the overlap between PC binding sites in the anterior and posterior wing disc compartment, as obtained by the BEDtools "intersect" function. For ASX and Calypso, the bed files were a

kind gift from Dr. Jürg Müller (Scheuermann et al., 2010). The mappability file for dm6 genome with 25 nt reads (the smallest size in the compared data) was generated using the Peakseq code (http://archive.gersteinlab.org/proj/PeakSeq/ Mappability_Map/Code/). The overall size of the mappable genome was used as the effective genome size for the GAT software (https://github.com/AndreasHeger/gat) to assess the significance of the overlap between peaks of Cyclin G and other factors (Heger et al., 2013). As GAT performs a two-tailed test, it displays low p-values both for significant overlap and exclusion (as between Cyclin G and H3K27me3).

Gene overlap significance assessment was made as follows: under the null hypothesis, genes that are enriched for ASX, Calypso, PC, PSC, PH, RNAPolII or H3K27me3 in wild type imaginal discs of third instar larvae should not exhibit any bias towards Cyclin G targets. Thus, the overlap between $\mathbf{n}$ enriched genes and $\mathbf{K}$ Cyclin G targets genes should be explained by random sampling without replacement of $\mathbf{n}$ genes within the total amount $\mathbf{N}$ of *Drosophila melanogaster* genes. The amount of overlap under the null hypothesis $\mathbf{X}$ follows a hypergeometric law: $X \sim HY(K, N, n)$. The significance of the observed overlap $\mathbf{k}$ was computed as the probability of observing $\mathbf{X}$ higher or equal to $\mathbf{k}$ under the null hypothesis: $\mathrm{P}(\mathrm{X} \geq \mathrm{k})$.

Acknowledgments

We thank Dr. Emmanuèle Mouchel-Vielh and Dr. Jean-Michel Gibert for stimulating discussions and critical reading of the manuscript, the Bloomington Stock Center for fly strains, Dr. Jürg Müller for the alleles of *Asx* and *caly* and for the ASX and Calypso ChIP bed files, Dr. Maria Dominguez and Dr Sergio Juarez-Carreño for the *dilp3-Gal4, R19B09-Gal4, npf-Gal4, pdf-Gal4, per-Gal4, ptth-Gal4* and *tsh-Gal4* drivers. This work was funded by the Centre National de la Recherche Scientifique (CNRS), Université Pierre et Marie Curie (UPMC), Sorbonne Universités (grant SU-14-R-CDV-05-1 to FP), and Fondation ARC pour la Recherche sur le Cancer (grant PJA20131200314 to FP). The École Normale Supérieure genomic platform was supported by the France Génomique national infrastructure, funded as part of the "Investissements d'Avenir" program managed by the Agence Nationale de la Recherche (contract ANR-10-INBS-09). CAD was funded by a doctoral fellowship from the MESR (Ministère de l'Enseignement Supérieur et de la Recherche). JD was funded by a doctoral fellowship from the MESR and by the Fondation pour la Recherche médicale (FDT20160435164).

Figures

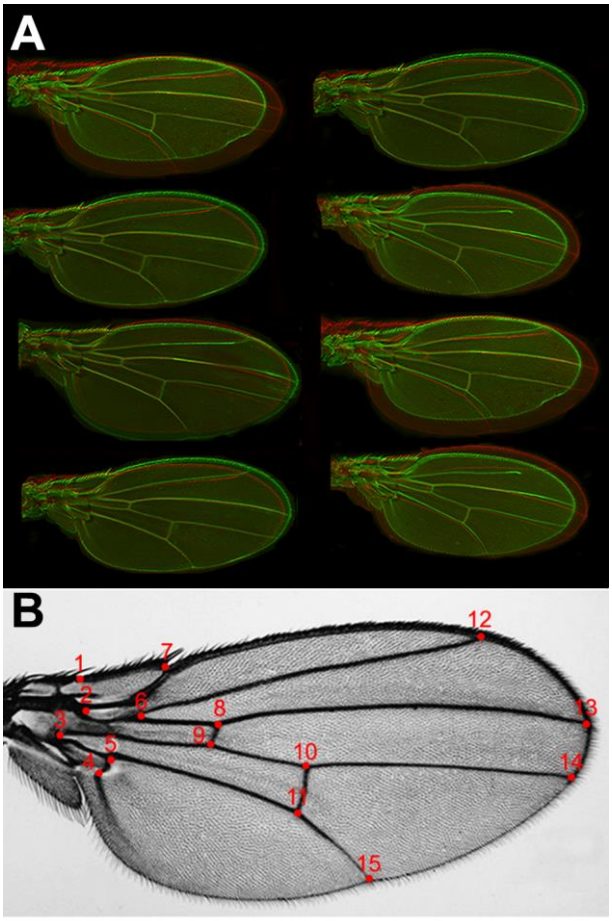

Figure 1: Acquisition of morphometric data.

A – Superimposition of the left and right wings of a sample of *da-Gal4, UAS-CycG*$^{\Delta P}$ flies (left wings in red, right wings in green) showing high asymmetry.

B - Red dots show the 15 landmarks digitized on the wings. FA10 was computed using these landmarks obtained from the left and right wings of at least 30 females randomly sampled from the population as described (Debat et al., 2011).

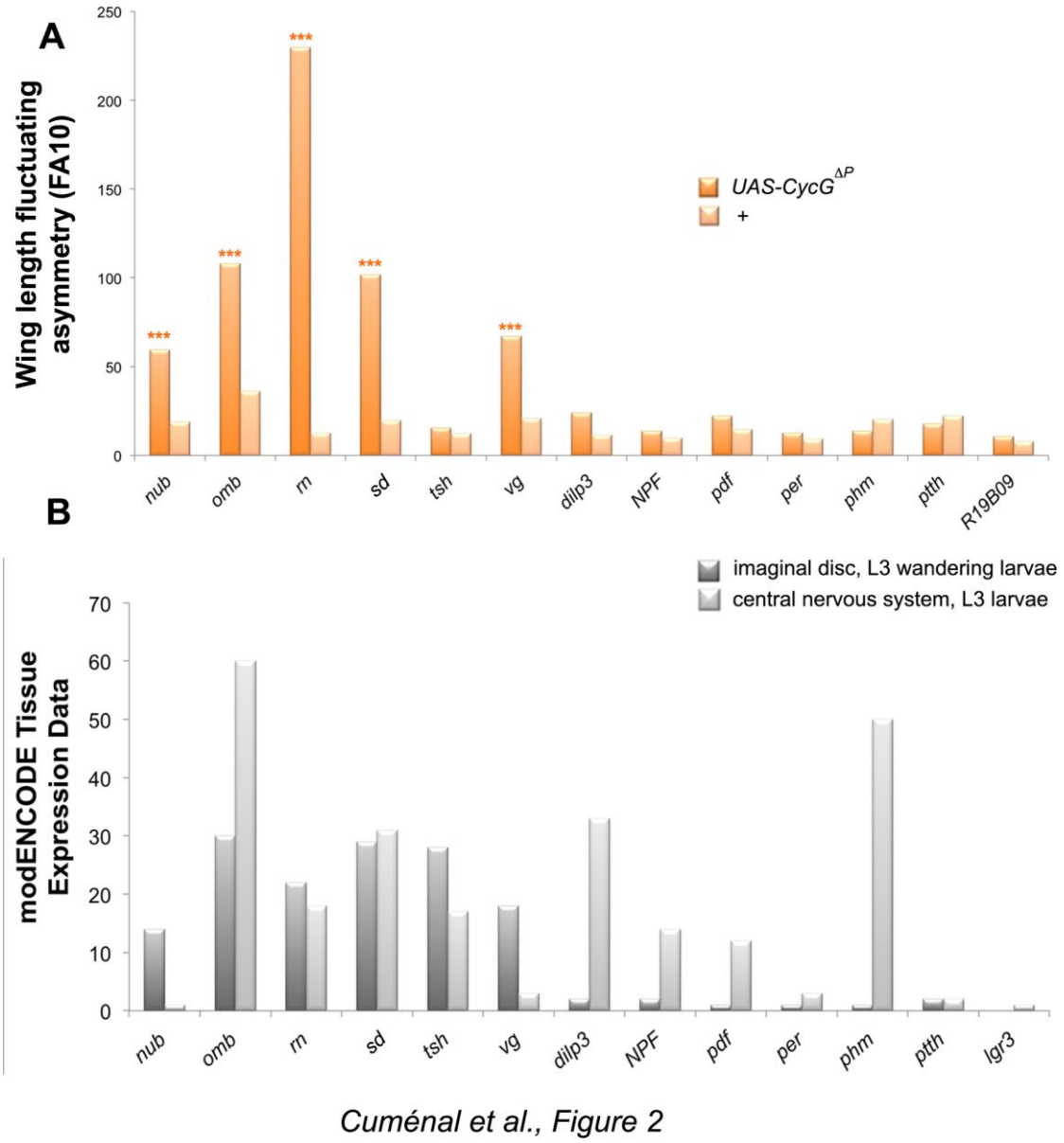

Figure 2: Local deregulation of *CycG* induces high fluctuating asymmetry.

A – Wing length fluctuating asymmetry (FA10) of females bearing a Gal4 driver either associated with *UAS-CycG$^{\Delta P}$* (dark orange) or alone (light orange). Wing length was measured as the distance between landmarks 3 and 13. (F-tests, *** p-value<0.001-. (Source data are provided in Table 1_Source_Data.xls).

B – Expression of the driver genes in 3rd instar larva wing imaginal discs (dark grey) and central nervous system (light grey) as indicated in modENCODE (Graveley et al., 2011).

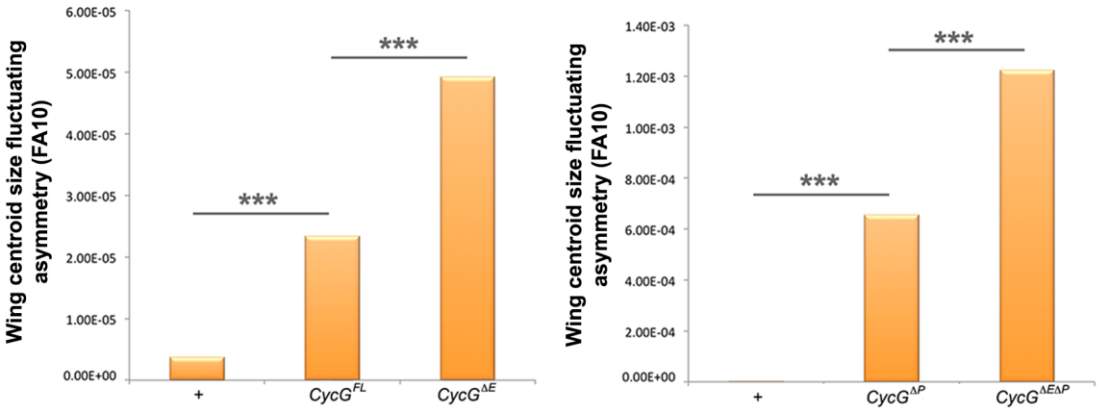

Cumenal et al., Figure 3

Figure 3: The ETP interacting domain limits *CycG*-induced fluctuating asymmetry

A – Centroid size fluctuating asymmetry (FA10) of females *da-Gal4*/+ (+), *+/UAS-Myc-CycG^{FL}; da-Gal4*/+, (*CycG^{FL}*) and *+/UAS-Myc-CycG$^{\Delta E}$*; *da-Gal4,* (*CycG$^{\Delta E}$*).

B – Centroid size fluctuating asymmetry (FA10) of females *da-Gal4*/+ (+), *+/ UAS-Myc-CycG$^{\Delta P}$; da-Gal4*/+ (*CycG$^{\Delta P}$*) and *+/UAS-Myc- CycG$^{\Delta E\Delta P}$; da-Gal4*/+ (*CycG$^{\Delta E\Delta P}$*).

(F-tests, *** p-value<0.001).

(Source data are provided in Table 2_Source_Data.xls).

Wing centroid size was calculated using the 15 landmarks described in Figure 1B.

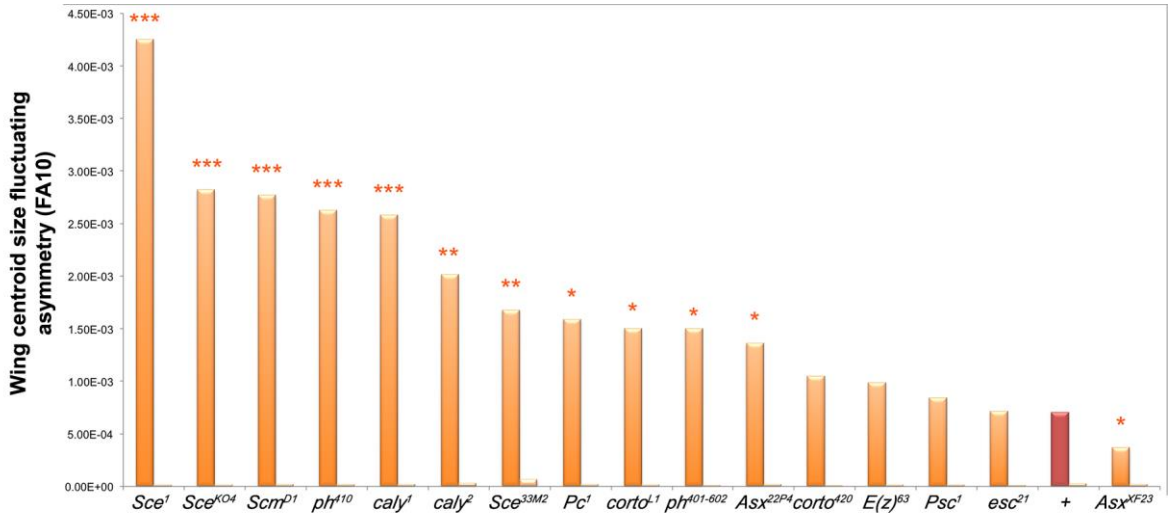

Cumenal et al., Figure 4

Figure 4: *CycG* interacts with several *PcG* and *ETP* genes for developmental stability.

Centroid size fluctuating asymmetry (FA10) of *ETP* or *PcG* heterozygous mutant females combined with *da-Gal4, UAS-CycG$^{\Delta P}$* (dark orange; *da-Gal4, UAS-CycG$^{\Delta P}$*; *PcG*/+ or *da-Gal4, UAS-CycG$^{\Delta P}$*; *ETP*/+) and *ETP* or *PcG* heterozygous mutant females combined with *da-Gal4* (light orange; *da-Gal4*/+*; PcG*/+ or *da-Gal4*; *ETP*/+). In brown (+), centroid size fluctuating asymmetry of *da-Gal4, UAS-CycG$^{\Delta P}$*/+ and *da-Gal4*/+ females. (Source data are provided in Table 3_Source_Data.xls).

(F-tests, *p-value<0.05; ** p-value<0.01; *** p-value<0.001).

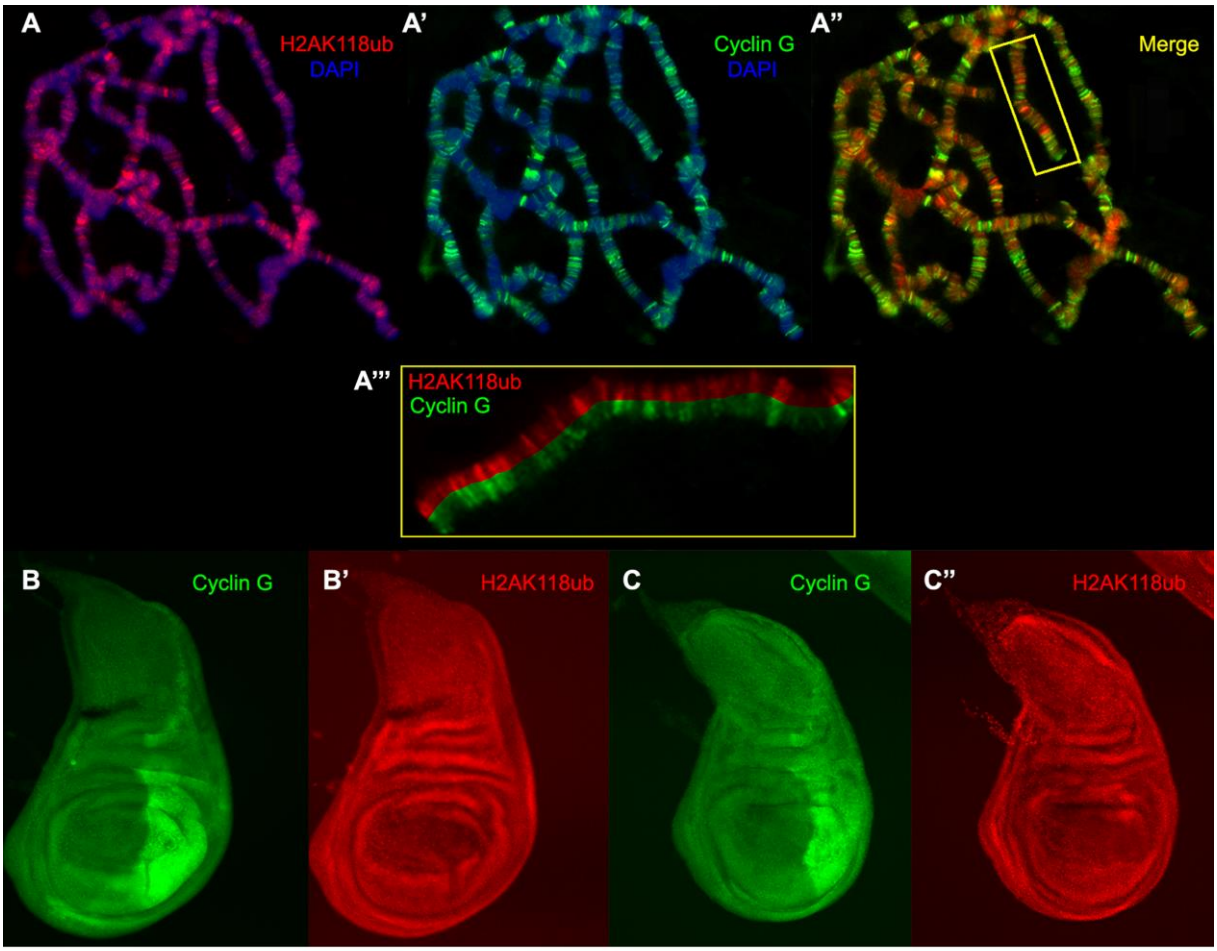

Cumenal et al., Figure 5

Figure 5: Cyclin G co-localizes with H2AK118ub at many sites on polytene chromosomes; expression of *CycG$^{\Delta P}$* does not modify the bulk of H2AK118ub.

A, A', A" – Immunostaining of polytene chromosomes from *w^{1118}* third instar larvae. H2AK118ub (red), Cyclin G (green), DAPI (blue). **A''' –** Close-up of the box showed in A".

B, B' – Wing imaginal discs of 3rd instar larvae expressing *CycG$^{\Delta P}$* in the posterior compartment under control of the *engrailed-Gal4* driver, stained with anti-Cyclin G (green) and anti-H2AK118ub (red).

C, C' – Wing imaginal discs of 3rd instar larvae expressing *CycG$^{\Delta E\Delta P}$* in the posterior compartment under control of the *engrailed-Gal4* driver, stained with anti-Cyclin G (green) and anti-H2AK118ub (red).

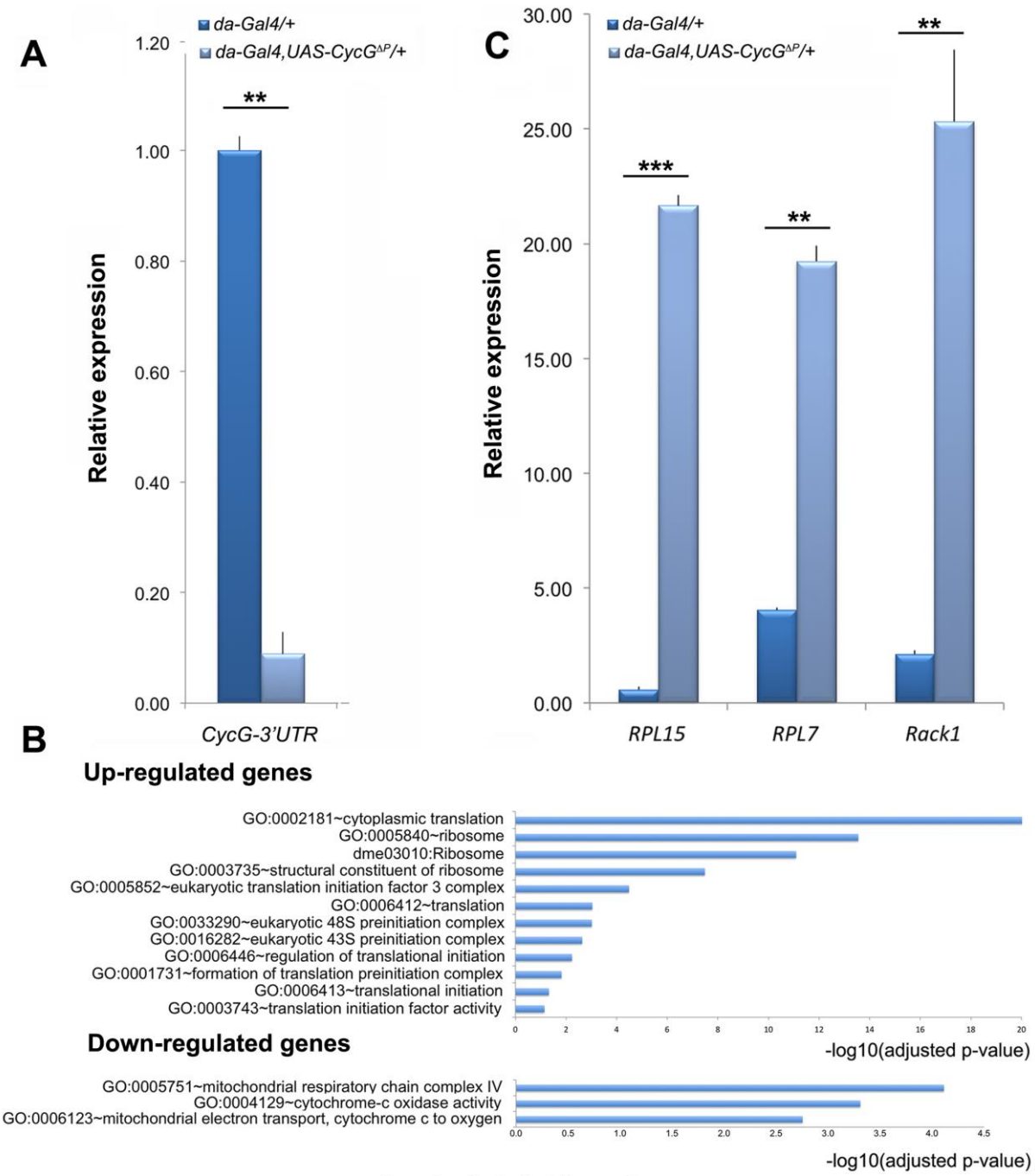

Cuménal et al., Figure 6

Figure 6: Genes deregulated in wing imaginal discs expressing *CycG$^{\Delta P}$*.

A – RT-qPCR analysis of endogenous *CycG* expression in *da-Gal4,UAS-CycG$^{\Delta P}$/+* and *da-Gal4/+* wing imaginal discs. Expression of *CycG* was normalized on the geometric mean of *Lam* and *rin* (Table S3). Two biological replicates (called 1 and 2) were performed per experiment. (t-tests, ** p-value<0.01). Error bars correspond to standard deviation.

B – Ontology of up-regulated and down-regulated genes in *da-Gal4, UAS-CycG$^{\Delta P}$/+ versus da-Gal4/+* wing imaginal discs. Gene ontology analysis was performed with DAVID (Huang et

al., 2009; Huang et al., 2009).

C – RT-qPCR analysis of *RPL15*, *RPL7* and *Rack1* expression in *da-Gal4, UAS-CycG$^{\Delta P}$*/+ and *da-Gal4*/+ wing imaginal discs. . Expression of *RPL15*, *RPL7* and *Rack1* were normalized on the geometric mean of *Lam* and *rin* (Table S5). Two biological replicates (called 1 and 2) were performed per experiment. (t-tests, ** p-value<0.01). Error bars correspond to standard deviation. (t-tests, ** p-value<0.01; *** p-value<0.001).

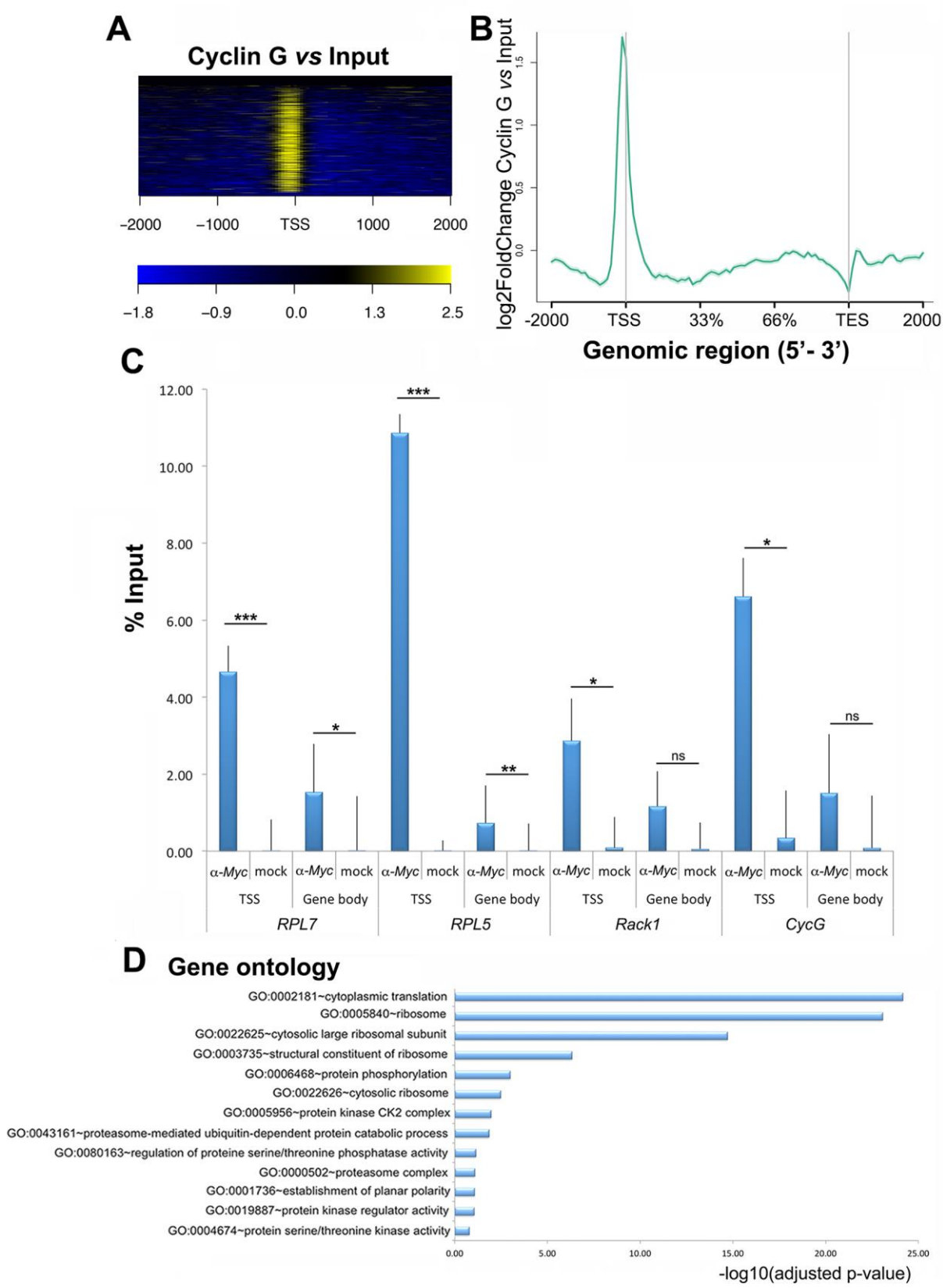

Cuménal et al., Figure 7

Figure 7: Identification of Cyclin G genome-wide binding sites in wing imaginal discs.

A – Heat-map showing the enrichment of Cyclin G over the Input signal on the TSS of 889 genes. TSS: Transcriptional Start Site; TES: Transcriptional End Site.

B – Average profile of Cyclin G signal over these genes shown as an aggregation plot.

C – ChIP-qPCR analysis of *RPL7, RPL5, Rack1* and *CycG*. IPs were performed either with Myc antibody (α-Myc) to reveal the presence of Cyclin G, or with rabbit IgG as negative control (mock). qPCR were performed using oligonucleotide primers located either at the TSS or in the gene body as indicated in Table S1. Error bars represent the coefficient of variation (CV) (Table S7).

D – Ontology of the 889 genes. Gene ontology analysis was performed with DAVID (Huang et al., 2009; Huang et al., 2009).

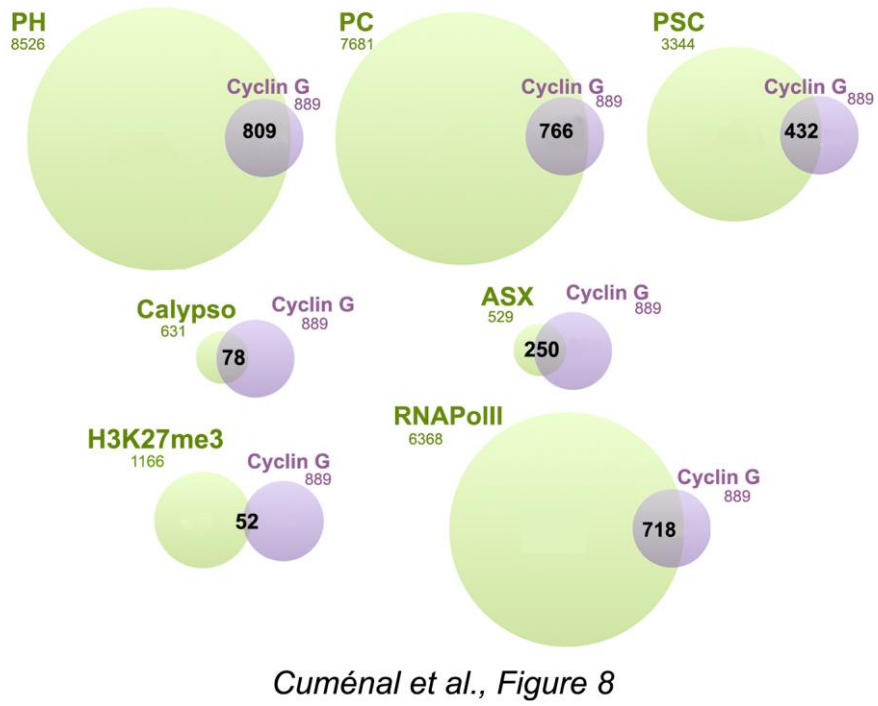

Figure 8: Cyclin G shares target genes with PRC1, ASX and RNAPolII but not with Calypso.

Venn diagrams showing the intersection between Cyclin G-bound genes in *+/ UAS-Myc-CycG$^{\Delta P}$; da-Gal4/+,* wing imaginal discs and PH, PC, PSC, ASX, Calypso and RNApolII in wild-type wing imaginal discs.

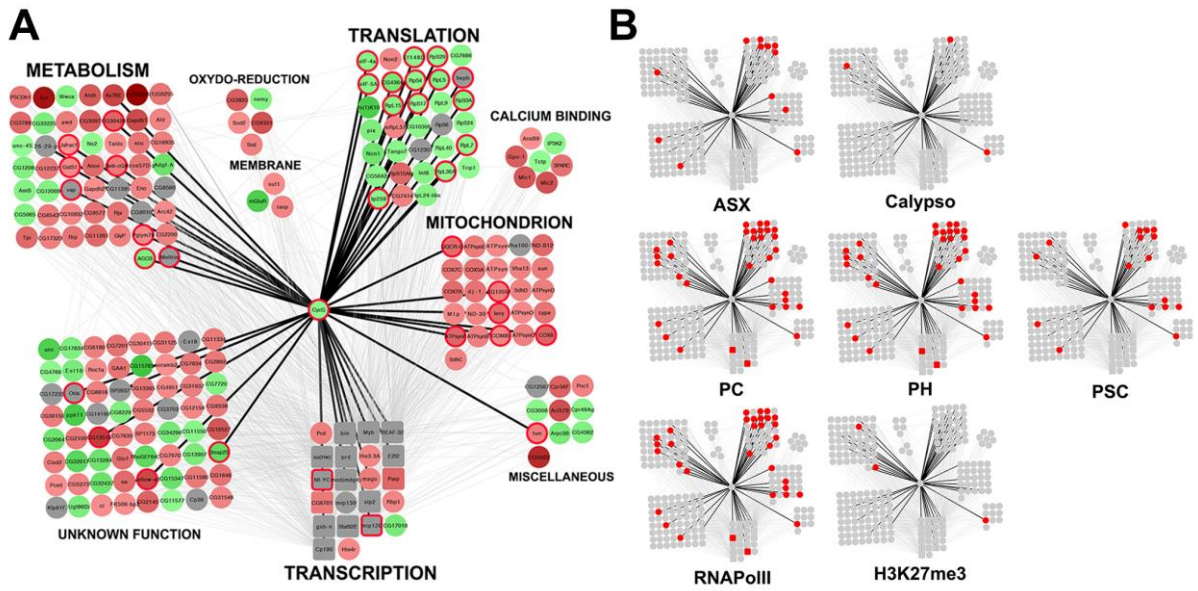

Cuménal et al., Figure 9

Figure 9: Functional subnetwork identified in wing imaginal discs expressing *CycG$^{\Delta P}$*.

A – Schematic representation of a sub-network of 222 genes centred on Cyclin G and identified using JactiveModules (Z score 48.53) (Ideker et al., 2002). In this sub-network, 65 genes were up-regulated in *da-Gal4, UAS-CycG$^{\Delta P}$ versus da-Gal4/+* wing imaginal discs (green gradient), 124 genes were down-regulated (red gradient), and 33 genes were not significantly deregulated (grey). Genes bound by Cyclin G are circled in red. Transcription factor genes are represented by squares. Genes were clustered depending on their function. Black edges correspond to interactions discovered in the present study. Grey edges correspond to interactions described in the literature and imported into the WID network using DroID (Murali et al., 2011).

The WID.xmml and CycG_subnetwork.xmml files are provided.

B – Genes bound by ASX, Calypso, PC, PH, PSC, or RNAPolII, or enriched in H3K27me3 in the sub-network are represented in red.

	n		FA10		Df			
	UAS-CycG$^{\Delta P}$	+	*UAS-CycG$^{\Delta P}$*	+	*UAS-CycG$^{\Delta P}$*	+	F	p-value
nub-Gal4	28	30	59.34	18.80	26.25	26.45	3.1561	2.34E-03
omb-Gal4	30	30	107.90	36.17	28.41	27.88	2.9829	2.87E-03
rn-Gal4	30	30	229.69	12.59	28.80	25.30	18.2390	9.60E-11
sd-Gal4	30	30	101.85	19.83	28.56	26.45	5.1367	3.64E-05
tsh-Gal4	29	30	15.49	12.32	23.89	22.27	1.2576	2.97E-01
vg-Gal4	30	30	67.11	20.90	28.45	26.67	3.2107	1.88E-03
dilp3-Gal4	30	28	23.90	11.51	26.97	23.71	2.0776	4.02E-02
NPF-Gal4	29	28	13.90	9.90	25.09	22.98	1.4048	2.12E-01
pdf-Gal4	30	30	22.14	14.75	24.60	25.09	1.5012	1.60E-01
per-Gal4	28	27	12.69	9.09	23.12	21.53	1.3963	2.23E-01
phm-Gal4	30	30	13.81	20.18	23.86	27.06	1.4609	1.80E-01
ptth-Gal4	29	30	17.62	22.14	25.17	26.30	1.2565	3.39E-01
R19B09-Gal4	30	30	10.76	7.81	23.15	21.87	1.3782	2.32E-01

Table 1: Size fluctuating asymmetry of flies expressing *CycGΔP* with different Gal4 drivers.

Size fluctuating asymmetry was estimated with the FA10 index using landmarks 3 and 13 (Palmer and Strobeck, 1992) as described previously (Debat et al., 2011). Standard F-tests were used to compare FA values between genotypes. Df: degrees of freedom.*CycGΔP*: cDNA encoding the protein deleted of the PEST domain. n: number of females measured. (Source data are provided in Table 1_Source_Data.xls).

				+/da-Gal4		+/UAS-CycG^{FL}; da-Gal4/+		+/UAS-CycG$^{\Delta E}$; da-Gal4/+		+/UAS-CycG$^{\Delta P}$; da-Gal4/+	
Genotype	n	FA10	Df	F	p-value	F	p-value	F	p-value	F	p-value
da-Gal4/+	89	3.73E-06	16.37	-	-						
+/UAS-CycG^{FL}; da-Gal4/+	89	2.34E-05	72.82	6.27	9.30E-05	-	-				
+/UAS-CycG$^{\Delta E}$; da-Gal4/+	90	4.92E-05	85.78	13.19	4.49E-07	2.10	6.96E-04	-	-		
+/UAS-CycG$^{\Delta P}$; da-Gal4/+	111	6.57E-04	108.76	176.01	7.08E-16	28.06	4.52E-35	13.34	6.63E-28	-	-
+/UAS-CycG$^{\Delta E\Delta P}$; da-Gal4/+	95	1.22E-03	93.28	328.22	5.34E-18	52.32	7.18E-44	24.88	1.12E-37	1.86	9.32E-04

Table 2: Centroid size fluctuating asymmetry of flies expressing different versions of Cyclin G.

Centroid size fluctuating asymmetry was estimated with the FA10 index using the 15 landmarks (Palmer and Strobeck, 1992) as described previously (Debat et al., 2011). Standard F-tests were used to compare FA values between genotypes. Df: degrees of freedom. n: total number of females analysed. *CycG^{FL}*: cDNA encoding the full-length protein; *CycG$^{\Delta E}$*: cDNA encoding a protein deleted of the ETP-interacting domain; *CycG$^{\Delta P}$*: cDNA encoding a protein deleted of the PEST domain; *CycG$^{\Delta E\Delta P}$*: cDNA encoding a protein deleted of both domains (Source data are provided in Table 2_Source_Data.xls).

Class	Gene	Allele	Allele class	Reference
ETP	*Additional sex combs*	*Asx*^{22P4}	no protein detected	Scheuermann et al., 2010
		Asx^{XF23}	loss of function	Simon et al., 1992
	corto	*corto*^{420}	loss of function	Salvaing et al., 2006
		corto^{L1}	amorphic	Salvaing et al., 2006
PcG	*calypso*	*caly*^{1}	no protein detected	Scheuermann et al., 2010
	calypso	*caly*^{2}	no protein detected	Scheuermann et al., 2010
	Enhancer of zeste	*E(z)*^{63}	loss of function	Beuchle et al., 2001
	extra sexcombs	*esc*^{21}	amorphic	Gindhart and Kaufman, 1995
	Polycomb	*Pc*^{1}	amorphic	Capdevilla et al., 1986
	polyhomeotic	*ph-d*^{401}*ph-p*^{602}	null	Dura et al., 1987
	polyhomeotic proximal	*ph-p*^{410}	loss of function	Dura et al., 1987
	Posterior sex combs	*Psc*^{1}	hypomorphic	Adler et al., 1989
	Sex combs extra	*Sce*^{1}	null	Gorfinkiel et al., 2004
	Sex combs extra	*Sce*^{33M2}	loss of function	Fritsch et al., 2003
	Sex combs extra	*Sce*^{KO4}	null	Gutiérrez et al., 2012
	Sex comb on midleg	*Scm*^{D1}	amorphic	McKeon and Brock, 1991,

Table 3: Polycomb and Enhancer of Polycomb and Trithorax alleles used in this study.

References

Adler, P.N., Charlton, J., and Brunk, B. (1989). Genetic interactions of the *suppressor 2 of zeste* region genes. *Dev Genet 10*, 249-260. doi:10.1002/dvg.1020100314

Arora, M., Packard, C.Z., Banerjee, T., and Parvin, J.D. (2015). RING1A and BMI1 bookmark active genes via ubiquitination of chromatin-associated proteins. *Nucleic Acids Res 44*, 2136-2144. 10.1093/nar/gkv1223

Arora, M., Zhang, J., Heine, G.F., Ozer, G., Liu, H.W., Huang, K., and Parvin, J.D. (2012). Promoters active in interphase are bookmarked during mitosis by ubiquitination. *Nucleic Acids Res 40*, 10187-0202. doi:10.1093/nar/gks820

Barabasi, A.L., and Albert, R. (1999). Emergence of scaling in random networks. *Science 286*, 509-512.

Beck, S., Faradji, F., Brock, H., and Peronnet, F. (2010). Maintenance of Hox gene expression patterns. *Adv Exp Med Biol 689*, 41-62.

Beuchle, D., Struhl, G., and Müller, J. (2001). Polycomb group proteins and heritable silencing of *Drosophila* Hox genes. *Development 128*, 993-1004.

Bischof, J., Maeda, R.K., Hediger, M., Karch, F., and Basler, K. (2007). An optimized transgenesis system for *Drosophila* using germ-line-specific *varphiC31* integrases. *Proceedings of the National Academy of Sciences 104*, 3312-17.

Breuker, C.J., Patterson, J.S., and Klingenberg, C.P. (2006). A single basis for developmental buffering of *Drosophila* wing shape. *PLoS One 1*, e7. doi:10.1371/journal.pone.0000007

Bustin, S.A., Benes, V., Garson, J.A., Hellemans, J., Huggett, J., Kubista, M., Mueller, R., Nolan, T., Pfaffl, M.W., et al. (2009). The MIQE guidelines: minimum information for publication of quantitative real-time PCR experiments. *Clin Chem 55*, 611-622. doi:10.1373/clinchem.2008.112797

Coléno-Costes, A., Jang, S.M., de Vanssay, A., Rougeot, J., Bouceba, T., Randsholt, N.B., Gibert, J.M., Le Crom, S., Mouchel-Vielh, E., et al. (2012). New partners in regulation of gene expression: the Enhancer of Trithorax and Polycomb Corto interacts with methylated Ribosomal Protein L12 via its chromodomain. *PLoS Genet 8*, e1003006. doi:10.1371/journal.pgen.1003006

Colombani, J., Andersen, D.S., and Léopold, P. (2012). Secreted peptide Dilp8 coordinates Drosophila tissue growth with developmental timing. Science *336*, 582-85.

doi:10.1126/science.1216689

Debat, V., and Peronnet, F. (2013). Asymmetric flies: The control of developmental noise in *Drosophila. Fly* (Austin) *7*, 1-8. doi: 10.4161/fly.23558

Debat, V., Bloyer, S., Faradji, F., Gidaszewski, N., Navarro, N., Orozco-Terwengel, P., Ribeiro, V., Schlötterer, C., Deutsch, J.S., and Peronnet, F. (2011). Developmental Stability: A Major Role for Cyclin G in *Drosophila melanogaster*. *PLoS Genet 7*, e1002314. doi:10.1371/journal.pgen.1002314

Debat, V., Milton, C.C., Rutherford, S., Klingenberg, C.P., and Hoffmann, A.A. (2006). Hsp90 and the quantitative variation of wing shape in *Drosophila melanogaster. Evolution 60*, 2529-538.

Dellino, G.I., Schwartz, Y.B., Farkas, G., McCabe, D., Elgin, S.C., and Pirrotta, V. (2004). Polycomb silencing blocks transcription initiation. *Mol Cell 13*, 887-893.

Dongen, S.V. (2006). Fluctuating asymmetry and developmental instability in evolutionary biology: past, present and future. *J Evol Biol 19*, 1727-743. doi:10.1111/j.1420-9101.2006.01175.x

Dupont, C.A., Dardalhon-Cuménal, D., Kyba, M., Brock, H.W., Randsholt, N.B., and Peronnet, F. (2015). *Drosophila* Cyclin G and epigenetic maintenance of gene expression during development. *Epigenetics Chromatin 8*, 18. doi:10.1186/s13072-015-0008-6

Faradji, F., Bloyer, S., Dardalhon-Cuménal, D., Randsholt, N.B., and Peronnet, F. (2011). *Drosophila melanogaster* Cyclin G coordinates cell growth and cell proliferation. *Cell Cycle 10*, 1-14. Erratum (2014) *Cell Cycle 13*, 2480-2480.

Feder, M.E., and Hofmann, G.E. (1999). Heat-shock proteins, molecular chaperones, and the stress response: evolutionary and ecological physiology. *Annual review of physiology 61*, 243-282.

Ferres-Marco, D., Gutierrez-Garcia, I., Vallejo, D.M., Bolivar, J., Gutierrez-Aviño, F.J., and Dominguez, M. (2006). Epigenetic silencers and Notch collaborate to promote malignant tumours by Rb silencing. *Nature 439*, 430-36. doi:10.1038/nature04376

Fritsch, C., Beuchle, D., and Müller, J. (2003). Molecular and genetic analysis of the Polycomb group gene *Sex combs extra/Ring* in *Drosophila. Mech Dev 120*, 949-954. doi:10.1016/s0925-4773(03)00083-2

García-Bellido, A. (2009). The cellular and genetic bases of organ size and shape in *Drosophila. Int J Dev Biol 53*, 1291-1303. doi:10.1387/ijdb.072459ag

García-Bellido, A.C., and García-Bellido, A. (1998). Cell proliferation in the attainment of constant sizes and shapes: the Entelechia model. *Int J Dev Biol 42*, 353-362.

Garelli, A., Gontijo, A.M., Miguela, V., Caparros, E., and Dominguez, M. (2012). Imaginal discs secrete insulin-like peptide 8 to mediate plasticity of growth and maturation. *Science 336*, 579-582. doi:10.1126/science.1216735

Gaytán de Ayala Alonso, A., Gutiérrez, L., Fritsch, C., Papp, B., Beuchle, D., and Müller, J. (2007). A genetic screen identifies novel polycomb group genes in *Drosophila. Genetics 176*, 2099-2108. doi:10.1534/genetics.107.075739

Geisler, S.J., and Paro, R. (2015). Trithorax and Polycomb group-dependent regulation: a tale of opposing activities. *Development 142*, 2876-887. doi:10.1242/dev.120030

Gildea, J.J., Lopez, R., and Shearn, A. (2000). A screen for new trithorax group genes identified little imaginal discs, the *Drosophila melanogaster* homologue of human retinoblastoma binding protein 2. *Genetics 156*, 645-663.

Graveley, B.R., Brooks, A.N., Carlson, J.W., Duff, M.O., Landolin, J.M., Yang, L., Artieri, C.G., van Baren, M.J., Boley, N., et al. (2011). The developmental transcriptome of *Drosophila melanogaster. Nature 471*, 473-79. doi:10.1038/nature09715

Grimaud, C., Negre, N., and Cavalli, G. (2006). From genetics to epigenetics: the tale of Polycomb group and trithorax group genes. *Chromosome Res 14*, 363-375. doi:10.1007/s10577-006-1069-y

Grossniklaus, U., and Paro, R. (2014). Transcriptional Silencing by Polycomb-Group Proteins. *Cold Spring Harb Perspect Biol 6*. doi:10.1101/cshperspect.a019331

Gutiérrez, L., Oktaba, K., Scheuermann, J.C., Gambetta, M.C., Ly-Hartig, N., and Müller, J. (2012). The role of the histone H2A ubiquitinase Sce in Polycomb repression. *Development 139*, 117-127. doi:10.1242/dev.074450

Heger, A., Webber, C., Goodson, M., Ponting, C.P., and Lunter, G. (2013). GAT: a simulation framework for testing the association of genomic intervals. *Bioinformatics 29*, 2046-48. doi:10.1093/bioinformatics/btt343

Huang, D.W., Sherman, B.T., and Lempicki, R.A. (2009). Systematic and integrative analysis of large gene lists using DAVID bioinformatics resources. *Nat Protoc 4*, 44-57. doi:10.1038/nprot.2008.211

Huang, D.W., Sherman, B.T., and Lempicki, R.A. (2009). Bioinformatics enrichment tools: paths toward the comprehensive functional analysis of large gene lists. *Nucleic Acids*

Res 37, 1-13. doi:10.1093/nar/gkn923

Huynh, C.Q., and Zieler, H. (1999). Construction of modular and versatile plasmid vectors for the high-level expression of single or multiple genes in insects and insect cell lines. *J Mol Biol 288*, 13-20.

Ideker, T., Ozier, O., Schwikowski, B., and Siegel, A.F. (2002). Discovering regulatory and signalling circuits in molecular interaction networks. *Bioinformatics 18 Suppl 1*, S233-240.

Kim, D., Pertea, G., Trapnell, C., Pimentel, H., Kelley, R., and Salzberg, S.L. (2013). TopHat2: accurate alignment of transcriptomes in the presence of insertions, deletions and gene fusions. *Genome Biol 14*, R36. doi:10.1186/gb-2013-14-4-r36

Kingston, R.E., and Tamkun, J.W. (2014). Transcriptional Regulation by Trithorax-Group Proteins. *Cold Spring Harb Perspect Biol 6* doi:10.1101/cshperspect.a019349

Kitano, H. (2004). Biological robustness. *Nat Rev Genet 5*, 826-837. doi:10.1038/nrg1471

Langmead, B., and Salzberg, S.L. (2012). Fast gapped-read alignment with Bowtie 2. *Nat Methods 9*, 357-59. doi:10.1038/nmeth.1923

Lawrence, M., Huber, W., Pagès, H., Aboyoun, P., Carlson, M., Gentleman, R., Morgan, M.T., and Carey, V.J. (2013). Software for computing and annotating genomic ranges. *PLoS Comput Biol 9*, e1003118. doi:10.1371/journal.pcbi.1003118

Leamy, L., Klingenberg, C., Sherratt, E., Wolf, J., and Cheverud, J. (2015). The Genetic Architecture of Fluctuating Asymmetry of Mandible Size and Shape in a Population of Mice: Another Look. *Symmetry 7*, 146-163. doi:10.3390/sym7010146

Leamy, L.J., Routman, E.J., and Cheverud, J.M. (2002). An epistatic genetic basis for fluctuating asymmetry of mandible size in mice. *Evolution 56*, 642-653. doi:10.1038/sj.hdy.6800637

Leamy, L.J., Workman, M.S., Routman, E.J., and Cheverud, J.M. (2005). An epistatic genetic basis for fluctuating asymmetry of tooth size and shape in mice. *Heredity* (Edinb) *94*, 316-325. doi:10.1038/sj.hdy.6800637

Leamy, L.J.L., and Klingenberg, C.P.K. (2005). The genetics and evolution of fluctuating asymmetry. *Annu. Rev. Ecol. Evol. Syst. 36*, 1-21. doi:10.1146/annurev.ecolsys.36.102003.152640

Lee, H.G., Kahn, T.G., Simcox, A., Schwartz, Y.B., and Pirrotta, V. (2015). Genome-wide activities of Polycomb complexes control pervasive transcription. *Genome Res 25*,1170-

81. doi: 10.1101/gr.188920.11

Levy, S.F., and Siegal, M.L. (2008). Network hubs buffer environmental variation in *Saccharomyces cerevisiae. PLoS Biol 6*, e264. doi:10.1371/journal.pbio.0060264

Li, Q., Brown, J.B., Huang, H., and Bickel, P.J. (2011). Measuring reproducibility of high-throughput experiments. *The annals of applied statistics 5*, 1752-779.

Love, M.I., Huber, W., and Anders, S. (2014). Moderated estimation of fold change and dispersion for RNA-seq data with DESeq2. *Genome Biol 15*, 550. doi:10.1186/s13059-014-0550-8

McAdams, H.H., and Arkin, A. (1997). Stochastic mechanisms in gene expression. Proc Natl Acad Sci USA *94*, 814-19.

Milton, C.C., Huynh, B., Batterham, P., Rutherford, S.L., and Hoffmann, A.A. (2003). Quantitative trait symmetry independent of Hsp90 buffering: distinct modes of genetic canalization and developmental stability. *Proc Natl Acad Sci USA 100*, 13396-3401. doi:10.1073/pnas.1835613100

Murali, T., Pacifico, S., Yu, J., Guest, S., Roberts, G.G., and Finley, R.L. (2011). DroID 2011: a comprehensive, integrated resource for protein, transcription factor, RNA and gene interactions for *Drosophila*. *Nucleic Acids Res 39*, D736-743. doi:10.1093/nar/gkq1092

Neto-Silva, R.M., Wells, B.S., and Johnston, L.A. (2009). Mechanisms of growth and homeostasis in the *Drosophila* wing. *Annu Rev Cell Dev Biol 25*, 197-220. doi:10.1146/annurev.cellbio.24.110707.175242

Newman, M.E.J. (2003). The structure and function of complex networks. *SIAM Review 45*, 167-256.

Nijhout, F., and Davidowitz, G. (2003). Developmental Perspectives on Phenotypic Variation, Canalization, and Fluctuating Asymmetry. In Developmental instability, causes and consequences, M. Polak, eds. (New York: Oxford University Press).

Okada, H., Ebhardt, H.A., Vonesch, S.C., Aebersold, R., and Hafen, E. (2016). Proteome-wide association studies identify biochemical modules associated with a wing-size phenotype in *Drosophila melanogaster. Nat Commun 7*, 12649. doi:10.1038/ncomms12649

Palmer, A.R., and Strobeck, C. (1992). Fluctuating asymmetry as a measure of developmental stability: Implications of non-normal distributions and power of statistical tests. *Acta Zool. Fennica 191*, 57-72.

Palmer, R.A. (1994). Fluctuating asymmetry analysis: a primer. In Developmental Instability: Its Origins and Evolutionary Implications (T. A. Markow. Netherlands, Kluwer Academic Publishers).

Parker, N.F., and Shingleton, A.W. (2011). The coordination of growth among Drosophila organs in response to localized growth-perturbation. *Dev Biol 357*, 318-325. doi:10.1016/j.ydbio.2011.07.002

Pengelly, A.R., Kalb, R., Finkl, K., and Müller, J. (2015). Transcriptional repression by PRC1 in the absence of H2A monoubiquitylation. *Genes Dev 29*, 1487-492. doi:10.1101/gad.265439.115

Queitsch, C., Sangster, T.A., and Lindquist, S. (2002). Hsp90 as a capacitor of phenotypic variation. *Nature 417*, 618-624. doi:10.1038/nature749

Quinlan, A.R., and Hall, I.M. (2010). BEDTools: a flexible suite of utilities for comparing genomic features. *Bioinformatics 26*, 841-42.

Rajala, T., Häkkinen, A., Healy, S., Yli-Harja, O., and Ribeiro, A.S. (2010). Effects of transcriptional pausing on gene expression dynamics. *PLoS Comput Biol 6*, e1000704. doi:10.1371/journal.pcbi.1000704

Rutherford, S, Hirate, Y, and Swalla, BJ (2007). The Hsp90 capacitor, developmental remodeling and evolution: The robustness of gene networks and the curious evolvability of metamorphosis. Cr*it Rev Biochem Mol 42*, 355-372.

Rutherford, S., Knapp, J.R., and Csermely, P. (2007). Hsp90 and developmental networks. *Adv Exp Med Biol 594*, 190-97. doi:10.1007/978-0-387-39975-1_16

Rutherford, S.L., and Lindquist, S. (1998). Hsp90 as a capacitor for morphological evolution. *Nature 396*, 336-342. doi:10.1038/24550

Salvaing, J., Decoville, M., Mouchel-Vielh, E., Bussière, M., Daulny, A., Boldyreva, L., Zhimulev, I., Locker, D., and Peronnet, F. (2006). Corto and DSP1 interact and bind to a maintenance element of the *Scr* Hox gene: understanding the role of Enhancers of trithorax and Polycomb. *BMC Biol 4*, 9. doi:10.1186/1741-7007-4-9

Salvaing, J., Nagel, A.C., Mouchel-Vielh, E., Bloyer, S., Maier, D., Preiss, A., and Peronnet, F. (2008a). The enhancer of trithorax and polycomb corto interacts with cyclin G in *Drosophila. PLoS One 3*, e1658. doi:10.1371/journal.pone.0001658

Salvaing, J., Mouchel-Vielh, E., Bloyer, S., Preiss, A., and Peronnet, F. (2008b). Regulation of Abd-B expression by Cyclin G and Corto in the abdominal epithelium of Drosophila.

Hereditas 145, 138-146. doi:HRD2067 [pii]10.1111/j.0018-0661.2008.02067.x

Sanchez, A., Choubey, S., and Kondev, J. (2013). Regulation of noise in gene expression. *Annu Rev Biophys 42*, 469-491. doi:10.1146/annurev-biophys-083012-130401

Sangster, T.A., Salathia, N., Undurraga, S., Milo, R., Schellenberg, K., Lindquist, S., and Queitsch, C. (2008). HSP90 affects the expression of genetic variation and developmental stability in quantitative traits. *Proc Natl Acad Sci USA 105*, 2963-68. doi:10.1073/pnas.0712200105

Schaaf, C.A., Misulovin, Z., Gause, M., Koenig, A., Gohara, D.W., Watson, A., and Dorsett, D. (2013). Cohesin and polycomb proteins functionally interact to control transcription at silenced and active genes. *PLoS Genet 9*, e1003560. doi:10.1371/journal.pgen.1003560

Scheuermann, J.C., de Ayala Alonso, A.G., Oktaba, K., Ly-Hartig, N., McGinty, R.K., Fraterman, S., Wilm, M., Muir, T.W., and Müller, J. (2010). Histone H2A deubiquitinase activity of the Polycomb repressive complex PR-DUB. *Nature 465*, 243-47. doi:10.1038/nature08966

Scheuermann, J.C., Gutiérrez, L., and Müller, J. (2012). Histone H2A monoubiquitination and Polycomb repression: the missing pieces of the puzzle. *Fly* (Austin) *6*, 162-68. doi:10.4161/fly.20986

Sen, P., Dang, W., Donahue, G., Dai, J., Dorsey, J., Cao, X., Liu, W., Cao, K., Perry, R., et al. (2015). H3K36 methylation promotes longevity by enhancing transcriptional fidelity. *Genes Dev 29*, 1362-376. doi:10.1101/gad.263707.115

Shen, L., Shao, N., Liu, X., and Nestler, E. (2014). ngs.plot: Quick mining and visualization of next-generation sequencing data by integrating genomic databases. *BMC Genomics 15*, 284. doi:10.1186/1471-2164-15-284

Siegal, M.L., and Bergman, A. (2002). Waddington's canalization revisited: developmental stability and evolution. *Proc Natl Acad Sci USA 99*, 10528-532. doi:10.1073/pnas.102303999

Simon, J., Chiang, A., and Bender, W. (1992). Ten different Polycomb group genes are required for spatial control of the abdA and AbdB homeotic products. *Development 114*, 493-505.

Soto, M.C., Chou, T.B., and Bender, W. (1995). Comparison of germline mosaics of genes in the Polycomb group of *Drosophila melanogaster. Genetics 140*, 231-243.

Takahashi, H., Okada, Teramura, and Tsujino (2011). Deficiency mapping of the genomic

regions associated with effects on developmental stability in *Drosophila melanogaster. Evolution 65*, 3565-577.

Vallejo, D.M., Juarez-Carreño, S., Bolivar, J., Morante, J., and Dominguez, M. (2015). A brain circuit that synchronizes growth and maturation revealed through Dilp8 binding to Lgr3. *Science 350*, aac6767. doi: 10.1126/science.aac6767.

Vandesompele, J., De Preter, K., Pattyn, F., Poppe, B., Van Roy, N., De Paepe, A., and Speleman, F. (2002). Accurate normalization of real-time quantitative RT-PCR data by geometric averaging of multiple internal control genes. *Genome Biol 3*, research0034.1-c0034.11.

Van Valen, L. (1962). A study of fluctuating asymmetry. *Evolution 16*, 125-142.

Venkatesh, S., Smolle, M., Li, H., Gogol, M.M., Saint, M., Kumar, S., Natarajan, K., and Workman, J.L. (2012). Set2 methylation of histone H3 lysine 36 suppresses histone exchange on transcribed genes. *Nature 489*, 452-55. doi:10.1038/nature11326

Weinberger, L., Voichek, Y., Tirosh, I., Hornung, G., Amit, I., and Barkai, N. (2012). Expression Noise and Acetylation Profiles Distinguish HDAC Functions. *Mol Cell 47*, 193-202. doi:10.1016/j.molcel.2012.05.008

Wodarz, A., Hinz, U., Engelbert, M., and Knust, E. (1995). Expression of crumbs confers apical character on plasma membrane domains of ectodermal epithelia of *Drosophila. Cell 82*, 67-76.

Yamada, T., and Bork, P. (2009). Evolution of biomolecular networks: lessons from metabolic and protein interactions. *Nat Rev Mol Cell Biol 10*, 791-803. doi:10.1038/nrm2787

Yeyati, P.L., Bancewicz, R.M., Maule, J., and van Heyningen, V. (2007). Hsp90 selectively modulates phenotype in vertebrate development. *PLoS Genet 3*, e43. doi:10.1371/journal.pgen.0030043

Yu, H., Kim, P.M., Sprecher, E., Trifonov, V., and Gerstein, M. (2007). The importance of bottlenecks in protein networks: correlation with gene essentiality and expression dynamics. *PLoS Comput Biol 3*, e59. doi:10.1371/journal.pcbi.0030059

Zhang, Y., Liu, T., Meyer, C.A., Eeckhoute, J., Johnson, D.S., Bernstein, B.E., Nusbaum, C., Myers, R.M., Brown, M., et al. (2008). Model-based analysis of ChIP-Seq (MACS). *Genome Biol 9*, R137. doi:10.1186/gb-2008-9-9-r137

SUPPLEMENTARY DATA

Table S1: Centroid size fluctuating asymmetry of flies expressing *CycGΔP* combined with different *PcG* or *ETP* mutant all

Centroid size fluctuating asymmetry was estimated with the FA10 index using the 15 landmarks (Palmer and Strobeck, 1992) as described previously (Debat et al., 2011). Standard F-tests were used to compare FA values between genotypes. Df: degrees of freedom. (Source data are provided in Table 3_Source_Data.xls).

Table S2: List of the 530 genes deregulated in *da-Gal4/+, UAS-CycGΔP* wing imaginal discs as compared to *da-Gal4/+* wing imaginal di

Table S3: Measure of endogenous *CycG* expression by RT-qPCR.

AE: amplification efficiency. Expression of *RPL15, RPL7* and *Rack1* were normalized on the geometric mean of *Lam* and *rin*. Two biological replicates (called 1 and 2) were performed per experiment. t-tests were performed to compare expression of *CycG* in *da-Gal4, UAS-CycG$^{\Delta P}$/+* and *da-Gal4/+* wing imaginal disc.

Table S4: Ontology of genes deregulated in *UAS-CycG$^{\Delta P}$, da-Gal4/+* wing imaginal discs.

Table S5: Validation of RNA-seq experiments by RT-qPCR.

AE: amplification efficiency. Expression of *RPL15, RPL7* and *Rack1* were normalized on the geometric mean of *Lam* and *rin.* Two biological replicates (called 1 and 2) were performed per experiment. t-tests were performed to compare expression of these genes in *da-Gal4, UAS-CycG$^{\Delta P}$/+ and da-Gal4/+* wing imaginal discs.

Table S6: List of the 889 genes bound by Cyclin G in wing imaginal discs.

Table S7: Validation of ChIP-seq experiments by RT-qPCR.

AE: amplification efficiency. Cq of the Input were adjusted taking dilution into account. Results were normalized in comparison to the Input.

Table S8: List of the 62 genes deregulated in *da-Gal4, UAS-CycGΔP/+* wing imaginal discs and bound by Cyclin G at the TSS.

Table S9: Comparison of fragments bound by Cyclin G with fragments bound by ASX, Calypso, PC, PH, PSC, RNAPolII, or enriched in H3K27me3 in 3rd larval instar wing imaginal discs.

Table S10: Primers used in this study.

Coordinates on the *Drosophila* genome (dm6, r6.13)

Table S11: RNA-seq of wing imaginal discs.

Table S12: ChIP-seq of wing imaginal discs.

Supplementary tables and figures

New nomenclature for proteins from the small ribosome subunit				
New name*	**Taxonomic range****	**Bacteria name**	**Yeast name**	**Human name**
bS1	B	S1	-	-
eS1	A E	-	S1	S3A
uS2	B A E	S2	S0	SA
uS3	B A E	S3	S3	S3
uS4	B A E	S4	S9	S9
eS4	A E	-	S4	S4
uS5	B A E	S5	S2	S2
bS6	B	S6	-	-
eS6	A E	-	S6	S6
uS7	B A E	S7	S5	S5
eS7	E	-	S7	S7
uS8	B A E	S8	S22	S15A
eS8	A E	-	S8	S8
uS9	B A E	S9	S16	S16
uS10	B A E	S10	S20	S20
eS10	E	-	S10	S10
uS11	B A E	S11	S14	S14
uS12	B A E	S12	S23	S23
eS12	E	-	S12	S12
uS13	B A E	S13	S18	S18
uS14	B A E	S14	S29	S29
uS15	B A E	S15	S13	S13
bS16	B	S16	-	-
uS17	B A E	S17	S11	S11
eS17	A E	-	S17	S17
bS18	B	S18	-	-
uS19	B A E	S19	S15	S15
eS19	A E	-	S19	S19
bS20	B	S20	-	-
bS21	B	S21	-	-
bTHX	B	THX	-	-
eS21	E	-	S21	S21
eS24	A E	-	S24	S24
eS25	A E	-	S25	S25
eS26	E	-	S26	S26
eS27	A E	-	S27	S27
eS28	A E	-	S28	S28
eS30	A E	-	S30	S30
eS31	A E	-	S31	S27A
RACK1	E	-	Asc1	RACK1

Table S 1. Small subunit r-proteins conversion table

** b, bacterial; e, eukaryotic; u, universal*

*** B, bacteria; A, archaea; E, eukaryotes*

Taken from (Ban et al., 2014).

New nomenclature for proteins of the large ribosome subunit				
New name*	**Taxonomic range****	**Bacteria name**	**Yeast name**	**Human name**
uL1	B A E	L1	L1	L10A
uL2	B A E	L2	L2	L8
uL3	B A E	L3	L3	L3
uL4	B A E	L4	L4	L4
uL5	B A E	L5	L11	L11
uL6	B A E	L6	L9	L9
eL6	E	-	L6	L6
eL8	A E	-	L8	L7A
bL9	B	L9	-	-
uL10	B A E	L10	P0	P0
uL11	B A E	L11	L12	L12
bL12	B	L7/L12	-	-
uL13	B A E	L13	L16	L13A
eL13	A E	-	L13	L13
uL14	B A E	L14	L23	L23
eL14	A E	-	L14	L14
uL15	B A E	L15	L28	L27A
eL15	A E	-	L15	L15
uL16	B A E	L16	L10	L10
bL17	B	L17	-	-
uL18	B A E	L18	L5	L5
eL18	A E	-	L18	L18
bL19	B	L19	-	-
eL19	A E	-	L19	L19
bL20	B	L20	-	-
eL20	E	-	L20	L18A
bL21	B	L21	-	-
eL21	A E	-	L21	L21
uL22	B A E	L22	L17	L17
eL22	E	-	L22	L22
uL23	B A E	L23	L25	L23A
uL24	B A E	L24	L26	L26
eL24	A E	-	L24	L24
bL25	B	L25	-	-
bL27	B	L27	-	-
eL27	E	-	L27	L27
bL28	B	L28	-	-
eL28	E	-	-	L28
uL29	B A E	L29	L35	L35
eL29	E	-	L29	L29
uL30	B A E	L30	L7	L7
eL30	A E	-	L30	L30
bL31	B	L31	-	-
eL31	A E	-	L31	L31
bL32	B	L32	-	-
eL32	A E	-	L32	L32
bL33	B	L33	-	-

New name*	Taxonomic range**	Bacteria name	Yeast name	Human name
eL33	A E	-	L33	L35A
bL34	B	L34	-	-
eL34	A E	-	L34	L34
bL35	B	L35	-	-
bL36	B	L36	-	-
eL36	E	-	L36	L36
eL37	A E	-	L37	L37
eL38	A E	-	L38	L38
eL39	A E	-	L39	L39
eL40	A E	-	L40	L40
eL41	A E	-	L41	L41
eL42	A E	-	L42	L36A
eL43	A E	-	L43	L37A
P1/P2	A E	-	P1/P2 (AB)	P1/P2 (αβ)

Table S 2. Large subunit r-proteins conversion table.

** b, bacterial; e, eukaryotic; u, universal*

*** B, bacteria; A, archaea; E, eukaryotes*

Taken from (Ban et al., 2014).

New name	Previous name	Earlier designations			
eS1	S1A		rp10A		PLC1
	S1B		rp10B		PLC2
uS2	S0A				NAB1A
	S0B				NAB1B
uS3	S3	S3	rp13	YS3	
uS4	S9A	S13	rp21	YS11	
	S9B				SUP46
eS4	S4A	S7A	rp5	YS6	
	S4B	S7B			
uS5	S2	S4	rp12	YS5	SUP44
eS6	S6A	S10A	rp9	YS4	
	S6B	S10B			
uS7	S5	S2	rp14	YS8	
eS7	S7A		rp30		
	S7B				
uS8	S22A	S24A	rp50	YS22	
	S22B	S24B			
eS8	S8A	S14A	rp19	YS9	
	S8B	S14B			
uS9	S16A		rp61R		
	S16B				
uS10	S20				URP2
eS10	S10A				
	S10B				
uS11	S14A		rp59A		CRY1
	S14B		rp59B		CRY2
uS12	S23A	S28A	rp37	YS14	
	S23B	S28B			
eS12	S12	S12			
uS13	S18A				
	S18B				
uS14	S29A	S36A		YS29	
	S29B	S36B			
uS15	S13	S27a		YS15	
uS17	S11A	S18A	rp41A	YS12	
	S11B	S18B	rp41B		
eS17	S17A		rp51A		
	S17B		rp51B		
uS19	S15	S21	rp52		
eS19	S19A	S16aA	rp55A	YS16A	
	S19B	S16aB	rp55B	YS16B	
eS21	S21A	S26A			
	S21B	S26B			
eS24	S24A				
	S24B				
eS25	S25A	S31A	rp45	YS23	
	S25B	S31B			

New name	Previous name	Earlier designations			
eS26	S26A				
	S26B				
eS27	S27A		rp61	YS20	
	S27B				
eS28	S28A	S33A		YS27	
	S28B	S33B			
eS30	S30A				
	S30B				
eS31	S31	S37		YS24	UBI3
uL1	L1A				SSM1A
	L1B				SSM1B
uL2	L2A	L5A	rp8	YL6	
	L2B	L5B			
uL3	L3	L3	rp1	YL1	TCM1
uL4	L4A	L2A	rp2	YL2	
	L4B	L2B			
uL5	L11A	L16A	rp39A	YL22	
	L11B	L16B	rp39B		
uL6	L9A	L8A	rp24	YL11	
	L9B	L8B			
eL6	L6A	L17A	rp18	YL16	
	L6B	L17B			
eL8	L8A	L4A	rp6	YL5	
	L8B	L4B			
uL10	P0				A0
uL11	L12A	L15A		YL23	
	L12B	L15B			
uL13	L16A	L21A	rp22	YL15	
	L16B	L21B	rp23		
eL13	L13A				
	L13B				
uL14	L23A	L17aA		YL32	
	L23B	L17aB			
eL14	L14A				
	L14B				
uL15	L28	L29	rp44	YL24	CYH2
eL15	L15A	L13A	rp15R	YL10	
	L15B	L13B			
uL16	L10				GRC5
uL18	L5	L1a		YL3	
eL18	L18A		rp28A		
	L18B		rp28B		
eL19	L19A	L23A	rp15L	YL14	
	L19B	L23B			
eL20	L20A	L18A			
	L20B	L18B			
eL21	L21A				URP1
	L21B				

New name	Previous name	Earlier designations			
uL22	L17A	L20A		YL17	
	L17B	L20B			
eL22	L22A	L1c	rp4	YL31	
	L22B				
uL23	L25	L25	rp16L	YL25	
uL24	L26A	L33A		YL33	
	L26B	L33B			
eL24	L24A	L30A	rp29	YL21	
	L24B	L30B			
eL27	L27A				
	L27B				
uL29	L35A				SOS1
	L35B				SOS2
eL29	L29			YL43	
uL30	L7A	L6A	rp11	YL8	
	L7B	L6B			
eL30	L30	L32	rp73	YL38	
eL31	L31A	L34A		YL28	
	L31B	L34B			
eL32	L32				
eL33	L33A	L37A	rp47	YL37	
	L33B	L37B			
eL34	L34A				
	L34B				
eL36	L36A	L39		YL39	
	L36B				
eL37	L37A	L43		YL35	
	L37B				
eL38	L38				
eL39	L39	L46		YL40	PUB2
eL40	L40A				UBI1
	L40B				UBI2
eL41	L41A	L47A		YL41	
	L41B	L47B			
eL42	L42A	L41A		YL27	
	L42B	L41B			
eL43	L43A				
	L43B				
P1	P1A			YP1α	A1
	P1B	L44’		YP1β	Ax
P2	P2A	L44		YP2α	A2
	P2B	L45		YP2β	

Table S 3. Yeast r-proteins conversion table.

Please note that small subunit RACK1/Asc1 is not included, as it was not considered a ribosomal protein before 2004 (Gerbasi et al., 2004). Adapted from (Planta and Mager, 1998).

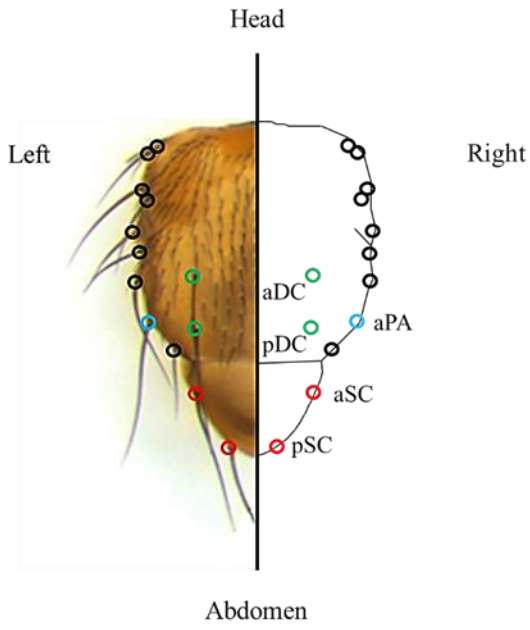

Figure S 1 Schematic representation of the macrochaete pattern on the thorax of a wild type drosphila melanogaster thorax.
aDC and pDC: anterior and posterior dorsocentral bristles (green), aSC and pSC: anterior and posterior scutellar bristles (red), aPA: anterior post-alar bristle (in blue).
The schematic representation of a wild-type macrocheate pattern is juxtaposed to the thorax of a wild-type individual. Realised by Heloïse Grunchec.

			Preliminary observations			
	K3A	**ΔK3**	**K3Y**	**P2QK3R**	**P2LK3E**	**ΔK3F4**
Homozygote viability	Sub-viable	Sub-viable	Viable	Viable	Viable	Lethal
Developmental delay	Dominant	Recessive	None	None	None	Dominant
Minute bristles	Dominant	Recessive	ND	ND	ND	Dominant
Bristle duplications	Dominant	Recessive	ND	ND	ND	Dominant
Ectopic veins	Dominant	None	Recessive	None	Recessive	ND

Table S 4. Summary of the phenotypes of uL11 mutants.
The $uL11^{K3Y}$, $uL11^{P2QK3R}$, and $uL11^{P2LK3E}$ alleles were established as homozygous stock lines without isogenisation. They were only observed as homozygotes; therefore, it is not known whether any of their phenotypes are dominant. The $uL11^{\Delta K3F4}$ allele was established on the SM5 balancer chromosome without isogenisation. ND, No Data.

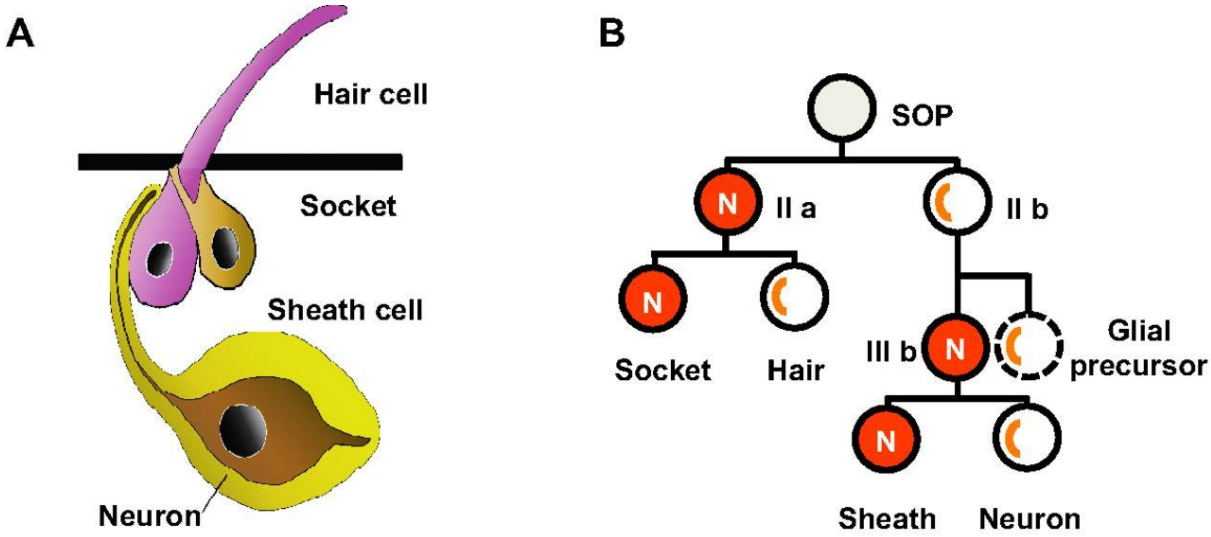

Figure S 2. The bristle cell lineage in Drosophila.
*(**A**) A mechanosensory bristle of* Drosophila *consisting of four cells: a hair cell, a socket cell, a sheath cell and a neuron. (**B**) Once a sensory organ precursor (SOP) cell has been generated within the proneural cluster in the ectoderm it undergoes three rounds of asymmetric cell division to form the different cell types of a sensory bristle. The first division gives rise to two cells (IIa and IIb), then IIb divides further into IIIb and into a glial cell that undergoes apoptosis. The final division of IIa generates the hair and socket cells (outer cells), while IIIb gives rise to a neuron and a sheath cell (inner cells) of the terminally differentiated organ. Asymmetric Notch signaling (N) is necessary at each cell division to specify cell fates: the Notch inhibitor Numb is asymmetrically distributed between the two daughter cells (orange), resulting in high Notch signaling in one daughter, and low activity in the other. Taken from (Koch et al., 2013).*

Translation is an essential metabolic activity in all cells, carried by ribosomes. These large complexes are synthetized in the nucleolus, and require the coordinated expression of 4 ribosomal RNA, 80 ribosomal proteins, and more than 200 assembly factors. Indeed, their biogenesis is both complex and expensive, consuming more than half of the energy in proliferating cells. As the cellular need for ribosomes varies with environmental or metabolic conditions, it is no surprise that their synthesis is tightly regulated in response to a number of cues. Many mechanisms ensure that the intensity of ribosome biogenesis is coupled to cell homeostasis. One of them is the ability of ribosomal proteins to regulate gene expression at many levels, ranging from the translation specificity to the activation or repression of transcription. Many of these functions are performed off the ribosome, and are therefore termed extraribosomal. Our team has discovered a new extraribosomal function of ribosomal protein uL11 in *Drosophila*. Indeed, when it is trimethylated on lysine 3 (uL11K3me3), it associates with Corto, a transcription factor of the Enhancers of Trithorax and Polycomb family. By studying their genome-wide binding profile on chromatin in S2 cells, we show that these proteins are distributed along different patterns, and that uL11K3me3 specifically binds a subset of active genes enriched in ribosome biogenesis components. Additionally, we generated the first genetic alleles for *Drosophila uL11* and describe the molecular screening method that we employed. Last, we studied the phenotypes of *uL11* alleles that delete or replace lysine 3. We describe that their *Minute*-like phenotypes suggest an essential role for the N-terminal domain of uL11, but that it may not result from the association between Corto and uL11K3me3.

Key words: Translation, Transcription, Epigenetics, Ribosome biogenesis, uL11, RpL12, Corto, Homeostasis.

Contrôle épigénétique de l'homéostasie de la biogenèse des ribosomes

La traduction est une activité métabolique essentielle dans les cellules, réalisée par les ribosomes. Ces particules sont synthetisées dans le nucléole, ce qui nécessite l'expression coordonnée de 4 ARN ribosomaux, 80 protéines ribosomales, et plus de 200 facteurs d'assemblage. En effet, leur biogenèse est complexe et coûteuse, sollicitant plus de la moitié de l'énergie des cellules en prolifération. La quantité de ribosomes requise varie selon les conditions environnementales et métaboliques, et de ce fait, leur synthèse est modulée en réponse à de nombreux stimuli. De nombreux mécanismes assurent la coordination de la biogenèse des ribosomes et de l'homéostasie cellulaire. L'un d'eux est la capacité des protéines ribosomiques à réguler l'expression des gènes à tous les niveaux, depuis la spécificité de la traduction jusqu'à l'activation ou la répression transcriptionnelle des gènes. Nombre de ces fonctions sont effectuées hors du ribosome et sont donc qualifiées d'extraribosomales. Notre équipe a mis en évidence une nouvelle fonction extraribosomale de la protéine ribosomale uL11 chez la Drosophile. En effet, quand sa lysine 3 est triméthylée (uL11K3me3), elle interagit avec Corto, un facteur de transcription de la famille des Enhancers de Trithorax et Polycomb. En étudiant leur fixation à la chromatine, nous avons montré que ces protéines se répartissent différemment à l'échelle du génome, et que uL11K3me3 est présente au niveau d'un sous-ensemble de gènes actifs enrichi en composants de la biogenèse des ribosomes. De plus, nous avons généré les premiers allèles génétiques du gène *uL11* chez la Drosophile, et nous décrivons la stratégie de crible moléculaire employée pour leur identification. Finalement, nous avons étudié les phénotypes des mutants de *uL11* dont la lysine 3 est délétée ou substituée. Nous décrivons que leurs phénotypes ressemblent à ceux des mutants Minute, et suggèrent que le domaine N-terminal de uL11 possède une fonction essentielle, mais peut-être indépendante de l'association entre uL11K3me3 et Corto.

Mots clés : Traduction, Transcription, Epigénétique, Biogenèse des ribosomes, uL11, RpL12, Corto, Homéostasie.